THE ROLE OF CHEMOKINE (C-C MOTIF) LIGAND 2 IN INFLAMMATION, OXIDATIVE STRESS, AGING AND METABOLISM

Fedra Nicaury Luciano Mateo

ADVERTIMENT. L'accés als continguts d'aquesta tesi doctoral i la seva utilització ha de respectar els drets de la persona autora. Pot ser utilitzada per a consulta o estudi personal, així com en activitats o materials d'investigació i docència en els termes establerts a l'art. 32 del Text Refós de la Llei de Propietat Intel·lectual (RDL 1/1996). Per altres utilitzacions es requereix l'autorització prèvia i expressa de la persona autora. En qualsevol cas, en la utilització dels seus continguts caldrà indicar de forma clara el nom i cognoms de la persona autora i el títol de la tesi doctoral. No s'autoritza la seva reproducció o altres formes d'explotació efectuades amb finalitats de lucre ni la seva comunicació pública des d'un lloc aliè al servei TDX. Tampoc s'autoritza la presentació del seu contingut en una finestra o marc aliè a TDX (framing). Aquesta reserva de drets afecta tant als continguts de la tesi com als seus resums i índexs.

ADVERTENCIA. El acceso a los contenidos de esta tesis doctoral y su utilización debe respetar los derechos de la persona autora. Puede ser utilizada para consulta o estudio personal, así como en actividades o materiales de investigación y docencia en los términos establecidos en el art. 32 del Texto Refundido de la Ley de Propiedad Intelectual (RDL 1/1996). Para otros usos se requiere la autorización previa y expresa de la persona autora. En cualquier caso, en la utilización de sus contenidos se deberá indicar de forma clara el nombre y apellidos de la persona autora y el título de la tesis doctoral. No se autoriza su reproducción u otras formas de explotación efectuadas con fines lucrativos ni su comunicación pública desde un sitio ajeno al servicio TDR. Tampoco se autoriza la presentación de su contenido en una ventana o marco ajeno a TDR (framing). Esta reserva de derechos afecta tanto al contenido de la tesis como a sus resúmenes e índices.

WARNING. Access to the contents of this doctoral thesis and its use must respect the rights of the author. It can be used for reference or private study, as well as research and learning activities or materials in the terms established by the 32nd article of the Spanish Consolidated Copyright Act (RDL 1/1996). Express and previous authorization of the author is required for any other uses. In any case, when using its content, full name of the author and title of the thesis must be clearly indicated. Reproduction or other forms of for profit use or public communication from outside TDX service is not allowed. Presentation of its content in a window or frame external to TDX (framing) is not authorized either. These rights affect both the content of the thesis and its abstracts and indexes.

The role of chemokine (C-C motif) ligand 2 in inflammation, oxidative stress, metabolism and aging

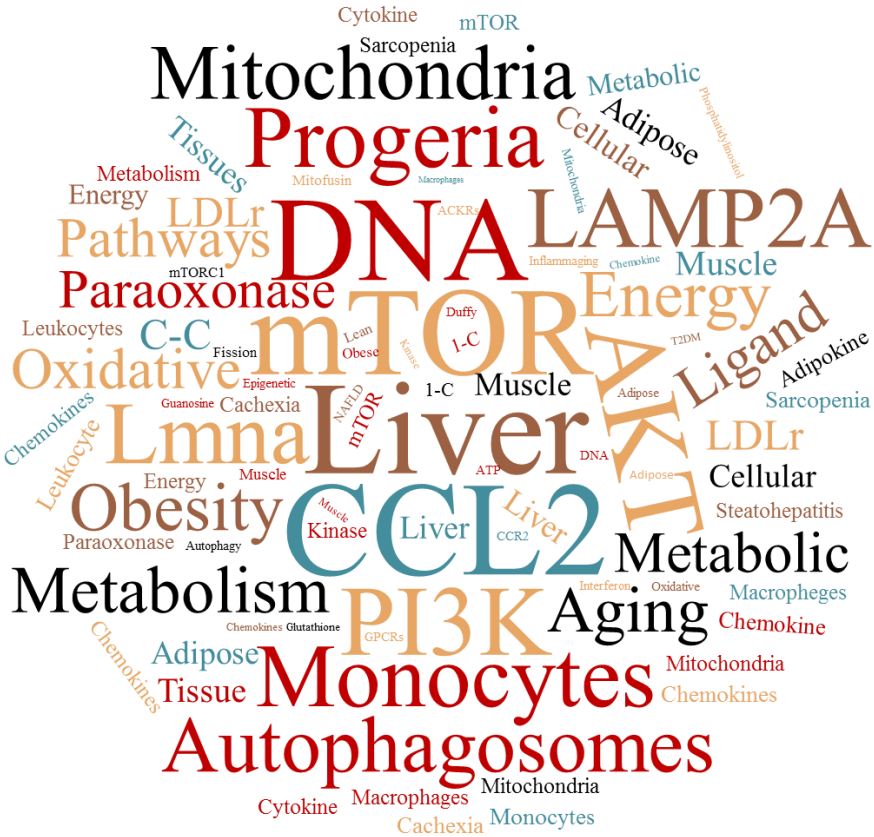

Fedra N. Luciano Mateo
PhD Dissertation
2019

UNIVERSITAT ROVIRA I VIRGILI
THE ROLE OF CHEMOKINE (C-C MOTIF) LIGAND 2 IN INFLAMMATION, OXIDATIVE STRESS, AGING AND METABOLISM
Fedra Nicaury Luciano Mateo

UNIVERSITAT ROVIRA I VIRGILI
THE ROLE OF CHEMOKINE (C-C MOTIF) LIGAND 2 IN INFLAMMATION, OXIDATIVE STRESS, AGING AND METABOLISM
Fedra Nicaury Luciano Mateo

Fedra N. Luciano Mateo

The role of chemokine (C-C motif) ligand 2 in inflammation, oxidative stress, aging and metabolism

PhD Thesis

Supervised by

Prof. Josep Lluís Domingo Roig
Prof. Jorge Joven Maried

Department of Basic Medical Sciences

UNIVERSITAT
ROVIRA i VIRGILI

Reus
2019

UNIVERSITAT ROVIRA I VIRGILI
THE ROLE OF CHEMOKINE (C-C MOTIF) LIGAND 2 IN INFLAMMATION, OXIDATIVE STRESS, AGING AND METABOLISM
Fedra Nicaury Luciano Mateo

UNIVERSITAT
ROVIRA i VIRGILI
FACULTAT DE MEDICINA I CIÈNCIES DE LA SALUT
DEPARTAMENT DE CIÈNCIES MÈDIQUES BÀSIQUES

Carrer Sant Llorenç, 21
43201 Reus
Tel. 977 759 306
Fax. 977 759352

TO WHOM IT MAY CONCERN

WE STATE that the present study, entitled **"The role of chemokine (C-C motif) ligand 2 in inflammation, oxidative stress, aging and metabolism"**, presented by **Fedra N. Luciano Mateo** with the purpose of obtaining the degree of Doctor, has been carried out under our supervision at the **Department of basic medical sciences** of this University.

Reus, 9th April 2019

Doctoral Thesis Supervisor/s

Prof. Josep Lluís Domingo

Prof. Jorge Joven

UNIVERSITAT ROVIRA I VIRGILI
THE ROLE OF CHEMOKINE (C-C MOTIF) LIGAND 2 IN INFLAMMATION, OXIDATIVE STRESS, AGING AND METABOLISM
Fedra Nicaury Luciano Mateo

"Do not be afraid to ask the question that is important to you and go after it fearlessly. Be yourself with determination and resilience because these are key to succeed in science"

Lydia Lynch, PhD
Harvard medical school and Trinity College Dublin, Ireland

UNIVERSITAT ROVIRA I VIRGILI
THE ROLE OF CHEMOKINE (C-C MOTIF) LIGAND 2 IN INFLAMMATION, OXIDATIVE STRESS, AGING AND METABOLISM
Fedra Nicaury Luciano Mateo

A mi Madre,
Gracias por quitar las piedras de mi camino

UNIVERSITAT ROVIRA I VIRGILI
THE ROLE OF CHEMOKINE (C-C MOTIF) LIGAND 2 IN INFLAMMATION, OXIDATIVE STRESS, AGING AND METABOLISM
Fedra Nicaury Luciano Mateo

Acknowledgements

Acknowle

UNIVERSITAT ROVIRA I VIRGILI
THE ROLE OF CHEMOKINE (C-C MOTIF) LIGAND 2 IN INFLAMMATION, OXIDATIVE STRESS, AGING AND METABOLISM
Fedra Nicaury Luciano Mateo

Es imposible resumir todas las personas a las que tengo que dar las gracias por hacer realidad este pequeño reto personal. El camino no ha sido una línea recta, más bien una montaña rusa con sus momentos buenos y momentos malos. Pero les agradezco a todas aquellas personas que han hecho de este trayecto un camino inolvidable.

En primer lugar, al Dr. Jorge Joven por confiar en mí y en mi trabajo, incluso cuando ni yo misma me lo creí. Gracias por todas y cada una de las lecciones desde el "*net i pulit*" al "*no te fíes ni de tu padre*" las cuales guardo con cariño y aprecio. Al Dr. Jordi Camps, gracias por escucharme, aceptar mis ideas y tener la santa paciencia de leer mis primeras versiones, corregirme y guiarme en todo este proceso. Sin duda alguna no habría podido conseguirlo sin su infinita ayuda y paciencia. Al Dr. Domingo, gracias por la oportunidad y la confianza.

Al personal de estabulario: Juan, Esperanza, Celeste y Carolina. Gracias por toda la ayuda que me habéis proporcionado durante estos años. Este trabajo sin vosotros no se hubiese podido llevar a cabo. Al personal de Tecnatox: Elga, Jordi, Anabel, Neus y Tania, gracias por las horas dedicadas y por estar siempre dispuestas a ayudarme cuando no sabía por dónde ir.

Gracias a todos los CRBeros por cada uno de los momentos compartidos. En primer lugar, a Esther, Anabel y Marta, mis mentoras, por abrirme las puertas del CRB, guiarme, y enseñarme a trabajar en un laboratorio como es debido. Por la cantidad de horas invertidas y el trabajo codo con codo en el laboratorio y el estabulario, y por contagiarme vuestro amor por la ciencia y el trabajo bien hecho. A Salva, gracias por la paciencia y por estar dispuesto a tenderme la mano siempre que te he necesitado, sin importar el día o los kilómetros que tengamos de por medio. Especialmente le doy las gracias a Anna, con quien inicié este reto. Siempre has ido un paso por delante y me has ayudado en todo, tanto en lo profesional como en lo personal. A Isa, gracias por tus sabios consejos.

A Gerard, mi primer *pollito oficial.* Gracias por la dedicación, por las horas, por no negarte nunca a ninguna de mis locuras, por muy cansado que te encontraras, siempre me respondías con un: "*No pateixis ho faig amb molt de gust*". Sin lugar a dudas, gracias por tus infinitas ganas de aprender y tu entusiasmo por la ciencia. Mí consejo para ti es que luches y te hagas oír con fuerza. Si tienes una idea ve a por ella con determinación y firmeza. A Eli, pocas veces se tiene la oportunidad de conocer personas como tú, con tanta determinación y energía. Gracias por el apoyo tanto en lo

profesional como en lo personal. Gracias a todos los alumnos de prácticas que me han acompañado y ayudado durante todo este tiempo. Especialmente a Heura, Ion, Javi, Patri, Imane, Marc y Pedro. Gracias por vuestras infinitas ganas de aprender.

I had the great opportunity to travel to Ireland and work at Trinity College Dublin. Thank you to Dr. Lynch for the chance to work in your lab and learn from the best about the immunometabolism. Thank you for your time. Thank you to Aaron, Lydia Dyck, Hanna, Joey, Roisin and all the members of the group for the opportunity to learn new techniques and make very good friends.

Empiezo el terreno personal dando las gracias a Noemí. Te añado en esta lista, porque sinceramente no sé dónde colocarte. Has estado ahí en los momentos de más trabajo, en los días más complicados y de mayor colapso, en los momentos de risas, pero sobre todo en los llantos y lágrimas. No existen palabras de gratitud suficientes para tu infinito apoyo. Quiero también dar las gracias a tu padre: Joan, por acogerme, velar por mí y mi estabilidad como si fuera una más de tus niñas. A la mami Tere, gracias por escucharme y aconsejarme.

A Pedro y a su familia, gracias por celebrar mis victorias, apoyarme en las derrotas y secar mis lágrimas cuando ha hecho falta. A Aida, gracias por ser mi familia en Reus y aceptar que mi casa es tu casa, este proyecto también es tuyo.

A mí Alejandra, todo esto empezó gracias a ti y tu: "*Venga Fedra prueba en el CRB, seguro que te cogen"*. Con esa frase comenzó todo esto y a ese verano del 2012 ordenando bloques de parafina. Este proyecto comenzó ese verano. Eres una amiga incondicional, de esas que duermen en el sofá para dejarte su cama, de las que te van a buscar a la estación lloviendo a mares y arrastran una maleta por Irlanda para que yo no tenga que dar un paso sola. Este proyecto también es tuyo.

A todos los miembros de mi larga familia, pero sobre todo a mis madres, mi abuela y mis tías. Mujeres que me han enseñado que no importa las veces que tropiece porque lo importante es poder levantarse, quitarse el polvo y volver al ruedo. Que cuando se tienen sueños, ambiciones y metas, lamerse las heridas no es la solución sino parte del camino. Que nuestro futuro lo construimos nosotros y el lugar de origen no es un impedimento, sino un punto a mi favor.

Index

Index

UNIVERSITAT ROVIRA I VIRGILI
THE ROLE OF CHEMOKINE (C-C MOTIF) LIGAND 2 IN INFLAMMATION, OXIDATIVE STRESS, AGING AND METABOLISM
Fedra Nicaury Luciano Mateo

Index

Abbreviations

Abbrevi

UNIVERSITAT ROVIRA I VIRGILI
THE ROLE OF CHEMOKINE (C-C MOTIF) LIGAND 2 IN INFLAMMATION, OXIDATIVE STRESS, AGING AND METABOLISM
Fedra Nicaury Luciano Mateo

Abbreviations

1-C: One carbon

4EBP1: Eukaryotic translation initiation factor 4E-binding protein 1

4-HNE: 4-hydroxy-2-nonenal

5-hmC: 5-hydroxymethilcytosine

5-mC: 5-methylcytosine

5-mTHF: 5-methyltetrahydrofolate

ACKRs: Atypical receptors

AKT: Protein kinase B

ALT: Alanine aminotransferase

AMPK: AMP activate protein kinase

AP-1: Activator protein 1

AST: Aspartate aminotransferase

ATG: Autophagy related protein

ATP: Adenosine triphosphate

ATP: Adenosine triphosphate

B2M: Beta-2-Microglobulin

BHMT: Betaine-homocysteine methyltransferase

CaMKKIIβ: Calmodulin-dependent protein kinase IIβ

CCL2: C-C motif ligand 2

CCR2: C-C motif chemokine receptor type 2

CD: Chow diet

CD11b: Cluster of differentiation molecule 11b

CD163: Cluster of differentiation molecule 163

CLEC4F: C-type lectin domain family 4 member

CMA: Chaperone-mediated autophagy

D6: D6 chemokine receptor

DAG: Diacylglycerol

DARC: Duffy antigen receptor for chemokine

DNMT: DNA methyltransferases

Drp: Dynamin relate protein

FAD: Flavin adenine nucleotide

FAH: Fumarate hydratase

GDP: Guanosine diphosphate

GLUT-4: Glucose transporter 4

GPCRs: G-protein-coupled cell surface receptors

GSH: Reduced glutathione

GSSG: Glutathione disulfide

GTP: Guanosine triphosphate

H2O2: Hydrogen peroxide

HDL: High density lipoprotein

HFD: High fat diet

IFN-α: Interferon alpha

IKK: IkB kinase

IL: Interleukin

iNOS: Inducible nitric oxide synthase

Interferon γ: Interferon gamma

IP3: Phosphatidylinositol 1.4.5 triphosphate

IRS: Insulin receptor substrate

JNK: Protein N-terminal kinase

KC: Kupffer cell

LAMP2A: lysosome associated membrane protein type 2

LC3: Microtubule-associated protein 1A/1B-light chain 3

LDL: Low density lipoprotein

LKB1: Liver kinase B1

LPL: Lipoproteinlipase

LPS: Lipopolysaccharide

Mfn2: Mitofusin 2

mTOR: Mammalian target of rapamycin

NAD: Adenine dinucleotide

NADPH: Nicotinamide adenine dinucleotide

NAFLD: Non-alcoholic fatty liver disease

NASH: Non-alcoholic steatohepatitis

NASH: Non-alcoholic steatohepatitis

NF-κB: Nuclear factor κB

NK: Natural killer

NO: Nitric oxide

OPA1: Optic atrophy protein

OXPHOS: Oxidative phosphorylation

PDGF: Platelets derived growth factor

PI3K: Phosphatidylinositol 3 kinase

PINK1: Protein kinase 1

PIP2: Phosphatidylinositol 4.5 diphosphate

PIP3: Phosphatidylinositol triphosphate

PKC: Protein kinase C

PLC: Phospholipase

PON: Paraoxonase

Ractor: Regulatory associated protein of mTOR

Rictor: Rapamycin-insensitive companion

ROS: Reactive oxygen species

SAH: S-adenosylhomocysteine

SAM: S-adenosylmethionine

SAPS: Senescence associated secretory phenotype

SDH: succinate dehydrogenase

SOD: Superoxide dismutase

SREBP-1: Sterol regulatory element-binding protein 1

STAT3: Signal transducer and activator of transcription 3

T2DM: Type 2diabetes mellitus

TAG: Triglyceride

TCA or CAC: Tricarboxylic acid cycle or citric acid cycle

TET: Ten- Elven translocation

TFG-β: Transforming grow factor

THF: Tetrahydropholate

THF: Tetrahydropholate

TLRs: Toll-like receptor

TNFR: Tumor necrosis factor receptor

TNFα: Tumor necrosis factor alfa

TSC: Tuberous sclerosis complex

ULK1: Unc-51 like kinase 1 complex

VLDL: Very low-density lipoproteins

UNIVERSITAT ROVIRA I VIRGILI
THE ROLE OF CHEMOKINE (C-C MOTIF) LIGAND 2 IN INFLAMMATION, OXIDATIVE STRESS, AGING AND METABOLISM
Fedra Nicaury Luciano Mateo

Abstract

Abstract

UNIVERSITAT ROVIRA I VIRGILI
THE ROLE OF CHEMOKINE (C-C MOTIF) LIGAND 2 IN INFLAMMATION, OXIDATIVE STRESS, AGING AND METABOLISM
Fedra Nicaury Luciano Mateo

Abstract

Metabolism and immune system are closely interconnected and their interactions play an important role in whole-body homeostasis [1]. This emerging idea has provided the new concept of immunometabolism. Immunometabolism has been separated into two main research branches: cellular and tissue immunometabolism [2].

Tissue immunometabolism, one of the main aspects of this thesis, focalizes on how immune cells can regulate the tissue metabolism with the aim to induce adaptation to environmental challenges. When cellular adaptation fails, and malfunction becomes extreme, additional leukocytes are recruited to help the tissue in order to cope with these particular stress conditions [2,3]. For instance, during an infection, an increase of neutrophils and other immunitary cells involved in acute inflammation has been observed. The activation, proliferation, differentiation and polarization of these immune cells cause significant metabolic stress, which can compromise the cellular metabolism, homeostasis and energetics requirements [4].

The deregulation of immune cells mobilization and chronic metabolic stress promote metabolic abnormalities in non-immune pathologies such as obesity, type 2 diabetes mellitus (T2DM), cardiovascular and neurodegenerative diseases, or arteriosclerosis [3]. The mechanisms of these variations in the immunological profile, which affect systemic metabolism, remain unclear. Nevertheless, experimental evidence supports an association between immune cell differentiation and tissue metabolic reprogramming. These alterations can affect the most important nutrient-sensing pathways as AMP-activate protein kinase (AMPK) and mammalian target of rapamycin (mTOR) pathway [3,5–7], which play a critical role in the generation of these chronic conditions.
Moreover, tissue metabolic reprograming should not be limited to local effects. The disturbances of metabolic tissues such as liver, muscle and adipose tissue can induce systemic metabolic alterations, a fact which may affect the general homeostasis and cause a vicious cycle of inflammation.

The main problem of tissue immunometabolism is when cellular adaptation fails. This can trigger the appearance of extreme conditions in which cells may die, therefore compromising systemic metabolism. All these alterations give place to metabolic pathologies as insulin resistance, T2DM, liver steatosis and cardiovascular diseases. Growing evidences support that chemokines play a

crucial role in all these processes. In detail, the increase of chemokine C-C motif ligand 2 (CCL2) in metabolic diseases may be an outstanding component in the regulation of metabolism. The key question is if the increase of CCL2 is whether the cause or the consequence of the problem.

For this reason, we explored the effect of CCL2 ablation in the metabolism of mice with an important background of hyperlipidemia, hepatic steatosis and metabolic syndrome. In addition, we investigated if that effect might be conditioned by diet. Obtained results are presented in the first study. Our results denoted that CCL2 ablation could be a therapeutic target especially in non-alcoholic fatty liver disease (NAFLD) development. In CCL2 deficient mice, histologic alterations and fatty liver disease were abrogated. Moreover, we observed an improvement in oxidative stress and inflammation. All these alterations were associated with a normalization of metabolic disturbances and an increase of selective autophagy.

Obtained results open a brief to other questions. For example, does CCL2 function go further to its chemoattracting capacity? Can this chemokine affect the systemic energy metabolism? In order to answer these questions, we generated targeted CCL2 cisgenic mice, which overexpressed CCL2 in all tissues. Achieved results are presented in study 2. We explored different metabolic tissues and results confirmed that CCL2 overexpression has a drastic effect in liver and especially in muscle metabolism. Unlike CCL2 deficiency, CCL2 overexpression was associated with hepatic steatosis and an increase in liver alterations markers. All our results suggest an inefficient liver ATP synthesis, which together with important metabolic alterations, may have led to liver dysfunction. However, these animals showed considerable muscle fragility and a hyperactivation of catabolic pathways. These results suggest that the effect of CCL2 overexpression is tissue-dependent.

In study 3 we evaluated the effect of CCL2 overexpression in a mice model of *Hutchinson-Gilford progeria syndrome*, a model of accelerated aging. These mice have the capacity to develop all metabolic alterations associated to aging such as sarcopenia, lipodystrophy, insulin resistance, cardiovascular alterations, cachexia, oxidative stress, mitochondrial dysfunction and cellular senescence. Our results demonstrate that overexpression of CCL2 promotes systemic alterations in *Hutchinson-Gilford progeria mice.* These mice developed general fibrosis and enhanced metabolic alterations related to accelerate aging.

The finding of therapeutic targets for the treatment of metabolic diseases is an important point in current investigations in our research group. The conclusions of this thesis suggest that CCL2 could be an important therapeutic target in different metabolic diseases.

UNIVERSITAT ROVIRA I VIRGILI
THE ROLE OF CHEMOKINE (C-C MOTIF) LIGAND 2 IN INFLAMMATION, OXIDATIVE STRESS, AGING AND METABOLISM
Fedra Nicaury Luciano Mateo

Introduction

Introdu

UNIVERSITAT ROVIRA I VIRGILI
THE ROLE OF CHEMOKINE (C-C MOTIF) LIGAND 2 IN INFLAMMATION, OXIDATIVE STRESS, AGING AND METABOLISM
Fedra Nicaury Luciano Mateo

Introduction

1. Immunometabolism

Immunometabolism is the interplay between immunological and metabolic processes [3]. Specifically, this new field tries to understand how immune cells can adapt their metabolism to different microenvironments, and how systemic metabolism could be affected by the variation of immune cells population [2]. For this reason, immunometabolism can be divided in two disciplines: cellular and tissue immunometabolism [2].

Cellular immunometabolism is focused in how changes in systemic metabolism can induce alteration in the immune parameters and contribute immune cell activation and proliferation [8]. In contrast, tissue immunometabolism is focused in how immune cells can infiltrate in a tissue and cause a metabolic reprogramming to help the organism adapt to metabolic changes [2,8].

Even though metabolism and immunity have been interwoven since the beginning of life, immunometabolism is an emerging field that has grown in recent years. The first connection between metabolism and immunity was proposed in the middle 1980's by Ceramic and colleagues [9], who discovered that macrophages incubated with lipopolysaccharides could induce resistance to glucose intake and lipoprotein lipase in adipocytes. This work represented the cornerstone in the contemporary immunometabolism. Soon after, Hotamisligil and colleagues associated this observation with inflammation. Hotamisligil showed that adipose tissue from obese rodents exhibited an increase of tumor necrosis factor alpha (TNFα) and its neutralization resulted in an improvement of insulin sensitivity and glucose metabolism [10]. Subsequent studies demonstrated that the administration of TNFα caused insulin resistance and impaired glucose metabolism. Hence, they described the different mechanisms that take part in this process [11,12].

Recently, immunometabolism has attracted the interest of the scientific community due to its clear association with non-immune pathologies such as obesity, diabetes, hyperlipidemia and NAFLD. The etiology of all these pathologies is linked with immune cell mobilization and low-grade of inflammation, a fact which contributes to metabolic dysregulation [3,13,14].

Nowadays, it has been recognized the role of immunometabolism in metabolic organs and the way different immune cell subpopulations can contribute to tissue metabolic homeostasis or dysfunction [15,16]. For instance, a type 2 or anti-inflammatory immunity predominates in adipose tissue under physiological conditions. This anti-inflammatory status is represented by the increase of T-regulatory cells (*Tregs*), eosinophils, T-helper 2 (Th2) lymphocytes or M2-like macrophages. These cells can produce cytokines such as interleukin 4 or 13 (IL-4 or IL-13) that contribute to the main role of adipose tissues (energy storage) and other functions such as thermogenesis (Figure 1) [16–18].

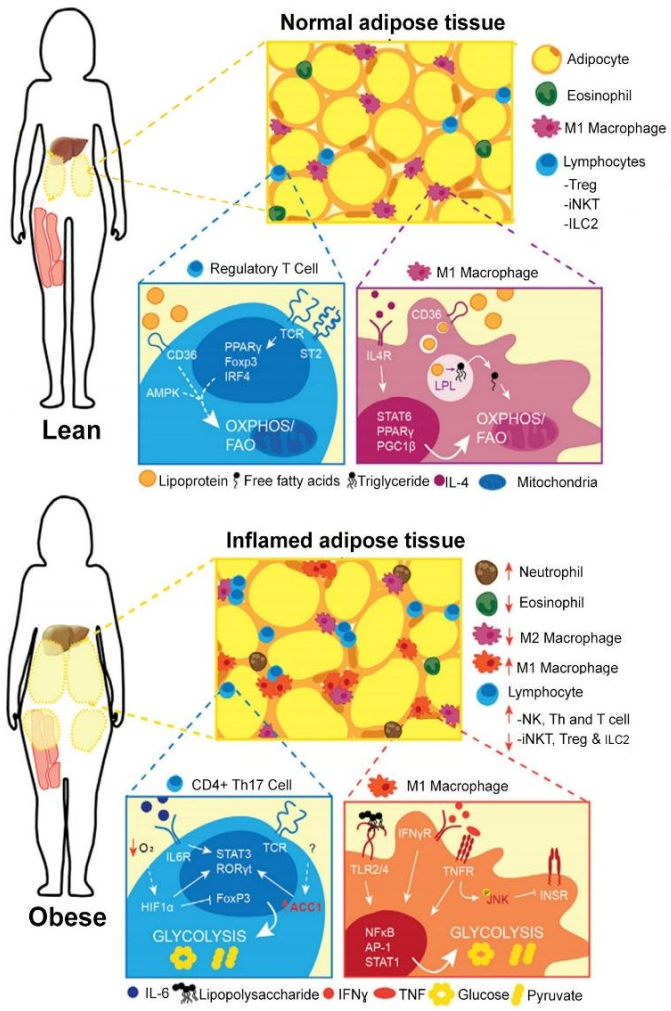

Figure 1: Schematic representation of immunometabolic convergence in lean and obese adipose tissue. Lean adipose tissue is characterized by an enrichment of anti-inflammatory immune cells whose phenotype is driven by metabolic changes induced by the adipose tissue microenvironment. Overfeeding and obesity induce multiple changes in the adipose microenvironment that can alter the metabolic program of adipose resident cells and promote inflammation. Additionally, signaling from pro-inflammatory cytokines can shift macrophage metabolism and promotes their pro-inflammatory properties. Acronyms used were: natural killer (NKT); Invariant natural killer (iNKT); type 2 innate lymphoid cells (ILC2); Interleukin4 and 6 (IL-4 and IL-6); Proinflamatory and antiinflammatory macrophages (M1 and M2 macrophge), Tumor necrosis factor (TNF). Figure adapted from Lynch *et al* 2016 [1].

On the other hand, adipose tissue impairment (for instance in obesity) promotes adipose tissue dysfunction and the increase of pro-inflammatory components (type 1 immunity) such as inflammatory cytokines, or adipokines, including leptin, TNFα or CCL2. These chemokines and adipokines contribute to the recruitment of new immune cells and promote the pro-inflammatory proliferation of resident cells. This condition can induce metabolic stress response, tissue alterations, fibrosis and metabolic dysfunction [1,19–22]. However, the problem begins when the inflammatory microenvironment generated in obesity directly contributes to the activation of immune receptors, such as Toll-like receptor (TLRs), interleukin 1 receptor type I (IL-1RI) and tumor necrosis factor receptor (TNFR). These receptors generate the activation of different inflammatory pathways that can contribute to locally and/or systemically metabolic alterations [23].

As in adipose tissues, liver can be affected during the obesity through an increase of pro-inflammatory immune cells. This condition can promote histological and metabolic alterations in the liver [13,16]. Even though mechanisms that control these modifications are unknown, several studies have shown that macrophages have a pivotal role in all of these processes through the activation of resident liver immunitary cells (Kupffer cells) or through the infiltrated monocytes or macrophages [12,24,25]. These alterations contribute to chemokines overexpression. Chemokines promote blood-derived monocyte infiltration into the liver, exacerbating liver inflammation [16,26] and stimulating other immune cells (Figure 2).

During liver injury, the number of monocyte derived macrophages and Kupffer cell population increase. These macrophages are activated by hepatocytes leading to the release of pro-inflammatory mediators that promote liver injury progression. Populations of macrophages increase their secretion of pro-inflammatory cytokines and stimulate hepatocyte lipogenesis and cell death [27].

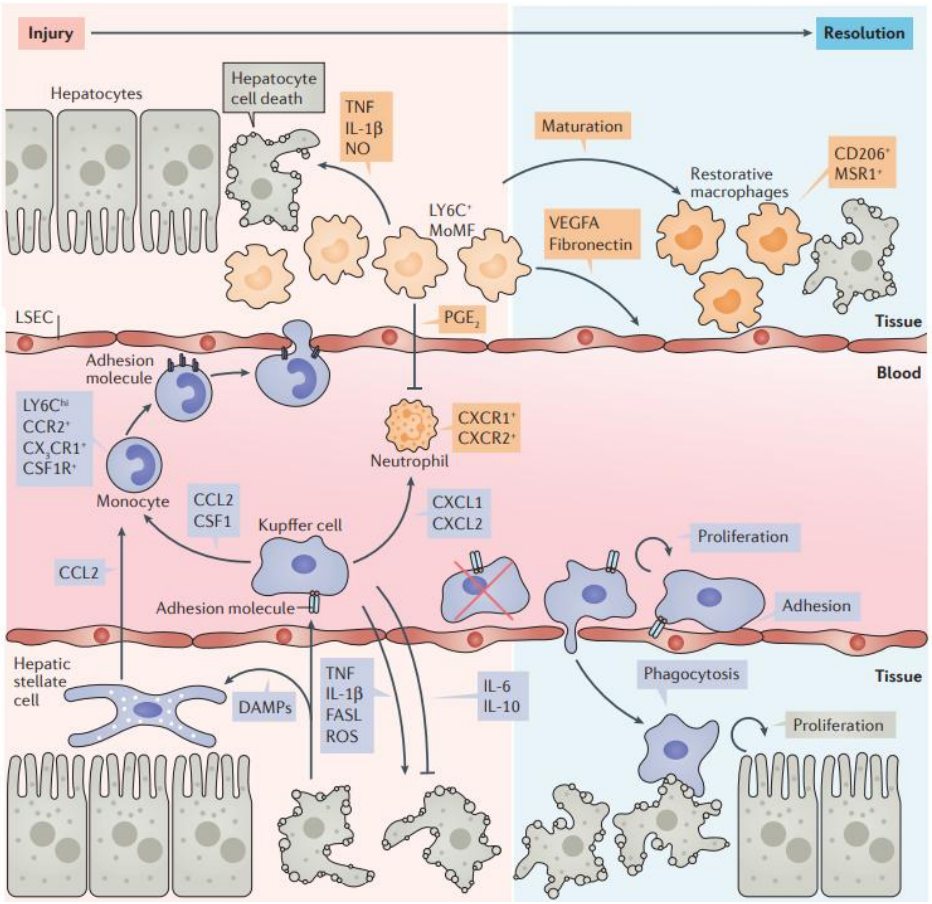

Figure 2. Resident Kupffer cells and infiltrating monocytes and macrophages in liver injury. Liver injury induces the activation of resident Kupffer cells and the infiltration of monocyte-derived macrophages, hence leading to the infiltration of monocytes into areas of inflammation. Acronyms used were: CCL2, CC-chemokine ligand 2; CCR2, CC-chemokine receptor 2; CSF1, macrophage colony-stimulating factor 1; CSF1R, CSF1 receptor; CX3CR1, CX3C-chemokine receptor 1; CXCR, CXC-chemokine receptor; CXCL, CXC-chemokine ligand; DAMPs, damage-associated molecular patterns; FASL, FAS ligand; IL-1β, interleukin-1β; LSEC, liver sinusoidal endothelial cell; MSR1, macrophage scavenger receptor 1; NO, nitric oxide; PGE2, prostaglandin E2; ROS, reactive oxygen species; TNF, tumour necrosis factor; VEGFA, vascular endothelial growth factor A. Figure extracted from Krekel *et al* 2017 [27].

Thus, further investigations of the different immune parameters can open novel therapeutic targets to control the whole-body's metabolism in metabolic diseases. A possible target could be chemokines and cytokines, which are responsible of macrophage infiltration and polarization.

2. *Chemokines*

Chemokines are a protein family formed by a group of 50 polypeptides with low molecular weight (8-15 kDa) which have from 20 to 70 percent homology in amino acid sequences. Chemokines are chemotactic cytokines whose interaction with its receptor is determinant for the immune response regulation to sites of inflammation or injury [28–30]. Chemokines are classified into four classes based on their structure and function: γ-Chemokine (motif C), β-Chemokine (motif CC), α-Chemokine (motif CXC) and δ-Chemokine (motif CX_3C) [28]. As seen in Figure 3, the main difference between each chemokine is the relative position of their two first cysteine residues. γ-Chemokines have only one of the first two cysteines. In β-Chemokines, these two cysteine residues are contiguous to each other. In α-Chemokines, one amino acid separates the first two cysteine residues and in δ-Chemokines, the first two cysteine residues are separated by three amino acids [31,32].

Figure 3: Chemokines classification based on the relation between the cysteine residues and disulfide interaction. From left γ- Chemokine (motif C), β-Chemokine (motif CC), α-chemokine (motif CXC), δ-Chemokine (motif CX3C).

The main function of chemokines is to provide cell migration directionality during inflammation, injury or homeostasis alterations. For this, chemokines induce the activation of specific G-protein-coupled cell surface receptors (GPCRs) which are composed by seven transmembrane helical segments (Figure 4). These receptors are expressed on some cells, whereas they are inducible on others [31]. In humans, four CXC chemokine receptors, eight CC receptors and one CX_3C receptor have been identified [31]. All of them are able to interact with different chemokines [28].

GPCRs receptors are functionally linked to phospholipases and their activation induce the mobilization of calcium from intracellular stores. The subsequently downstream pathway triggers conformational changes of leukocyte integrins, which promote cell adhesion and extravasation.

More specifically, the activation of GPCRs induces a conformational change of guanosine diphosphate (GDP) to guanosine triphosphate (GTP), with a subsequent activation of phospholipase C (PLC), producing phosphatidylinositol 1,4,5 triphosphate (IP3) and dialcyl-glycerol (DAG) from one molecule of phosphatidylinositol 4,5 diphosphate (PIP2). IP3 stimulates calcium mobilization, whereas DAG produces the activation of protein kinase C (PKC) leading to leukocyte activation. Consequently, these actions produce cell chemotaxis, adhesion and extravasation [33].

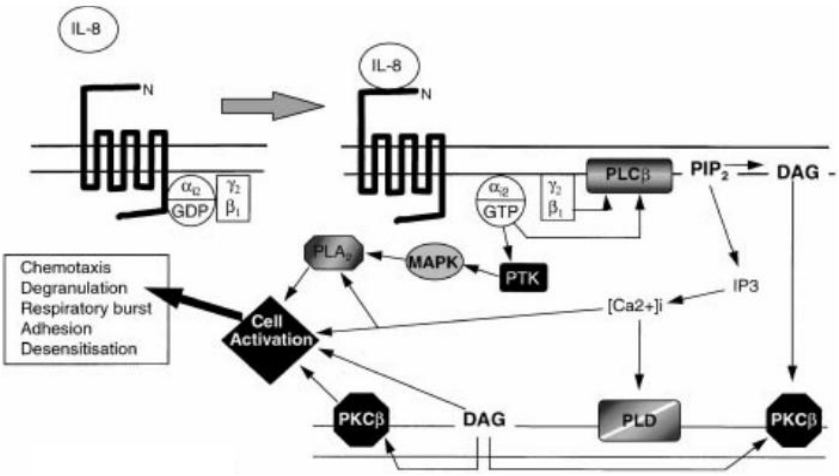

Figure 4: Model of chemokine receptor activation and signal transduction for IL-8 and neutrophils. Acronyms used were interleukin 8 (IL-8), guanosine diphosphate (GDP), guanosine triphosphate (GTP), phospholipase C (PLC), phosphatidylinositol 4,5 diphosphate (PIP2), phosphatidylinositol 1,4,5 triphosphate (IP3) , dialcyl-glycerol (DAG) and protein kinase C activation (PKC). Figure extracted from Murdoch *et al* 2000 [33]

Growing evidences support that chemokines transmit cell signals, which generate multiple responses relate to chemotaxis among other functions. Specifically, the increase of CCL2 in metabolic diseases suggests that this chemokine may play a systemic role in the regulation of metabolism [34,35].

2.2 Chemokine (C-C motif) ligand 2

CCL2 or monocyte chemoattractant protein 1 (MCP-1) is one of the most characterized chemokines. Structurally, CCL2 belongs to CC chemokines subfamily [36] and has two different molecular weights: 9 and 13 kDa according to their levels of O-glycosylation [36,37]. Like other chemokines, CCL2 has 3 different domains: N-terminal domain with disulfide bonds that stabilize the molecule, four regions of β-sheet and α-helix that overlies the sheets (Figure 5). In humans, the gene responsible of CCL2 expression is located in chromosome 17 (chr.17, q11.2) and its expression can be induced by different inflammatory factors as platelet-derived growth factor, interleukins 1 and 4 (IL-1 and IL4), TNF-α, vascular endothelial growth factors and Interferon gamma (IFN-γ) [36,38]. CCL2 can be produced by many cell types such as fibroblasts, epithelial, smooth muscle, mesangial, astrocytic and microglial. However, monocytes and macrophages are the main source of CCL2 [36,38–40].

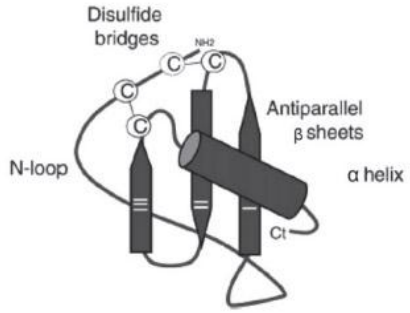

Figure 5: Structure of CCL2. Figure extracted from Chew *et al* 2012 [202]

2.2.1 CCL2 receptors and signals transduction pathways

The main CCL2 receptor is CCR2 (C-C motif chemokine receptor type 2). As all chemokine receptors, CCR2 belongs to GPCRs family and is located on leukocytes surface [36]. CCR2 is encoded by a gene situated on the short arm of chromosome 3 [41].

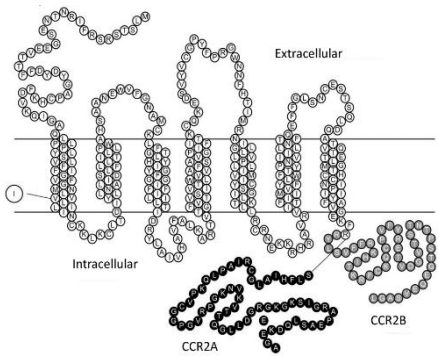

Figure 6: Structure of the CCR2A and CCR2B molecules. Figure adapted from Bartoli *et al* 2001 [203].

Like any other GPCRs proteins, CCR2 has seven hydrophobic domains linked by intra and extracellular loops (Figure 6). Moreover, it has an extracellular N-terminal domain, which is responsible for binding ligands with high affinity such as CCL2, CCL7, CCL8, CCL12, and CCL13 [42]. Furthermore, CCR2 has a C-terminal intracellular domain, whose main function is the regulation of intracellular reactions [42]. The

different C-terminal amino acid sequences determine the CCR2 isoform. There are two different CCR2 isoforms: CCR2A and CCR2B. CCR2A can be expressed by mononuclear cells and vascular smooth muscle cells. CCR2B is expressed by Natural Killers (NK) cells and monocytes [38]. CCR2A and CCR2B can induce different signaling pathways, but CCR2B isoform represents 90% of the total CCR2 receptors expressed on mononuclear cells [42,43].

Despite the fact that chemoattractant function of CCL2 is regulated by GPCRs proteins, CCL2 has other silent or atypical receptors (ACKRs) [44–46]. These receptors neither transmit any signal nor induce extracellular response. ACKRs regulate CCL2 concentration, aiming to regulate the inflammatory response [47]. The most important CCL2 atypical receptors are Duffy antigen receptor for chemokine (DARC) and D6 chemokine receptor (D6) [32,45].

2.2.2 Biological function

The most important function of CCL2 is monocyte recruitment during inflammatory processes or under chronic inflammatory conditions. In detail, during the inflammation the number of blood monocytes derived from bone marrow increases. These immune cells migrate into the inflammatory focus and contribute to generate a pro-inflammatory microenvironment, CCL2 has distinct role throughout this process. Under inflammatory conditions CCL2 induces a chemokine gradient that contributes to the recruitment of circulating monocytes into the inflamed tissue. In inflamed tissue, CCL2 induces the secretion of inflammatory cytokines [48].

Thus, CCL2 has a determinant role in the development and progression of much inflammatory pathology associated with monocyte infiltration including allergic reactions, bacterial infections and arthritis [41]. Moreover, several studies associate CCL2 overexpression with other metabolic pathologies such as arteriosclerosis, cancer, nephropathies, obesity and diabetes [36,38,41,49,50]. This finding suggests that CCL2 may be involved in different biological processes mostly unrelated to chemotaxis.

2.2.3 Chemokine (C-C motif) ligand 2 and metabolic disorders

Metabolic diseases are different pathologies, congenital or acquired, that affect cell function, thus causing a systemic problem. In our society, the most common metabolic diseases are diabetes, cancer, cardiovascular disease, hypercholesterolemia, non-alcoholic fatty liver disease and obesity. All these pathologies are the main causes of death and disability worldwide.

Mechanistically, metabolic diseases are characterized by oxidative stress, hypoxia, mitochondrial dysfunction, an increase of free fatty acids and an increase of inflammatory chemokines. All these alterations induce a vicious cycle which perpetuates metabolic disorders [51].

Different studies have elucidated the role of chemokines and their receptors in several metabolic diseases. The interaction between chemokines and receptors can induce several signaling pathways, which in turn, can influence different molecular and cellular processes. Thus, alterations in chemokines/receptors axis lead to numerous human diseases [52,53]. This fact has been demonstrated using genetically modified mice, antibody or inhibitor-mediated neutralization and epidemiological studies in humans [38].

Several studies have demonstrated that CCL2 and its receptor CCR2 are related to the pathogenesis of different inflammatory and metabolic diseases such as cancer, obesity, insulin resistance, atherosclerosis and non-alcoholic fatty liver disease; thus, becoming an interesting and highly studied target for novel therapeutic strategies [7,54].

2.2.3.1 Chemokine (C-C motif) ligand 2, Obesity and Insulin Resistance

Obesity is a pathology associated with the increase of size and number of adipocytes [55]. This pathology is correlated with a chronic, low grade inflammation and an increase of pro-inflammatory cytokines and adipokines [56]. In 1993, Hotamisligil and Spiegelman were the first to establish a relation between inflammation and adipose tissue. They found an interrelation between obesity and the increase of TNFα levels [10]. Nowadays, adipose tissue expansion is related with an increase of another inflammatory cytokine such as CCL2. CCL2 is upregulated during obesity and it is supposed that this chemokine could play a determinant role in monocyte recruitment during over-

intake conditions and insulin resistance [49,57–59]. In fact, some researchers suggest that the increase of inflammatory monocyte recruitment could increase the risk to develop type 2 diabetes mellitus and insulin resistance [60].

In physiological conditions, insulin induces the activation of insulin receptor substrate (IRS) in cells. This interaction causes the activation of IRS downstream signaling. Under normal conditions, this process could be regulated through feedback mechanisms, which ensure that metabolic homeostasis is maintained. In inflammatory conditions, the interaction between insulin and insulin receptor could be interrupted. In consequence, the activation of IRS and its downstream signaling cannot be carried out. This is the first step in the development of insulin resistance, hyperglycemia and hyperinsulinemia [60,61].

Insulin signaling pathway regulates the metabolism of carbohydrates, lipids and proteins though the activation of components such as phosphatidylinositol 3 kinase (PI3K) and protein kinase B (AKT). Thus, insulin resistance can induce overwhelming consequences in cell homeostasis.

From a functional point of view, the relation between inflammation and insulin resistance is associated with c-Jun N-terminal kinases (JNK) and IκB kinases (IKK) activation. Both kinases are stimulated by inflammatory components and are overexpressed in obesity. It has been shown that JNK and IKK activation cause serine phosphorylation in IRS-1, which attenuates the IRS-1 downstream insulin signaling pathway. Moreover, its inhibition may have beneficial effects for the treatment of insulin resistance [60,61].

To sum up, even though the role of inflammation in insulin resistance is still poorly understood, the use of anti-inflammatory strategies may be a successful alternative for the treatment of insulin resistance. The recruitment and regulation of inflammatory monocytes and macrophages through the use of CCL2 or CCR2 antagonists can be a therapeutic strategy in the regulation of glucose concentration and insulin resistance.

2.2.3.2 Chemokine (C-C motif) ligand 2 and Oxidative Stress

Oxidative stress is an imbalance between free radicals or reactive oxygen species (ROS) production and antioxidants defenses [62]. Free radicals are molecules with unpaired electrons which have a high reactive capacity. Consequently, these molecules can quickly induce alterations in nearby components.

Moreover, ROS are highly reactive molecules, which can have unpaired electrons or oxygen-based radicals. ROS include superoxide (O^{2-}), hydrogen peroxide (H_2O_2), hydroxyl radical (OH^-), nitric oxide (NO), hypochlorite (ClO^-) and peroxynitrite (ONOO-). Low concentrations of these components are necessary for cell survival. However, in pathologies such as obesity, diabetes, cardiovascular alterations and hyperlipemia there is an overproduction of free radical and ROS. High concentrations of these components can induce modifications in proteins, carbohydrate, lipids and DNA. All these alterations can compromise cell survival [62,63].

In physiological conditions, ROS and free radicals are generated either from extracellular sources of oxygen by the action of NADPH oxidase (NOX) or from the mitochondrial respiratory chain. However, in adverse conditions, several factors could contribute to ROS and free radicals overproduction including hyperglycemia, an increase in muscle activity, and high levels of lipids, endothelial ROS and chronic inflammation [64–66].

To counteract these hostile conditions, the organism possesses several antioxidant enzymes. The most important are: superoxide dismutase, glutathione peroxidase, catalase and paraoxonase 1 (PON1).

- Superoxide dismutase has two isoforms, copper-zinc (CuZn-SOD) and manganese (Mn-SOD). CuZn is associated with cytosol, whereas Mn-SOD is associated with mitochondria. Both isoforms convert superoxide (O2-) in hydrogen peroxide (H2O2) [67].

- Glutathione peroxidase is able to reduce hydrogen peroxide (H_2O_2) using reduced glutathione (GSH) as an electron donor by generating glutathione disulphide (GSSG) and water (H_2O) [68,69].

- Catalase reduces H_2O_2 into oxygen and water without any endogenous reducing agents [62]. It is located in liver, erythrocytes and kidneys.
- Paraoxonase-1 is an enzyme linked to high density lipoproteins (HDL) and protects low-density lipoproteins (LDL) against oxidation. This enzyme has paraoxonase, lactonase and arylesterase activities. PON1 belongs to the paraoxonase family, which is composed by three enzymes with high structural homology: PON1, PON2 and PON3. All three PON enzymes degrade lipid peroxides in LDL and HDL [70]. The main difference between these enzymes remains in their localization in the organism. PON1 and PON3 are mainly expressed in the kidney and liver and are localized in the circulation bounded to HDL particles. Conversely, PON2 is an intracellular enzyme not found in the circulation, which reduces intracellular oxidative stress and decreases apoptosis [71].

Several studies demonstrated that the imbalance between antioxidant enzymes and pro-oxidant components can potentially increase the inflammatory response. This chronic inflammation may elevate ROS levels, generating a vicious cycle which may alter cell survival.

The link between oxidative stress and inflammation can be found at different levels. For instance, in cancer, the increase of inflammatory cells stimulates ROS production which promotes tumor development through the increase of DNA damage [72]. Moreover, neutrophils and macrophages can produce O_2, H_2O_2, OH^-, ONOO- contributing to the increase of ROS damage [62]. On the other hand, inflammatory cells also produce soluble mediators such as cytokines and chemokines, which induce the recruitment of inflammatory cells and the production of more reactive species. These chemokines activate signal transduction pathways and cause changes in transcription factors, such as nuclear factor κB (NF-κB), signal transducer and activator of transcription 3 (STAT3), hypoxia-inducible factor-1α (HIF-1α), activator protein-1 (AP-1), nuclear factor of activated T cells, and NF-E2 related factor-2 (Nrf2), which mediate the cellular stress responses. This sustained inflammatory/oxidative microenvironment can damage the neighboring cells and compromise cellular survival at a systemic level [72].

Collectively, inflammation and oxidative stress conditions are a systemic problem. Thus, stopping the vicious cycle of oxidation/inflammation can be a clinical target for the progression of many

diseases. CCL2 or its receptor (CCR2) can be a therapeutic target for its implication in immune cell recruitment and inflammatory processes.

2.2.3.3 Chemokine (C-C motif) ligand 2 and Non-alcoholic Fatty Liver Disease

NAFLD is one of the most prevalent liver pathologies worldwide. Nowadays, this pathology is considered to be the hepatic manifestation of metabolic syndrome [73]. NAFLD is characterized by the presence of significant amount of lipid accumulation in the liver in the absence of excessive alcohol consumption.

These hepatic fatty depots result in a wide histological spectrum of liver damage ranging from simple steatosis to non-alcoholic steatohepatitis (NASH), fibrosis, cirrhosis, and hepatocellular carcinoma and liver failure [73–75] (Figure 7). NAFLD is related to visceral obesity, insulin resistance, dyslipidemia and hypertension. Nevertheless, the molecular mechanisms of generation and development of this disorder are not completely understood. However, alterations in free fatty acid metabolism due to an inappropriate diet seem to play a fundamental role [76–79].

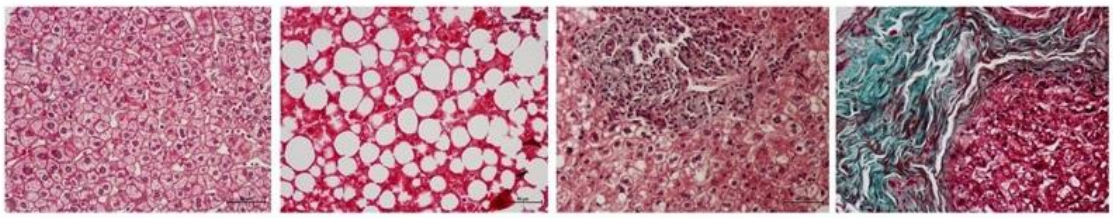

Figure 7: Nonalcoholic fatty liver disease progression. From left simple steatosis, steatosis, non-alcoholic steatohepatitis, fibrosis.

The most accepted theory, which explains the development and pathogenesis of NAFLD, is based on successive processes. Briefly, the first step of NAFLD development is simple steatosis. This condition is caused by an increase in the uptake and synthesis of fatty acids and a decrease in their oxidation or secretion [80]. This disequilibrium is observed in pathologies such as obesity or hyperinsulinemia, pathologies in which insulin resistance is a determinant factor. It has been demonstrated that insulin resistance increases the hepatic *de novo* lipogenesis and impairs the inhibition of adipose tissue lipolysis. Consequently, insulin resistance causes adipose tissue hypertrophy, which compromises the adipocytes ability to store fat, resulting in an increase of free fatty acids into the

circulation. Free fatty acids are then misrouted from their primary storage site to ectopic sites like skeletal muscle or liver.

In the liver, this unusual lipid accumulation causes lipotoxicity, and a recruitment of inflammatory mediators such as cytokines, chemokines and adipokines, which results in important hepatic alterations like chronic inflammation, mitochondrial dysfunction and fibrosis [75].

Mitochondrial dysfunction causes oxidative stress due to a deregulation of the antioxidant capacity, resulting in an excessive production of ROS and, then, hepatocyte death. This process is characterized by an increase in pro-inflammatory cells, mainly macrophages. In this situation, resident macrophages (Kupffer cells) and recruited macrophages are responsible to produce inflammatory mediators that could maintain the inflammatory state and ROS production [79].

Chronic inflammation and ROS overproduction cause stellate cells activation. Stellate cells produce collagen, which results in liver fibrosis and an increase of chemoattractant chemokines. Overproduction of chemokines promotes a vicious cycle of inflammation and fibrosis that can trigger liver failure.

Several studies correlated the CCL2 overexpression with NAFLD progression and development [75,81,82]. Along the same line of study, some investigators have demonstrated that the inactivation of CCL2 or its receptor (CCR2) reduces hepatic steatosis, NASH progression and insulin resistance [83]. Although the mechanisms are not well-known yet, CCL2/CCR2 axis could be a therapeutic target in NAFLD progression [84].

2.2.3.4 Chemokine (C-C motif) ligand 2 and aging

Aging is a biological phenomenon characterized by the loss of cellular functions caused by the progressive functional decline of the organism [85,86]. In consequence, aging has been associated with the development and progression of diseases such as cancer, diabetes, cardiovascular disorders, and neurodegenerative diseases. For these reasons, understanding the causes and mechanisms that control aging has been a field of great interest [85].

Aging may arise from multiple causes: genomic instability, telomere shortening, epigenetic alterations, loss of proteostasis, deregulated nutrient sensing, mitochondrial dysfunction, cellular senescence, stem cell exhaustion and chronic inflammation or "*Inflammaging"* [87]. This latter has aroused the interest of many researchers because epidemiology studies associated chronic inflammatory conditions with an increase of co-morbidities relate to aging such as Alzheimer's disease, atherosclerosis, macular degeneration and degenerative arthritis among others [86,88].

Chronic inflammation may be produced from multiple causes. Mainly, inflammation causes an increase of leukocyte infiltration, which can promote structural alterations and cellular damage. Consequently, these alterations induce the overproduction of cytokines, like CCL2, that amplify or modulate the inflammatory response. In physiological conditions, all these processes generate tissue repairments. However, during aging, all these processes result in a chronic low-grade inflammation, with the aim to repair damaged tissue. When these situations exceed a threshold often induce the detriment of normal tissue function [89,90].

On the other hand, it has been shown that chronic inflammation also might be due to cellular senescence. Cellular senescence is a physiological state in which cells cannot divide. This process is a consequence of metabolic adaptation in response to damage and stress. Senescent cells can produce pro-inflammatory cytokines (the senescence associated secretory phenotype or SASP), which have the capacity to modify tissue microenvironment and induce permanent inflammation [89–91]. This may aggravate this aging phenotype at a systemic level because inflammatory cytokines can induce senescence in other cells [92]. Nowadays, many researches are trying to find an inflammatory molecule that can measure the i*nflammaging*. In many studies, an association between CCL2 levels and aging has been demonstrated. CCL2 is considered to be a marker of

chronic inflammation because it is a SASP and can promote secondary senescence in healthy cells [93–97]. Several studies suggest that SASP can propagate the *inflammaging* from cell to cell via cell interactions and promote the inflammatory pathway activation in host cells [98]. Thus, CCL2 can be a therapeutic target in *inflammaging* progression and aging associate pathologies.

2.2.3.4.1 Hutchinson-Gilford progeria syndrome

Hutchinson-Gilford Progeria Syndrome (HGPS) or progeria syndrome is a premature aging disorder, which affects 1 in 4 million newborns worldwide. HGPS was first described by Jonas Hutchinson and Hastings Gilford in 1886 and 1897 respectively [99]. The study of HGPS has opened a new perspective about aging diseases and their several comorbidities. It is characterized by the early development of multiple biological alterations and aging-associated symptoms, including a lack of subcutaneous fat, alopecia, muscle weakness, osteoporosis, growth impairment, sclerotic skin, hair loss, joint contractures and progressive cardiovascular disease. All these conditions induce the death due to heart attacks and strokes in childhood (14.6 years old) mainly from myocardial infarction [100,101].

Genetically, this syndrome is produced by a mutation in the exon 11 of the LMNA gene, which encodes for lamin A and C, being both components of the nuclear envelope [99,102,103]. Normally, lamin A is produced via post-translational modifications of prelamin A, which includes different steps: Firstly, the farnesyltransferase farnesylates the cysteine residue at the C-terminal cysteine-serine-isoleucine-methionine motif. Then, three C-terminal amino acids are removed, enabling methylation of the new C-terminus by isoprenylcysteine carboxyl methyltransferase. Subsequently, the enzyme ZMPSTE24/FACE endoprotease removes the 15 C-terminal tripeptides, which includes the farnesylated and carboxymethylated cysteine [104,105] (Figure 8). Afterwards, mature Lamin A is incorporated into the nuclear lamina.

In contrast, HGPS patients present a mutant prelamin A isoform with a lack of 50 amino acids. In consequence, the cleavage site of the enzyme ZMPSTE24 /FACE does not exist, resulting in the accumulation of permanently farnesylate and uncleaved lamin A isoform named progerin [99,102,106].

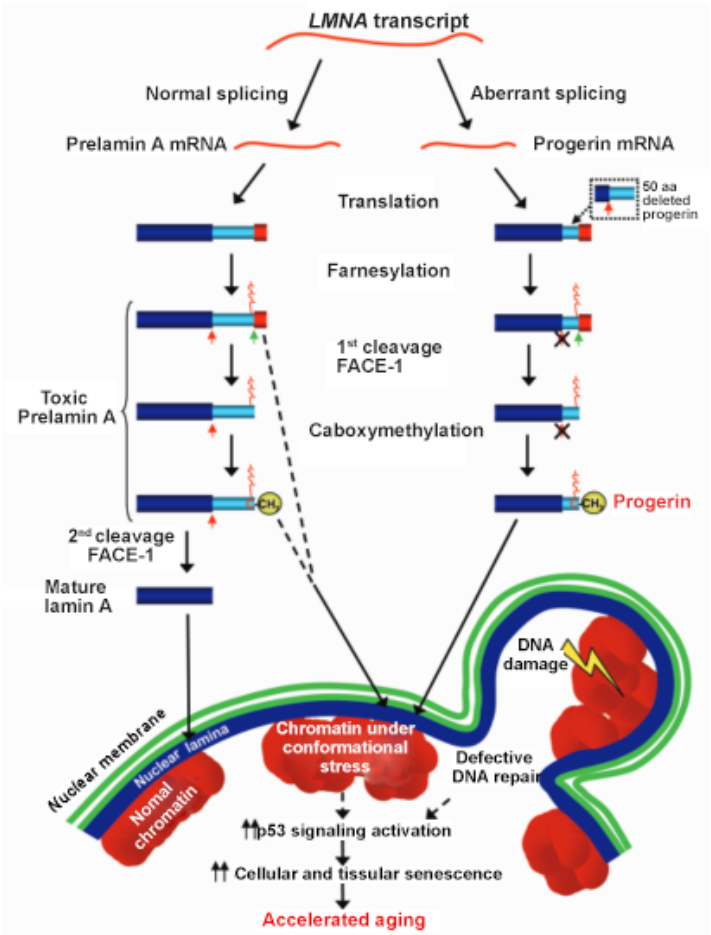

Figure 8. Molecular mechanisms underlying immature Lamin A induced progeria. In wild type mice LMNA locus produce prelamin A mRNA. HGPS induce the deletion of 50 aminoacids from exon 11 yields the aberrant progerin mRNA. Prelamin A undergoes three additional post-translational modifications for the production of producing mature lamin A. HGPS cannot complete lamin A maturation, accumulating toxic prelamin A. Both farnesylated progerin and prelamin A assemble in the nuclear lamina, altering the stability of the nuclear envelope and causing conformational chromatin stress, as well as defective recruitment of DNA repair factors. Accumulated DNA damage and altered chromatin would activate a p53-signaling pathway, inducing cell and tissue senescence and eventually leading to accelerated aging. Figure extracted from Cadiñanos *et al* 2005 [107].

Lamin A is an important part of the nucleus structure; thus, one of the most important consequences of progerin accumulation are the dramatic changes in nuclear morphology, and alterations in of cellular functions, including DNA replication and repair, chromatin organization, signal transduction and gene transcription [108][99,101]. Nuclear morphology alterations induce an increase in the stiffness of the cells and, consequently, affect the response against mechanical stress in the vasculature, bones and joints [99]. However, the most severe medical problems for progeria syndrome patients are the cardiovascular alterations.

Although these patients do not show alterations in LDL, HDL, cholesterol levels, triglycerides and C-reactive protein, they are susceptible to develop cardiovascular diseases. For instance, it has been demonstrated that these patients have suffered heart failure, left ventricular diastolic dysfunction, ventricular hypertrophy, cardiac fibrosis, heart valve dysfunction, intima-media thickening, vascular fibrosis, arteriosclerosis and hypertension [108,109]. All these vascular alterations are closely related to aging development and progression [106].

Moreover, it has been demonstrated that progerin accumulation induces nuclear envelope abnormalities, hyperactivation of p53 signaling pathway due to nuclear DNA damage, cellular senescence, stem cell dysfunction and the development of progeroid-like phenotype [107].

Thus, the development of animal models with this genetic syndrome can provide an experimental and useful framework to investigate the basis of aging associated pathologies and assess a therapeutic strategy against these alterations. There are many different animal models to study progeria syndrome and to explore the mechanisms that regulate this pathology. However, *Zmpste24* null (*Zmpste24*$^{-/-}$*)* and *LMNA*^{G609G} have similar characteristics and are closely related to progeria syndrome [102,105,110,111].

Zmpste24$^{-/-}$ was the first mice model of HGPS. These mice do not have *Zmpste24 enzyme but* show all metabolic characteristics of progeria syndrome: progerin accumulation, hyperactivation of p53 pathway, cellular senescence, cell dysfunction, defective DNA repair and progeroid like phenotype [112*]. LMNA*^{G609G} has genetic similarity with HGPS, although it presents the same physical and biochemical phenotype as *Zmpste24*$^{-/-}$ [113].

Both animal models have led to a better understanding of premature aging disorders and their clinical and metabolic manifestations. Consequently, these mice allow the study of all hallmarks and molecular processes associated to aging and could also contribute to the development of a suitable therapeutic approach for progeria syndrome and aging [112].

2.2.3.5 Chemokine (C-C motif) ligand 2 and Mitochondrial Dysfunction

Mitochondria are an essential components of eukaryote cells which control several important biological processes such as adenosine triphosphate (ATP) synthesis, central carbon metabolism, regulation of calcium ions homeostasis, generation of ROS, activation of apoptosis and maintenance of intracellular redox potential [114]. All of them are necessary process for the cell to survive.

Metabolic imbalance of nutrient signal input, energy production and/or oxidative respiration results in mitochondrial dysfunction. Mitochondrial dysfunction is defined as the incapacity of mitochondria to generate and sustain enough ATP levels. Thus, mitochondrial dysfunction causes dramatic alterations in cell homeostasis and consequently in the entire organism [115]. It has been demonstrated that mitochondrial dysfunction contributes to many common disorders such as, diabetes, NAFLD, cardiovascular disease or obesity. These pathologies are characterized by aberrant ROS production, a defective mitochondrial biogenesis, disruption in mitochondrial dynamics, inappropriate apoptosis regulation, an inefficient ATP production, alteration in mitochondrial signaling pathways, and overproduction of different inflammatory cytokines as CCL2 and cell failure [116,117].

Fortunately, in physiological conditions, mitochondria have the plasticity to adapt its structure and functionality according to cell energetic requirements (Figure 9) through a process denominated as mitochondrial dynamics. Mitochondrial dynamics is a general term that comprises the process of fission and fusion, mitochondrial trafficking and mitophagy [117,118]. This process is considered to be the quality control of mitochondrial functionality. Fusion promotes mitochondrial interconnection, which contributes to energy dissipation and rapid provision. Fusion optimizes mitochondrial function and plays a beneficial role in the maintenance of long-term starvation through ATP synthesis maximization. In contrast, mitochondrial fission promotes segregation of mitochondrial damage and facilitates its elimination by mitophagy [119].

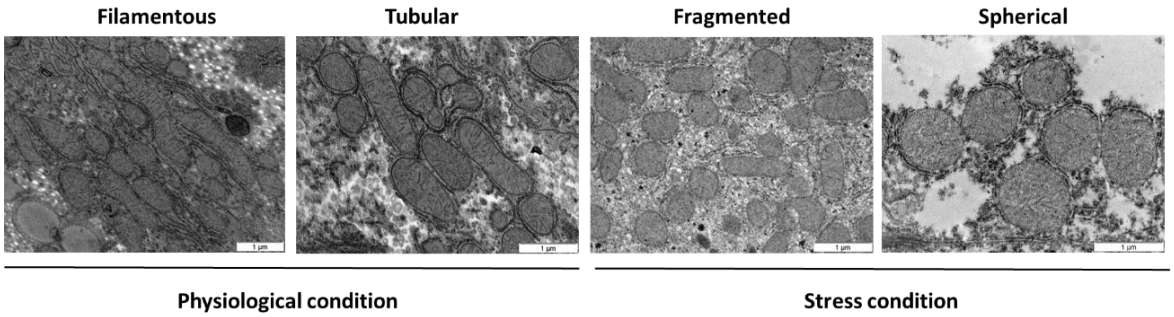

Figure 9: Net mitochondrial morphology. Physiological conditions are represented with filamentous and tubular mitochondrial. Stress conditions are represented with fragmented and spherical mitochondrial.

Mitophagy is a selective kind of autophagy (described later in point 3.2), which helps in the degradation of impaired mitochondria. The different processes that control mitophagy and mitochondrial dynamics are not clearly understood. However, some research relates these processes with the action of proteins such as dynamin relate protein (Drp1), mitofusin 1 (Mfn1), mitofusin 2 (Mfn2) or optic atrophy protein 1 (OPA1) [120,121].

At a structural level, mitochondrial fusion is controlled by Mfn1 and Mfn2, both GTPases and OPA1. This process requires the fusion of outer and inner membranes which gives the mitochondria an elongated structure (Figure 9 and Figure 10). Mfn1 and Mfn2 are involved in the outer membrane fusion process and OPA1 mediate the inner membrane fusion.

Fusion is closely related to membrane potential and oxidative phosphorylation (OXPHOS) system. Thus, alterations in mitochondrial fusion result in variations in the membrane potential and differences in ATP synthesis.

During the fusion, two mitochondria approach to each other. Then, Mfn1 form an intramolecular coiled coil that may link mitochondria. This interconnection is the first step for membrane fusion and initiates the lipid bilayer mixing and the outer membrane fusion. Subsequently, inner membranes are mixed by the interaction of OPA1. Fusion process enhances the mitochondrial capacity and maintain genetic and biochemical homogeneity.

Mitochondrial fission is executed by Drp1, which is a cytosolic protein activated by oxidative stress, bacterial infection or inflammation. As described above, fission is a division process that produces one or more mitochondria. Mitochondria division occurs in contact to endoplasmic reticle. For this, Drp1 needs to interact with four mitochondrial localized adaptors: mitochondrial fission factor (MFF), mitochondrial dynamics proteins (MiD49 and MiD51) and fission 1 (FIS1). Unlike fusion process, fission is inhibited by an increase in OXPHOS [122].

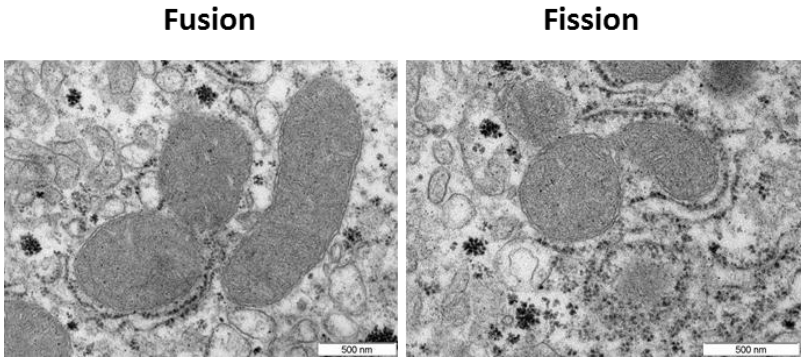

Figure 10: Mitochondrial dynamic. Left: mitochondrial fusion. Right: mitochondrial fission

Thus, modifications in mitochondrial dynamics can induce important metabolic alterations. Therefore, mitochondrial defects have been accepted as key features in energy metabolism disturbances. For this reason, new therapeutic strategies for metabolic alterations are focused on the regulation of mitochondrial function and biogenesis [6,114].

3 Energy metabolism

Energy metabolism is the process by with the organism generates ATP through the breakdown of nutrients such as carbohydrates, proteins and fats. This process is the main energy production and takes place in the mitochondria through the OXPHOS complexes [123].

In general, the main substrate for energy metabolism is glucose, which is metabolized in three steps: glycolysis, tricarboxylic (or citric) acid cycle (TCA or CAC) and finally OXPHOS (Figure 11). Briefly, one molecule of glucose is converted into two molecules of pyruvate through a sequence of steps. In the first step, glucose is phosphorylated by hexokinase generating glucose-6-phosphate. This process prevents the escape of glucose from the cell. Subsequently, glucose-6-phosphate is converted to fructose-6-phosphate by glucose-6-phosphate isomerase. This isomerization allows fructose-6-phosphate phosphorylation generating fructose-1.6-bisphosphate.

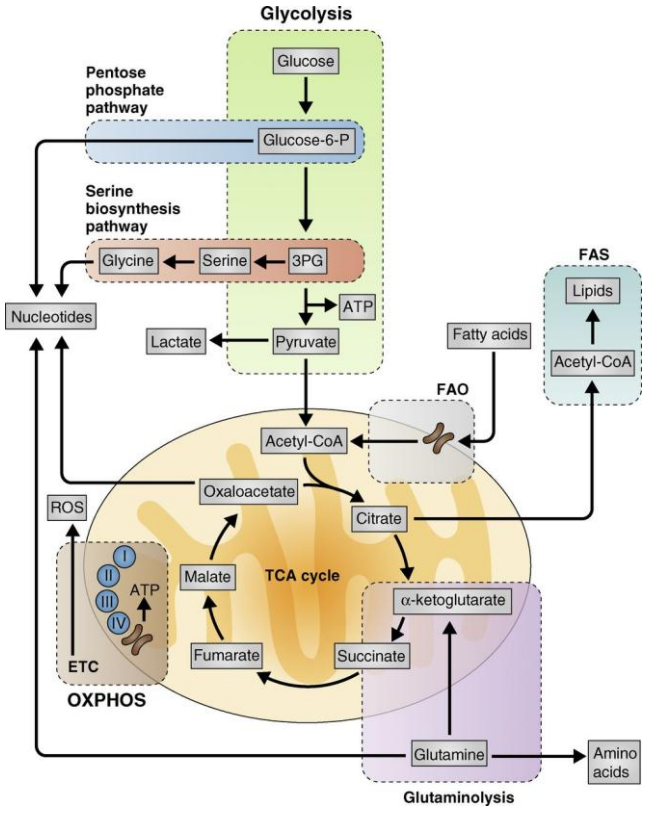

Figure 11: Schematic representation of energy metabolism. Energy metabolism is the process by with the organism generates ATP through the breakdown of nutrients such as carbohydrates, proteins and fats. ATP is the molecular currency of energy in the cell. The first of these, glycolysis, involves the enzymatic breakdown of glucose to pyruvate in the cytoplasm. The TCA cycle encompasses the second pathway, where pyruvate is converted to acetyl-CoA in the mitochondria and shuttled through several enzymatic reactions to generate reducing equivalents to fuel OXPHOS. Other substrates can also be metabolized in the TCA cycle, such as glutamine via glutaminolysis or fatty acids via β-oxidation (FAO). These connected biochemical pathways can also provide metabolic precursors for biosynthesis. Figure extracted from Bruck *et al* 2015 [124] .

The next step induces the split of fructose-1.6-bisphosphate into dihydroxyacetone phosphate and glyceraldehyde-3-phosphate. The last phase of glycolysis includes the subsequently transformation of glyceraldehyde-3-phosphate into 3 phosphoglycerate, phosphoenolpyruvate and pyruvate. Then, in aerobic conditions pyruvate is converted to acetyl coenzyme A (Acetyl-CoA) which enters the TCA cycle though the pyruvate dehydrogenase complex. In anaerobic conditions, pyruvate is used for lactate synthesis [8].

In CAC cycle, Acetyl-CoA is completely oxidized into three molecules of CO2. For this is necessary sequences of metabolic reaction, which providing energy for the respiratory chain or OXPHOS complex and the reduction of cofactors as nicotinamide adenine dinucleotide (NAD^+) and flavin adenine nucleotide (FAD^{2+}). The first phase of CAC is the condensation of Acetyl-CoA and oxaloacetate to generate citrate, which is regulated by the enzyme citrate synthase. Next, citrate is converted to cis-aconitate and then to isocitrate being both processes regulated by aconitase. The isocitrate generated is converted to α-ketoglutarate by isocitrate dehydrogenase. In this step is reduced form of nicotinamide adenine dinucleotide (NADH2) from NAD^+, which will be subsequently used in OXPHOS complex. α-ketoglutarate is decarboxylated by the α-ketoglutarate dehydrogenase complex and is converted to succinyl-CoA. Succinyl-CoA is converted to succinate, which in turn is oxidized to fumarate by succinate dehydrogenase. This reaction is produced in the inner mitochondrial membrane and involves the reduction of FAD^{2+} to FADH2, which provides electrons for the respiratory chain. Next, fumarate is hydrated by fumarate hydratase generating L-malate, which is oxidized to oxaloacetate by L-malate dehydrogenase. In this reaction another NADH is produced [8,125].

During all of CAC cycle, one molecule of ATP, three molecules of NADH and one of $FADH_2$ is produced. NADH and $FADH_2$, will be used in the respiratory chain for the ATP production. These processes take place in the mitochondria.

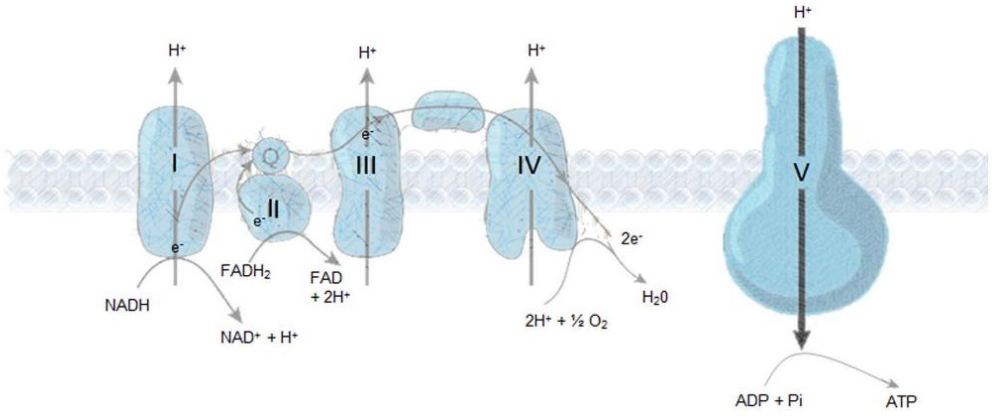

Figure 12: Respiratory chain system in mammalian mitochondria. Complex I or NADH/ubiquinone oxidoreductase; complex II or succinate dehydrogenase, complex III or cytochrome C reductase, complex IV or cytochrome C oxidase, complex V or ATPase.

Respiratory chain is a system of four complexes that are involved in electron transfer in aerobic conditions. The main function of the respiratory chain the regulation of electron and proton transport which aims to generate ATP. This system is composed by five complexes and two electron carriers (Figure 12). Complex I or NADH/ubiquinone oxidoreductase is the first complex. Its activation takes place by the electrons from NADH produced in CAC. Complex II or succinate dehydrogenase is the second source of electrons, which conducts the electrons from $FADH_2$ provided during succinate oxidation to ubiquinone. The ubiquinone reduction causes the pass of electrons to the cytochrome C reductase or complex III and subsequently to complex IV or cytochrome C oxidase. The latter is responsible of oxygen reduction to water [126].
The mitochondrial membrane potential is generated by the respiratory chain. Its complexes actives ATPase, which is the last step for the ATP synthesis [5,127].

All these processes are regulated according to the energetic needs of the cell. High AMP/ATP ratio induces the activation of different metabolic signaling pathways induce the activation of all described steps. For this reason, these molecules are considered cell energy sensors [128].

3.1 PI3K/AKT/mTOR pathway

The PI3K/AKT/mTOR signaling pathway has a central role in the prevention of aberrant cellular proliferation and in the maintenance of glucose homeostasis. PI3K/AKT/mTOR signaling pathway is responsible to ensure that cells do not grow under conditions of energy stress or nutrient starvation. Thus, if this pathway is perturbed, it contributes to the development of different human diseases such as cancer, immunological and neurological disorders, diabetes, localized tissue overgrowth and cardiovascular disease. PI3K/AKT/mTOR signaling pathway participates in a broad range of cellular regulatory processes, including cell growth, proliferation and metabolism (Figure 13) [129–132]. For this reason, PI3K/AKT/mTOR pathway is a potential target for the clinical treatment of numerous metabolic diseases [133–135].

As shown in figure 13, PI3K/AKT/mTOR pathway begins when growth factors such as insulin-like growth factor, platelet-derived growth factor or other components as mitogens, hormones, or nutrients activate PI3K. Structurally, PI3K is composed by a catalytic subunit (p110) and three regulatory subunits (p85, p55, or p50). PI3K activation induces the phosphorylation of PIP2, which generates phosphatidylinositol triphosphate (PIP3). In turn, PIP3 induces the phosphorylation of AKT1, which can be phosphorylated at threonine 308 and serine 473 (Ser473). AKT1 activated form induces the inactivation of the tuberous sclerosis complex (TSC), which is composed by TSC1 and TSC2. This inactivation of TSC induces the activation of mTOR [136,137].

mTOR is a serine/threonine protein kinase which is evolutionarily conserved in humans. It is one of the most important energy sensors and is ubiquitously expressed. Several studies have revealed a broad spectrum of functions for this molecule, including cell cycle progression, cell proliferation, angiogenesis, and apoptosis [132,138,139].

Structurally, mTOR generates 2 functionally and structurally distinct complexes: mTORC1 (mTOR complex 1) and mTORC2 (mTOR complex 2). mTORC1 is compose by mTOR kinase, regulatory associated protein of mTOR (raptor), and mLST8 (also known as GβL). mTORC1 is primarily responsible for nutrient and growth factor signal sensing. In contrast, mTORC2 consists of three subunits that include mTOR kinase, mLST8 and rapamycin-insensitive companion (Rictor). Unlike mTORC1, mTORC2 function is not well understood yet [140,141].

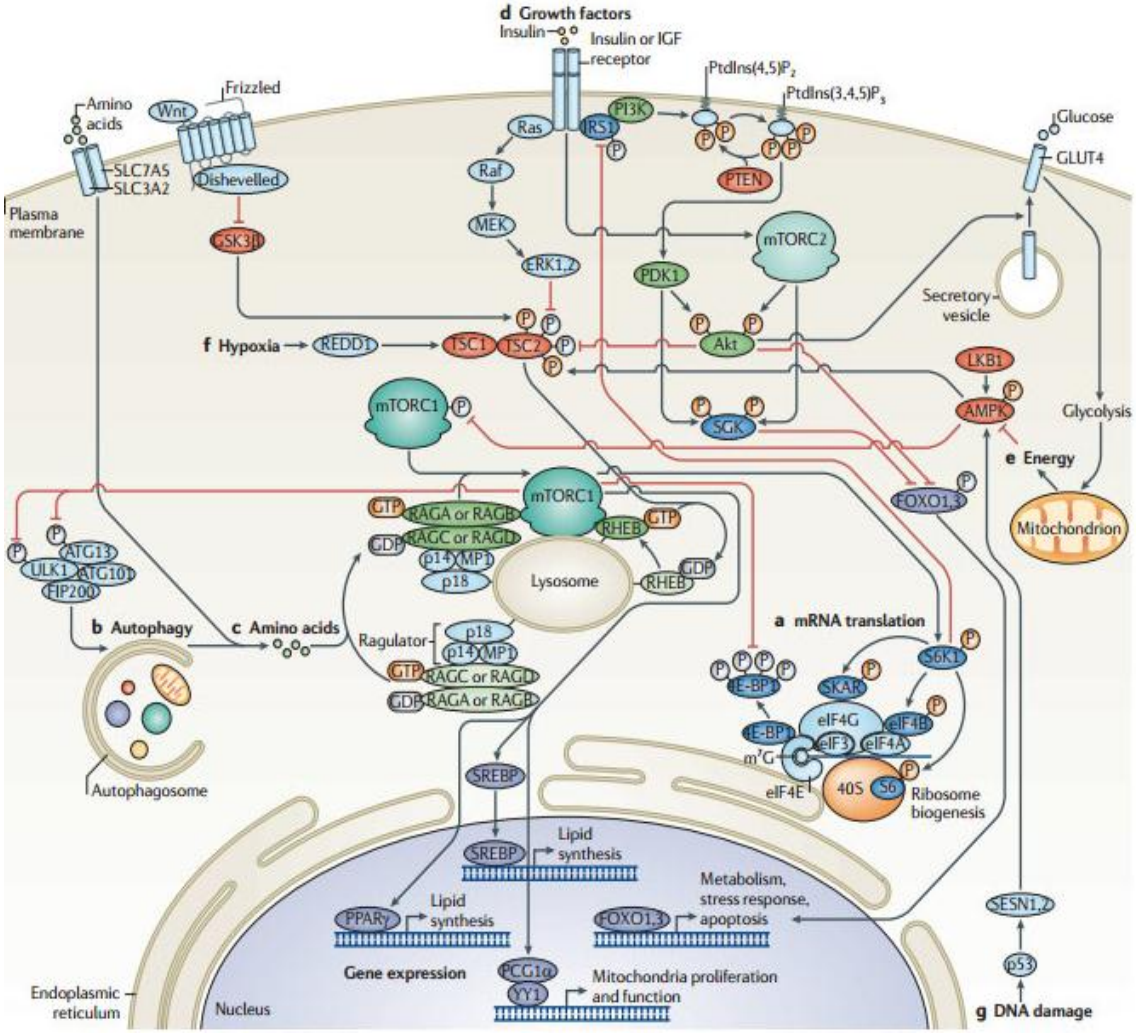

Figure 13: PI3K/AKT/mTOR signaling pathway. PI3K/AKT/mTORC1 signaling pathway is one of the detachable pathways involved in the cell homeostasis. The most detachable acronyms used were: eukaryotic translation initiation factor 4E-binding protein 1 (4EBP1); protein kinase B (AKT); AMP-activated protein kinase (AMPK), G protein beta subunit-like (GβL), mammalian target of rapamycin complex 1 and mammalian target of rapamycin complex 2 (mTORC1/mTORC2 respectively); ribosomal protein S6 kinase beta-1 (p70S6K); phosphatidylinositol bisphosphate (PIP2); phosphatidylinositol triphosphate (PIP3); regulatory associated protein of mTOR (Raptor); rapamycin-insensitive companion of mTOR (Rictor); tuberous sclerosis complex 1 and T tuberous sclerosis complex 2 (TSC1/TSC2 respectively); phosphoinositide 3-kinases (PI3K). Figure extracted from Sabatini *et al* 2011 [141].

Another key component in the maintenance of energy homeostasis is AMP-activated protein kinase (AMPK). AMPK is a heterodimeric serine/threonine kinase shaped by three subunits: two regulatory (β and γ) and one catalytic (α). Unlike mTOR, AMPK is active when AMP/ATP ratio increases. For instance, during metabolic stress induced by low nutrient intake or prolonged exercise.

AMPK is activated by the phosphorylation of the subunit α at threonine 172 and its activation leads to an increase in ATP production pathways [142]. AMPK phosphorylation is controlled by the liver kinase B1 (LKB1) and calmodulin-dependent protein kinase IIβ (CaMKKIIβ) [143]. Nonetheless, AMPK has a close relationship with mTORC1; AMPK induces the direct phosphorylation of TSC2, and consequently mTORC1 inhibition [143].

3.2 Autophagy

Autophagy is one of the most powerful systems for cellular clean-up, which is responsible for the degradation of all type of macromolecules (proteins, lipids, nucleic acids and sugars), organelles or any type of abnormality caused by extra or intracellular components. All these components can be recycled to generate new molecules or for ATP synthesis under starving conditions. Even though starvation is one of the most important triggers of the autophagy process, it can be affected by different diseases such as NAFLD, hepatocellular carcinoma, viral infections or sarcopenia [144,145]. The study of this process has shown that three types of autophagy can co-exist: macroautophagy, microautophagy and chaperone-mediated autophagy (CMA) [146,147]. All of them are mechanistically different.

In macroautophagy, the cytosolic materials are sequestered inside double-membrane vesicles (autophagosomes) and delivered into lysosomes for their degradation (Figure 14). The main steps are induction or initiation, nucleation, membrane elongation, enclosure and, finally, the fusion with the lysosome.

Several proteins are involved in this recycling pathway, but the most characterized are autophagy related proteins (ATG). These proteins are responsible for the development of the different parts of the autophagosome formation. The activation of Unc-51 like kinase 1 complex (ULK1 or ATG1) is the first step for the macroautophagy. The activity of these complexes is controlled by mTORC1 and

AMPK. In starvation, mTORC1 is inactivated and in consequence ULK1 promotes the activation of class III PI3K nucleation complex and the PI3P binding complex, which induces the activation of membrane insolation. Subsequently, ATG12-ATG5 and microtubule-associated protein 1A/1B-light chain 3 (LC3) conjugation systems are engaged to isolation membrane, which enables the elongation and closure of autophagosome. The final step in macroautophagy is the fusion of autophagosome with the lysosome, which induces the cargo degradation and recycling of breakdown components. The cargo recognition and recruitment to the autophagosome is regulated by various autophagy receptors. One of them is p62 or Sequestosome-1 which recognizes the different proteins and organelles targeted for degradation [148–150].

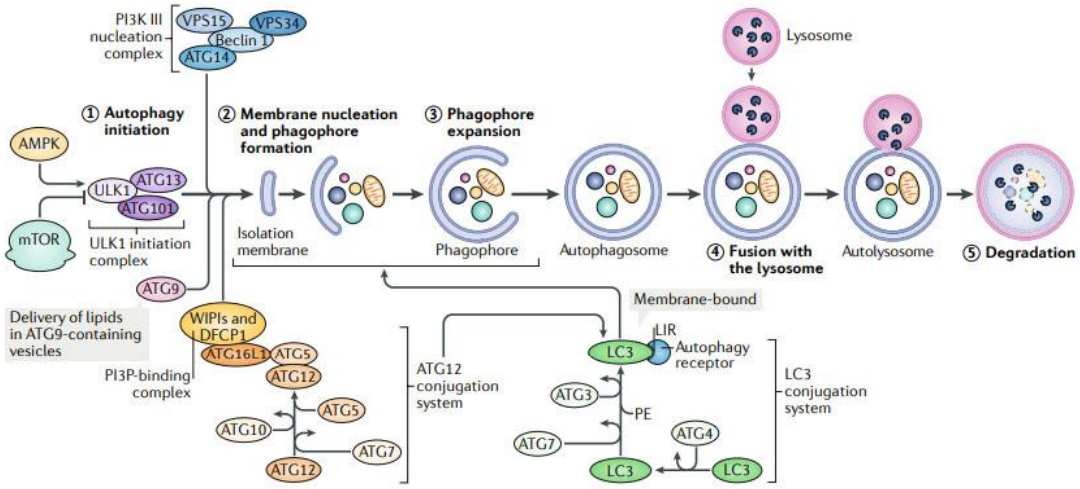

Figure 14: Macroautophagy pathway. Acronyms used were: AMP-activated protein kinase, AMPK; mammalian target of rapamycin complex (mTOR); phosphoinositide 3-kinases (PI3K); Unc-51 like kinase 1 complex (ULK1 or ATG1); autophagy relate protein (ATG), microtubule-associated protein 1A/1B-light chain 3, (LC3); phosphatidylinositol-3-phosphate (PI3P). Figure extracted from Hansen *et al* 2018 [148]

The mechanisms that control microautophagy are completely different to macroautophagy. In microautophagy, cargo degradation is produced by invagination of lysosomal membrane, which induces the internalization of cytosolic material in lysosome for its degradation [148].

In CMA, the cargo is recognized in the cytosol by a chaperone that brings them to the lysosomes, where crosses the membrane through a translocation complex for its subsequent degradation. That is why CMA is considered to be a type of selective autophagy. However, this kind of autophagy only degrades proteins. Mechanistically, CMA substrates must contain a specific target motif, which is identified by a cytosolic chaperone (HSC70). Subsequently, the combination of chaperone and cargo is identified by a lysosome receptor. The most characterized receptor for the CMA is the lysosome associated membrane protein type 2A (LAMP-2A) [144,151,152].

Collectively, the three types of autophagy are cellular mechanisms designed to reach the homeostatic balance. Alterations in autophagy processes induce the accumulation of abnormal or dysfunctional material, which can compromise the cell survival. In this context, several diseases have been associated with impaired autophagy like neurodegenerative diseases, cancer, aging, inflammation, obesity and liver diseases [153,154]. For this reason, an improvement in the understanding of the autophagy regulation should provide substantial information for new therapeutic manipulations. In fact, all processes that modulate autophagy are not currently known. The regulation of macroautophagy, has been the most studied issue. As discussed above, regulation of macroautophagy occurs via mTORC1 and AMPK. mTORC1 leads to autophagy inhibition through the inactivation of ULK1 complex. In contrast, under starving conditions, nutrient depletion induces AMPK activation and, in consequence, mTORC1 is inhibited and macroautophagy is activated. For this reason, the uses of pharmacologic targets to manipulate autophagy are focused in mTORC1 antagonists and AMPK activators. For instance, it has been shown that rapamycin (which is the most available mTORC1 antagonist) or metformin (which is an AMPK activator) have a remarkable repercussion in autophagy [155–159]. Nevertheless, the search for drugs that modulate autophagy is a process that is strongly studied. For this, understanding how inflammation, overnutrition or metabolic alterations affect autophagy is essential.

4 *One carbon metabolism and DNA methylation*

One carbon metabolism (1-C) is a complex metabolic pathway, which provides carbon units that are used by different chemical reactions including cellular biosynthesis, regulation of redox potential and epigenetic status [160]. This cyclic process has three different pathways: folate cycle, methionine cycle and trans-sulphuration pathway, being the first two the most studied (Figure 15) [161].

The folate cycle starts with the folic acid acquired by the diet. Folic acid is reduced to dihydrofolate (DHF) using NADPH, which is reduced again to generate tetrahydrofolate (THF). These reactions allow the incorporation of the reduced folic acid to folate cycle. Once built into the cycle, THF can be used for synthetizing 5,10-methylene-THF, 5-methyl-THF, 10-formyl-THF and 5-formly THF. 5-methyl-THF is used for the homocysteine remethylation to generate methionine [162].

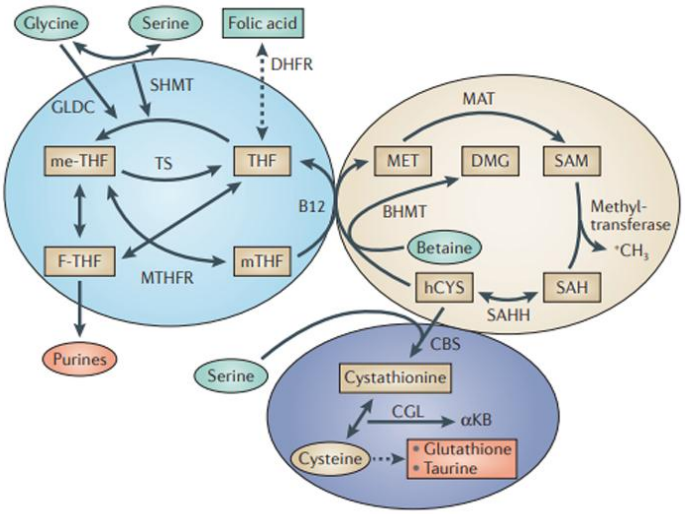

Figure 15: Schematic representation of 1-C metabolism. The folate cycle, the methionine cycle and trans-sulphuration pathway are different metabolic pathways that exist independently. The folate cycle and methionine cycle are the most detachable components of the one carbon. Betaine hydroxymethyltransferase (BHMT); Dihydrofolate reductase (DHFR); Dimethylglycine (DMG); Glycine decarboxylase (GLDC); Thymidylate synthase (TS); Tetrahydrofolate (THF); 5,10-methylene-THF (me-THF); 5-methyltetrahydrofolate (mTHF); methylenetetrahydrofolate reductase (MTHFR); 10-formyltetrahydrofolate (F-THF); Homocysteine (hCYS); Vitamin B12 (B12); cystathionine lyase (CGL); α-ketobutyrate (αKB). Figure extracted from Locasale *et al*2013 [160].

Homocysteine remethylation is the cornerstone of methionine cycle. This process has a great physiological importance because methionine allows the synthesis of S-adenosylmethionine (SAM). SAM is the methyl donor for DNA methylation, and when this takes place SAM is converted to S-adenosylhomocysteine (SAH). Alterations in methionine synthesis lead to changes in the ratio of SAM to SAH and may impact many methylation reactions, including DNA methylation.

DNA methylation is the transference of a methyl group to the 5th position of cytosine adjacent to guanines in CpG island [163], generating 5-methylcytosine (5mC) which is the epigenetic mark of DNA methylation. CpG islands could be hyper or hypomethylated, which results in an alteration on transcriptional regulation [164]. Hypermethylation is associated with gene suppression and in contrast, hypomethylation is associated with gene activation. The prevalence of hypermethylation or hypomethylation is linked to different metabolic alterations like obesity, diabetes or NAFLD.

DNA methylation is regulated by DNA methyltransferases (DNMTs) or DNA demethylases. There are three different DNMTs: DNMT1, DNMT3A, and DNMT3B. DNMT1 is the responsible for DNA stability and DNMT3A and DNMT3B are responsible for de novo DNA methylation [165]. The methyl group used in DNA and histone methylation comes from one carbon metabolism [166]. Thus, deregulation in one carbon metabolism induces an important alteration in the DNA methylation.

DNA demethylation is regulated by Ten-Elven translocation 1 (TET1), which oxidizes the 5mC residues to 5-hydroxymethylcytosine (5-hmC) and subsequently in 5-formylcytosine and 5-carboxylcytosine. The biological functions of all of these intermediate structures have not been elucidated yet but an increase in 5-hmC is considered to be an epigenetic mark for DNA demethylation [165].

UNIVERSITAT ROVIRA I VIRGILI
THE ROLE OF CHEMOKINE (C-C MOTIF) LIGAND 2 IN INFLAMMATION, OXIDATIVE STRESS, AGING AND METABOLISM
Fedra Nicaury Luciano Mateo

Hypothesis and aims

Hypothesi

UNIVERSITAT ROVIRA I VIRGILI
THE ROLE OF CHEMOKINE (C-C MOTIF) LIGAND 2 IN INFLAMMATION, OXIDATIVE STRESS, AGING AND METABOLISM
Fedra Nicaury Luciano Mateo

Hypothesis

C-C motif ligand 2 may play a determinant role in metabolic alterations through the regulation of signaling molecules involved in inflammation, oxidative stress and aging.

Aims

- To explore the effect of CCL2 ablation in the metabolism of mice with an important background of hyperlipidemia, hepatic steatosis and metabolic syndrome. Furthermore, we investigate whether that effect may be conditioned by diet.

- To determine the effects of a systemic CCL2 overexpression in the energy and 1-C metabolism of liver and muscle and to evaluate its implication in the regulation of metabolic reprogramming through the regulation of mTOR and AMPK signaling pathway.

- To evaluate the effect of CCL2 overexpression in an animal model of accelerated aging.

UNIVERSITAT ROVIRA I VIRGILI
THE ROLE OF CHEMOKINE (C-C MOTIF) LIGAND 2 IN INFLAMMATION, OXIDATIVE STRESS, AGING AND METABOLISM
Fedra Nicaury Luciano Mateo

Materials and methods

Materials

UNIVERSITAT ROVIRA I VIRGILI
THE ROLE OF CHEMOKINE (C-C MOTIF) LIGAND 2 IN INFLAMMATION, OXIDATIVE STRESS, AGING AND METABOLISM
Fedra Nicaury Luciano Mateo

Study 1

Chemokine (C-C motif) ligand 2 gene ablation protects low-density lipoprotein and paraoxonase-1 double deficient mice from liver injury, oxidative stress and inflammation

UNIVERSITAT ROVIRA I VIRGILI
THE ROLE OF CHEMOKINE (C-C MOTIF) LIGAND 2 IN INFLAMMATION, OXIDATIVE STRESS, AGING AND METABOLISM
Fedra Nicaury Luciano Mateo

Mice generation, genotyping and experimental design

Low density lipoprotein receptor single deficient mice (*Ldlr$^{-/-}$)* and CCL2 single deficient mice (*ccl2$^{-/-}$)* were purchased from Jackson Laboratories (Bar Harbor, Maine, USA) and the University of California in Los Angeles kindly donated *pon1$^{-/-}$* mice. All strains were backcrossed >10 generations to ensure C57BL/6J genetic background. From their progeny, we first generated by breeding double-deficient mice in pon1 and ldlr (*pon1$^{-/-}$, ldlr$^{-/-}$;* PLKO). Then, we generated another strain adding ccl2 deficiency (*ccl2$^{-/-}$, pon1$^{-/-}$, ldlr$^{-/-}$*; CPLKO). PLKO mice and littermates without mutations (wild type, WT) were used as controls to investigate the effects of CCL2 deficiency.

Mice genotyping was performed using DNA isolated from the tail. *ccl2* and/or *pon1* mRNA expressions were analyzed from homogenized tails (Figure.16) and livers (Figure.17) [167,168]. Handling of animals was performed by dedicated staff in accordance with current regulations and supervision by the Ethics Committee on Animal Experimentation of the Universitat Rovira i Virgili (protocols 4815 and GC-URV-0235-03.18.2014) following European guidelines (Directive 2010/63/EU).

Homozygous strains were viable and reproduced without difficulty under controlled temperature (22°C), humidity (50%) and light/dark cycle 12/12 h in a stress-free environment and fed a CD prepared by Scientific Animal Food & Engineering, Augy, France and water ad libitum. The animals were randomly allocated to experimental groups, and the investigators responsible for the assessment of outcomes had no previous knowledge of the experimental group to which the animals belonged. No animals were excluded from the analysis. Selected male CPLKO, PLKO and WT mice (n = 16, each) at 10 weeks of age were allocated into two dietary groups (n = 8, each) to compare the pon1- and ccl2-related effects and to assess the differential response against caloric intake provided by CD or HFD (Ssniff Spezialdiäten GmbH, Soest, Germany), over 14 weeks. At the beginning of the study, other littermates (n=3-4 for each strain) were used to confirm similar histologic features in their livers at this age. Information on supplied nutrients by both diets may be found in Table 1.

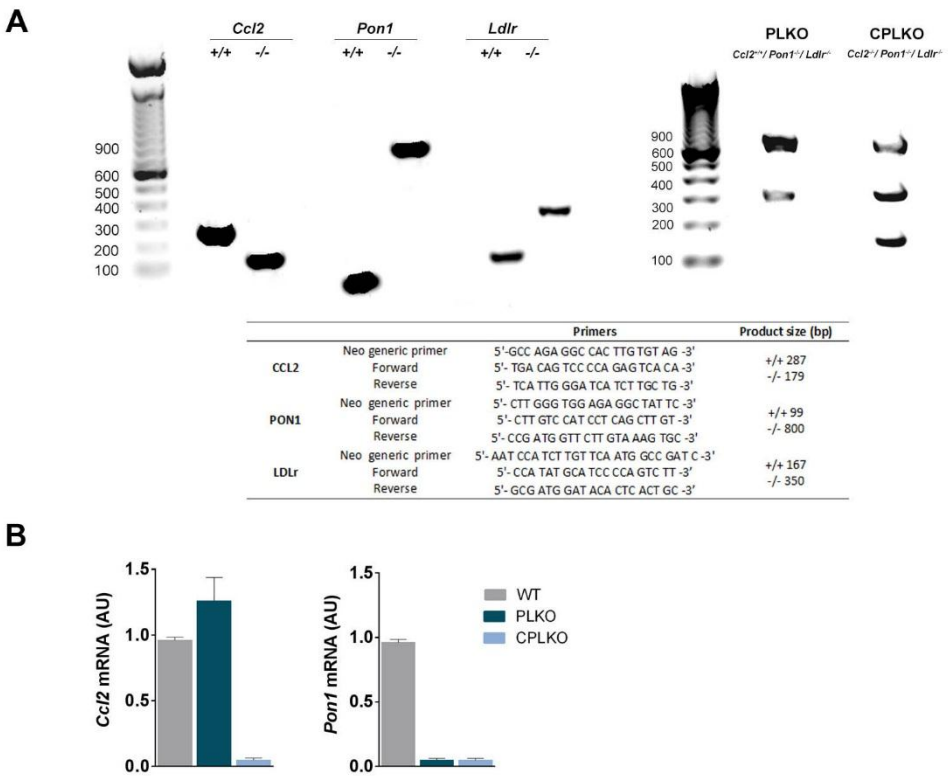

Figure 16. Genotyping and liver mRNA expression in mice generation. (A) Electrophoretic assessment and primers used in genotyping. (B) Expression of *pon1* and *ccl2* mRNA in liver homogenates of 24-week-old male genetically modified mice and control littermates (WT). PLKO denotes *ccl2*$^{+/+}$, *pon1*$^{-/-}$, *ldlr*$^{-/-}$ and CPLKO denotes *ccl2*$^{-/-}$, *pon1*$^{-/-}$, *ldlr*$^{-/-}$.

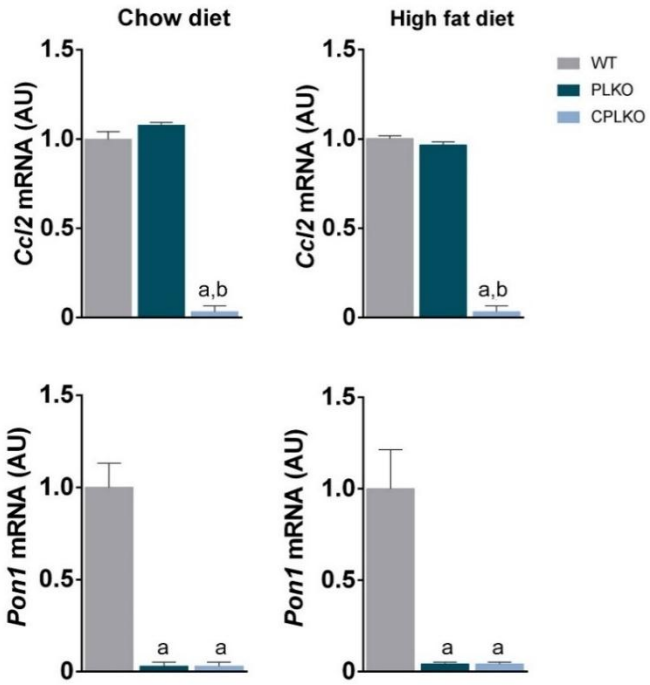

Figure 17. Relative hepatic mRNA expression of the chemokine (C-C motif) ligand 2 (*Ccl2*) and paraoxonase-1 (*Pon1*) in wild type (WT), PLKO and CPLKO mice. PLKO stands for $ccl2^{+/+}$, $pon1^{-/-}$, $ldl^{-/-}$ and CPLKO stands for $ccl2^{-/-}$, $pon1^{-/-}$, $ldlr^{-/-}$. Values are shown as mean ± SEM. [a] $P < 0.001$, with respect to wild type mice; [b] $P < 0.001$, with respect to PLKO animals.

Sample collection and biochemical analyses

One week before sacrifice, glucose tolerance tests (GTT) were performed on fasted (4 h) mice after intraperitoneal glucose (2 g/kg body weight) administration. Glucose concentrations were determined in blood from the tail immediately before and 15, 30, 60 and 120 min with test strips adapted to the Accuchek sensor system (Roche Diagnostics, Barcelona, Spain). At sacrifice, blood was obtained by intracardiac puncture to measure serum glucose, cholesterol, and triglyceride concentrations, and aspartate aminotransferase (AST) and alanine aminotransferase (ALT) activities in an automated analyzer Roche Cobas Mira Plus (Roche Diagnostics).

	CD	HFD
Crude protein (%)	16.1	24.1
Crude fat (%)	3.1	34.6
Crude fibre (%)	3.9	7.2
Carbohydrate (available) (%)	71.8	24.8
Crude ash (%)	4.2	8.5
Nitrogen free extracts (%)	43.5	23.3
Energy density (Kcal/g (Kj/g))	3.3 (14.0)	5.7 (24)
Calories from protein (%)	19.3	19
Calories from fat (%)	8.4	60
Calories from carbohydrate (%)	72.4	21
Calcium (%)	1.4	1.0
Phosphorus (%)	1.0	0.7
Sodium (%)	0.5	0.2
Magnesium (%)	0.3	0.2
Potassium (%)	1.5	1.0
Chloride (%)	0.7	-
Cholesterol (mg/kg)	ND	265
Lysine (%)	3.9	2
Methionine (%)	1.5	0.8
Cystine (%)	1.1	0.5
Met+Cys (%)	ND	1.3
Threonine (%)	ND	1.1
Tryptophan (%)	0.9	0.3
Arginine (%)	4.8	0.9
Histidine (%)	ND	0.8
Valine (%)	ND	1.6
Isoleucine (%)	ND	1.3
Leucine (%)	ND	2.4
Phenylalanine (%)	ND	1.3
Phe+Tyr (%)	ND	2.6
Glycine (%)	0.4	0.5
Glutamic acid (%)	ND	5.4
Aspartic acid (%)	ND	1.8
Proline (%)	ND	2.8
Alanine (%)	ND	0.8
Serine (%)	ND	1.4
Vitamin A (IU/kg)	7500	15000
Vitamin D_3 (IU/kg)	1000	1500
Vitamin E (IU/kg)	120	225
Vitamin K (as menadione) (mg/Kg)	2.5	20
Thiamin (B_1) (mg/Kg)	7	16
Riboflavin (B_2) (mg/Kg)	6.5	16
Pyridoxime (B_6) (mg/Kg)	2.6	18
Cyanocobalamin (B_{12}) (µg/Kg)	20	30
Nicotinic acid (mg/Kg)	75	45
Pantothenic acid (mg/Kg)	17	55
Folic acid (mg/Kg)	0.5	19
Biotin (µg/Kg)	40	310
Choline-Chloride (mg/Kg)	1600	2300
Iron (mg/Kg)	280	139
Manganese (mg/Kg)	90	82
Zinc (mg/Kg)	64	56
Copper (mg/Kg)	18	12
Iodine (mg/Kg)	ND	1.0
Selenium (mg/Kg)	ND	0.1
Cobalt (mg/Kg)	ND	0.1

Table 1. Nutritional composition of chow diet (CD) and high fat diet (HFD).

Quantitative RT-PCR

Total RNA was extracted using the RNeasy kit (Qiagen, Barcelona, Spain) and was retrotranscribed using the Reverse Transcription System kit (Applied Biosystems; Invitrogen, Barcelona, Spain). Real-time PCR (qPCR) was conducted on a 7900HT Fast Real-Time PCR System using TaqMan Gene Expression Assays (Applied Biosystems). The results normalized according to the expression level of Beta-2-Microglobulin (B2M) mRNA.

Histological analyses and immunochemistry

Livers were frozen in liquid N_2 and stored at -80°C and/or fixed in formalin (formaldehyde 3.7-4% buffered to pH=7 and stabilized with methanol 1-1.5%) until analysis. Adequate sections were stained with hematoxylin and eosin to evaluate liver impairment according to a scoring system as described [169]. For immunohistochemistry, procedures were performed as described with few modifications [168]. Briefly, after deparaffinization and rehydration of 2 µm liver sections, antigens were retrieved in 0.15 mol/L sodium citrate or Tris 10 mM/EDTA 1 mM buffer at pH=6 or pH=9 in a microwave oven until reaching 90ºC. Bovine serum albumin (2%) and hydrogen peroxide (1%) were sequentially used to block nonspecific binding sites and endogenous peroxidase and rinsed with phosphate buffered saline. Then, sections were incubated with the corresponding primary antibody, the appropriate secondary antibody and detected with reagents described in Table 2. All sections were counterstained with Mayer's hematoxylin and quantified via image analysis (at least 10 fields for each sample) using ImageJ software (National Institutes of Health, USA). To assess differences in oxidation and inflammation and to explore macrophage heterogeneity in healthy and diseased liver, we stained macrophages for C-Type Lectin Domain Family 4 Member F (CLEC4F), antigen F4/80, cluster of differentiation molecule 11B and 163 (CD11b and 163), and 4-hydroxy-2-nonenal (4-HNE) [27,170,171]

Western blot analyses

Frozen liver tissue (20 mg) from each animal was homogenized in 300 µL of lysis buffer composed of 0.25 M sucrose, 1 mM Pefabloc SC (Sigma-Aldrich, Saint Louis, MI, USA), and a phosphatase inhibitor cocktail (Hoffman-La Roche, Basel, Switzerland) using a sonicator (Branson Sonifer 150, Thistle Scientific, Glasgow, UK). Western blotting was performed by denaturing 50 µg of protein at 100 °C for 5 min in Laemmli sample buffer and β-mercaptoethanol. For protein separation, 8%-14% sodium dodecyl sulfate-polyacrylamide gel was used, and proteins were transferred onto a polyvinylidene difluoride or nitrocellulose membrane (Thermo Fisher, Barcelona, Spain). Before the primary antibody incubation, membranes were blocked with nonfat milk or bovine serum albumin at 5% in Tris, sodium chloride and 1% Tween-20 (pH=7.4). Reagents and further details may be found in Supplementary Table S2. Bands were detected with a SuperSignal West Femto chemiluminescent substrate (Pierce, Rockford, IL, USA), and the analysis was performed with a ChemiDoc system (Bio-Rad Laboratories, Madrid, Spain). Bands were analyzed and quantified using Image Lab 2.0 software (Bio-Rad Laboratories). Specifically, we measured the expression of molecules involved in the regulation of energy metabolism and autophagy-lysosomal function, including the PI3K-p85, AKT, AKT- pS473, mTOR, mTOR- pS2448, autophagy-related protein7 (Atg7), AMPK, AMPK- pT172, 4EBP1-p37/46, LC3-I and LC3-II and LAMP2 [129,132,146]. Fumarylacetoacetate hydrolase (FAH) was used as a reference protein [172].

Measurement of energy-balance metabolites in liver tissue (gas chromatography)

Metabolomic analysis was performed as previously reported [123]. Briefly, 100 mg of liver tissue was placed in 1 mL of methanol/water (8:2), mixed with D4-succinic acid (MeOH-D4s) as a standard at a final concentration of 0.01 µM, and homogenized with a Precellys 24 homogenizer (Izasa, Barcelona, Spain). Samples were stored at -20 ºC for 2 h to precipitate the proteins and centrifuged at 15,000 rpm for 10 minutes at 4 ºC. The supernatants were collected and stored at -80 ºC. At the moment of analysis, samples were dried with N2 and derivatized with methoxylamine hydrochloride dissolved in pyridine (40 mg/ml) and N-methyl-N-trimethylsilyl trifluoroacetamide. The analysis was with a 7890A gas chromatograph coupled with an electron impact source to a

7200 quadrupole time-of-flight mass spectrometer (GC-MS-EI) (Agilent Technologies, Santa Clara, USA).

Measurement of glutathione, glutathione disulfide and methionine cycle-related metabolites (liquid chromatography)

Metabolites were measured as described [173]. For the most common methionine cycle-related metabolites, 25 mg of liver tissue was added to 1 mL of an extraction solution containing methanol:water (8:2 v/v), 1% ascorbic acid (m/v) and 0.5% β-mercaptoethanol (v/v) and homogenized with Precellys 24 homogenizer (Izasa). After protein precipitation, samples were centrifuged at 14,000 rpm for 10 minutes at 4°C, the supernatant was collected, dried under N2, resuspended in 100 µL of ultrapure type 1 water containing 50 mM ammonium acetate + 0.2% formic acid and placed into vials for analysis. Five milliliters of sample were injected into an ultrahigh-pressure liquid chromatography-quadrupole time of flight mass spectrometer (Agilent Technologies, Santa Clara, USA) (UHPLC). To attain optimal results, GSH and GSSG were measured individually. Briefly, 50 mg of liver tissue was added to 500 µL of 100 mM N-ethylmaleimide, 152 mM NaCl in 1 mM acetic acid, and homogenized with a Precellys 24 homogenizer (Izasa). We used 200 µL of 8 M trichloroacetic acid for cell lysis and protein precipitation. Then, N-ethylmaleimide was removed by adding 10 mL of dichloromethane. Samples were centrifuged at 14,000 rpm, 4°C for 10 minutes, and 10 µL were injected into the UHPLC. Data quantification was performed using the calibration curves of each standard.

Statistical analyses

We used the nonparametric Mann-Whitney U-tests for comparisons between two groups according to the distribution of results in the measured variables. All statistical analyses and relevant graphics were performed with GraphPad Prism software 6.01 (GraphPad Software, San Diego, CA, USA).), SPSS Software (IBM SPSS Statistics for Windows, Version 21.00 Armonk, NY: IBM Corp) and MetaboAnalyst 3.0 (www.metaboanalyst.ca). Differences were considered statistically significant when the p value was ≤ 0.05. Unless otherwise indicated, the results are expressed as the mean ± standard error of the mean.

	Antigen	*Antibody*	*1ry Dilution*	*2ry Antibody*	*2ry Dilution*
Macrophage marker	F4.80	F4.80 antibody, ab100790 (Abcam, Cambridge, UK)	1:100	Goat α-rabbit HRP, P0448 (Dako, Agilent, California, USA)	1:200
Kupffer cells	CLEC4F	CLEC4F/CLECSF13 Antibody, AF2784 (AF2784, Minneapolis, USA)	1:100	Goat α-rabbit HRP, P0448 (Dako, Agilent, California, USA)	1:200
Pro-inflammatory macrophages marker	CD11b	CD11b antibody, ab133357 (Abcam, Cambridge, UK)	1:4000	Goat α-rabbit HRP, P0448 (Dako, Agilent, California, USA)	1:200
Anti-inflammatory macrophages markers	CD163	CD163, antibody, ab182422 (Abcam, Cambridge, UK)	1:500	Goat α-rabbit HRP, P0448 (Dako, Agilent, California, USA)	1:200
Oxidative stress marker	4HNE	Anti-HNE, MHN-100P (Genox, Baltimore, MD, USA)	1:1000	Goat anti-rabbit IgG, BA-1000 (Vector)	1:200
Insulin receptor	PI3K-p85	PI3K antibody, #4257 (Cell signalling, Massachusetts, USA)	1:1000	Goat α-rabbit HRP, P0448 (Dako, Agilent, California, USA)	1:5000
	Akt-p S473	p-Akt antibody, #4060 (Cell signalling, Massachusetts, USA)	1:1000	Goat α-rabbit HRP, P0448 (Dako, Agilent, California, USA)	1:5000
	Akt	AKT antibody, #4685 (Cell signalling, Massachusetts, USA)	1:1000	Goat α-rabbit HRP, P0448 (Dako, Agilent, California, USA)	1:5000
Energy sensors	mTOR-p S2448	pmTOR antibody,#2971 (Cell signalling, Massachusetts, USA)	1:1000	Goat α-rabbit HRP, P0448 (Dako, Agilent, California, USA)	1:2000
	mTOR	mTOR Antibody, #2972 (Cell signalling, Massachusetts, USA)	1:1000	Goat α-rabbit HRP, P0448 (Dako, Agilent, California, USA)	1:2000
	P4E-BP1	P4E-BP1 antibody #2855 (Cell signalling, Massachusetts, USA)	1:100	Goat α-rabbit HRP, P0448 (Dako, Agilent, California, USA)	1:5000
	AMPK-P T172	pAMPK antibody, #2531 (Cell signalling, Massachusetts, USA)	1:1000	Goat α-rabbit HRP, P0448 (Dako, Agilent, California, USA)	1:5000
	AMPK	AMPK antibody #2532S (Cell signalling, Massachusetts, USA)	1:1000	Goat α-rabbit HRP, P0448 (Dako, Agilent, California, USA)	1:5000
Autophagy markers	Atg7	Atg7 Antibody, #8558 (Cell signalling, Massachusetts, USA)	1:1000	Goat α-rabbit HRP, P0448 (Dako, Agilent, California, USA)	1:5000
	LC3	LC3B Antibody, #2775S (Cell signalling, Massachusetts, USA)	1:1000	Goat α-rabbit HRP, P0448 (Dako, Agilent, California, USA)	1:5000
	LAMP2A	LAMP2A antibody, ab125068 (Abcam, Cambridge, UK)	1:1000	Goat α-rabbit HRP, P0448 (Dako, Agilent, California, USA)	1:2000

Table 2. Antibodies and dilutions used in immunohistochemical and western blot analyses in the study 1.

Study 2

Metabolic reprogramming: The role of chemokine (C-C motif) ligand 2 in liver tissue and muscle metabolism

UNIVERSITAT ROVIRA I VIRGILI
THE ROLE OF CHEMOKINE (C-C MOTIF) LIGAND 2 IN INFLAMMATION, OXIDATIVE STRESS, AGING AND METABOLISM
Fedra Nicaury Luciano Mateo

Animals and experimental design

We employed male *Ccl2* cisgenic mice (*CgCcl2,* n=8) with a C57BL/6J genetic background. These animals have an additional copy of CCL2 gene in the Gt (ROSA) 26Sor locus of the mouse genome and were obtained via recombination in embryonic stem cells [174]. Strains were backcrossed >10 generations to maintain homozygous. Littermates without mutations were used as control (WT). All mice were maintained under controlled temperature (22ºC), humidity (50%) and light/dark cycle 12/12h. Mice were fed a normal standard diet (CD) from Scientific Animal Food & Engineering (SAFE, Augy, France) and water at libitum for 22 weeks. These procedures were approved by the Ethics Review Committee for Animal Experimentation of Rovira i Virgili University (protocols 4815 and GC-URV-0235-03.18.2014) following European guidelines (Directive 2010/63/EU).

Sample collection and laboratory measurements

At sacrifice, blood was obtained by intracardiac puncture to measure serum glucose, cholesterol, and triglyceride concentrations and AST and ALT activities in an automated analyzer Roche Cobas Mira Plus (Roche Diagnostics, Basel, Switzerland). Tissues were frozen in liquid N_2 and stored at -80 ºC and/or fixed in formalin (3.7-4% formaldehyde buffered to pH=7 and stabilized with 1-1.5% methanol) until analysis.

Analysis of tissue CCL2 concentrations

To check the effectiveness of the genetic modification we measured CCL2 concentrations in liver, pancreas, muscle, and white and brown adipose tissues by ELISA (Preprotech, London UK). Thirty mg of selected tissues were homogenized by using a sonicator (Branson Sonifer 150, Thistle Scientific, Glasgow, UK) in 50 mM Tris, with 1 mM EDTA, 1% Igepal CA-630, 150 mM NaCl, 0.10% Triton, 50 mM NaF, 100 mM phenylmethanesulfonyl fluoride (PMS), and 1 mM Na_3VO_4. Measurements were performed with 200 µg of protein.

Histological analyses and immunohistochemistry

Liver and muscle tissues were fixed in formalin. Two µm of tissue sections were stained with hematoxylin and eosin and Sirius red to evaluate histological alterations. For immunohistochemical analyses we used 10 mM Tris /1 mM EDTA at pH=6 as antigen retrieval in a microwave oven until reaching 90ºC for 30 min. Bovine serum albumin (2%) was used to block nonspecific binding. Endogen peroxidase was blocked by hydrogen peroxide. Then, sections were incubated with F4/80 antibody (ab100790, Abcam, Cambridge, UK), which is a marker of macrophages, and a secondary antibody (P0448, Dako, Agilent, CA, USA). All sections were counterstained with Mayer's hematoxylin.

Western blot analyses

Twenty mg of frozen liver and muscle tissues from each animal were homogenized by using a sonicator (Branson Sonifer 150). For hepatic tissue, we used the protocol described in the study 1. For muscle, we used 300 µL of lysis buffer composed of 50 mM Tris, 1 mM EDTA, 1 % Igepal CA-630, 150 mM NaCl, 0.10 % Triton, 50 mM NaF, 100 mM phenylmethanesulfonyl fluoride (PMS) and 1 mM Na_3VO_4.

We measured the expression of pro-inflammatory and anti-inflammatory makers and molecules involved in the regulation of energy metabolism and autophagy-lysosomal function, including: CD11b, CD163, TNFα, liver arginase, PON1, PI3K-p85, AKT, AKT- pS473, phospho-S6 ribosomal protein (S6-Ps235/236), S6 ribosomal protein, translocase of the outer membrane 20 (TOM20), Mfn2, AMPK, AMPK- pT172, OXPHOS, LC3-I and LC3-II, sequestosome 1 or p62/SQSTM1 and the LAMP2A [27,144,170,175]. FAH and vinculin were used as reference proteins. Western blots were performed using the protocol described in the study 1. Reagents and further details are shown in Table 3.

Measurement of energy-balance and one-carbon metabolites in liver and muscle tissue and statistical analyses were performed according to the methods described in the study 1.

Antigen	*Antibody*	*1ry Dilution*	*2ry Antibody*	*2ry Dilution*
CD11b	CD11b antibody, ab133357 (Abcam, Cambridge, UK)	1:1000	Goat α-rabbit HRP, P0448 (Dako, Santa Clara, CA, USA)	1:5000
TNFα	TNFα antibody, #3707 (Cell signalling, Danvers, MA, USA)	1:1000	Goat α-rabbit HRP, P0448 (Dako, Santa Clara, CA, USA)	1:5000
CD163	CD163, antibody, ab182422 (Abcam, Cambridge, UK)	1:1000	Goat α-rabbit HRP, P0448 (Dako, Santa Clara, CA, USA)	1:5000
F4/80	F4/80, antibody, ab100790 (Abcam, Cambridge, UK)	1:100	Goat α-rabbit HRP, P0448 (Dako, Santa Clara, CA, USA)	1:200
Arginase	Liver arginase, antibody, ab91279 (Abcam, Cambridge, UK)	1:10000	Goat α-rabbit HRP, P0448 (Dako, Santa Clara, CA, USA)	1:5000
PON1	In-house	1:200	Goat α-rabbit HRP, P0448 (Dako, Santa Clara, CA, USA)	1:1000
PI3K-p85	PI3K antibody, #4257 (Cell signalling, Danvers, MA, USA)	1:1000	Goat α-rabbit HRP, P0448 (Dako, Santa Clara, CA, USA)	1:5000
Akt pS473	p-Akt antibody, #4060 (Cell signalling, Danvers, MA, USA)	1:1000	Goat α-rabbit HRP, P0448 (Dako, Santa Clara, CA, USA)	1:5000
Akt	AKT antibody, #4685 (Cell signalling, Danvers, MA, USA)	1:1000	Goat α-rabbit HRP, P0448 (Dako, Santa Clara, CA, USA)	1:5000
S6 ps235/236	pS6 antibody, #4856 (Cell signalling, Danvers, MA, USA)	1:1000	Goat α-rabbit HRP, P0448 (Dako, Santa Clara, CA, USA)	1:5000
S6	S6 antibody, #2217 (Cell signalling, Danvers, MA, USA)	1:1000	Goat α-rabbit HRP, P0448 (Dako, Santa Clara, CA, USA)	1:5000
AMPK pT172	pAMPK antibody, #2531 (Cell signalling, Danvers, MA, USA)	1:1000	Goat α-rabbit HRP, P0448 (Dako, Santa Clara, CA, USA)	1:5000
AMPK	AMPK antibody #2532S (Cell signalling, Danvers, MA, USA)	1:1000	Goat α-rabbit HRP, P0448 (Dako, Santa Clara, CA, USA)	1:5000
OXPHOS	OXPHOS Rodent , antibody, ab ab110413 (Abcam, Cambridge, UK)	1:250	Goat α-mouse HRP, P0447 (Dako, Santa Clara, CA, USA)	1:5000
LC3	LC3B Antibody, #2775S (Cell signalling, Danvers, MA, USA)	1:1000	Goat α-rabbit HRP, P0448 (Dako, Santa Clara, CA, USA)	1:5000
LAMP2A	LAMP2A antibody, ab125068 (Abcam, Cambridge, UK)	1:1000	Goat α-rabbit HRP, P0448 (Dako, Santa Clara, CA, USA)	1:2000
P62	P62 Antibody, #5114 (Cell signalling, Danvers, MA, USA)	1:1000	Goat α-rabbit HRP, P0448 (Dako, Santa Clara, CA, USA)	1:5000
FAH	FAH antibody #ABN526 (Millipore, Burlington, MA, USA)	1:1000	Goat α-rabbit HRP, P0448 (Dako, Santa Clara, CA, USA)	1:2000
Vinculin	Vinculin antibody, ab73412 (Abcam, Cambridge, UK)	1:1000	Goat α-rabbit HRP, P0448 (Dako, Santa Clara, CA, USA)	1:2000
TOM20	TOM20 antibody, #42406 (Cell signalling, Danvers, MA, USA)	1:1000	Goat α-rabbit HRP, P0448 (Dako, Santa Clara, CA, USA)	1:5000
Mfn2	Mfn2 antibody, ab124773 (Abcam, Cambridge, UK)	1:1000	Goat α-rabbit HRP, P0448 (Dako, Santa Clara, CA, USA)	1:2000
UCP-1	UCP-1, antibody, ab10983(Abcam, Cambridge, UK)	1:100	Goat α-rabbit HRP, P0448 (Dako, Santa Clara, CA, USA)	1:200

Table 3. Antibodies used in western blot and immunohistochemical analyzed in study 2 and study 3

UNIVERSITAT ROVIRA I VIRGILI
THE ROLE OF CHEMOKINE (C-C MOTIF) LIGAND 2 IN INFLAMMATION, OXIDATIVE STRESS, AGING AND METABOLISM
Fedra Nicaury Luciano Mateo

Study 3

Overexpression of chemokine (C-C motif) ligand 2 promotes fibrosis and metabolic alterations leading to accelerated aging

UNIVERSITAT ROVIRA I VIRGILI
THE ROLE OF CHEMOKINE (C-C MOTIF) LIGAND 2 IN INFLAMMATION, OXIDATIVE STRESS, AGING AND METABOLISM
Fedra Nicaury Luciano Mateo

Animals and experimental design

Mice used in this study were of C57BL/6J genetic background carrying the following genetic modifications: Cisgenic mice (*CgCcl2*) were generated in our laboratory as previously described [174]; *Lmna* $^{G609G+/-}$ were kindly donated by the University of Oviedo. These lines were used to generate an accelerated aging mice model with ubiquitous *Ccl2* expression (*Lmna* $^{G609G+/-}$ */CgCcl2*$^{-/+}$). Mice genotyping was performed using DNA isolated from the tail (Figure 17A). The second progeny obtained by breeding of *Lmna* $^{G609G+/-}$ */CgCcl*$^{+/-}$ showed a characteristic phenotype (lower body weight, are smaller and are not fertile) (Figure 17B). Then, for this study we only used the first progeny of heterozygous *Lmna* $^{G609G+/-}$ */CgCcl*$^{+/-}$ mice. Wild type (WT) and *Lmna*$^{G609G-/+}$ were used as controls groups.

All mice were maintained under controlled temperature (22ºC), humidity (50%) and light/dark cycle 12/12h. Mice were fed a normal standard diet (CD) from Scientific Animal Food & Engineering (SAFE, Augy, France) and water *ad libitum*. The experimental and scientific procedures were performed conformed to EU Directive 2010/63/EU and Ethics Review Committee for Animal Experimentation of Rovira I Virgili University (protocols 4815 and GC-URV-0235-03.18.2014).

Longevity studies, sample collection and histological analysis

The study started at 4 weeks of age. Animals were assessed weekly and sacrificed according to senescence criterial proposed by Takeda et al [176], which are presented in Table 4.

At sacrifice, tissues were frozen in liquid N2 and stored at -80 ºC and/or fixed in formalin (formaldehyde 3.7-4% buffered to pH=7 and stabilized with methanol 1-1.5%) until analysis. All tissues were stained with hematoxylin and eosin, Sirius red staining and visualized in a light microscope. For immunohistochemistry we used the protocol described in the study 1. Reagents and further details are shown in Supplementary Table S3.

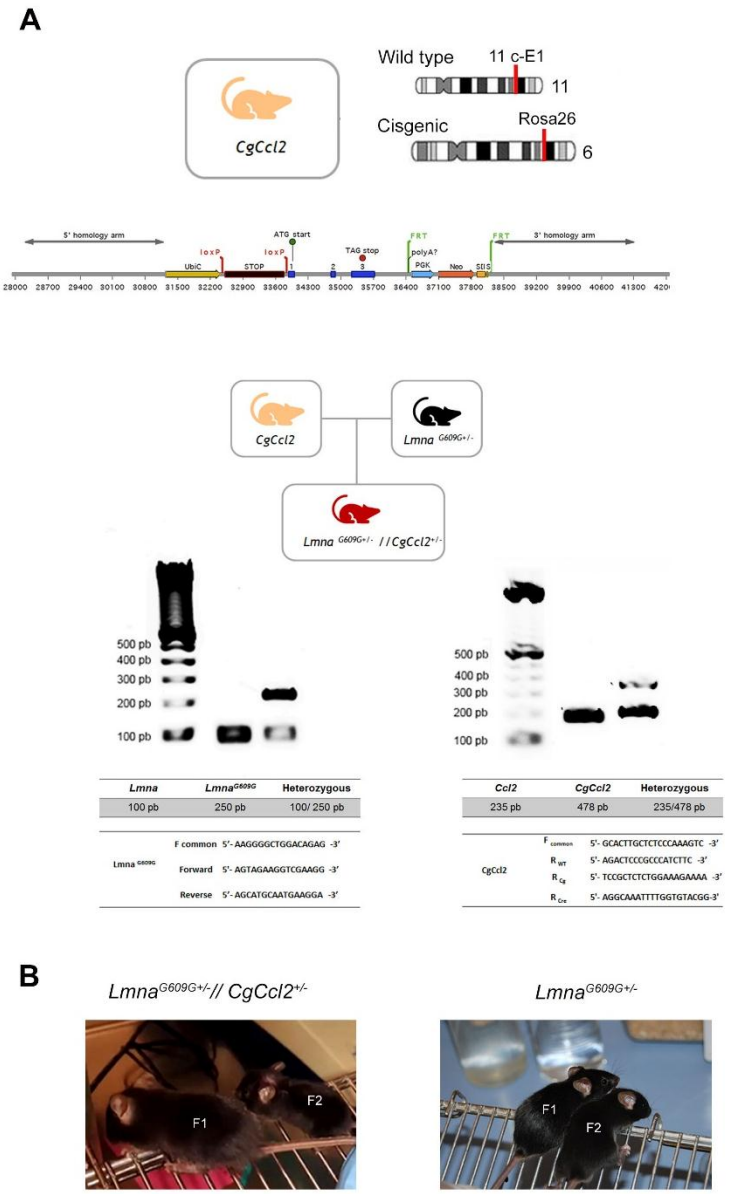

Figure 17. **Generation of *Lmna* $^{G606G\ +/-}$ */CgCcl2* $^{+/-}$ mice.** *(*A) Schematic representation of the wild-type allele for C-C motif ligand 2 gene (*Ccl2*) which is located in the region 11 C-E1 of chromosome 11. The cisgenic vector is inserted in the ROSA26 locus of chromosome 6. Electrophoretic assessment and primers used in genotyping of *Lmna* $^{G606G\ +/-}$ */CgCcl2* $^{+/-}$. (B) Phenotype of the fist (F1) and second (F2) littermates obtaining by the breeding of *Lmna* $^{G606G\ +/-}$*/CgCcl2* $^{+/-}$ and *Lmna*$^{G606G+/-}$. *Lmna* $^{G606G\ +/-}$*/CgCcl2* $^{+/-}$ denote heterozygous progeria and CCL2 cisgenic mice. *Lmna* $^{G606G\ +/-}$ denote progeria mice.

	Grade 0	*Grade 1*	*Grade 2*	*Grade 3*	*Grade 4*
Behavior					
Reactivity	The most intensive exploratory response observed within 30 seconds	Normal behavior	Abnormal grait with no lessening of agility and behavior patterns and restlessness	Definite decrease in agility and behavior patterns	Does not move voluntarily but will move if nudged	Immobile
Passivity	Escape reaction from pinching of the nuchal skin or from hanging by the forelimb	Natural escape reaction to pinching	Decrease in escape reaction to pinching	Loss of escape reaction to pinching. Preserved righting reaction to manual turn over	Neither escape reaction to pinching nor righting to hanging by the forelimb.	Escape reaction nil
Appearance					
Glossiness	Glossiness	Natural gloss	Decrease in gloss	Complete disappearance of gloss	Complete disappearance of gloss and hair appears dirty	Complete disappearance of gloss and hair looks very dirty
Coarseness	Coarseness of hair on the head, nuca and dorsum determined according to the number of palpable, fine clumps of hair	No coarseness	Coarseness of less than an area of the head	Coarseness of less than double the area of the head	Coarseness of less than 3 times area of the head	Coarseness of over 3 times area of the head
Loss of hair	Loss or thinning of hair on the head, nuca and dorsum except for changes due to ulcer or Periophthalmic lesions	Neither loss or thinning of hair	A. Loss of hair in less than an area of the head. B. Thinning of hair in less than 1/2 of total area	A. Loss of hair in over one area of the head, less than in 1/4 of total area. B. Thinning if hair in more than 1/2 of total area	Loss of hair in more than 1/4, in less than 1/2 of total area.	Loss of hair in over 1/2 of total area
Skin ulcers	Ulcer or healed ulcer on entire skin except for changes associated with Periophthalmic lesions	No evidence of ulcer	Healed ulcer or ulcer with scab	Ulcer without healing tendency, in less than one area of the head	Ulcer without healing tendency in more than one area of the heard, in less than 1/4 area of all the skin.	Ulcer without healing tendency in more than 1/4 area of whole skin
Eyes					
Periophthalmic lesions	Catarrhal changes in the periophthalmic area or swelling of the palpebra	No changes	Catarrhal changes limited to periophthalmic area or swelling of palpebra	Catarrhal changes extending to nose	Catarrhal changes extending further	
Lordokyphosis of the spine	Examined by inspection and palpation	Natural anteroposterior curvature	Increased curvature disappears with digital pressure on the dorsum	Increased curvature disappears with a combination of manual cephalocaudal traction and digital pressure on the dorsum	permanent curvature	Lordokyphosis of the spine

Table 4. Criteria for grading score of senescence in mice

Global DNA methylation

For DNA isolation muscle tissues were dissolved in 200 µl lysis buffer of DNA Micro Kit (Catalog no. 56304, Qiagen, Germany), and incubated with proteinase K overnight at 56°C. DNA was extracted according to the manufacturer's protocol (DNeasy Blood & Tissue Kit, Qiagen) and DNA concentration was determined at 260 nm using the NanoDrop ND-1000 spectrophotometer (Nanodrop Technologies Inc., Wilmington, NC, USA). Then, 5-mC and 5-hmC were detected using the genomic DNA through ultra-high-pressure liquid chromatography (UHPLC) coupled with an iFunnel electrospray ionization source (ESI) and a 6490 triple quadrupole mass spectrometer (QqQ-MS), hydrolyzed following the method provide by Rossella et al [177]. Briefly, 200 µL of 88% formic acid was added to dry DNA (2.5 µg) and incubated at 140 ºC for 90 minutes. Samples were cooled at room temperature and evaporated under N2, resuspended in 100 µL of 0.1% formic acid and placed into chromatographic vials. Detection of 5-mC, 5-hmC and guanine was carried out by injecting 5 µL of hydrolyzed DNA into a 1290 Infinity UHPLC coupled with a quadrupole mass spectrometer (QqQ-MS) (Agilent Technologies, Santa Clara). Metabolites were quantified using standard calibration curves to calculate the proportions of methylated and hydroxymethylated DNA according to the total amount of guanine.

Analysis of CCL2, western blot, measurement of energy-balance and 1-C carbon metabolites and statistical analyses were performed according to the methods described in the study 1.

Results

Result

UNIVERSITAT ROVIRA I VIRGILI
THE ROLE OF CHEMOKINE (C-C MOTIF) LIGAND 2 IN INFLAMMATION, OXIDATIVE STRESS, AGING AND METABOLISM
Fedra Nicaury Luciano Mateo

Study 1

Chemokine (C-C motif) ligand 2 gene ablation protects low-density lipoprotein and paraoxonase-1 double deficient mice from liver injury, oxidative stress and inflammation

UNIVERSITAT ROVIRA I VIRGILI
THE ROLE OF CHEMOKINE (C-C MOTIF) LIGAND 2 IN INFLAMMATION, OXIDATIVE STRESS, AGING AND METABOLISM
Fedra Nicaury Luciano Mateo

Results

Metabolic phenotypes, including liver histology and distribution of macrophages, were sensitive to CCL2 *deficiency*

PLKO and CPLKO mice had a significantly lower body weight than WT animals when given diet CD. In contrast, weight increased similarly in all strains when HFD (Figure 18 A). Moreover, serum cholesterol, triglycerides and glucose concentrations were significantly higher in the HFD groups than in the CD groups, and PLKO and CPLKO mice had higher values than WT animals. All strains became glucose intolerant when fed HFD but without significant differences among strains, and serum glucose remained lower in mice with *ccl2* deficiency. Serum AST and ALT activities were higher in PLKO mice than in WT animals, while CPLKO mice had levels of these enzymes similar to those of the WT group (Figure 18 B). These findings suggested a differential hepatic response that was confirmed histologically (Figure 19). Minor fat accumulation was observed in PLKO mice fed CD, and prominent liver steatosis was observed when fed HFD. In contrast, CPLKO mice did not develop steatosis irrespective of the administered diet (Figure 19 A).

The immunohistochemical expression of 4-HNE was low in WT mice and very high in PLKO animals. The expression of 4-HNE in CPLKO mice was similar to that of WT animals, indicating a similar degree of oxidative stress (Figure 19 B). Again, the expected higher oxidative stress in *pon1*-deficient mice was averted by the added deficiency in *ccl2* (CPLKO), suggesting that CCL2 may potentially induce major metabolic changes, inhibit the inflammatory response, or both.

Differences between PLKO and CPLKO mice were observed through the differential abundance of liver macrophages with different phenotypes. PLKO mice fed a CD diet had a lower expression of CLEC4F, indicating a lower amount of Kupffer cells. This alteration was corrected in CPLKO animals. However, we did not find any significant difference in this marker in mice given HFD (Figure 20 A). A significant subset of macrophages was positive for F4/80 antigen with expected potent phagocytic activity and ROS production capacity. PLKO mice did not change their relative abundance of these macrophages, but in mice deprived of *ccl2,* the relative proportion of F4/80+ cells remained significantly lower when fed either CD or HFD (Figure 20 B). A relatively low percentage of macrophages were positive for CD11b staining, which increased in fat-challenged mice in all strains. CD11b is a marker of pro-inflammatory macrophages, and the increase was

lower in CPLKO animals (Figure 20 C). Finally, to assess the putative reparative function of some macrophages and the functional adaptation to environmental challenges, we also measured CD163+ cells. This antigen is a marker of anti-inflammatory macrophages, and we found that PLKO mice had a significant decrease in the proportion of CD163-stained cells with respect to WT mice. The additional CCL2 deficiency counteracted such reduced expression (Figure 20 D). We also measured the hepatic mRNA expression of *CD11b* and *CD163*, which confirmed the immunohistochemical analyses in mice fed with CD, although we did not observe any significant differences in animals fed with HFD (Figure 21).

Taken together, our findings show that CCL2 axis alters the metabolic phenotype of mice challenged with fat accumulation and may reshape the functional capacity of liver macrophages.

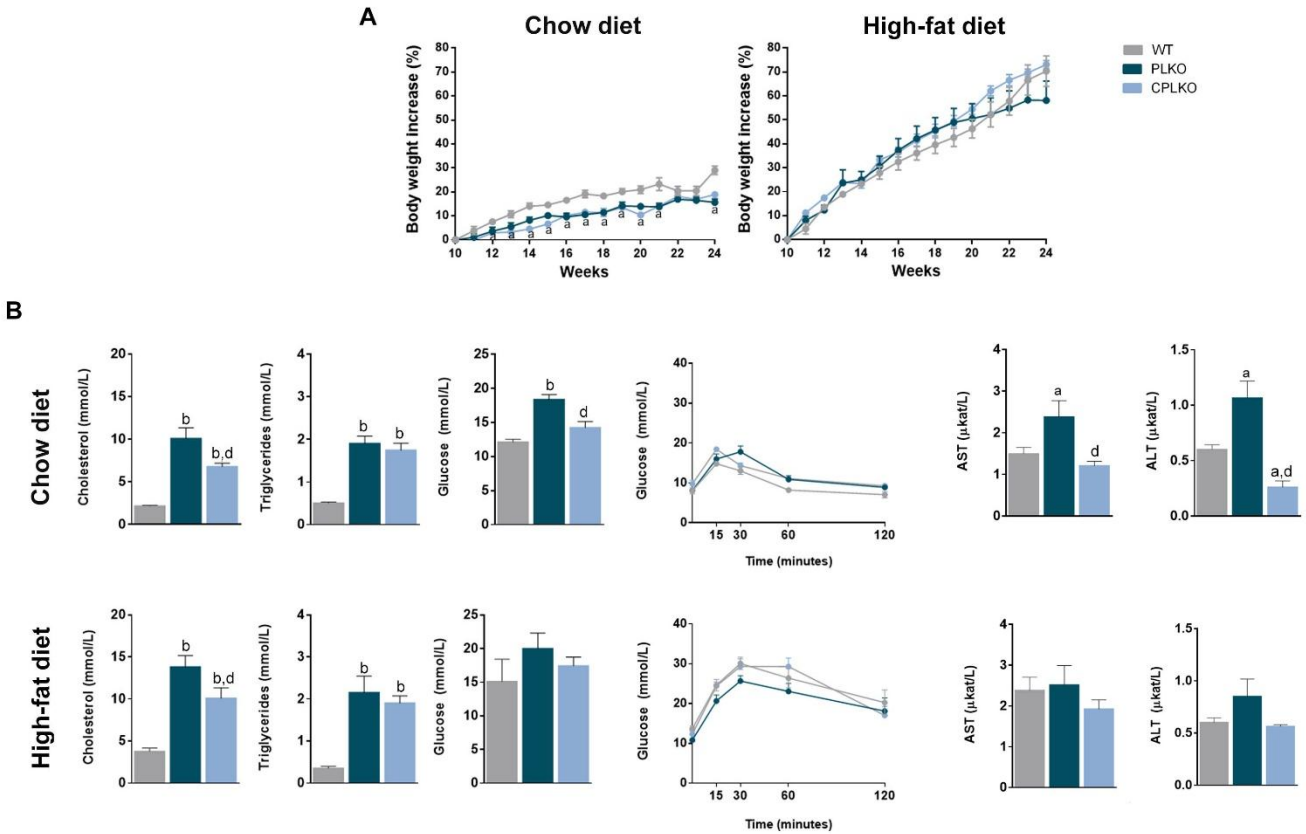

Figure 18. Selected metabolic features in genetically modified mice. The results for (A) Body weight increase and (B) biochemical variables. PLKO denotes *ccl2*$^{+/+}$, *pon1*$^{-/-}$, *ldlr*$^{-/-}$ and CPLKO denotes *ccl2*$^{-/-}$, *pon1*$^{-/-}$, *ldlr*$^{-/-}$. Values are mean ± SEM (n=8 per genotype and dietary condition) ^{a} $P < 0.05$, ^{b} $P < 0.001$, with respect to control littermates (WT); ^{c} $P < 0.05$, ^{d} $P < 0.001$, with respect to PLKO.

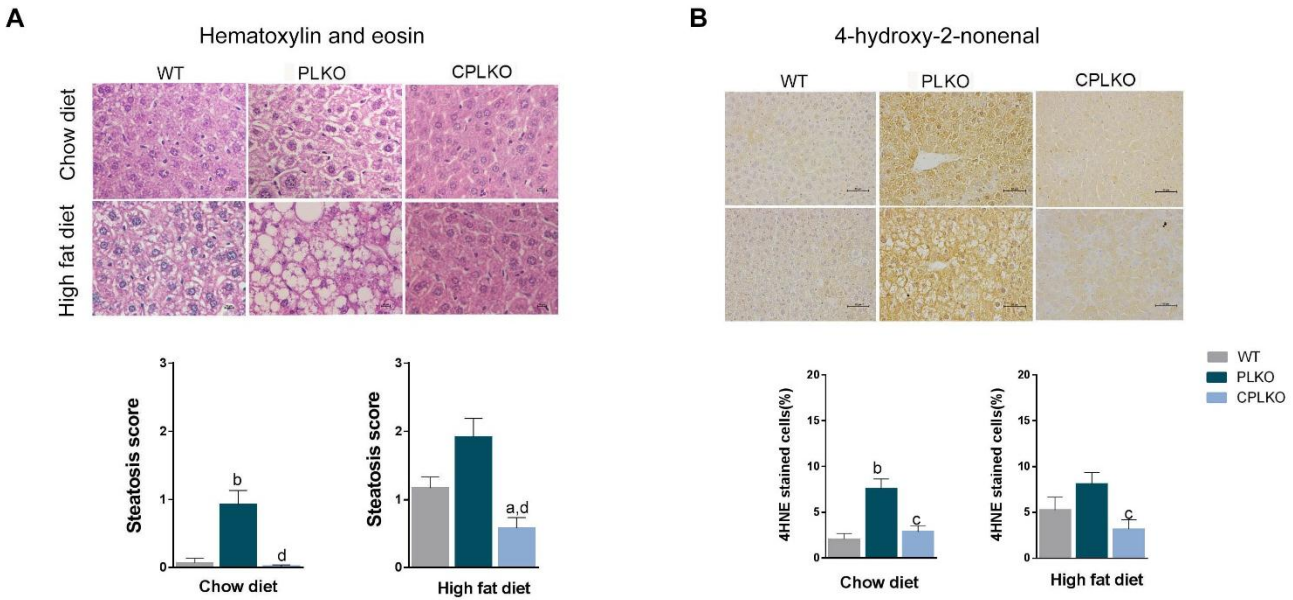

Figure 19. Hepatic histological features. Representative microphotographs (bars indicate magnification) of liver sections stained with (A) hematoxylin and eosin and against (B) 4-hydroxy-2-nonenal (4-HNE). PLKO denotes *ccl2*$^{+/+}$, *pon1*$^{-/-}$, *ldlr*$^{-/-}$ and CPLKO denotes *ccl2*$^{-/-}$, *pon1*$^{-/-}$, *ldlr*$^{-/-}$. Values reported for the calculated steatosis score and 4HNE stained cells are mean ± SEM (n=8 per genotype and dietary condition) [a] $P < 0.05$, [b] $P < 0.001$, with respect to control littermates (WT); [c] $P < 0.05$, [d] $P < 0.001$, with respect to PLKO.

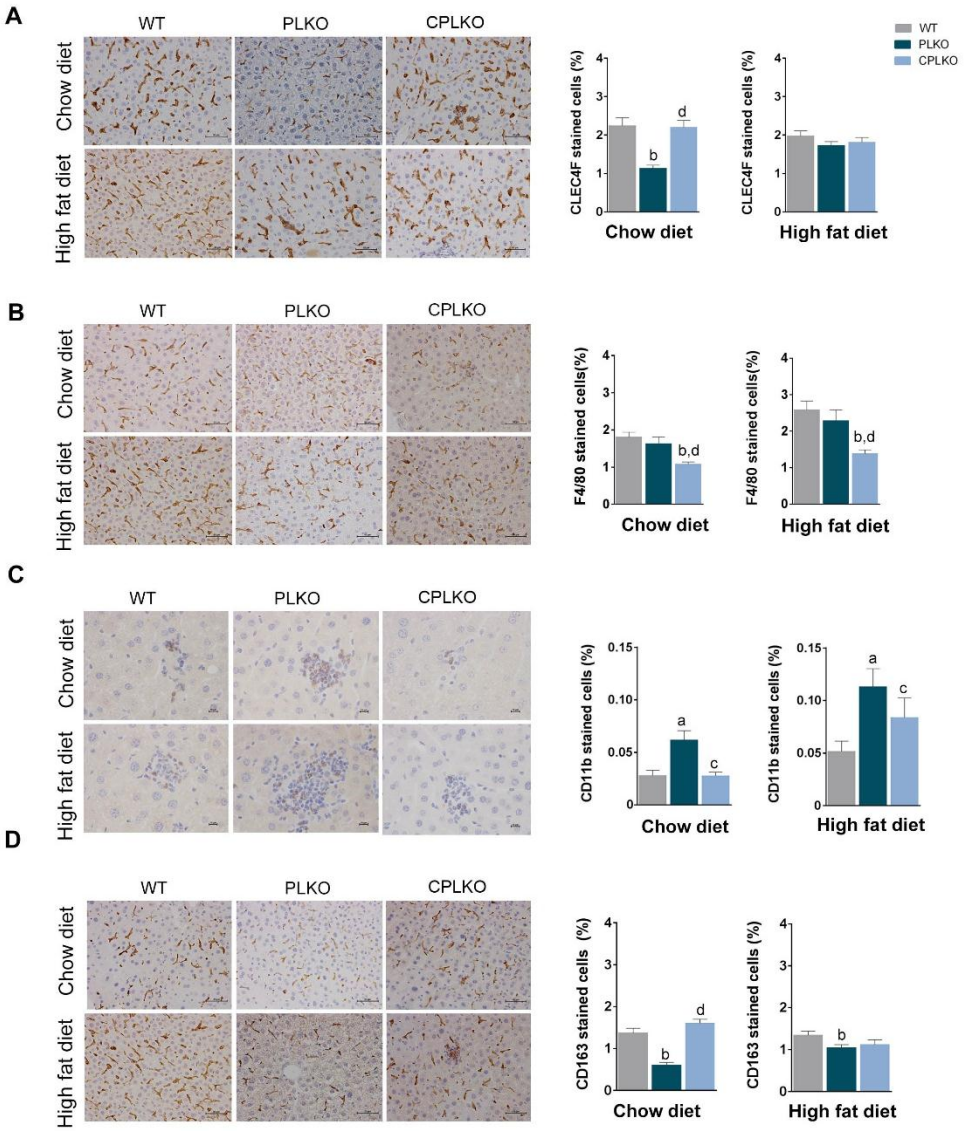

Figure 20. Hepatic macrophage relative density. Representative microphotographs (bars indicate magnification) illustrating immunohistochemical staining of (A) C-type lectin domain family 4 member F (CLEC4F), (B) F4/80, (C) cluster of differentiation 11b (CD11b) and (D) cluster of differentiation 163 (CD163). PLKO denotes *ccl2*$^{+/+}$, *pon1*$^{-/-}$, *ldlr*$^{-/-}$ and CPLKO denotes *ccl2*$^{-/-}$, *pon1*$^{-/-}$, *ldlr*$^{-/-}$. Values for the calculated stained cells (%) are mean ± SEM (n=8 per genotype and dietary condition) ^{a} $P < 0.05$, ^{b} $P < 0.001$, with respect to control littermates (WT); ^{c} $P < 0.05$, ^{d} $P < 0.001$, with respect to PLKO.

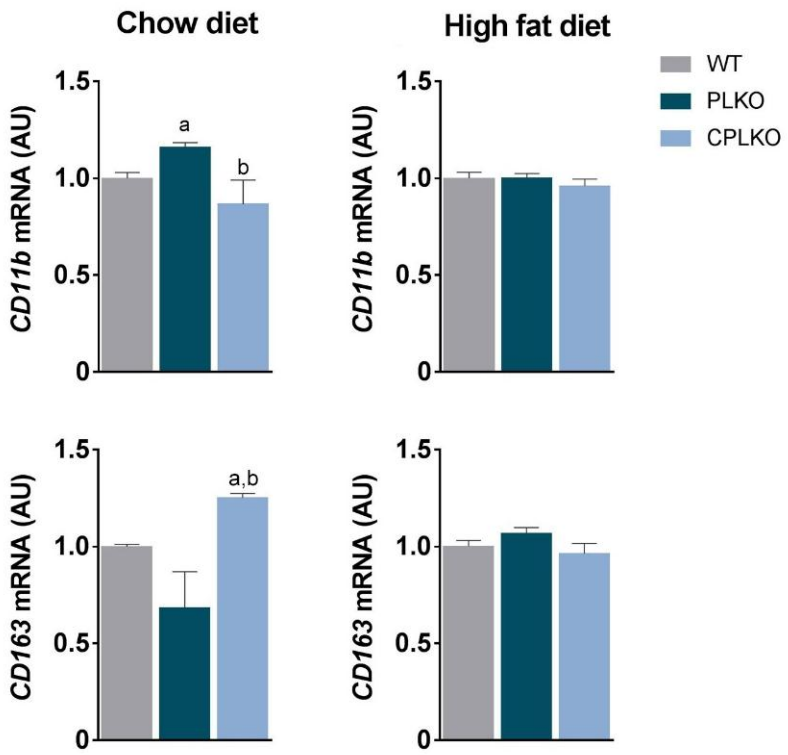

Figure 21. Relative hepatic mRNA expression of CD11b and CD163 antigens in wild type (WT), PLKO and CPLKO mice. PLKO stands for *ccl2*$^{+/+}$, *pon1*$^{-/-}$, *ldlr*$^{-/-}$ mice and CPLKO stands for *ccl2*$^{-/-}$, *pon1*$^{-/-}$, *ldlr*$^{-/-}$ animals. Values are mean ± SEM [a] $p < 0.05$, with respect to wild type mice; [b] $p < 0.05$, with respect to PLKO mice.

Oxidative stress and inflammation mediate energy metabolism-associated pathways

Targeted metabolomic analysis indicated that PLKO and CPLKO mice differ in their liver metabolism. Partial least square discriminant analysis visually indicates the role of the measured metabolites in discriminating among the different experimental groups. Separation among groups was more clearly shown in animals fed HFD, and the effects on the distribution among dietary groups were consistent. The standardized metabolite concentrations were represented as a heatmap, and most metabolites discriminated both genetic variations, including the effect of diet. Glycolysis and amino acid metabolism appear to be important to explain the differences superposed by *ccl2* deficiency, as shown by the ranked importance of metabolites without supervision via random forest analysis (Figure 22 and Table 5).

When comparing the metabolic response of PLKO and CPLKO mice with respect to normal (WT), we found an accumulation of glucose-6-phosphate together with increased proximal and distal metabolites, including fructose 6-phosphate, fructose 1,6-bisphosphate and ribose-5 phosphate, indicating a reduced entry of glucose carbon into mitochondrial biosynthetic metabolism and likely alterations in the pentose monophosphate shunt. In both strains, with minor dietary-induced differences, there was an apparent decoupling between glycolysis and CAC (Figure 23 A, B). Therefore, the induced mutations result in a state of relatively reduced hepatic oxidative metabolism. However, the accumulation of lactate and β-hydroxybutyrate quantitatively differed according to the ingestion of calories and were more evident in comparisons between PLKO and CPLKO mice, suggesting potential alternatives to provide CAC feeding. Notably, mice deprived from CCL2 significantly improved the function of the glycolytic pathway and connections with CAC. Hepatic mitochondria also support relevant pathways related to the ability of 4-carbon intermediates to move into (anaplerosis) and out of (cataplerosis) the CAC without undergoing oxidation. These metabolic activities are required for shuttling reducing equivalents and biosynthetic substrates to other pathways, and the relative accumulation of CAC intermediates, lactate, ketone bodies and amino acids suggests that CCL2 may influence the flux of anaplerosis and cataplerosis-associated pathways (Figure 23 C). Taken together, our results suggest that PON1 and CCL2 are closely related and may affect metabolic activities with the potential for ROS formation in liver mitochondria, contributing to oxidative stress and inflammation under these conditions.

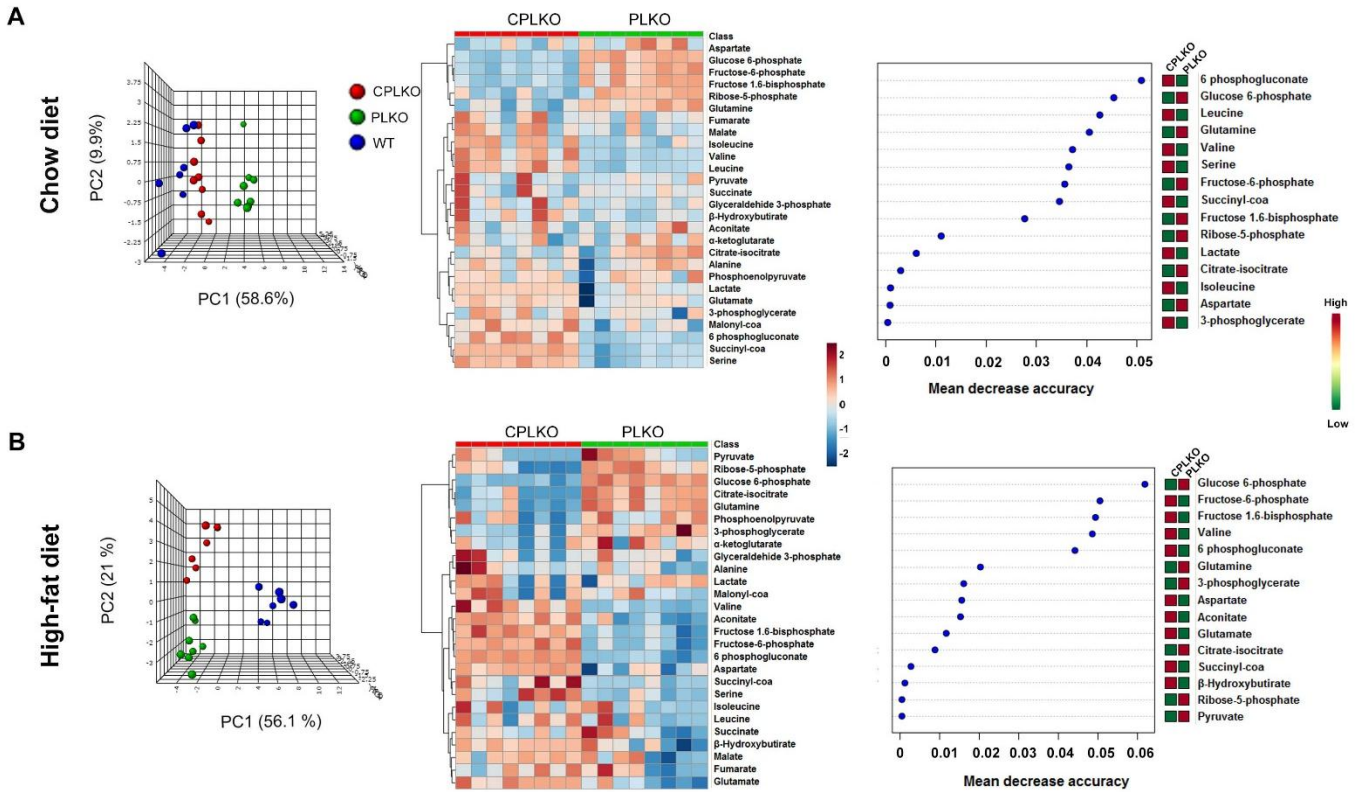

Figure 22. Dietary-induced changes and the effect of *pon1* and/or *ccl2* ablation in hepatic energy-balance metabolites. From left to right in mice segregated by dietary conditions (A and B), partial least square discriminant analysis to visualize how measured metabolites discriminate among strains, heatmap built using standardized metabolite concentrations, and random forests to rank the importance of metabolites without supervision. PLKO denotes *ccl2*$^{+/+}$, *pon1*$^{-/-}$, *ldlr*$^{-/-}$ and CPLKO denotes *ccl2*$^{-/-}$, *pon1*$^{-/-}$, *ldlr*$^{-/-}$.

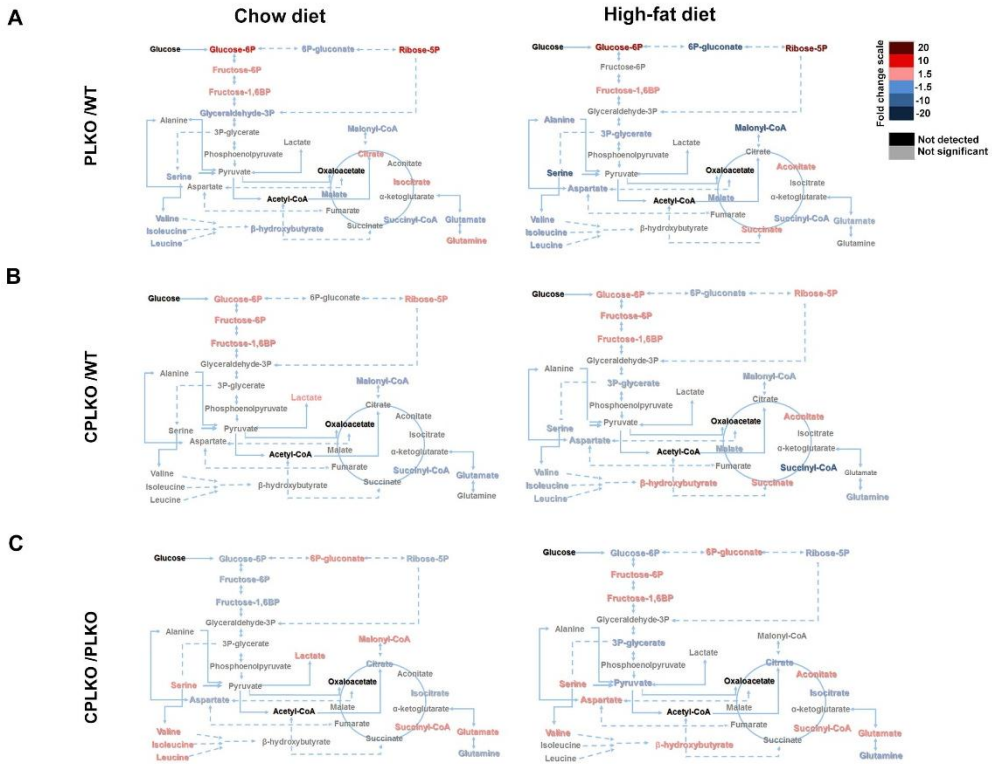

Figure 23. The relative impact of dietary fat on the levels of metabolites associated with energy metabolism in the liver. Comparisons were made assessing fold-changes according to the legend in mice with *pon1* deficiency (A) and *pon1* and *ccl2* deficiency (B) with respect to control littermates and between both strains (C). PLKO denotes *ccl2*$^{+/+}$, *pon1*$^{-/-}$, *ldlr*$^{-/-}$ and CPLKO denotes *ccl2*$^{-/-}$, *pon1*$^{-/-}$, *ldlr*$^{-/-}$.

	WT		*PL KO*		*CPL KO*	
Metabolites	**CD**	**HFD**	**CD**	**HFD**	**CD**	**HFD**
Glucose 6-phosphate	18.9 (14.6 - 18.9)	39.4 (37.4 - 39.4)	228.6 (201.1 - 266.4) [b]	410.8 (299.1 - 445.3) [b]	39.5 (30.6 - 54.6) [b,d]	50.9 (49.3 - 64.9) [b,d]
Fructose-6-phosphate	2.6 (1.9 - 3.2)	4.5 (2.6 - 5.4)	13.9 (10.4 - 17.2) [b]	5.3 (4.6 - 7.5)	5.4 (4.1 - 6.06) [b,d]	13.4 (13.1 - 18.7) [b,d]
Fructose 1.6-bisphosphate	8.3 (7.6 - 8.6)	12.6 (10.9 - 12.9)	42.1 (30.7 - 45.7) [b]	17.3 (14.6 - 22.9) [b]	14.1 (12.1 - 18.8) [b,d]	42.4 (35.5 - 49.5) [b,d]
Glyceraldehide 3-phosphate	7.1 (5.3 - 7.1)	3.6 (1.2 - 5.4)	4.7 (4.4 - 5.8) [a]	3.3 (2.8 - 3.4)	6.1 (4.6 - 11.1)	3.2 (2.5 - 5)
3-phosphoglycerate	36.6 (18.3 - 72.9)	26.2 (25.7 - 45.6)	22.4 (19.6 - 24.4)	9.5 (9.2 - 1) [b]	27.1 (18.7- 33.6)	5.9 (4.7 - 7.4) [b,d]
Phosphoenolpyruvate	73.3 (58.0 - 148.6)	58.1 (57.8 - 82.4)	86.4 (67.6 - 95.6)	64.2 (53.1 - 75.6)	86.6 (72.7 - 89.9)	47.2 (39.3 - 68.6)
Pyruvate	18.7 (15.7 - 20.8)	13.5 (12 - 15.5)	16.7 (16.1 - 18.2)	14.9 (12.6 - 16.8)	16.6 (14.9 - 23.2)	11.7 (11.7 - 14.7) [d]
Lactate	4942.2 (4941.4 -1509.5)	6248 (4984.5 - 8331)	11273.9 (9990.7 - 13532.1)	8608.5 (5800.8 - 10465.9)	15947.9 (15799.6 - 16145.6) [b,d]	9058.5 (3654.5 - 11769.1)
6 phosphogluconate	40 (37.5 - 62.5)	30.3 (18.3 - 43.7)	8.5 (7.7 - 11.1) [b]	5.9 (4.5 - 7.4) [b]	34.4 (18.2 - 51.4) [d]	14.6 (6.1 - 23.5) [b, c]
Ribose-5-phosphate	7.3 (7.1 - 21.7)	3.4 (2.5 - 7.9)	77.5 (67.2 - 97.6) [b]	71.1 (51.1 - 97.6) [b]	14.9 (9.8 - 44.7) [b,d]	24.5 (13.5 - 56.0) [b,d]
Citrate-isocitrate	1.1 (0.8 - 1.5)	0.8 (0.3 - 2.)	3.4 (1.3 - 4.7) [a]	2.3 (1.7 - 3.4)	1.5 (0.9 - 2.3) [c]	0.3 (0.3 - 0.8) [d]
Aconitate	393.9 (232.5 - 461.5)	36.6 (23.6 - 45.8)	275.1 (238.6 - 328.9)	88.1 (72.1 - 130.7) [b]	268.7 (210.5 - 385.6)	279.4 (205.4 - 324.2) [b,d]
α-ketoglutarate	0.7 (0.5 - 0.8)	0.5 (0.7 - 0.8)	0.6 (0.5 - 0.6)	0.5 (0.4 - 0.6)	0.5 (0.4 - 0.6)	0.4(0.3 - 0.5)
Succinyl-coa	152.8 (152.8 - 173.7)	304.9 (281.2 - 304.9)	37.8 (29.2 - 44.2) [b]	13.3 (13.2- 14.5) [b]	121.8 (120.5 - 128.3) [b,d]	22.2 (19.4 - 62.2) [b,d]
Succinate	75.1 (55.5 - 82.9)	41.4 (38.1 - 57.7)	75.3 (70.7 - 81.2)	60.7 (47.1 - 83.6) [a]	73.9 (48.5 - 170.3)	64.9 (57.1 - 73.3) [b]
Fumarate	7.5 (5 - 9.3)	3.7 (3.2 - 7.1)	5.8 (4.2 - 6.01)	3.6 (2.3 - 5.3)	6.2 (3.9 - 9.7)	4.2 (3.8 – 7.1)
Malate	328.7 (163.7 - 469.9)	299.6 (170.1 - 299.6)	149.08 (107.7 -173.1) [a]	71.5 (58.3 - 121.8) [b]	247.4 (129.7 - 335.3)	103.9 (102.9 - 113.6) [b]
Malonyl-coa	9.7 (8.1 - 12.6)	6.1 (3.3 - 7.1)	4.7 (3.8 - 5.5) [b]	1.1 (0.9 - 1.4) [b]	5.7 (5.549 - 7.373) [b,d]	1.5 (0.5 - 2.1) [b]
β-Hydroxybutirate	14.8 (12.6 - 14.8)	9.8 (7.4 - 11.9)	9.01 (6.9 - 10.6) [b]	10.2 (7.7 - 13.4)	13.239 (9.505 - 25.309)	14.5 (13.6 - 15.2) [b,d]
Glutamate	229.1(211.8 - 417.8)	98.6 (97.3 - 103.4)	121.3 (84.2 - 145.4) [b]	47.6 (29.6 - 69.9) [b]	158.5 (136.5 - 202.5) [b,d]	132.2 (101.4 - 160.8) [d]
Glutamine	1.2 (0.9 - 2.2)	1.8 (0.6 - 3.1)	3.4 (3.1 – 4.4) [b]	2.4 (1.6 - 3.1)	1.6 (0.9 - 2.2) [d]	0.4 (0.4 - 0.7) [b,d]
Alanine	931.1 (847.1 - 1135.4)	879.6 (874.2 – 885.1)	896.8 (674.9 - 1094.1)	564.1 (470.9 - 707.7) [b]	908.1 (742.9 - 1112.7)	655.9 (568.2 - 1144.4)
Serine	1447.4 (804.6 - 2419.3)	1653.3 (1591.3 - 1715.3)	392.4 (305.4 - 446.3) [b]	150.5 (136.9 - 211.1) [b]	935.4 (876.1 - 1225.9) [d]	495.5 (205.9 - 725.3) [b, c]
Valine	292 (239.1 - 405.1)	345.8 (243.5 - 397.8)	141.9 (130.2 - 47.5) [b]	87.2 (85.3 - 91.4) [b]	283.9 (189.1 - 359.3) [d]	132.7 (108.8 - 148.1) [b, d]
Isoleucine	50.7 (43.6 - 53.9)	92.9 (81.8 - 92.9)	32.6 (30.9 - 38.1) [b]	21.4 (20.7 - 31.1) [b]	49.2 (36.3 - 50.9) [d]	25.9 (20.8 - 33.7) [b]
Leucine	578.6 (467.4 - 578.6)	770.4 (758.6 - 782.2)	277.9 (243.8 - 295.8) [b]	142.3 (133.3 - 215.6) [b]	517.6 (403.3 - 686.3) [d]	200.5 (160.1 - 260.1) [b]
Aspartate	204.5 (199.4 - 697.5)	506.1 (296.3 – 715.8)	310.3 (203.3 - 446.6)	146.3 (76.1 - 211.6) [b]	198.8 (161.9 - 281.9) [d]	290.3 (270.5 - 301.1) [b,d]

Table 5. Hepatic energy-balance metabolites. Values are expressed in µM/ 100 mg of tissue (mean (interquartile range) illustrating dietary-based differences between standard chow diet (CD) or high fat diet (HFD) in all strains. PLKO denotes *ccl2*$^{+/+}$, *pon1*$^{-/-}$, *ldlr*$^{-/-}$ and CPLKO *ccl2*$^{-/-}$, *pon1*$^{-/-}$, *ldlr*$^{-/-}$; [a] $p<0.05$, [b] $p < 0.001$, with respect to WT; [c] $p < 0.05$, [d] $p< 0.001$ with respect to PLKO.

Oxidative stress-induced dysfunction in the liver methionine transmethylation and trans-sulfuration pathways may be restored by ccl2 deficiency

The liver regulates the flux of methionine through essential mechanisms affecting DNA, and protein methylation and the synthesis of the antioxidant glutathione. We observed significant differences in the levels of metabolites between PLKO and WT mice that were completely or partially averted in CPLKO animals (Table 6 and Figure 24). For instance, there was a significant 4-fold decrease in methionine concentrations in PLKO mice when compared with the other strains, and the difference was maintained when fed CD or HFD. Homocysteine levels were also lower in PLKO mice, suggesting a significantly reduced flux in transmethylation. There were major changes in SAM and SAH, substrate and product of essential methyltransferase reactions in PLKO mice. SAM levels were decreased in these animals, but differences only reached statistical significance when fed an HFD. In contrast, SAH levels increased dramatically, with a major impact on the SAM/SAH ratio. This decrease in the SAM/SAH ratio due to increased SAH correlated with homocysteine levels and probably suggests considerable alteration in the methylation status of hepatocytes. The SAM/SAH ratio in CPLKO mice was not different from that observed in WT mice, indicating reversal in causal mechanisms (Figure 24). The reduced flux in methionine transmethylation of PLKO mice affects the efficient utilization of methionine for the synthesis of GSH via the trans-sulfuration pathway. GSH is the most abundant antioxidant in hepatocytes and is critical for protecting cells from oxidative stress, acting as a free radical scavenger and inhibitor of lipid peroxidation. In PLKO mice, the GSH to GSSG ratio was extremely low, and we observed a greater mRNA expression of glutathione peroxidase and glutathione reductase than in WT and CPLKO animals (Figure 25). The GSH/GSSG ratio is an indicator of cellular health, and the reduced ratio indicates major cellular injuries because under normal conditions, reduced GSH represents up to 90% of cellular GSH. Interestingly, deficiency in CCL2 may be effective in maintaining hepatocytes' redox potential, but the levels were not completely reversed (Figure 25). Our findings suggest that measurement of the GSH/GSSG ratio in the liver may bear usefulness in research focused on specific NAFLD therapeutics and the potential relationship between oxidative stress and epigenetic mechanisms.

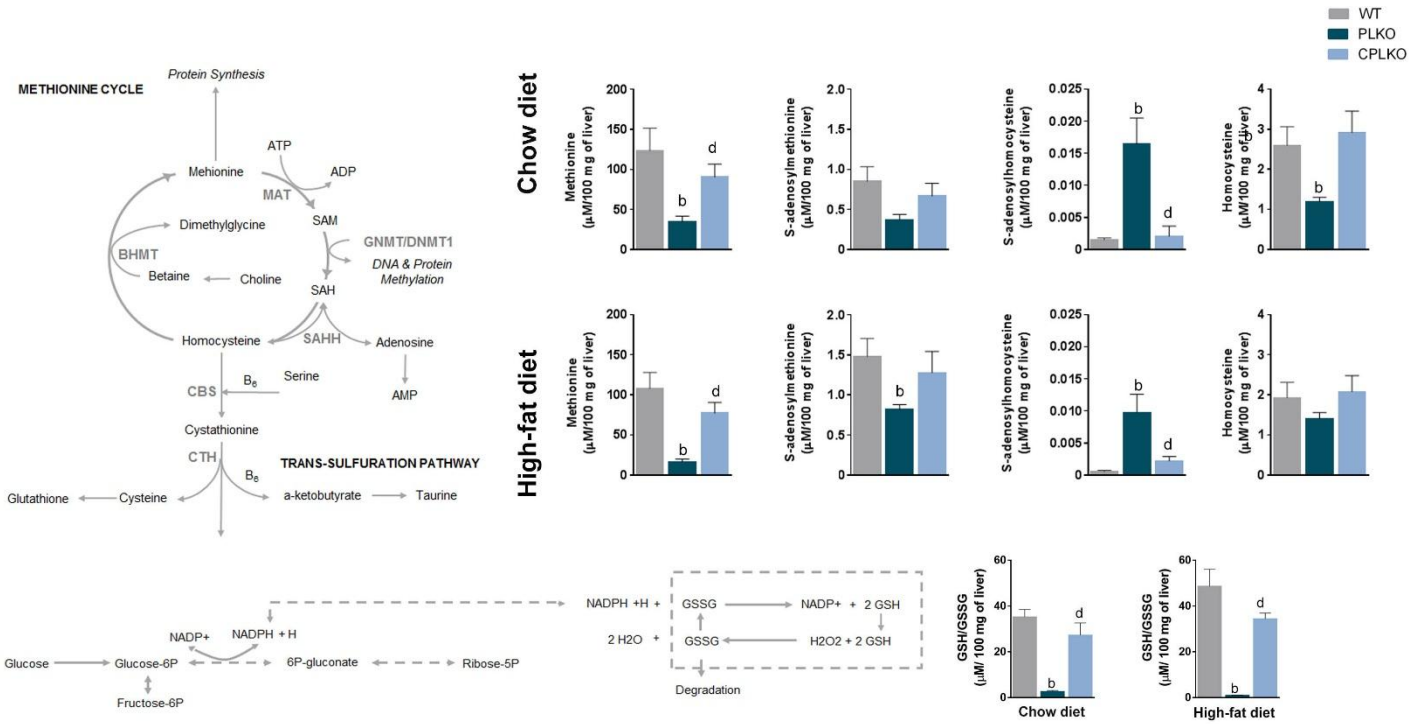

Figure 24. The relative impact of dietary fat on the levels of metabolites associated with the methionine cycle and trans-sulfuration pathways in the liver. PLKO denotes *ccl2*$^{+/+}$, *pon1*$^{-/-}$, *ldlr*$^{-/-}$ and CPLKO denotes *ccl2*$^{-/-}$, *pon1*$^{-/-}$, *ldlr*$^{-/-}$. Values are mean ± SEM (n=8 per genotype and dietary condition) ^{b} $P < 0.001$, with respect to WT; ^{d} $P < 0.001$, with respect to PLKO.

Metabolite	*WT*		*PLKO*		*CPLKO*	
	CD	**HFD**	**CD**	**HFD**	**CD**	**HFD**
Homocysteine	2.4 (2.1 - 2.9)	2.3 (2.1 - 2.7)	1.2 (1 - 1.4)	1.441 (1 - 1.6)[d]	2.1 (1.4 - 4.1)	2 (1.4 - 2.7)
Choline-Dimethlyglycine	15 (10.8 - 22.6)	10 (7.4 - 10.4)	11.7 (6.7 - 15.1)	12.9 (9 - 18.8)[a]	27.9 (21.4 - 48.4)[a,d]	15.6 (9.6 - 20.9) [d]
Betaine	0.02 (0.01 - 0.06)	0.1 (0.01 - 0.2)	0.1 (0.04 - 0.09)	0.1 (0.04 - 0.1)	0.003 (0.003 - 0.01) [b,d]	0.04 (0.03 - 0.1) [d]
Methionine	99 (70.2 - 231.3)	99.4 (72 - 185.6)	28.9 (19.2 - 48.4)[b]	11.5 (8.7 - 27.9)[a]	89.3 (47.3 - 118.2)[d]	64.1 (51 -120)
SAM	0.6 (0.4 - 1.2)	1.4 (1.1 - 1.9)	0.4 (0.3 - 0.7)	0.9 (0.7 - 0.9) [a]	0.6 (0.4 - 1)	1.3 (0.5 - 1.7)
SAH	0.001 (0.001 - 0.002)	0.0003 (0.0001 - 0.001)	0.01 (0.01 - 0.03) [b]	0.01 (0.01 - 0.02)[b]	0.001 (0.0003 - 0.001)	0.001 (0.001-0.004)[a]
AMP	10 (8.4 - 11.4)	7.3 (5.3 - 8.5)	15.8 (9.1 - 26.1)	16.5 (13.6 - 20.1)[b]	8.5 (5.8 - 24)	12.2 (8.6 - 22.3)[a]
Cystathionine	0.004 (0.003 - 0.011)	0.007 (0.002 - 0.01)	0.004 (0.002 - 0.01)	0.002 (0.001 - 0.005)	0.004 (0.002 - 0.01)	0.003 (0.001 - 0.01)
Taurine	93.3 (85.9 - 210.2)	1827.3 (1291.8 - 2577.1)	363.3 (311.8 - 501.)[b]	1171.1 (1118.7 - 1695.8)	1192.9 (361.1 - 1769.5)[b]	1313.9 (356.5 - 2485.2)
Glutathione disulfide (GSSG)	13.4 (11.4 - 13.9)	8.4 (7.1 - 13.6)	240.605 (238.4 - 266.2) [b]	772.9 (543.1 - 7313.6)[b]	14.1 (10.1-21.4)[d]	15.3 (12.9 - 18.9)[a]
Glutathione (GSH)	439.7 (351.1 - 581.7)	453.2 (361.5 - 476.3)	653.328 (596.1 - 725.2)[b]	1171.1 (1118.7 - 1695.8)[a]	414.4 (320.1 - 475.6)[d]	513.8 (425.5 - 688.3)

Table 6. Metabolites in methionine cycle and trans-sulfuration pathway. Values are expressed in µM/ 100 mg of tissue (mean (interquartile range)) illustrating dietary- based differences between standard chow diet (CD) or high fat diet (HFD) in all strains. PLKO denotes *ccl2*$^{+/+}$, *pon1*$^{-/-}$, *ldlr*$^{-/-}$ and CPLKO *ccl2*$^{-/-}$, *pon1*$^{-/-}$, *ldlr*$^{-/-}$; [a] $p < 0.05$, [b] $p < 0.001$, with respect to WT; [c] $p < 0.05$, [d] $p < 0.001$ with respect to PLKO.

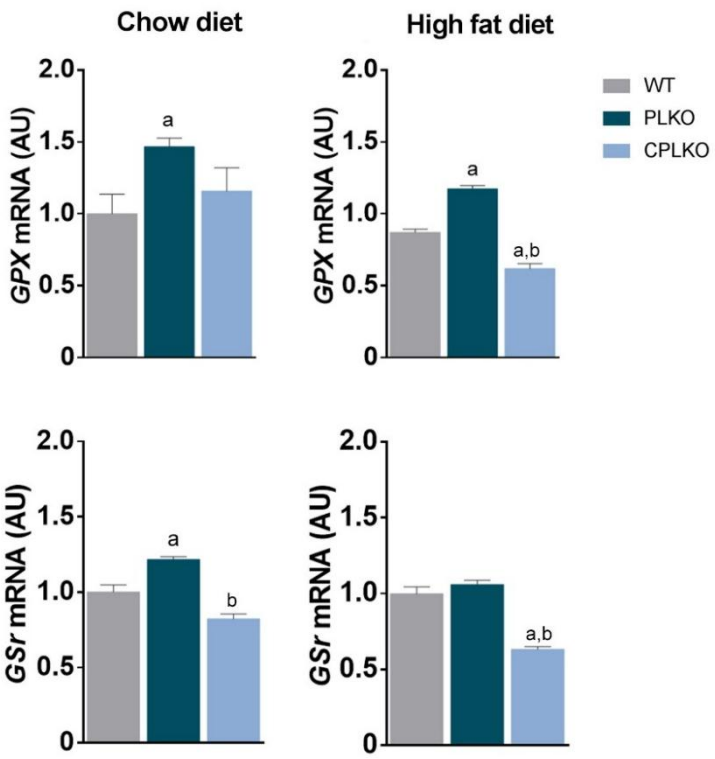

Figure 25. Relative hepatic mRNA expression of glutathione peroxidase (*Gpx*) and glutathione reductase (*Gsr*) in wild type (WT), PLKO and CPLKO mice. PLKO stands for *ccl2*$^{+/+}$, *pon1*$^{-/-}$, *ldlr*$^{-/-}$ mice, and CPLKO stands for *ccl2*$^{-/-}$, *pon1*$^{-/-}$, *ldlr*$^{-/-}$ animals. Values are mean ± SEM [a] $p < 0.05$, with respect to wild type mice; [b] $p < 0.05$, with respect to PLKO mice.

Assessment of the role of ccl2 in hepatic autophagy-lysosomal function

In the liver, autophagy not only contributes to the maintenance of normal hepatocyte functions but also may respond to pathogenic changes. Autophagy was essentially suppressed or clearly reduced in genetically modified mice with respect to WT mice as assessed by low levels of LC3 II/I ratio (Figure 26), probably indicating a direct relationship with PON1 deficiency and high oxidative stress. We examined the Atg7, which was highly dependent on dietary conditions but did not significantly differ among strains. In contrast, mTOR was highly activated in genetically modified strains, as shown by the significant increase in the ratio between the phosphorylated and the non-phosphorylated forms. These changes probably refer to mTORC1 as indicated by a significantly higher expression of P4EBP1 and were associated with low levels of AMPK activation. In addition, Akt was also highly activated in PLKO and CPLKO mice. Considering the induced changes in liver histologic features and metabolic perturbations by the ablation of *ccl2* in PLKO mice, the lack of differential effects in the Akt/AMPK/mTOR pathway or the repression of autophagy appears noteworthy (Figure 26). Then, we explored the expression of LAMP2A, which was significantly increased in CPLKO mice with respect to PLKO mice levels, with even more dramatic effects when mice were fed HFD, suggesting a potential role of chaperone-mediated autophagy in the remission of oxidative stress. Taken together, our data indicate that PON1 deficiency is associated with decreased autophagosome formation, which is independent of CCL2. In contrast, CCL2 might affect CMA.

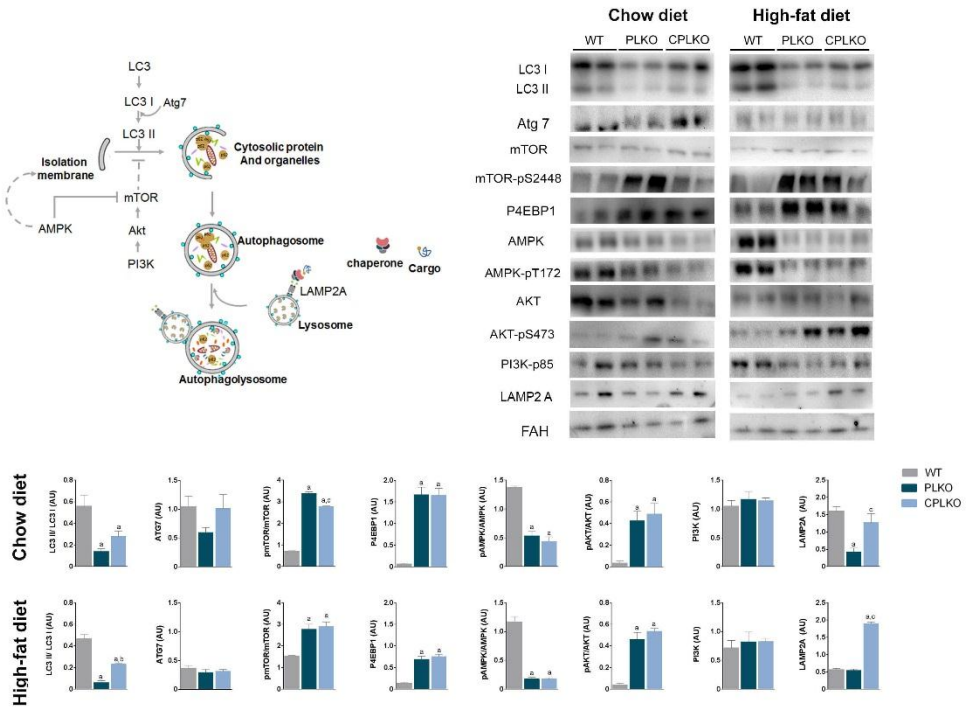

Figure 26. Overall assessment of autophagy-lysosomal function through Western blot analysis of selected molecules, including microtubule-associated protein 1A/1B light chain 3B (LC3), autophagy-related protein 7 (Atg7), mammalian target of rapamycin (mTOR), mTOR-p S448, eukaryotic translation initiation factor 4E-binding protein 1 (P4EBP1), AMP-activated protein kinase (AMPK) AMPK-p T172, protein kinase B (AKT), AKT-pS473, phosphoinositide 3-kinase p85 subunit (PI3K-p85), lysosome associated membrane protein 2 (LAMP2A), and fumarylacetoacetate hydrolase (FAH). PLKO denotes *ccl2*$^{+/+}$, *pon1*$^{-/-}$, *ldlr*$^{-/-}$ and CPLKO denotes *ccl2*$^{-/-}$, *pon1*$^{-/-}$, *ldlr*$^{-/-}$. Representative bands are from pooled liver homogenates from randomly selected samples. Values for calculations are mean ± SEM (n=8 per genotype and dietary condition); [a] $P < 0.05$, [b] $P < 0.01$, with respect to WT; [c] $P < 0.05$, with respect to PLKO.

Study 2

Metabolic reprogramming: The role of chemokine (C-C motif) ligand 2 in liver tissue and muscle metabolism

UNIVERSITAT ROVIRA I VIRGILI
THE ROLE OF CHEMOKINE (C-C MOTIF) LIGAND 2 IN INFLAMMATION, OXIDATIVE STRESS, AGING AND METABOLISM
Fedra Nicaury Luciano Mateo

Results

Phenotypic alterations associated to Ccl2 overexpression

CgCcl2 mice did not show any detectable difference in longevity, behavior or reproduction respect to WT. However, these mice showed a significantly lower body weight together with higher concentrations of serum glucose, cholesterol and triglycerides. Serum AST and ALT activities were also higher with respect to WT (Figure 27).

As expected, *CgCcl2* mice displayed higher CCL2 concentrations than WT animals in all tissues examined. *Ccl2* overexpression was associated to higher liver weight and lower muscle weight (Figure 28). For this, histological analysis was performed in liver and muscle. We observed that *CgCcl2* mice accumulated lipid droplets in the liver and had muscle atrophy and lower F4/80 stained cells as compared with WT animals, without any remarkable evidence of fibrosis (Figure 29 A). Moreover, we observed that these animals had a lower hepatic expression of pro-inflammatory markers such as CD11b and TNFα. In contrast, we found an upregulation of CD163, an anti-inflammatory marker. Despite of this data, *CgCcl2* mice did not show any significant alteration in PON1 expression, indicating a similar degree of oxidative stress. In muscular tissue we only found a significant decrease of TNFα expression (Figure 29 B). The levels of CD11b, CD163 and PON1 were similar to those of WT animals.

Ccl2 overexpression induced opposite changes in mitochondrial electron transport chain complexes in the liver and muscle.

We analyzed the protein levels of mitochondrial electron transport chain complexes (OXPHOS) to determine whether *Ccl2* overexpression is associated with mitochondrial alterations. *CgCcl2* mice had decreased hepatic levels of complexes I (CI-NDUFB8), III (CIII-UQCRC2), IV (MTCO1), and V (CVNDUFB8) but not of complex II (CII-SDHB). These results suggest that the hepatic ATP synthesis capacity is severely impaired or inactive. In addition, CgCcl2 mice had an increase of TOM20 protein concentration with respect to WT and a downregulation of MFN2, indicating that *Ccl2* overexpression induces alterations in liver mitochondrial quality and function. In contrast, when we analyzed the muscle tissue, we observed a hyperactivation of complexes I, II, IV, and V of OXPHOS, and a decrease in TOM20 expression, without any significant alterations in MFN2 (Figure 30).

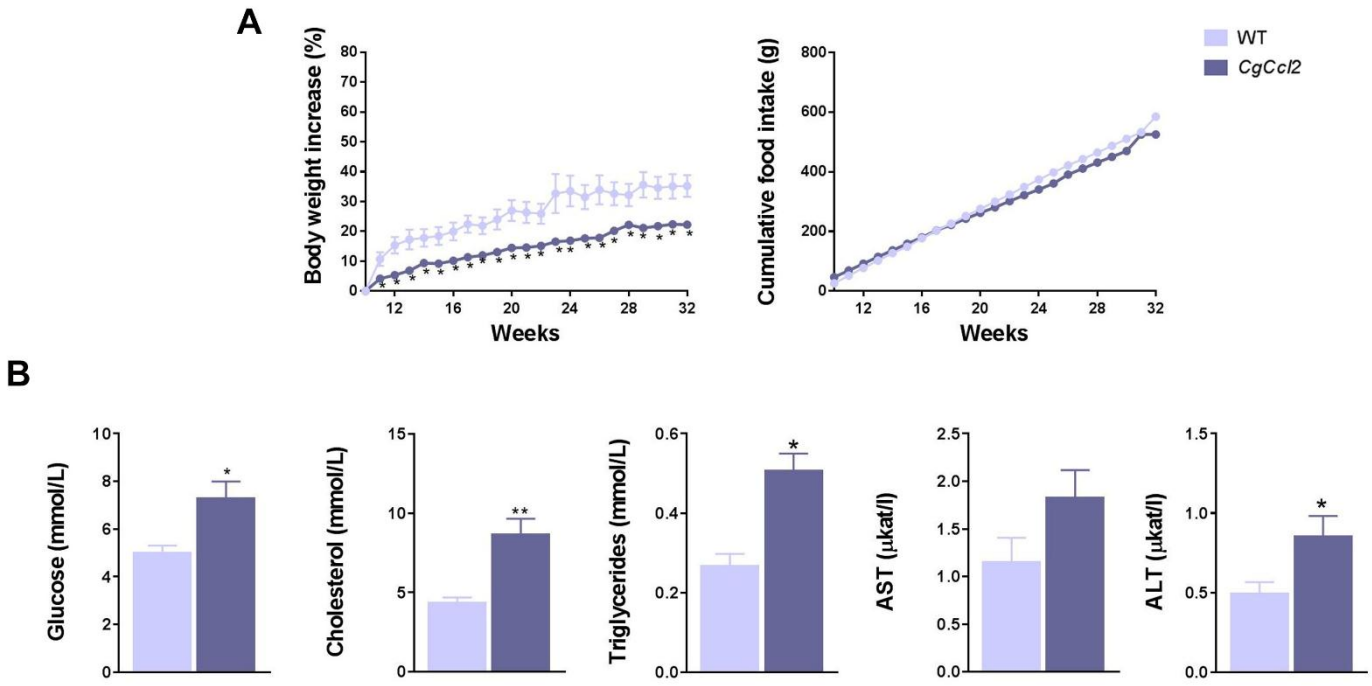

Figure 27. Selected metabolic features in wild type (WT) and *Ccl2* cisgenic mice (*CgCcl2*). Results are shown for (A) body weight increase and (B) biochemical variables. Values are mean ± SEM (n=8) * $p < 0.05$, ** $p < 0.001$, with respect to control littermates (WT).

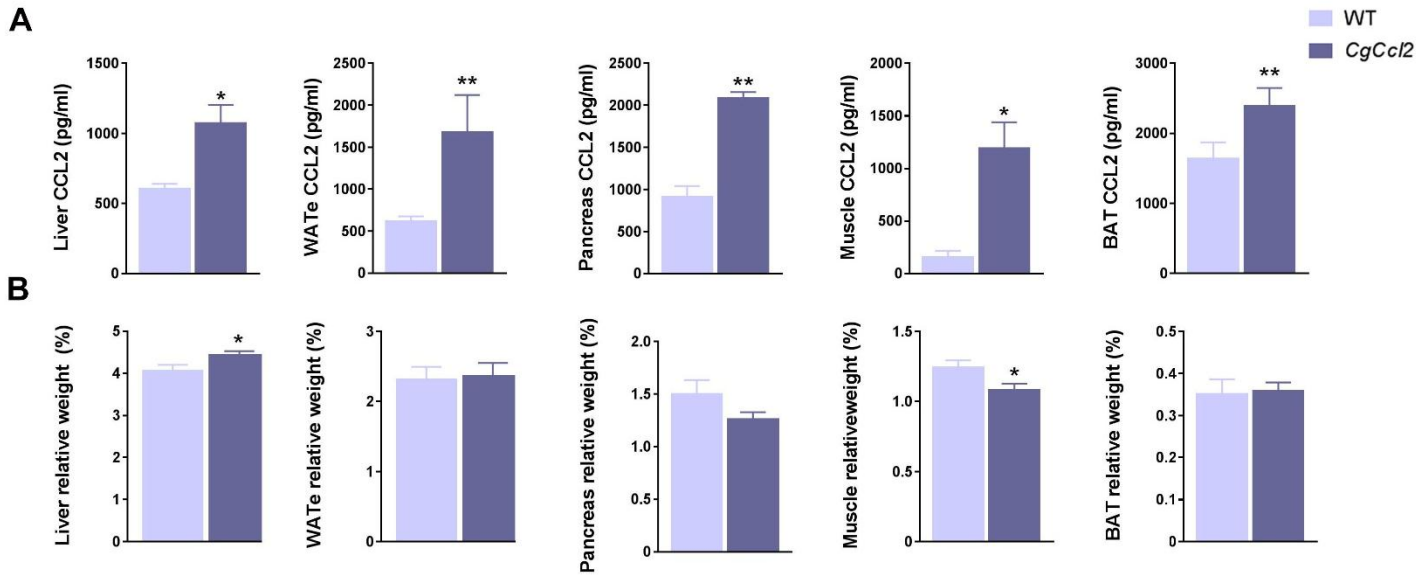

Figure 28. CCL2 overexpression in metabolic tissues. (A) CCL2 concentrations in liver, white adipose tissue (eWAT), pancreas, muscle and brown adipose tissue (BAT) in wild type (WT) and *Ccl2* cisgenic mice (*CgCcl2*). (B) Effect of Ccl2 overexpression in the weight of selected tissues. Results are shown as means ± SEM (n=8) * $p < 0.05$, ** $p < 0.001$, with respect to control littermates (WT).

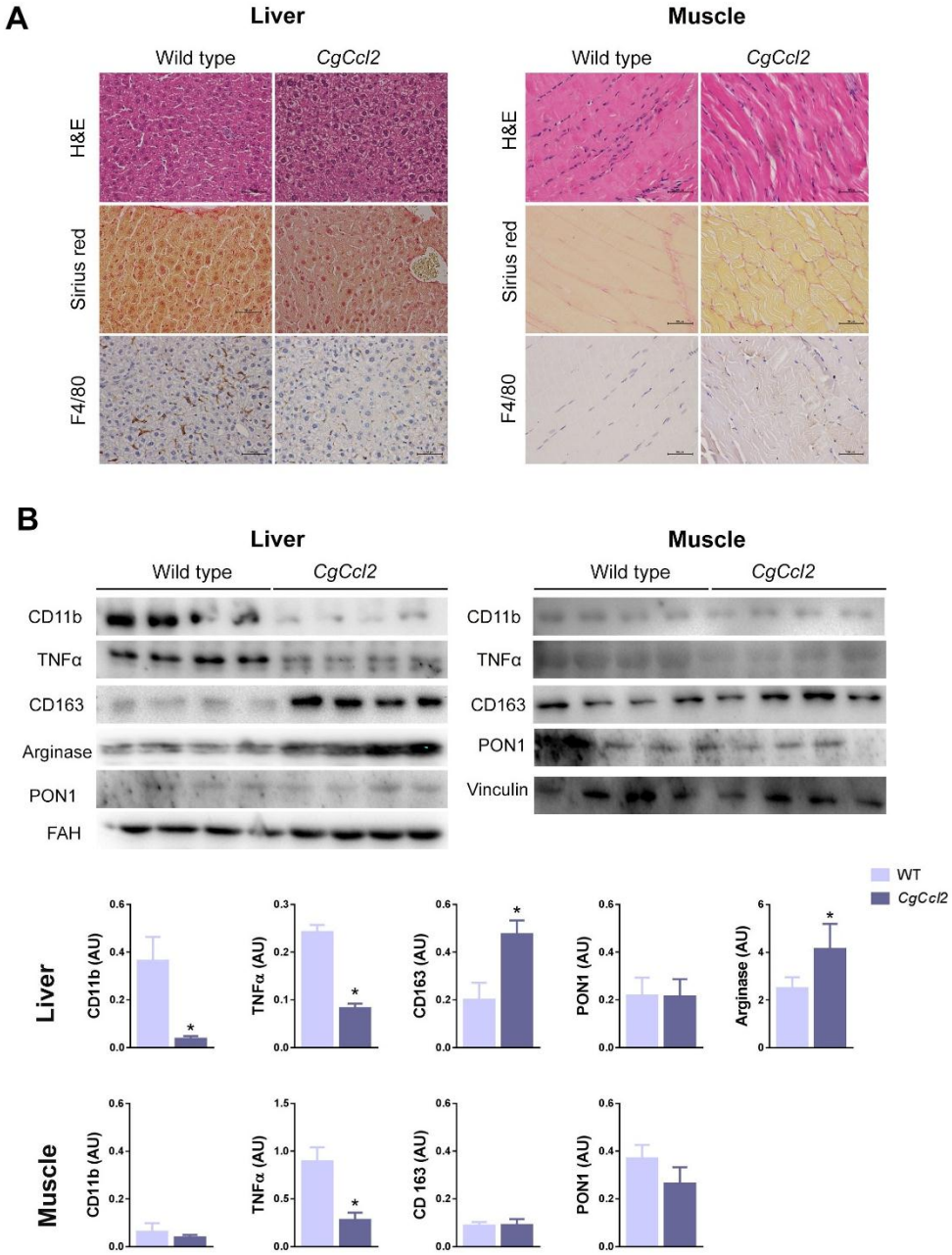

Figure 29. Influence of CCL2 overexpression in liver and muscle histological features, inflammation and oxidative stress. (A) Representative microphotographs of liver and muscle sections stained with hematoxylin and eosin (H&E), sirius red staining and F4/80 immunohistochemistry. (B) Western blot analysis of cluster of differentiation (CD) 11b, tumor necrosis factor (TNFα), CD163, liver arginase and paraoxonase 1 (PON1). Results are shown as means ± SEM (n=8) * $p < 0.05$ with respect to control littermates (WT).

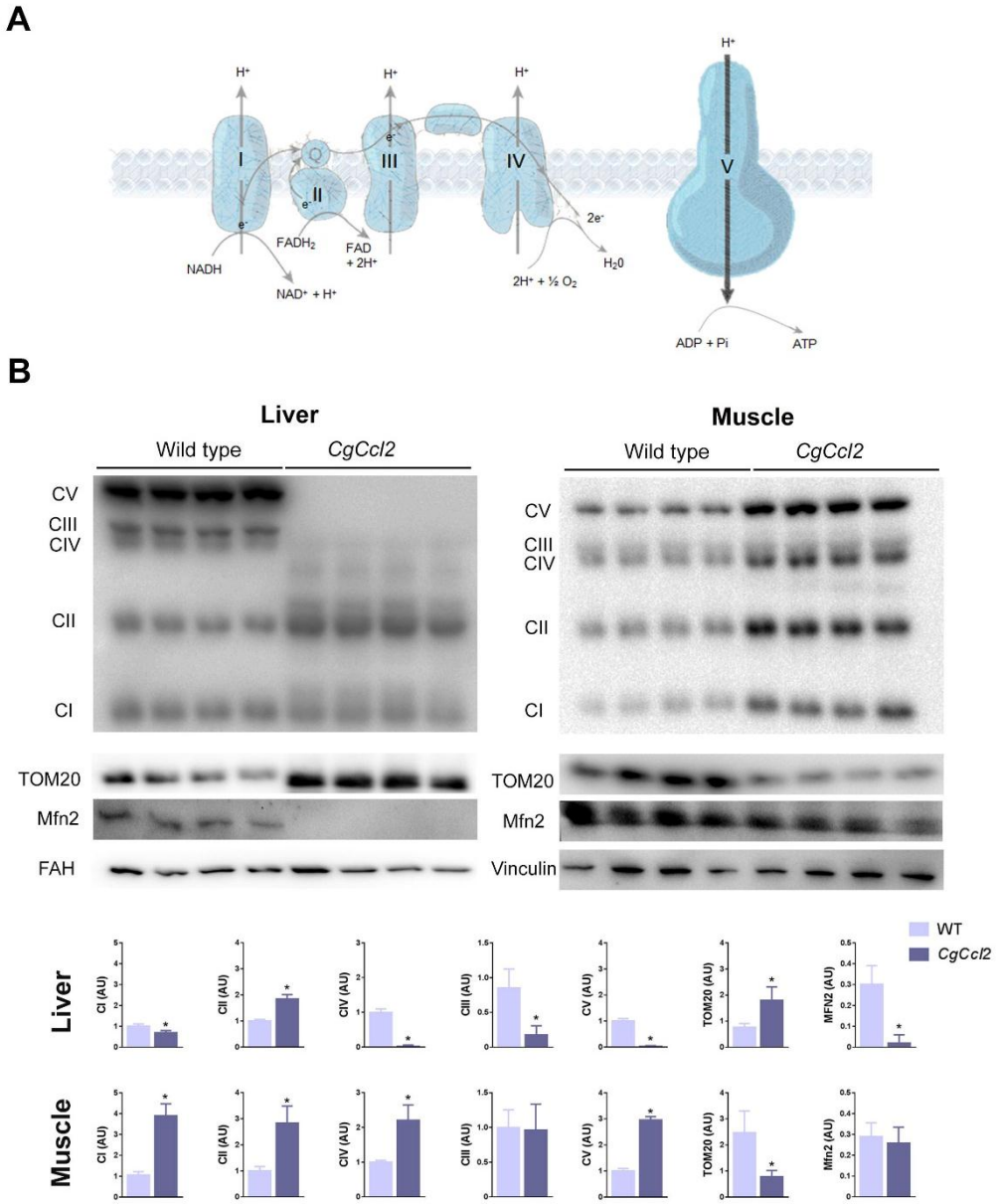

Figure 30. **Repercussion of CCL2 overexpression on the mitochondrial status.** (A) Schematic representation of oxidative phosphorylation complexes (OXPHOS). (B) Repercussion of CCL2 overexpression in OXPHOS, mitofusin 2 (MFN2) and translocase of the outer membrane (TOM20) in liver and muscle tissues. Results are shown means ± SEM; * $p < 0.05$, with respect to control littermates (WT).

Ccl2 overexpression induced different alterations in energy metabolism, one-carbon metabolism and autophagy in the liver and muscle

We further analyzed the energy metabolism and one-carbon metabolism to deepen into the molecular mechanisms by which *Ccl2* overexpression induces liver and muscle alterations. PLSDA analysis showed a clear segregation between *CgCcl2* and WT mice in both tissues. Results of energy-related metabolites are shown in Figure 31 and Supplementary Table 6.

In the liver, we observed important alterations in metabolites involved in the CAC (Figure 31 A). Specifically, we found lower concentrations of citrate, isocitrate, oxaloacetate, fumarate, together with higher levels of succinate in cisgenic mice compared to WT animals. These results confirm that *Ccl2* overexpression causes alterations in hepatic mitochondrial function. In contrast, the analysis of muscular tissue showed higher levels of all metabolites analyzed. The most remarkable changes were in glucose, 3 phosphoglycerates, pyruvate, lactate, ribose 5 phosphate, β-Hydroxybutyrate, succinate, aconitate and oxaloacetate concentrations (Figure 31 B). These results suggest an increase of anaerobic glycolysis and ketonic body synthesis as an ATP alternative source.

Results of one-carbon metabolites are shown in Figure 32 and Table 7. We found an alteration in the homocysteine transmethylation in the livers of *CgCcl2* mice with respect to WT (Figure 32 A). *Ccl2* overexpression induced a depletion of methionine and increases in choline, dimethylglycine, betaine, and 5-methyltetrahydrofolate, suggesting an alteration in the enzyme betaine homocysteine methyltransferase. On the other hand, we did not observe any remarkable alteration in one-carbon metabolism in muscle tissue (Figure 32 B).

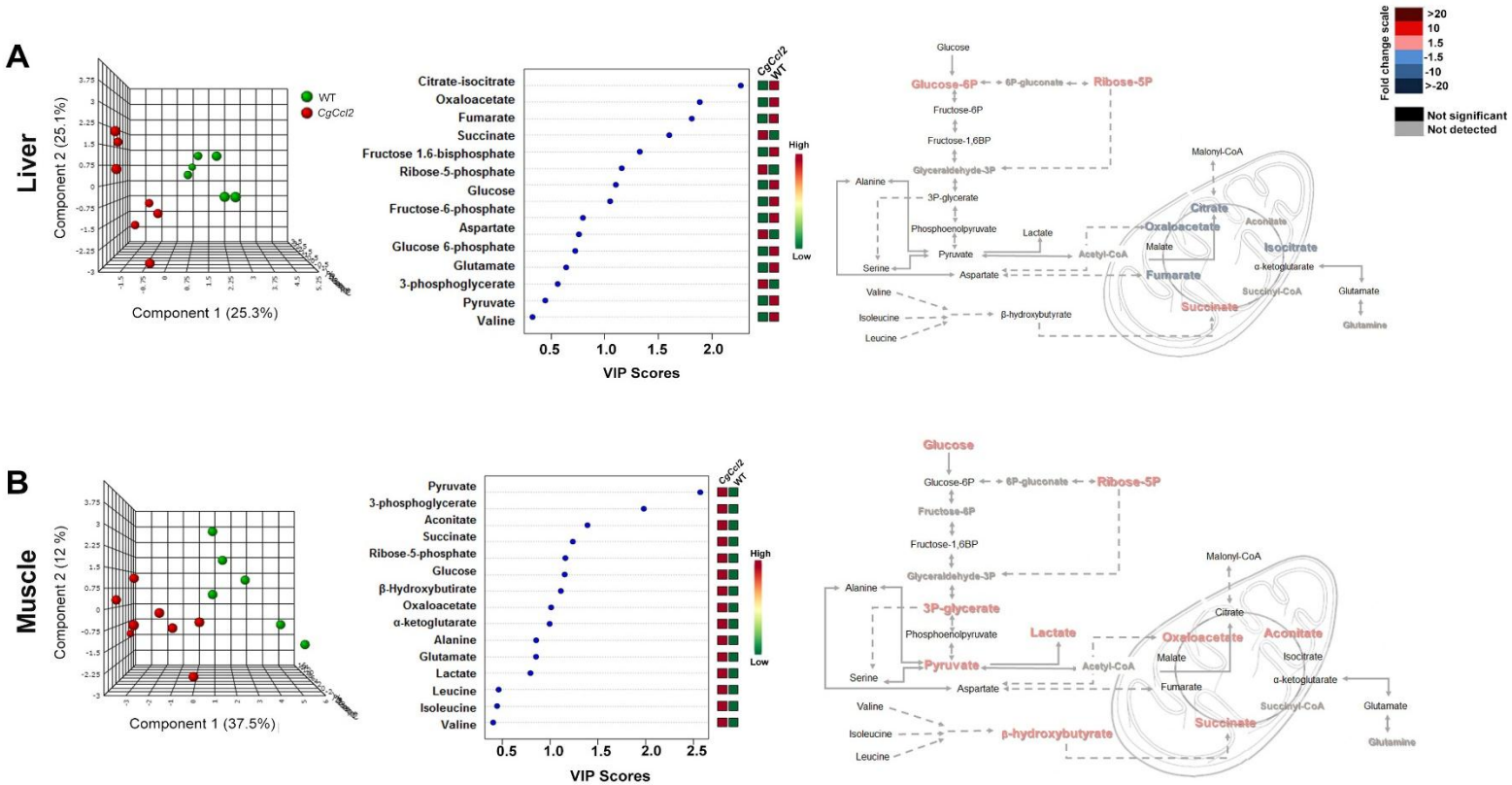

Figure 31. Repercussion of CCL2 overexpression on the levels of metabolites associated with energy metabolism in the liver. (A) and muscle tissue (B). From left to right, the partial least square discriminant analysis (PLSDA), variable importance in projection (VIP) score and fold changes of metabolite levels comparing cisgenic mice with wild type animals.

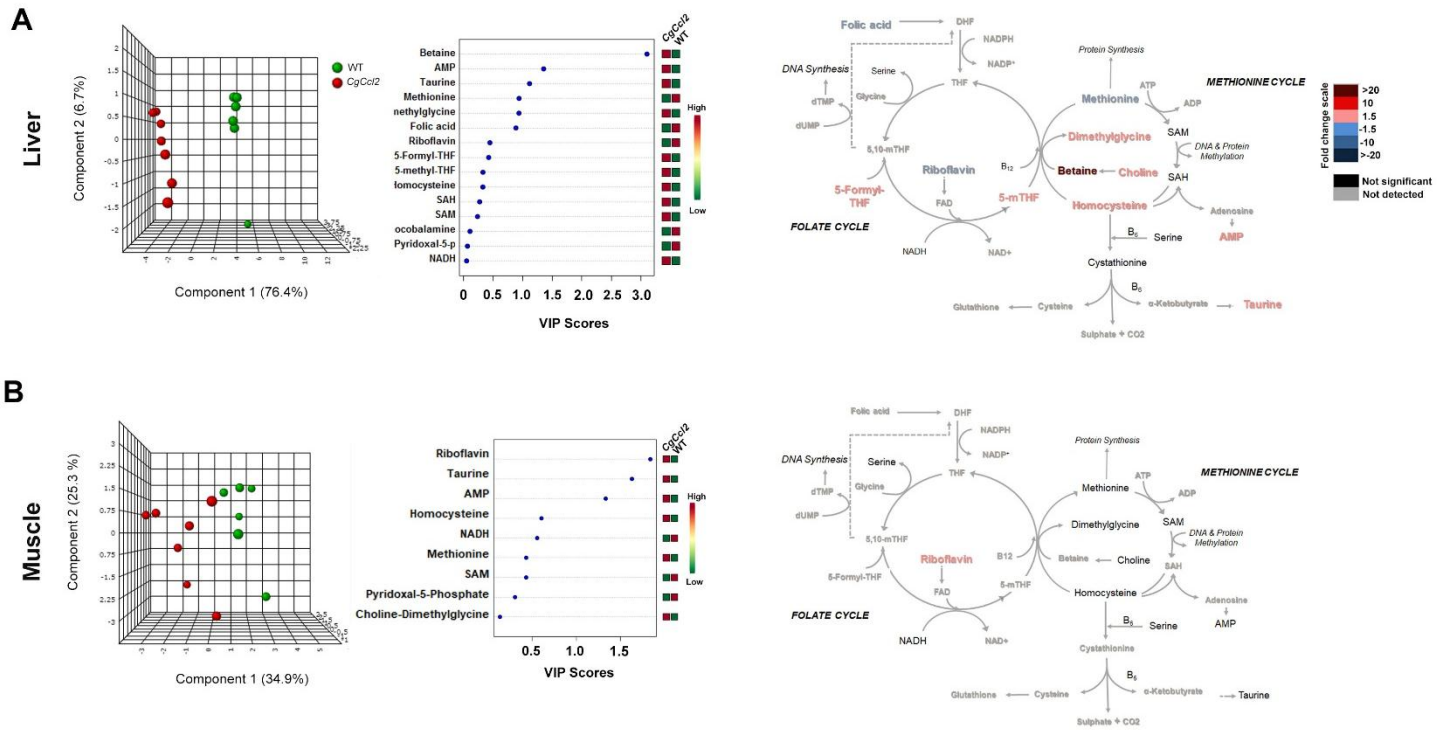

Figure 32. Repercussion of CCL2 overexpression on the levels of metabolites associated with one-carbon metabolism in the liver. (A) and muscle tissue (B). From left to right, the partial least square discriminant analysis (PLSDA), variable importance in projection (VIP) score and fold changes of metabolite levels comparing cisgenic mice with wild type animals.

	Liver		*Muscle*	
Metabolites	**Wild type**	***CgCcl2***	**Wild type**	***CgCcl2***
Glucose	53097.7 (42523.5-68695.5)	44395.8 (16996-55033.1)	373.4 (345-394.2)	726.3 (681.4-1314.1)*
Glucose 6-phosphate	45.1 (39.1-48.3)	103.6 (48.7-132.7)*	16 (12.8-18.8)	15.6 (10-25.8)
Fructose-6-phosphate	428.4 (258.9-552.7)	391.5 (136.6-474)	-	-
Fructose 1.6-bisphosphate	63.4 (52.3-85.7)	60.6 (11.8-94.4)	3.6 (2.4-13.4)	7 (2.9-10.8)
3-phosphoglycerate	15.7 (14.7-22.1)	22.3 (17.2-25)	1.9 (1.6-3.2)	5.8 (2.6-7.9)*
Phosphoenolpyruvate	8.1 (6.1-15.6)	9 (8.3-12.3)	0.5 (0.3-1.1)	0.5 (0.5-0.7)
Pyruvate	422 (325.7-570.5)	337.8 (247.5-491.5)	68.8 (54.8-221.2)	597.3 (499.3-675.2)*
Lactate	16199.3 (14922.1-16470.7)	14521.1 (12177.8-18810.5)	9815.7 (6626.5-16649.8)	17001 (8834.4-27368.7)*
Ribose-5-phosphate	27.6 (24.5-32.3)	55.1 (51.7-71)*	9 (7.8-10.7)	18.4 (16.6-30.2)*
Oxaloacetate	946.7 (701.9-1143.8)	464 (222.4-821.4)*	27.7 (15.7-33.4)	58.9 (48.4-66.9)*
Citrate-isocitrate	28.9 (14.9-39.8)	8.9 (6.8-17)*	51.6 (27.1-119.4)	53.1 (30.5-125.6)
Aconitate	-	-	11.5 (10.3-12.9)	35.8 (14.8-56.4)*
α-ketoglutarate	21.2 (15.2-26.9)	18.9 (10.7-28)	2.1 (1.2-5.1)	4.5 (1.2-7.8)
Succinate	382.9 (247.7-411.5)	471.5 (386.4-563.4)*	41.2 (38.1-79.1)	110.3 (110.3-126.8)*
Fumarate	485.3 (405.2-686.8)	323.4 (273.9-330.9)*	143.7 (56.9-217.6)	160 (116-167.3)
Malate	1191.6 (932.2-1552.4)	825.4 (614.7-1408)	322.2 (133.8-502)	373.3 (308.4-379.9)
β-Hydroxybutirate	216.4 (162.2-250)	215.8 (168.6-288.2)	38.4 (22-51.3)	76.1 (76.1-84.8)*
Glutamate	10659.9 (8844.7-15265.4)	9457.2 (6229.3-12508.3)	1673 (1212.6-2498.8)	2648.6 (1750.1-4824.8)
Alanine	515.8 (466.5-706.2)	517.3 (396.7-656.6)	362.2 (286.4-414.6)	508.2 (432.2-1155.3)
Serine	2282.2 (2261.4-2327.6)	2253.8 (2045.9-3281)	1007.8 (591.2-1375)	1008.1 (660.7-1749.1)
Valine	551.7 (469.8-702.5)	622.1 (339.3-788.6)	123.3 (75.9-201.2)	158.8 (95.9-252.4)
Isoleucine	568.6 (552.6-585.7)	603.8 (442.2-790.6)	77.1 (45-116.7)	101.3 (55.6-181)
Leucine	1440.7 (1398.9-1469.4)	1509.9 (1248.6-1886.2)	163.8 (102-260.6)	262.3 (124.5-389.6)
Aspartate	253.9 (226.8-332.6)	201.6 (154.9-276.5)	245 (108.4-374.3)	258.6 (207.4-343.2)

Table 6. Hepatic and muscle energy metabolites. Values are expressed in µM/ 100 mg of tissue (mean (interquartile range). ǂ Values are expressed in nM/100 mg of tissue**.** * $p < 0.05$, **$p < 0.001$ respect to wild type group. The lack of values denotes a significant number of observations under the limit of quantification.

	Liver		*Muscule*	
Metabolites	**Wild type**	***CgCcl2***	**Wild type**	***CgCcl2***
Cystathionine‡	6.7 (6.2-11.2)	8.8 (6.9-8.9)	-	-
Taurine	494.2 (274.4-541.1)	1027.7 (884.6-1582.1)*	1499.7 (601.8-3621.9)	2385.2 (1811.5-5839.9)
Choline-Dimethylglycine	13.9 (8.1-15.5)	36.9 (36.6-47.6)*	0.1 (0.1-0.2)	0.1 (0.1-0.2)
Betaine‡	15 (13.2-15.2)	1012.5 (448.6-1497.7)**	-	-
Homocysteine	0.7 (0.6-0.8)	1.1 (1-2.4)*	0.3 (0.3-0.4)	0.4 (0.2-0.7)
SAM	1.2 (0.9-1.4)	1.5 (1.5-1.6)	3.3 (1.7-4.5)	2.7 (2.3-2.9)
Methionine	42.1 (41-42.7)	9.9 (8.7-19.2)**	0.6 (0.6-0.7)	0.7 (0.3-1.2)
AMP	57.4 (56.1-61.8)	338.8 (338.8-407.9)**	3.7 (2.1-5.7)	7.7 (3.8-10.7)
NADH	12.5 (10.9-14.6)	13.8 (13-14.4)	1.7 (1.3-2.5)	1.5 (0.7-2.5)
SAH‡	33.5 (24.7-46.2)	52.1 (29.2-75.1)	-	-
Pyridoxal 5 phosphate	12.5 (12.5-12.5)	10.3 (9.4-14.1)	3.5 (2.2-7.1)	3.4 (3.4-3.4)
5-Methyl-tetrahydrofolate	4.2 (3.5-5.8)	7.4 (5.3-8.5)*	-	-
5-Formyl-tetrahydrofolate‡	32.8 (24.8-37.7)	65.6 (39-66.7)*	-	-
Folic acid	0.3 (0.3-0.3)	0.1 (0.1-0.1)*	-	-
Cyanocobalamin‡	3.4 (2.9-3.8)	2.9 (2.5-3.3)	-	-
Riboflavin	10.6 (9.5-13.9)	6.5 (5.7-6.5724)*	0.5 (0.2-0.9)	0.9 (0.9-1)*

Table 7. Hepatic and muscle one-carbon metabolites. Values are expressed in µM/ 100 mg of tissue (mean (interquartile range). ‡ Values are expressed in nM/100 mg of tissue**.** * $p < 0.05$, **$p < 0.001$ respect to wild type group. The lack of values denotes a significant number of observations under the limit of quantification.

We next explored the impact of *Ccl2* overexpression on different cell energetics sensors. As seen in Figure 33, the regulation of the energetic response was different in liver and muscle. In hepatic tissue, *Ccl2* overexpression induced an inactivation of AMPK respect to WT mice and the upregulation of mTORC1, expressed by low pAMPK/AMPK ratio and high pS6/S6 ratio. Resulting in low levels of LC3II/LC3I ratio, which suggests a reduction in autophagosome formation. Similarly, we observed a low expression of p62/SQSTM1 without changes in LAMP2A levels. These disturbances were accompanied of an inactivation of insulin growth factor pathway as indicated by a downregulation of its downstream components PI3K-P85 and pAKT/AKT ratio. On the contrary, in muscle, *CgCcl2* mice had a significant AMPK activation, associated with low levels of mTORC1 as indicated by the reduced phosphorylation of its targets pS6/S6 ratio. Consequently, we observed an activation of autophagy as shown by the significant increase in the LC3II/LC3I ratio and low levels of p62/SQSTM1. Next, we explored the expression of LAMP2A, which was inhibited, suggesting an inactivation of chaperone mediated autophagy, without any effecting the PI3K-P85 expression and pAKT/AKT ratio.

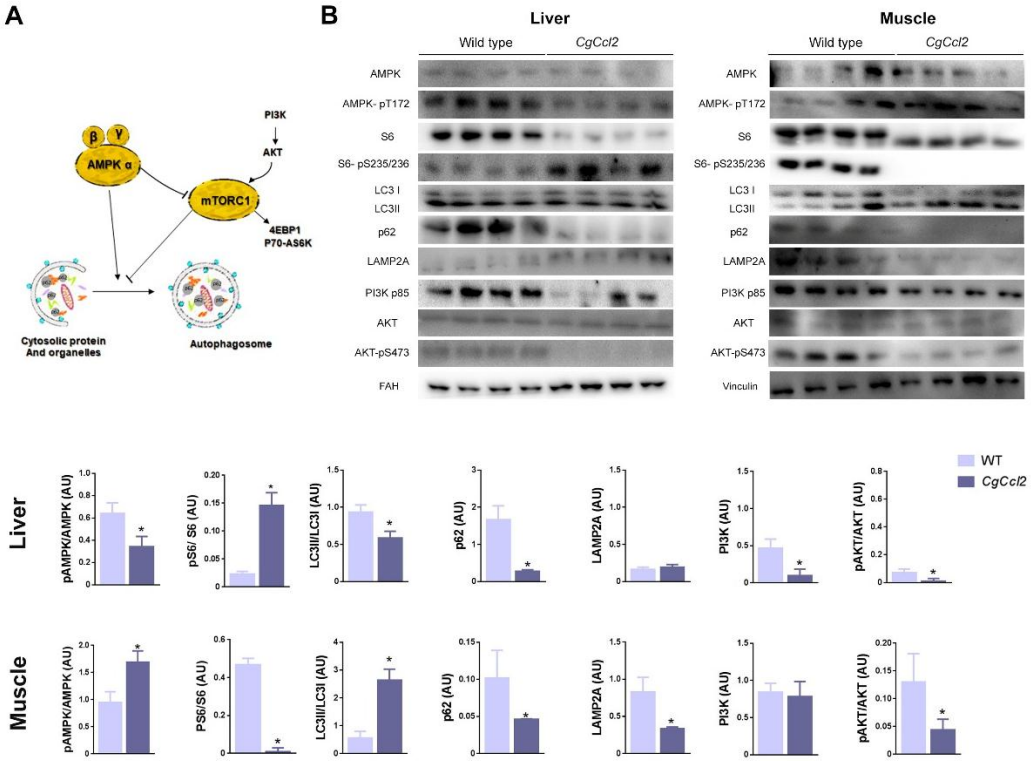

Figure. 33. **Overall assessment of CCL2 overexpression in PI3K/AKT/mTORC1 driven pathway by Western Blot analysis**. (A) Schematic representation of AMPK and MTOC1 role in autophagy. (B) Western Blot analysis of selected molecules, including phosphoinositide 3-kinase p85 subunit (PI3K-p85), protein kinase B (AKT), AKT-pS473, phospho-S6 ribosomal protein (S6-Ps235/236), S6 ribosomal protein, AMP-activated protein kinase (AMPK) AMPK-p T172, microtubule-associated protein 1A/1B light chain 3B (LC3), sequestosome 1 or p62/SQSTM1 (p62), lysosome associated membrane protein 2 (LAMP2A), fumarylacetoacetate hydrolase (FAH) and vinculin, in cisgenic mice (CgCcl2) and wild type animals. Results are shown as means ± SEM; * $p < 0.05$, with respect to control littermates (WT).

Study 3

Overexpression of chemokine (C-C motif) ligand 2 promotes fibrosis and metabolic alterations leading to accelerated aging

UNIVERSITAT ROVIRA I VIRGILI
THE ROLE OF CHEMOKINE (C-C MOTIF) LIGAND 2 IN INFLAMMATION, OXIDATIVE STRESS, AGING AND METABOLISM
Fedra Nicaury Luciano Mateo

Results

Ccl2 overexpression shortens the lifespan in accelerated aging mice model

Lmna $^{G609G+/-}$ */CgCcl2*$^{+/-}$ mice showed an ubiquitous *Ccl2* overexpression (Figure 34). When we performed the weekly evaluation of mice, we observed that WT developed a physiological weight increase. However, the *Lmna* $^{G609G+/-}$ mice showed lower body weight respect to WT and at 32 weeks, these mice started a gradual loss of body weight (Figure 35 A). *Lmna* $^{G609G+/-}$ */CgCcl2*$^{+/-}$ mice had a similar evolution as *Lmna* $^{G609G+/-}$ mice until 14 weeks. After these period *Lmna* $^{G609G+/-}$ */CgCcl2*$^{+/-}$ mice started to lose body weight. Subsequently, these mice showed a senescence phenotype faster than the other groups (Figure 35 B). At 20 weeks, *Lmna* $^{G609G+/-}$ */CgCcl2*$^{+/-}$ mice showed lipodystrophy, reduction in growth rate, body weight and lordokyphosis. In consequence *Lmna* $^{G609G+/-}$ */CgCcl2*$^{+/-}$ mice died before the *Lmna* $^{G609G+/-}$ mice.

We observed that *Lmna* $^{G609G+/-}$ mice lived until 38 weeks compared to the 20 weeks of *Lmna* $^{G609G+/-}$ */CgCcl2*$^{+/-}$ mice or the 104 weeks of WT mice (Figure 35 C).

Ccl2 overexpression induces sarcopenia, cachexia and fibrosis

At sacrifice, *Lmna* $^{G609G+/-}$ and *Lmna* $^{G609G+/-}$*/CgCcl2* $^{+/-}$ mice exhibited similar senescence phenotype and important histological alterations, loss of weight, muscle atrophy, fatigue and weakness, although *Lmna* $^{G609G+/-}$ */CgCcl2* $^{+/-}$ showed a more pronounced and earlier phenotype. Histological analysis showed important cardiovascular alterations. *Lmna* $^{G609G+/-}$ */CgCcl2* $^{+/-}$ mice displayed a significant loss of the aortic and femoral arterial structure. Furthermore, we observed an increase of collagen infiltration and F4/80 stained cells in the tunica media (Figure. 36). Similar alterations were observed in the cardiac muscle (Figure. 37). Moreover, Lmna $^{G609G+/-}$ /CgCcl2 $^{+/-}$ mice displayed a generalized loss of fat depots (Figure. 38), which were characterized by an increase in collagen infiltration, UCP-1 and F4/80 staining cells in brown and white adipose tissues.

Histological muscle analysis revealed that *Lmna* $^{G609G+/-}$ and *Lmna* $^{G609G+/-}$*/CgCcl2* $^{+/-}$ mice exhibited a clear cachexia and sarcopenia, which were characterized by a remarkable loss of muscle fiber structure and fibrosis (Figure 39). Also, quadriceps had a low number of F4/80 stained cells and low expression of TNFα and of the antioxidant enzyme PON1 respect to WT. Again, these alterations

were more pronounced in *Lmna* $^{G609G+/-}$ */CgCcl2*$^{+/-}$ mice (Figure 39 B). Moreover, these mice exhibited alterations of macrophage markers. *Lmna* $^{G609G+/-}$ */CgCcl2*$^{+/-}$ mice showed an increase in CD163 levels respect to control groups without alterations in CD11b.

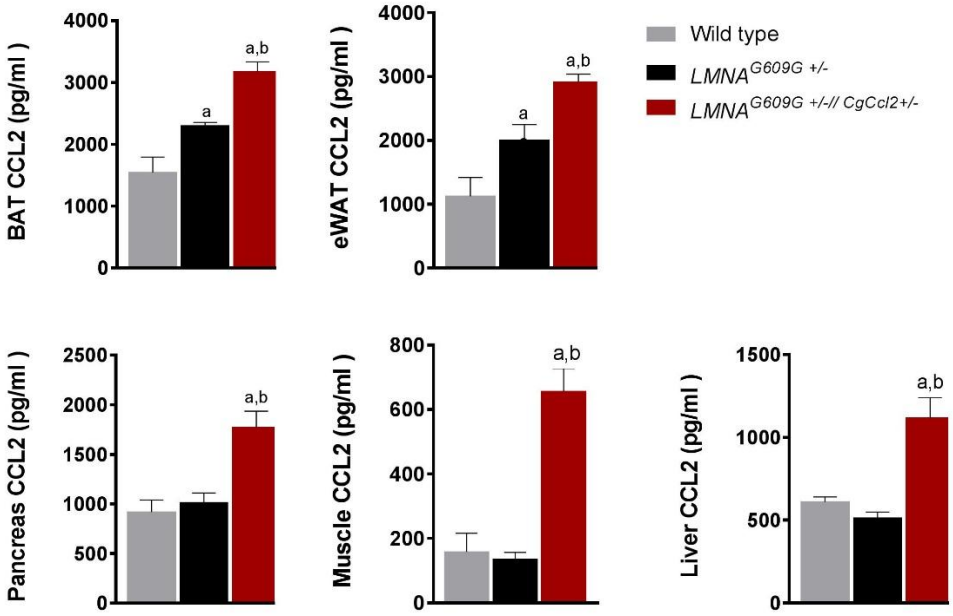

Figure 34. CCL2 concentrations in different metabolic tissues. CCL2 concentrations in the liver, white adipose tissue (eWAT), pancreas, muscle and brown adipose tissue (BAT) in wild type, *Lmna* $^{G609G\ +/-}$ and *Lmna* $^{G609G\ +/-}$*/ CgCcl2* $^{+/-}$ mice. Results are shown as means ± SEM (n=8). $^{a}p< 0.05$ respect to wild type mice, $^{b}p<0.05$ respect to *Lmna* $^{G609G\ +/-}$ by Mann–Whitney U test. *Lmna* $^{G606G\ +/-}$*/CgCcl2* $^{+/-}$ denotes heterozygous progeria and CCL2 cisgenic mice. *Lmna* $^{G606G\ +/-}$ denotes progeria mice.

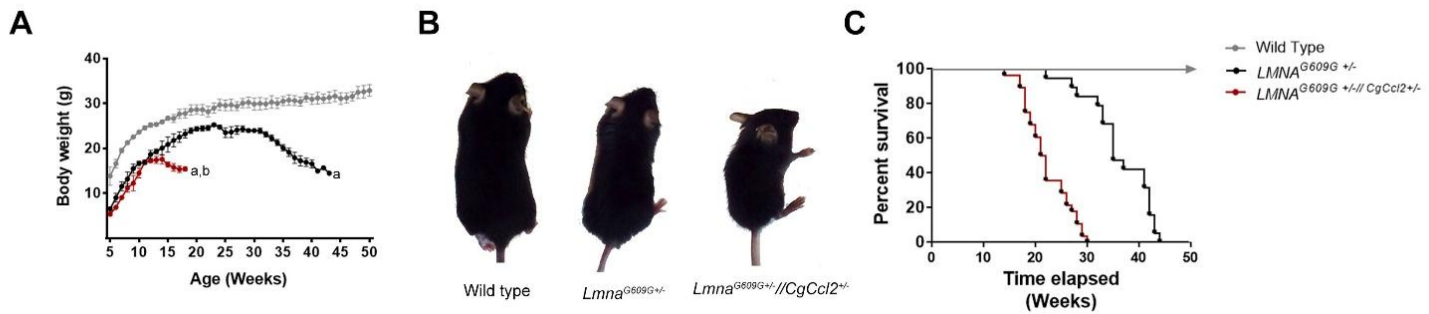

Figure 35. Phenotypes of wild type, *Lmna* $^{G609G+/-}$ and *Lmna* $^{G609G+/-}$*/CgCcl2* $^{+/-}$ (A) Cumulative plot of body weight increase versus age. Dots represents mean values, and error bars indicate de SEM. (B) Representative photographs of wild type, *Lmna* $^{G609G+/-}$ and *Lmna* $^{G609G+/-}$*/CgCcl2* $^{+/-}$ at 20 weeks of age. (C) Kaplan-Meier survival plots from wild type (n=20), *Lmna* $^{G609G+/-}$ *(n=28)* and *Lmna* $^{G609G+/-}$*/CgCcl2* $^{+/-}$ (n=34). *Lmna* $^{G606G+/-}$*/CgCcl2* $^{+/-}$ denotes heterozygous progeria and CCL2 cisgenic mice. *Lmna* $^{G606G+/-}$ denotes progeria mice.

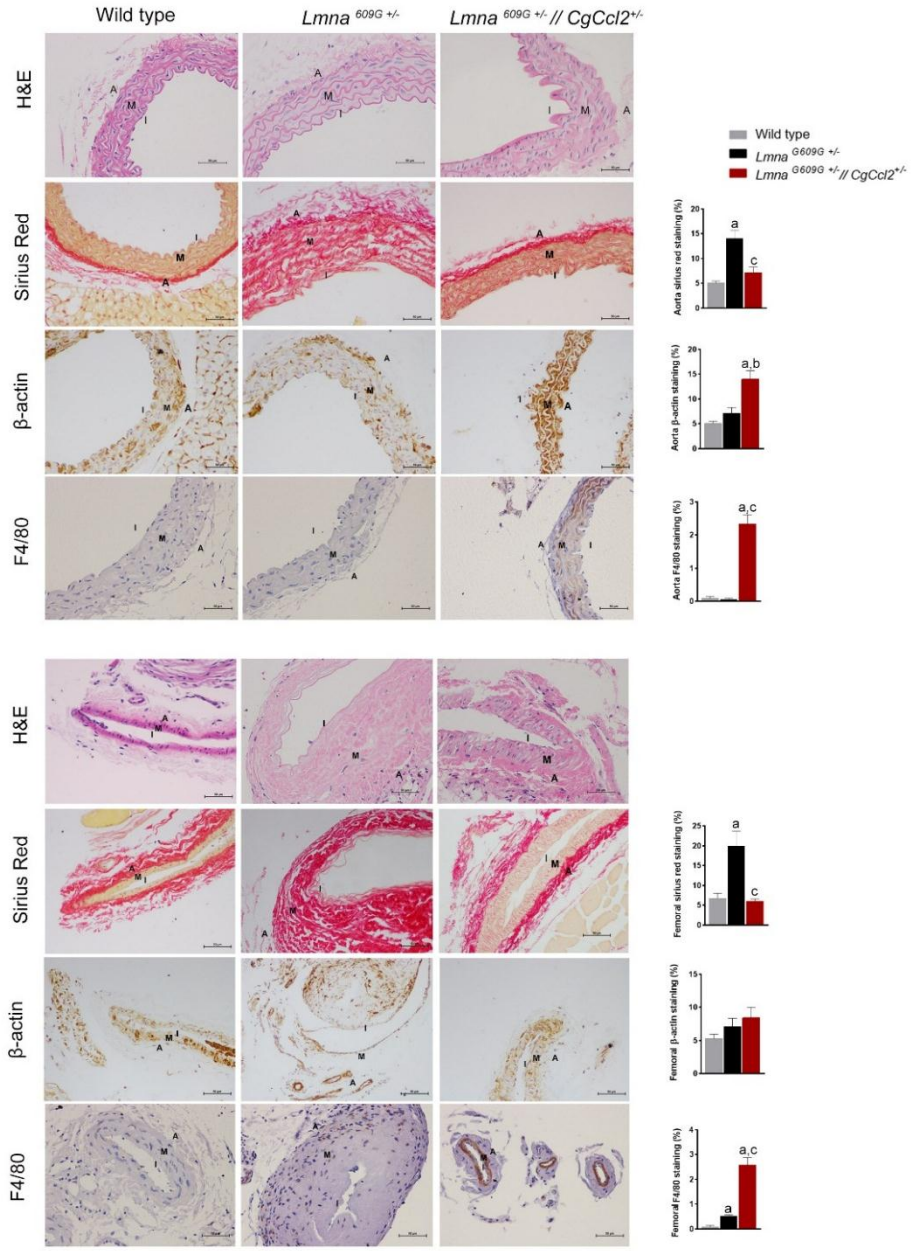

Figure 36. **Histology analysis of aorta and femoral arteries**. Representative micrographs of aorta and femoral arteries by Hematoxylin and Eosin (H&E), Sirius red staining and immunohistochemical analysis of β-actin and F4/80 cells. At right, the quantification of positive staining area. Results are shown as mean stained cells ± SEM. [a] p<0.001 respect to wild type mice, [b]p<0.05 respect to *Lmna* $^{G609G\ +/-}$, [c]p<0.001 respect to *Lmna* $^{G609G\ +/-}$ mice by Mann–Whitney U test. *Lmna* $^{G606G\ +/-}$*/CgCcl2* $^{+/-}$ denotes heterozygous progeria and CCL2 cisgenic mice. *Lmna* $^{G606G\ +/-}$ denotes progeria mice.

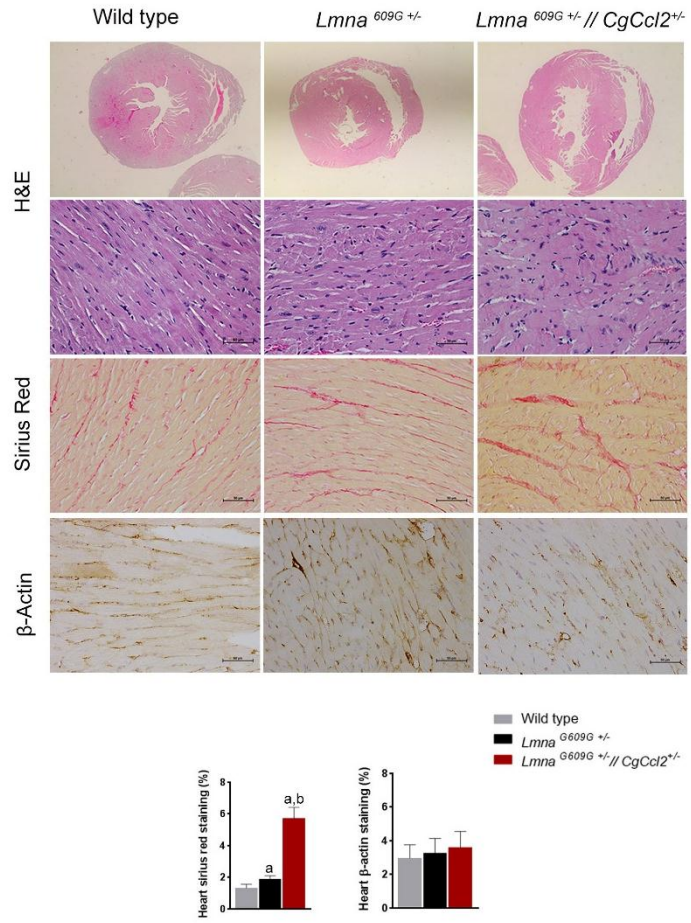

Figure 37. **Histology analysis of cardiac muscle.** Representative micrographs of heart by Hematoxylin and Eosin (H&E), Sirius red staining and immunohistochemical analysis of β-actin and staining cells and the quantification of positive staining area. Results are shown as means ± SEM. [a]p<0.05 respect to wild type mice, [b]p<0.05 respect to *Lmna* $^{G609G\ +/-}$ mice by Mann–Whitney U test. *Lmna* $^{G606G\ +/-}$*/CgCcl2* $^{+/-}$ denotes heterozygous progeria and CCL2 cisgenic mice. *Lmna* $^{G606G\ +/-}$ denotes progeria mice.

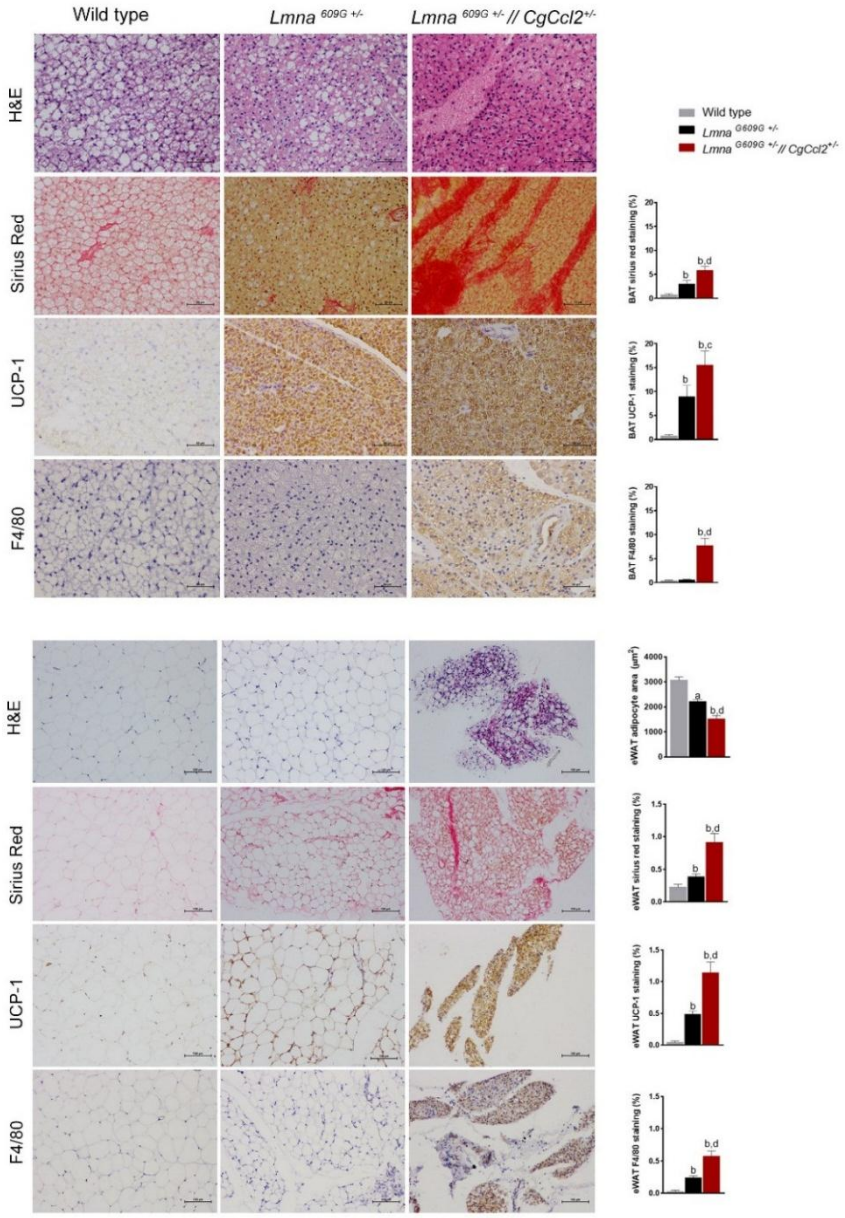

Figure 38. Histology analysis of brown and white adipose tissue (BAT and eWAT respectively). Representative micrographs of BAT and eWAT by Hematoxylin and Eosin (H&E), Sirius red staining and immunohistochemical of uncoupling protein one (UCP-1) and F4/80 cells. At right, the quantification of positive staining area. Results are shown as means ± SEM. [a]p<0.05 respect to wild type mice, [b]p<0.001 respect to wild type mice, [c]p<0.05 respect to *Lmna* $^{G609G\ +/-}$, [d]p<0.001 respect to *Lmna* $^{G609G\ +/-}$ mice by Mann–Whitney U test. *Lmna* $^{G606G\ +/-}$*/CgCcl2* $^{+/-}$ denotes heterozygous progeria and CCL2 cisgenic mice. *Lmna* $^{G606G\ +/-}$ denotes progeria mice.

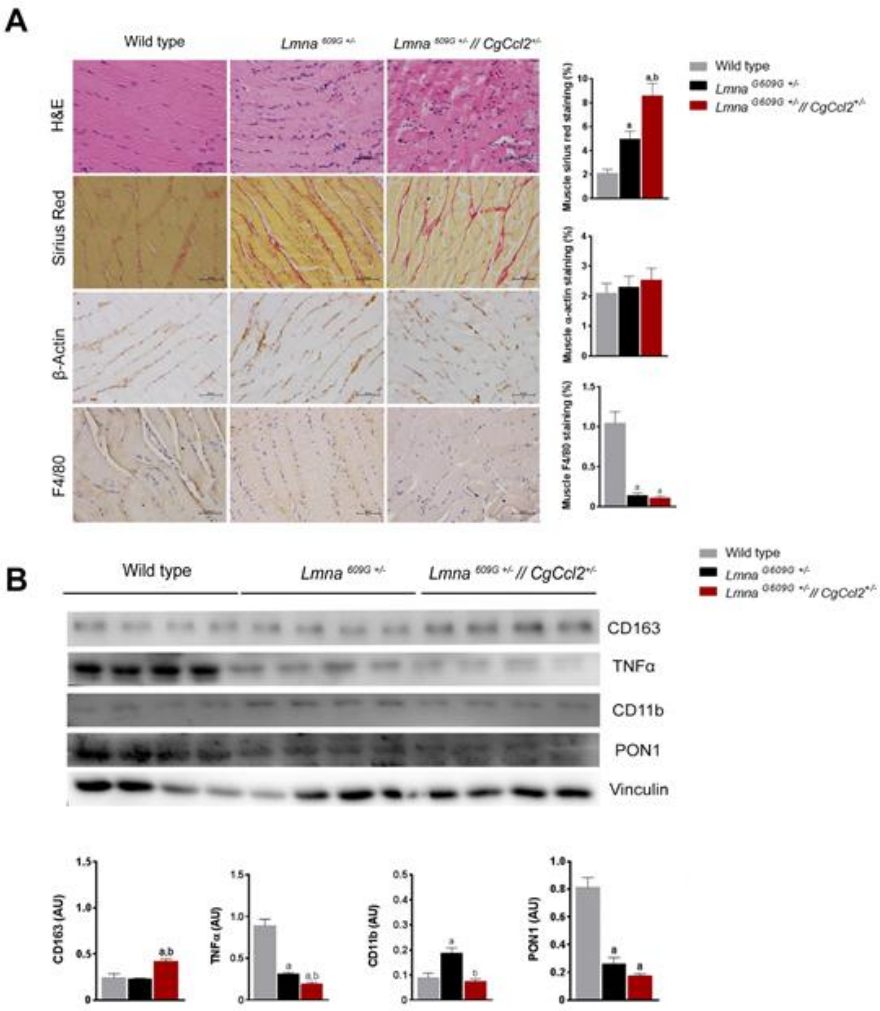

Figure 39. Muscle histology and western blot analysis. (A) Representative micrographs of muscle histology analysis by hematoxylin & eosin, Sirius red staining and immunohistochemical analysis of β-actin and F4/80 cells. At right, quantification of positively-stained cells (B) Overall assessment of macrophage polarization in muscle tissue though western blot of selected molecules, including cluster of differentiation (CD) 11 and 163, Tumor necrosis factor (TNFα) and Paraoxonase 1 (PON1). Value are mean ± SEM. [a]p< 0.05, respect to wild type mice. [b] p<0.05 with respect to *Lmna* $^{G609G+/-}$ mice by Mann–Whitney U test. *Lmna* $^{G606G+/-}$*/CgCcl2* $^{+/-}$ denotes heterozygous progeria and CCL2 cisgenic mice. *Lmna* $^{G606G+/-}$ denotes progeria mice.

Lmna $^{G609G+/-}$ mice present alterations in energy and one-carbon metabolism in muscle

To better understand changes induced by *Lmna $^{G609G+/-}$* mutation, we performed a metabolomic analysis in muscle from fasted *Lmna $^{G609G+/-}$* and WT mice. We selected this tissue due to its important implications in aging development. The partial least square discriminant analysis and the heatmap showed a clear distinction between animals from the both groups (Figure 40 A). Examination of individual metabolites showed that *Lmna $^{G609G+/-}$* mutation induced upregulation of all metabolites involved in energy metabolism with respect to WT. We emphasized the important increase in glucose metabolism and in all amino acids analyzed. We also noted alterations in glutamate, α-ketoglutarate, citrate-isocitrate, aconitate and succinate concentration (Figure 40 B and Table 8). *Lmna $^{G609G+/-}$* also increased riboflavin, homocysteine, methionine and downregulated 5-methyl-tetrahydrofolate (5-methyl-THF) and SAH without a significant alteration in DNA methylation (Figure 40 B and Figure 42). These results suggest that *Lmna $^{G609G+/-}$* mutation has an important impact in muscle metabolism without epigenetic perturbation.

Respect to wild type, the main alterations observed in *Lmna $^{G609G+/-}$/ CgCcl2$^{+/-}$* were an increase in branched-chain amino acids (valine, isoleucine and leucine), β-hydroxybutyrate, fructose 1.6 bisphosphate, glucose 6-phosphate and ribose-5-phosphate, together with a depletion in 3-phosphoglycerate and citrate-isocitrate (Figure 41 A). As regards 1-C metabolism, we observed an increase in riboflavin and methionine levels and a downregulation of 5 methyl-THF, SAM and SAH. These alterations in 1-C metabolism induced an increase of the percentage of 5-mC, which is a marker of DNA methylation (Figure 43). These results suggest that CCL2 has a role in the DNA methylation.

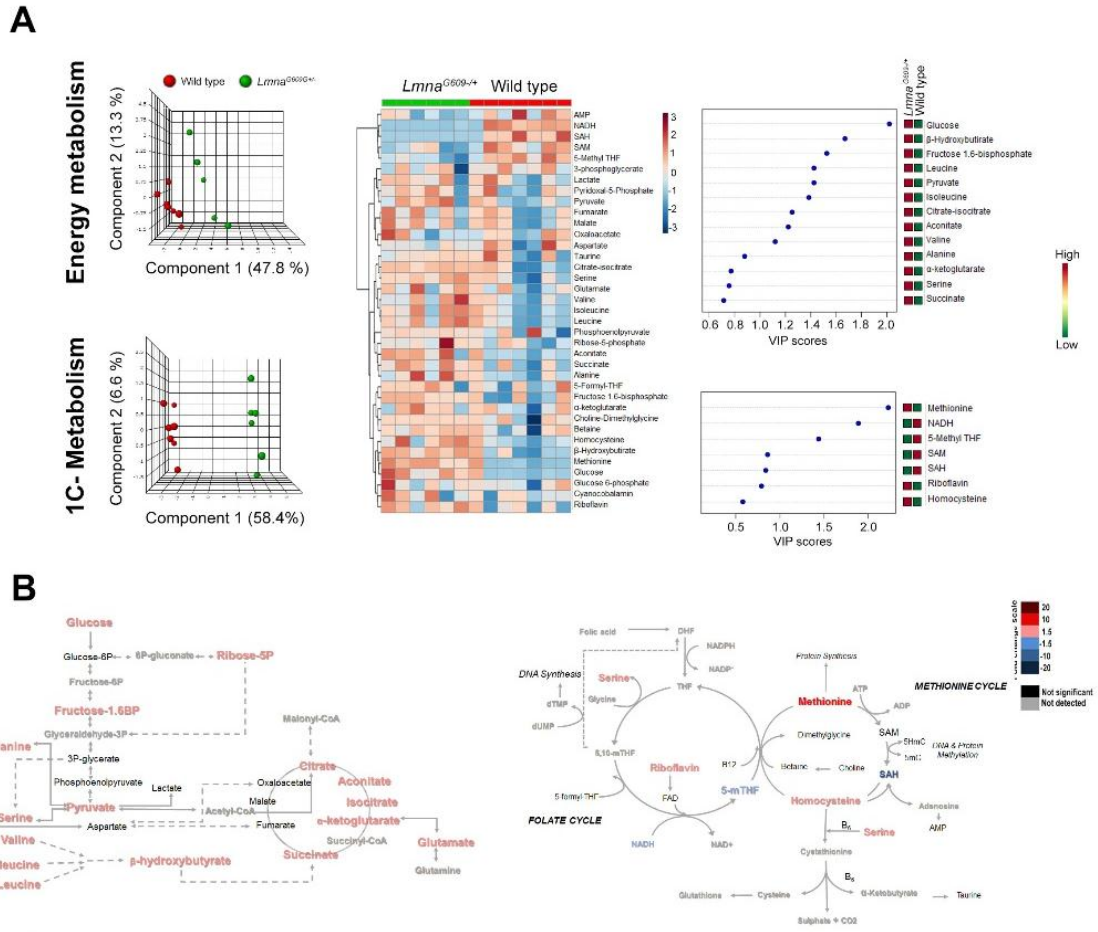

Figure 40. *Lmna* $^{G609G-/+}$ mutation induces important changes in energy and one carbon (1-C) metabolism. (A) Partial least square discriminant analysis (PLSDA), heatmap and variable importance in projection (VIP scores) of metabolites involved in energy and 1-C metabolism between wild type and *Lmna* $^{G609+/-}$ mice (B) The relative impact of Lmna $^{G609G-/+}$ mutation on the levels of metabolites associated with energy and 1-C metabolism. Comparisons were made assessing fold changes according to the legend. *Lmna* $^{G606G+/-}$ denotes progeria mice.

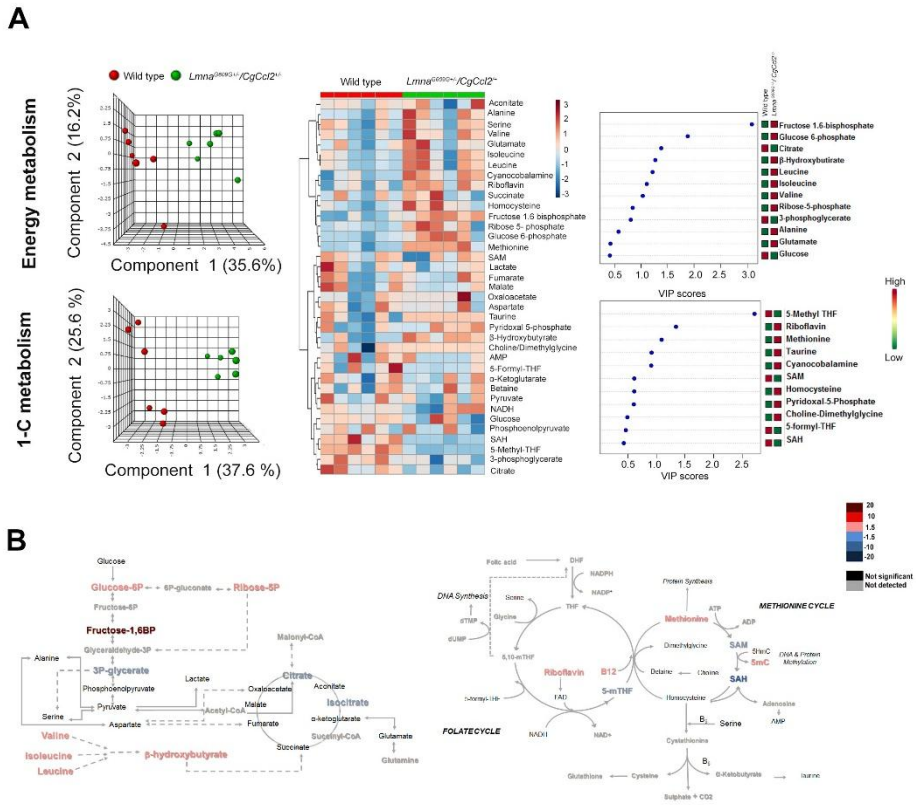

Figure 41. The relative impact of *Lmna* $^{G609G+/-}$ */CgCcl2* $^{+/-}$ mutation in the energy and one carbon (1-C) metabolism. (A) Partial least square discriminant analysis (PLSDA), heatmap and variable importance in projection (VIP scores) of metabolomic comparison between *Lmna* $^{G609G+/-}$ */CgCcl2* $^{+/-}$ *and* wild type mice (B) The relative impact of *Lmna* $^{G609G+/-}$ */CgCcl2* $^{+/-}$ mutation on the levels of metabolites associated with energy and 1C metabolism respect to wild type mice comparisons were made assessing fold changes according to the legend. *Lmna* $^{G606G+/-}$*/CgCcl2* $^{+/-}$ denotes heterozygous progeria and CCL2 cisgenic mice.

We explored whether the metabolomic alterations observed in *Lmna* $^{G609G+/-}$ could be reproduced in further *Lmna* $^{G609G+/-}$*/ CgCcl2*$^{+/-}$. When we compared the muscle metabolomic profile, we observed a clear distinction between groups (Figure 42 A). As it regards energy metabolism, *Lmna* $^{G609G+/-}$*/ CgCcl2*$^{+/-}$ mice showed alterations in glucose and CAC metabolism without significative alterations in amino acids concentrations with respect to *Lmna* $^{G609G+/-}$. Our results indicate that energy status of *Lmna* $^{G609G+/-}$*/ CgCcl2*$^{+/-}$ were different from *Lmna* $^{G609G+/-}$, suggesting a possible role of CCL2 in energy metabolism in Lmna ^{G609G} genetic background (Figure 42 B). *Lmna* $^{G609G+/-}$*/ CgCcl2*$^{+/-}$ mice induced different metabolic alterations than those observed in *Lmna* $^{G609G+/-}$ mice in 1-C metabolism. Thus, these mice showed a downregulation of methionine, choline-dimethylglycine, 5 methyl-THF and 5 formyl-THF. These alterations could be a consequence of the increase of SAM, SAH and AMP levels that we observed in *Lmna* $^{G609G+/-}$*/ CgCcl2*$^{+/-}$ respect to *Lmna* $^{G609G+/-}$. One of the most important consequences of SAM to SAH alterations is the increase in 5-mC (Figure 42 B and 43). Our result confirms that methionine metabolism has an important role in *Lmna* $^{G609G+/-}$ mice and could be influenced by CCL2.

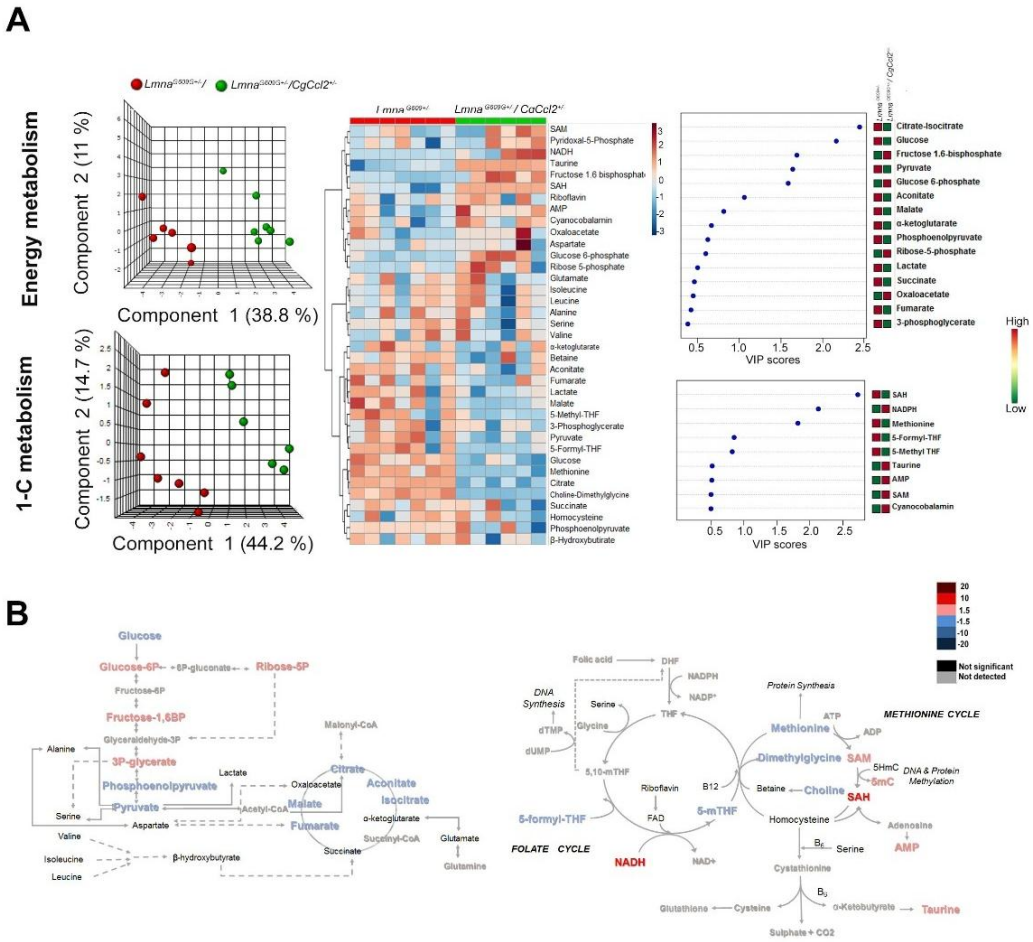

Figure 42. The relative impact of *CgCcl2 overexpression* in the energy and one carbon (1-C) metabolism of *Lmna* $^{G609G+/-}$. (A) Partial least square discriminant analysis (PLSDA), heatmap and variable importance in projection (VIP scores) of metabolomic comparation between *Lmna* $^{G609G+/-}$ and *Lmna* $^{G609G+/-}$ */CgCcl2* $^{+/-}$ (B) The relative impact of *Lmna* $^{G609G+/-}$ */CgCcl2* $^{+/-}$ mutation on the levels of metabolites associated with energy and 1C metabolism respect to *Lmna* $^{G609G+/-}$ mice. Comparisons were made assessing fold changes according to the legend. *Lmna* $^{G606G+/-}$*/CgCcl2* $^{+/-}$ denotes heterozygous progeria and CCL2 cisgenic mice. *Lmna* $^{G606G+/-}$ denotes progeria mice.

Metabolites	*Wild type*	*Lmna $^{G609G+/-}$*	*Lmna $^{G609G+/-}$ / CgCCL2$^{+/-}$*
Glucose	373.4 (345-394.2)	1101 (819.4-2248.1)[a]	175.6 (104.5-517.3)[c]
Glucose 6-phosphate	16 (12.8-18.8)	18.2 (14.1-19.7)	131.3 (77.4-166.3) [a,c]
Fructose-1.6-Bisphosphate	3.6 (2.4-13.4)	12.4 (12.4-19.9) [a]	87.9 (55.5-120.4) [a,c]
3-phosphoglycerate	1.9 (1.6-3.2)	1.3 (0.4-2.6)	1.4 (0.8-1.5) [a,c]
Phosphoenolpyruvate	0.5 (0.3-1.1)	0.7 (0.7-0.8)	0.3 (0.1-1.6) [c]
Pyruvate	68.8 (54.8-221.2)	475.6 (248.2-482.6) [a]	107.1 (40-142.4) [c]
Lactate	9815.7 (6626.5-16649.8)	12913.7 (4688.9-16340.4)	9730.5 (8019.7-10986.5)
Ribose-5-phosphate	9 (7.8-9)	10.4 (10.2 -10.7) [a]	20.9 (20.3-29.2) [a,c]
Oxaloacetate	27.7 (15.7-33.4)	19.8 (19.8-38.5)	29.2 (20.7-29.2)
Citrate-isocitrate	51.6 (27.1-119.4)	137.5 (137.5-137.5) [a]	22.8 (11.5-31) [a,d]
Aconitate	11.5 (10.3-12.9)	32.6 (29.4-34.6) [a]	12.7 (7.9-29.4)[c]
α-ketoglutarate	2.1 (1.2-5.1)	3.7 (1.2-5.2) [a]	1.6 (1.2-5.2)
Succinate	41.2 (38.1-79.1)	71.1 (66.5-104.5)[a]	47.8 (25.4-83.5)
Fumarate	143.7 (56.9-217.6)	337.4 (229.7-337.4)	131.9 (89.1-160.5)[c]
Malate	322.2 (133.8-502)	593 (387.8-704.6)	231 (203.7-326.1)[c]
β-Hydroxybutirate	38.4 (22-51.3)	129.9 (97.6-147.4) [a]	99.5 (82.9-111.9) [a]
Glutamate	1673 (1212.6-2498.8)	2798.1 (1842.4-3290.2) [a]	2058.4 (1558.2-3866.8)
Alanine	362.2 (286.4-414.6)	619.2 (396.8-1193.4) [a]	489.4 (342.4-855.5)
Serine	1007.8 (591.2-1375)	1585.4 (1360-2012.6) [a]	1309.3 (956.5-1466)
Valine	123.3 (75.9-201.2)	357.5 (164-814.4) [a]	258 (220.7-507.8) [a]
Isoleucine	77.1 (45-116.7)	317.9 (126.3-341.8) [a]	174.6 (101.1-438.8) [a]
Leucine	163.8 (102-260.6)	612.9 (287-851.5) [a]	416 (267.4-1153.4) [a]
Aspartate	245 (108.4-374.3)	195.5 (195.5-201.5)	206.3 (139-219.3)

Table 8. Muscle energy-balance metabolites. Values are expressed in µM/ 100 mg of tissue (mean and interquartile range). [a] $p < 0.05$, [b] $p < 0.001$ respect to wild type group; [c] $p<0.05$, [d] $p<0.001$ respect to Lmna$^{G609G+/-}$ by Mann–Whitney U test. *Lmna $^{G606G+/-}$/CgCcl2 $^{+/-}$* denotes heterozygous progeria and CCL2 cisgenic mice. *Lmna $^{G606G+/-}$* denotes progeria mice.

Metabolites	*Wild type*	*Lmna $^{G609G+/-}$*	*Lmna $^{G609G+/-}$ / CgCCL2$^{+/-}$*
Taurine	1499.7 (601.8-3621.9)	1952.7 (1407-2041.3)	3038.1 (2920.8-3038.1)[d]
*Choline-Dimethylglycine**	145.9 (69.1-216.1)	185.7 (185.7-189.4)	171.6 (171.0-171.8)[d]
*Betaine**	0.4 (0.2-0.5)	0.6 (0.5-0.6)	0.3 (0.3-0.6)
Homocysteine	0.3 (0.3-0.4)	0.7 (0.5-0.9)[a]	0.5 (0.3-0.9)
SAM	3.3 (1.7-4.5)	1.2 (0.7-2.0)	2.7 (0.5-2.1)[a,c]
Methionine	0.6 (0.6-0.7)	9.3 (6.4-12.2)[a]	1.6 (0.8-1.6)[a,d]
AMP	3.7 (2.1-5.7)	2.3 (1.5-2.9)	2.8 (2.8-3.8)[c]
NADH	1.7 (1.3-2.5)	0.2 (0.2-0.2)[a]	5 (0.2-3.8)[d]
*SAH**	0.1 (0.1-0.2)	0.01 (0.0-0.01)[a]	0.09 (0.07-0.1)[b,d]
Pyridoxal 5 phosphate	3.5 (2.2-7.1)	4.9 (4.4-6.4)	6.7 (4.1-9.6)
*5-Methyl-THF**	10.2 (8.8-20.1)	3.2 (1.2-3.2)[a]	1.1 (0.9-1.3)[a,c]
*5-Formyl-THF**	1.7 (0.7-2.8)	2.1 (2.1-2.1)	0.8 (0.8-1.3)[c]
*Cyanocobalamin**	0.4 (0.3-0.5)	0.5 (0.4-0.8)	0.8 (0.5-1)[a]
Riboflavin	0.5 (0.2-0.9)	1.2 (0.9-1.7)[b]	1.7 (0.9-2.2)[a]

Table 8. Muscle one-carbon metabolites. Values are expressed in µM/ 100 mg of tissue (mean (interquartile range). * Values are expressed in nM/100 mg of tissue. [a]p < 0.05, [b]p< 0.001 respect to wild type group; [c] p<0.05, [d] p<0.001 respect to Lmna $^{G609G+/-}$ by Mann–Whitney U test. *Lmna $^{G606G+/-}$/CgCcl2 $^{+/-}$* denotes heterozygous progeria and CCL2 cisgenic mice. *Lmna $^{G606G+/-}$* denotes progeria mice. SAM: s-adenosylmethionine; AMP: Adenosine monophosphate; SAH: s-adenosylhomocysteine; 5-Methyl-THF: 5-Methyl-tetrahydrofolate.

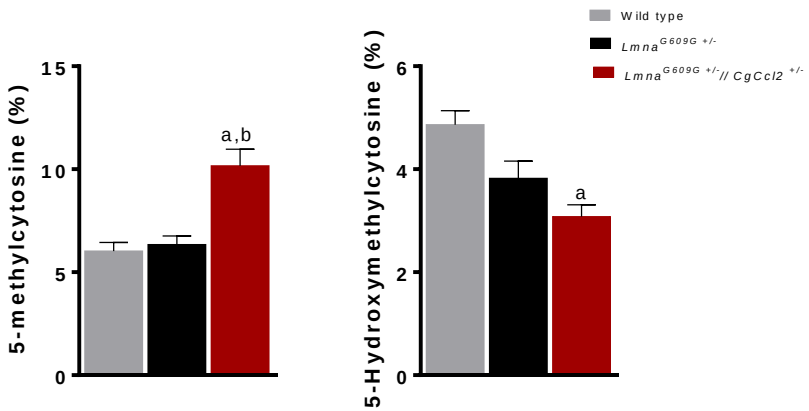

Figure 43. Effect of *Lmna* mutation on DNA Methylation in muscle tissue represented by the percentage of 5-methylcytosine and 5-hydroxymetilcytosine. Results are shown as means ± SEM (n=8) [a]p<0.05 respect to wild type mice, [b]p<0.05 respect to *Lmna* $^{G609G\ +/-}$ by Mann–Whitney U test. *Lmna* $^{G606G\ +/-}$*/CgCcl2* $^{+/-}$ denotes heterozygous progeria and CCL2 cisgenic mice. *Lmna* $^{G606G\ +/-}$ denotes progeria mice.

Lmna G609G+/- induces P53 activation and a downregulation of PI3K/AKT/mTOR pathway

Both mice with the Lmna mutation showed an upregulation of tumor suppressor p53. p53 is a transcription factor, which in stress conditions might control the cell growth through the regulation of AKT/mTOR pathways. Respect to wild type, both progeroid mice developed an inactivation of AKT and mTORC1, which are represented in the figure 44 as AKT-pS473 and S6-Ps235/236, without affecting PI3K-p85. Moreover, these mice showed an activation of AMPK- pT172, which resulted in the macroautophagy activation, indicated by an increase in LC3II/LC3I ration and clear reduction in sequestosome p62. These results were more evident in *Lmna* $^{G609G+/-}$*/ CgCcl2*$^{+/-}$ mice. However, *Lmna* $^{G609G+/-}$ mice showed a downregulation of LAMP2A, which is used as a CMA marker.

Moreover, we analyzed the protein levels of mitochondrial oxidative phosphorylation complexes (OXPHOS) to determine whether Lmna $^{G609G+/-}$ is associated with mitochondrial alterations. Progeroid mice revelated downregulation of complexes I (CI-NDUFB8) and II (CII-SDHB). However, only *Lmna* $^{G609G+/-}$*/ CgCcl2*$^{+/-}$ showed a decreased of III (CIII-UQCRC2), IV (MTCO1) and V (CVNDUFB8). These results suggest that the muscle ATP synthesis capacity is severely impaired or inactive in *Lmna* $^{G609G+/-}$*/ CgCcl2*$^{+/-}$. In addition, both group of mice had a decrease of TOM20 and MFN2 protein concentration. Progerin accumulation induced alterations in muscle mitochondria and fusion process

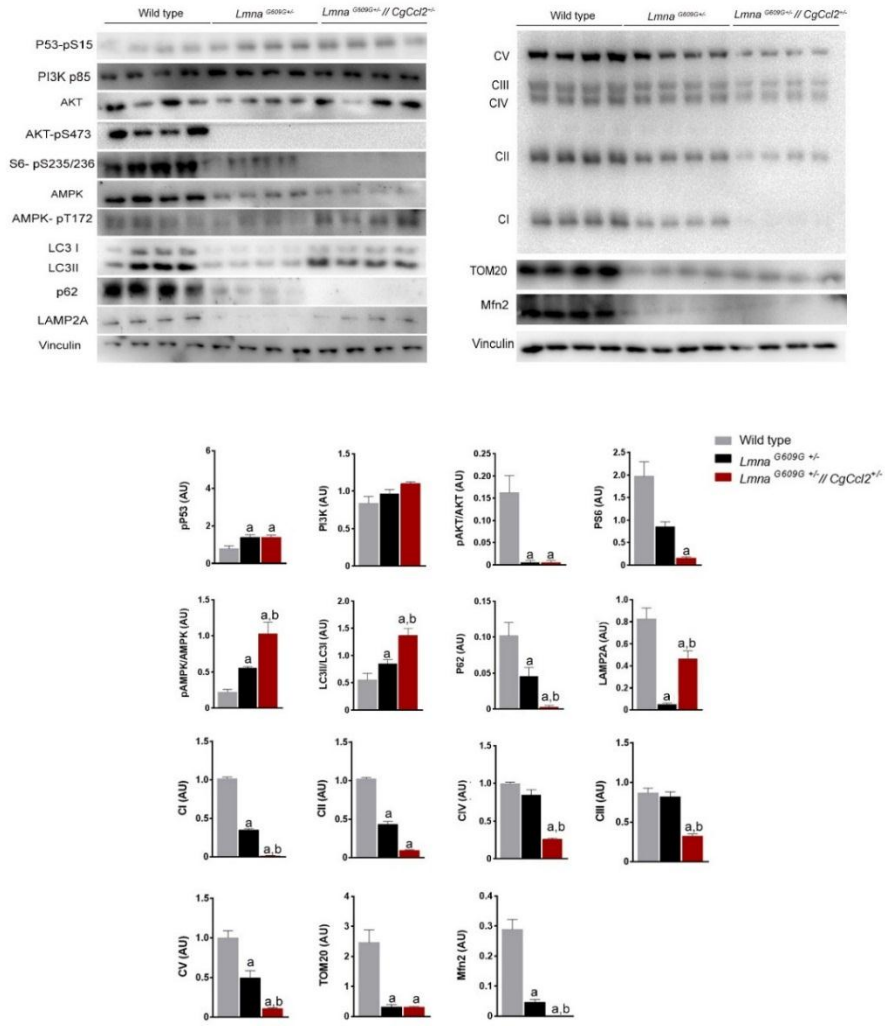

.

Figure 44. Overall assessment of p53 regulates the PI3K/AKT/mTORC1 pathway and mitochondrial dynamics. Western blot of selected molecules. Values are shown as mean ± SEM. [a]p< 0.05, respect to wild type mice. [b] p<0.05 with respect to *Lmna* $^{G609G+/-}$ by Mann–Whitney U test. *Lmna* $^{G606G+/-}$*/CgCcl2* $^{+/-}$ denote heterozygous progeria and CCL2 cisgenic mice. *Lmna* $^{G606G+/-}$ denote progeria mice. Acronyms used: phospho- tumor suppressor p53 (p53-pS15), Phosphoinositide 3-kinases (PI3K), Protein Kinase B (AKT) and phospho-Protein Kinase B (AKT-pS473), phospho-ribosomal protein S6 (S6-pS235/236), AMPK activated protein kinase (AMPK), phospho-AMPK activated protein kinase (AMPK pT172), Microtubule-associated proteins 1A/1B light chain 3B (LC3), p62, Lysosome-associated membrane protein 2 (LAMP2A), Translocase of outer membrane (TOM20), Mitofusin 2 (Mfn2), Vinculin and Complex I or NADH/ubiquinone oxidoreductase; complex II or succinate dehydrogenase, complex III or cytochrome C reductase, complex IV or cytochrome C oxidase, complex V or ATPase.

Discussion

Discussio

UNIVERSITAT ROVIRA I VIRGILI
THE ROLE OF CHEMOKINE (C-C MOTIF) LIGAND 2 IN INFLAMMATION, OXIDATIVE STRESS, AGING AND METABOLISM
Fedra Nicaury Luciano Mateo

Discussion

The maintenance of homeostasis under diverse metabolic diseases requires a complex relationship between organs, cells, hormones and cytokines converging at multiple metabolic pathways. Understanding the association between all of these components is determinant in the search of new therapeutics targets of metabolic diseases such as obesity, type II diabetes, NAFLD and cardiovascular diseases, which represent the main cause of death in western society. In this dissertation we demonstrated that the chemokine CCL2 could be an effective therapeutic target in NAFLD progression and accelerated aging.

Originally, CCL2 interaction with its receptor (CCR2) was associated to the regulation of monocytes and macrophages at the sites of inflammation, but the results of this dissertation demonstrated that *Ccl2* ablation or its overexpression could transmit cells signals that generate multiple response not related to chemotaxis function. In the **first study**, we showed that the *Ccl2* ablation partially or completely reverted most of liver metabolic alterations and histological features generated by oxidative stress and hyperlipemia. However, the mechanisms that establish the metabolic reprogramming in the hepatocytes in due to this *Ccl2* deficiency remain poorly understood.

Our analysis of the coupled oxidation-inflammation system reveals an *in vivo* essential role in liver disease and potential alternative strategies capable of delaying NAFLD development. Deprivation of PON1, an important component of antioxidant defenses, resulted in increased production of lipid peroxides, which correlated with fat accumulation and variations in the distribution of liver macrophages. Examination of energy metabolism in the livers of *Pon1* deficient mice suggested mitochondrial damage and decoupling from glycolysis, confirming that mitochondrial metabolism mediates in oxidative stress and inflammation in fatty liver [178]. Mitochondrial damage may cause an imbalance between ROS production. Potentially, overexpression of antioxidant defenses might improve lifespan and health span in mice [179]. The increase in glutathione peroxidase and glutathione reductase expression in PLKO mice can be interpreted as a mechanism of hepatocytes to defend against this oxidative stress. Consequently, the GSH/GSSG ratio in these mice was extremely low in PLKO mice. The oxidative stress status could interact with metabolism, more specifically the relative deficiency in methyl donors resembling the pro-oxidant, pro-inflammatory disturbances observed in mice fed methionine-choline deficient mice. Interestingly, most defects

were completely reversed by the concomitant *Ccl2* deficiency, most likely mediated by amelioration in macrophage functionality [180,181]. Although the liver has several types of immune cells macrophages represent one third of hepatic non-parenchymal cells and are considered the first response to liver injury, playing a major role in repair and regeneration processes [182,183].

Energy metabolism in the livers of CPLKO mice was also partially restored when compared with PLKO mice, of note these results were more evident when fed a standard diet. This data suggest that the prevention of obesity and dietary restraint is a crucial first step in protection of the liver [184] because obesity and overnutrition are causal in the altered expression of genes relevant for metabolism, oxidative stress and inflammation [41,150–152].

The analysis of energy sensors AMPK and mTORC1 activation were inversely related in both PLKO and CPLKO mice. A consequence of mTORC1 activation is autophagy inhibition, which induced a low LC3-II/LC3-I ratio [185]. Therefore, the livers of these mice were deprived of a crucial mechanism to cope with a variety of cellular stress. However, when we examined LAMP2A, we found that *Pon1* deficiency altered this mechanism, which was completely reversed by the addition of *Ccl2* deficiency. Accumulated evidence highlights the importance of autophagy in the maintenance of liver homeostasis and the involvement in the pathogenesis of NAFLD affecting hepatocytes and other hepatic cell types [150,186,187]. CMA participates in protein quality control by degrading oxidized and damaged proteins under stress conditions and contributes amino acids through the degradation of proteins. Indeed, it has been reported that high lipid concentrations can stimulate LAMP2A degradation through the modification of the lysosome membranes [188][189]
Therefore, this study demonstrates that CCL2 is a key molecule for the development of metabolic and histological alterations in the liver of mice sensitive to the development of hyperlipidemia and hepatic steatosis, a finding with potential to identify new therapeutic targets in liver diseases, which is important because there is no specific pharmacotherapy approved for NAFLD.

CCL2 deficiency denotes an improvement of liver metabolic alterations, suggesting an interconnection between this chemokine and metabolism. To investigate this aspect, in the **second study**, we generated targeted *Ccl2* cisgenic mice (*CgCcl2*), which overexpressed CCL2 in all tissues. *CgCcl2* mice showed considerable biochemical and histological alterations associated with energy metabolism and inflammatory status. These mice had a higher predisposition to fatty liver disease,

muscle weakness and significant changes in mitochondria biogenesis, autophagy, ATP synthesis and alterations through AMPK/ mTORC1 driven pathways. Additionally, we explored muscle and liver inflammatory status by the analyses of different macrophage markers. *CgCcl2* mice denoted a modulation of the functional difference in macrophage polarization with a shift towards low liver pro-inflammatory and high anti-inflammatory activity. However, muscle tissue did not show any remarkable alterations. The cause of these findings is not well known yet and new examinations using *Ccl2* liver or muscle specific cisgenic mice are necessary to determine the different mechanisms that control these changes. However, we suggest that these changes may represent an important issue in the development of macrophage-induced metabolic alterations in tissues. Thus, our data suggest that this chemokine has a key metabolic role in the cell homeostasis through the regulation of energy status, particularly in liver and muscle.

Overexpression of CCL2 results in dramatic alterations in biochemical parameters correlated with liver fat accumulation, muscle histological alterations and changes in macrophage plasticity. Examination of energy sensor AMPK/mTORC1, showed that *CgCcl2* mice had a different AMPK behavior in liver and muscle (inhibition in the liver, stimulation in the muscle) indicating distinct energy requirements. In liver, we observed an anabolic profile indicated by low pAMPK/AMPK ratio and high mTORC1 activity, impairment of autophagosome formation, decoupling of OXPHOS components and reduction of mitochondrial fusion. On the other side, skeletal muscle showed a catabolic profile indicated by the activation of AMPK, reduction of mTORC1, increased autophagy without mitochondrial fusion alterations, increased OXPHOS components, and increased levels of lactate and ketone bodies. These chronic high energy requirements of the muscle could induce skeletal muscle fragility and higher mitochondrial activity [189,190]. The mitochondria are the central components of energy metabolism because they are the final acceptors of metabolic substrates and are involved in oxidative phosphorylation, citric acid cycle and fatty acid oxidation [191]. Mitochondrial dynamics is regulated by the balance between fusion, fission and autophagy and alterations in some of these processes have an important repercussion in energy status and in cell metabolism [189,192]. Our results suggest that CCL2 can develop alterations in mitochondria status and the effect of CCL2 seems to be tissue-dependent.

The metabolomics analysis showed that livers of CgCcl2 mice had important changes in CAC cycle. These alterations have been linked to metabolic diseases such as diabetes, ischemia, and hypertension [193,194]. Moreover, our results suggested a link between this chemokine and liver methionine status. Methionine transmethylation is directed to maintain SAM concentration [162], thus methionine depletion induces important metabolic and histological alterations in liver which are related to lipid irregular accumulation in hepatocytes [165,181]. However, we did not find any remarkable alterations in one-carbon metabolism in muscle.

Collectively, this second study indicates that CCL2 and metabolism are closely interconnected. CCL2 overexpression induces metabolic alterations that can affect important processes for cell survival, such as mitochondrial dynamics, autophagy and the regulation of different energy sensors essential for the cell homeostasis.

Beyond these data, several studies demonstrated that CCL2 are correlated with chronological aging in humans and mice [93–95,97]. For this reason, in **study 3** we evaluated the effect of CCL2 overexpression in a mice model of *Hutchinson-Gilford progeria syndrome*, which is a model of accelerated aging. The chronic CCL2 overexpression induces an early senescence phenotype in progeria mice. These mice showed a premature degenerative change, including loss of fertility, sarcopenia, cachexia, dermal thinning and loss of subcutaneous fat. These ageing phenotypes correlate with a reduction in average lifespan (20 weeks in *Lmna* $^{G609G+/-}$*/ CgCcl2*$^{+/-}$ vs 38 weeks in *Lmna* $^{G609G+/-}$), suggesting that this chemokine is an important factor in aging development.

Lmna $^{G609G+/-}$*/ CgCcl2*$^{+/-}$ mice may help to clarify the relevance of systemic inflammation as a regulator of aging. Chronic low grade of inflammation is one of the hallmarks of aging and is closely related. Aging is stimulated by several soluble factors such as interleukins, inflammatory cytokines and growth factors that can affect surrounding cells [96]. Studies *in vitro* have demonstrated that CCL2 participates in the senescence associated secretory phenotype (SASP). SASP is a collection of different factors secreted by senescent cells which are able to induce secondary senescence in healthy tissues, reduce the fitness and promote aging [89,93,96,195]. SASP include several pro-inflammatory chemokines, which have a beneficial paracrine function; however, an unchecked production of these factors could cause detrimental effects in cell survival. Moreover, SASP may

disrupt tissue structure and induce disturbances in its function through the alteration of the immune system [96,195].

One of the most characterized senescence markers is p53, which was increased in both progeroid mice. p53 is a transcription factor that, in stress conditions inhibits cell proliferation through mTORC1 inhibition [196]. The mechanism that controls p53 and mTORC1 interaction is regulated by different means. For instance, it has been demonstrated that p53 induce the direct or indirect activation of AMPK, which is considered to be one of the most important inhibitors of mTORC1. Moreover, p53 also induced PTEN/PI3K/AKT to reduce mTORC1 activity [196,197]. This metabolic reprogramming causes drastic systemic alterations in cells being autophagy activation one of them. Autophagy promotes the recycling of damaged organelles in response to metabolic alterations or nutrient depletion [153][148]. Even though autophagy is considered to be one of the most important anti-aging mechanisms of the cells, we observed an increase in macroautophagy in both groups. Moreover, this increase in macroautophagy was associated with a mTORC1 inhibition and the upregulation of AMPK. Similar results were obtained by other groups using *Hutchinson-Gilford progeria* mice models [198,199].

We consider that macroautophagy activation can be an adaptation to the metabolic stress observed in these mice. Moreover, this dramatic increase is probably a compensation mechanism to the CMA impairment observed in both groups. Downregulation of chaperones are associated with a loss of protein degradation machinery [200,201], a fact which can explain the dramatic increase in amino acids concentration observed in *Lmna* $^{G609G+/-}$*/ CgCcl2*$^{+/-}$ and *Lmna* $^{G609G+/-}$. A decline in protein homeostasis is closely related to aging progression and degenerative diseases such as Alzheimer, Parkinson's, Huntington and cancer [200]. All these pathologies are characterized by mitochondrial dysfunction and alterations in ATP synthesis.

Mitochondria are the main source of cellular energy and mitochondrial stress can induce electron transport chain disruption and in consequence the ATP synthesis depletion. Here, we observed that both progeroid mice have an important mitochondrial dysfunction together with an alteration in mitochondrial dynamic, energy and one carbon metabolism. These alterations are enhanced with CCL2 overexpression. Previous studies have demonstrated that CCL2 overexpression can induce dramatic mitochondrial dysfunction and contributes to mitochondrial biogenesis decline [174].

Moreover, physiological aging *per se* contributes to mitochondrial alterations, which can be produced by different mechanisms including destabilization of respiratory chain complexes, changes in the lipid composition of mitochondrial membranes, oxidation of mitochondrial proteins or alterations in mitophagy process [87, 204, 205]. CCL2 seems to have a profound impact in these alterations. The combination between increased damage and reduced turnover in mitochondria, due to lower biogenesis and reduced clearance, may contribute to aging process in HGSP mice. In addition, several evidences suggest that mitochondrial dysfunction contributes to alterations in metabolic pathways and can alter epigenetic states. These changes can mark a milestone in terms of physiological aging.

Our findings demonstrate striking associations between CCL2 and aging in *Lmna* $^{G609G+/-}$ mice, suggesting that CCL2 could be an interesting target for the design of new therapeutic strategies for the treatment of progeria syndrome.

Collectively, our data confirm that CCL2 has an important metabolic function that goes beyond to its chemoattracting capacity.

Conclusions

Conclusion

UNIVERSITAT ROVIRA I VIRGILI
THE ROLE OF CHEMOKINE (C-C MOTIF) LIGAND 2 IN INFLAMMATION, OXIDATIVE STRESS, AGING AND METABOLISM
Fedra Nicaury Luciano Mateo

Conclusions

- ✓ Chemokine C-C motif ligand 2 is a key molecule to explain liver metabolic and histological alterations associated with high fat diet.

- ✓ Chemokine C-C motif ligand 2 overexpression affects cell survival, mitochondrial dynamics, autophagy and the regulation of energy sensors.

- ✓ Chemokine C-C motif ligand 2 impairs the senescence phenotype of mice with progeria syndrome (*Lmna*$^{G609G+/-}$).

- ✓ Our results suggest that chemokine C-C motif ligand 2 may be an important therapeutic target in metabolic diseases.

UNIVERSITAT ROVIRA I VIRGILI
THE ROLE OF CHEMOKINE (C-C MOTIF) LIGAND 2 IN INFLAMMATION, OXIDATIVE STRESS, AGING AND METABOLISM
Fedra Nicaury Luciano Mateo

References

Reference

UNIVERSITAT ROVIRA I VIRGILI
THE ROLE OF CHEMOKINE (C-C MOTIF) LIGAND 2 IN INFLAMMATION, OXIDATIVE STRESS, AGING AND METABOLISM
Fedra Nicaury Luciano Mateo

References

[1] Kohlgruber, A.C., LaMarche, N.M., Lynch, L., 2016. Adipose tissue at the nexus of systemic and cellular immunometabolism. Seminars in Immunology 28(5): 431–40.

[2] Man, K., Kutyavin, V.I., Chawla, A., Morris, C.A., Bunnell, B.A., Dhurandhar, N.V., et al., 2017. Tissue Immunometabolism: Development, Physiology, and Pathobiology. Cell Metabolism 25(1): 11–26.

[3] Mathis, D., Shoelson, S.E., Immunometabolism: an emerging frontier. Nature Reviews Immunology 11(2):81-83

[4] Rhoads, J.P., Major, A.S., Rathmell, J.C., 2017. Fine tuning of immunometabolism for the treatment of rheumatic diseases. Nature Reviews Rheumatology 13(5): 313–20.

[5] Rambold, A.S., Pearce, E.L., 2018. Mitochondrial Dynamics at the Interface of Immune Cell Metabolism and Function. Trends in Immunology 39(1): 6–18.

[6] Murphy, M.P., Hartley, R.C., 2018. Mitochondria as a therapeutic target for common pathologies. Nature Reviews Drug Discovery 17(12): 865–86.

[7] O'Connor, T., Borsig, L., Heikenwalder, M., 2015. CCL2-CCR2 Signaling in Disease Pathogenesis. Endocrine, Metabolic & Immune Disorders Drug Targets 15(2): 105–18.

[8] O'Neill, L.A.J., Kishton, R.J., Rathmell, J., 2016. A guide to immunometabolism for immunologists. Nature Reviews. Immunology 16(9): 553–65.

[9] Mahoney, J.R., Beutler, B.A., Le Trang, N., Vine, W., Ikeda, Y., Kawakami, M., et al., 1985. Lipopolysaccharide-treated RAW 264.7 cells produce a mediator that inhibits lipoprotein lipase in 3T3-L1 cells. Journal of Immunology (Baltimore, Md. : 1950) 134(3): 1673–5.

[10] Hotamisligil, G.S., Shargill, N.S., Spiegelman, B.M., 1993. Adipose expression of tumor necrosis factor-α: direct role in obesity-linked insulin resistance. Science 259(5091): 87–91.

[11] Miles, P.D., Romeo, O.M., Higo, K., Cohen, A., Rafaat, K., Olefsky, J.M., 1997. TNF-alpha-induced insulin resistance in vivo and its prevention by troglitazone. Diabetes 46(11): 1678–83.

[12] Hotamisligil, G.S., 2017. Foundations of Immunometabolism and Implications for Metabolic Health and Disease. Immunity 47(3): 406–20.

[13] Norata, G.D., Caligiuri, G., Chavakis, T., Matarese, G., Netea, M.G., Nicoletti, A., et al., 2015. The Cellular and Molecular Basis of Translational Immunometabolism. Immunity 43(3): 421–34.

[14] Wang, A., Luan, H.H., Medzhitov, R., 2019. An evolutionary perspective on immunometabolism. Science (New York, N.Y.) 363(6423): eaar3932.

[15] Exley, M.A., Hand, L., O'Shea, D., Lynch, L., 2014. Interplay between the immune system and adipose tissue in obesity. Journal of Endocrinology 223(2): R41–8.

[16] Chatzigeorgiou, A., Chavakis, T., 2015. Immune Cells and Metabolism. Springer, Cham 2016 (233):221-49.

[17] Van Dyken, S.J., Locksley, R.M., 2013. Interleukin-4- and Interleukin-13-Mediated Alternatively Activated Macrophages: Roles in Homeostasis and Disease. Annual Review of Immunology 31(1): 317–43.

[18] Molofsky, A.B., Nussbaum, J.C., Liang, H.-E., Van Dyken, S.J., Cheng, L.E., Mohapatra, A., et al., 2013. Innate lymphoid type 2 cells sustain visceral adipose tissue eosinophils and alternatively activated macrophages. The Journal of Experimental Medicine 210(3): 535–49.

[19] Kwon, H., Pessin, J.E., 2013. Adipokines Mediate Inflammation and Insulin Resistance. Frontiers in Endocrinology 4 (71): 1-13.

[20] Ouchi, N., Parker, J.L., Lugus, J.J., Walsh, K., 2011. Adipokines in inflammation and metabolic disease. Nature Reviews Immunology 11(2): 85–97.

[21] Chmelar, J., Chung, K.-J., Chavakis, T., 2013. The role of innate immune cells in obese adipose tissue inflammation and development of insulin resistance. Thrombosis and Haemostasis 109(03): 399–406.

[22] Fantuzzi, G., Faggioni, R., 2000. Leptin in the regulation of immunity, inflammation, and hematopoiesis. Journal of Leukocyte Biology 68(4): 437–46.

[23] Kumari, M., Heeren, J., Scheja, L., 2018. Regulation of immunometabolism in adipose tissue. Seminars in Immunopathology 40(2): 189–202.

[24] Lumeng, C.N., Bodzin, J.L., Saltiel, A.R., 2007. Obesity induces a phenotypic switch in adipose tissue macrophage polarization. Journal of Clinical Investigation 117(1): 175–84.

[25] Lumeng, C.N., Deyoung, S.M., Saltiel, A.R., 2007. Macrophages block insulin action in adipocytes by altering expression of signaling and glucose transport proteins. American Journal of Physiology-Endocrinology and Metabolism 292(1): E166–74.

[26] Miura, K., Yang, L., van Rooijen, N., Ohnishi, H., Seki, E., 2012. Hepatic recruitment of macrophages promotes nonalcoholic steatohepatitis through CCR2. American Journal of Physiology-Gastrointestinal and Liver Physiology 302(11): G1310–21.

[27] Krenkel, O., Tacke, F., 2017. Liver macrophages in tissue homeostasis and disease. Nature

Reviews Immunology 17(5): 306–21.

[28] Charo, I.F., Ransohoff, R.M., 2006. The many roles of chemokines and chemokine receptors in inflammation. The New England Journal of Medicine 354(6): 610–21.

[29] White, G.E., Iqbal, A.J., Greaves, D.R., 2013. CC chemokine receptors and chronic inflammation--therapeutic opportunities and pharmacological challenges. Pharmacological Reviews 65(1): 47–89.

[30] Luster, A.D., 1998. Chemokines--chemotactic cytokines that mediate inflammation. The New England Journal of Medicine 338(7): 436–45.

[31] Miller MC, Mayo KH, 2017. Chemokines from a Structural Perspective. International Journal of Molecular Sciences. 8(10). pii: E2088.

[32] Bonecchi, R., Galliera, E., Borroni, E.M., Corsi, M.M., Locati, M., Mantovani, A., 2009. Chemokines and chemokine receptors: an overview. Frontiers in Bioscience (Landmark Edition) 14: 540–51.

[33] Murdoch, C., Finn, A., 2000. Chemokine receptors and their role in inflammation and infectious diseases. Blood 95(10): 3032–43.

[34] Jin, T., Xu, X., Hereld, D., 2008. Chemotaxis, chemokine receptors and human disease. Cytokine 44(1): 1–8.

[35] Ransohoff, R.M., 2009. Chemokines and chemokine receptors: standing at the crossroads of immunobiology and neurobiology. Immunity 31(5): 711–21.

[36] Yadav, A., Saini, V., Arora, S., 2010. MCP-1: Chemoattractant with a role beyond immunity: A review. Clinica Chimica Acta 411(21-22): 1570–9.

[37] Xu, J., Fu, S., Peng, W., Rao, Z., 2012. MCP-1-induced protein-1, an immune regulator. Protein & Cell 3(12): 903–10.

[38] Deshmane, S.L., Kremlev, S., Amini, S., Sawaya, B.E., 2009. Monocyte Chemoattractant Protein-1 (MCP-1): An Overview. Journal of Interferon & Cytokine Research 29(6): 313–26.

[39] Cushing, S.D., Berliner, J.A., Valente, A.J., Territo, M.C., Navab, M., Parhami, F., et al., 1990. Minimally modified low density lipoprotein induces monocyte chemotactic protein 1 in human endothelial cells and smooth muscle cells. Proceedings of the National Academy of Sciences of the United States of America 87(13): 5134–8.

[40] Standiford, T.J., Kunkel, S.L., Phan, S.H., Rollins, B.J., Strieter, R.M., 1991. Alveolar macrophage-derived cytokines induce monocyte chemoattractant protein-1 expression from human pulmonary type II-like epithelial cells. The Journal of Biological Chemistry

266(15): 9912–8.

[41] Melgarejo, E., Medina, M.Á., Sánchez-Jiménez, F., Urdiales, J.L., 2009. Monocyte chemoattractant protein-1: A key mediator in inflammatory processes. The International Journal of Biochemistry & Cell Biology 41(5): 998–1001.

[42] Bose, S., Cho, J., 2013. Role of chemokine CCL2 and its receptor CCR2 in neurodegenerative diseases. Archives of Pharmacal Research 36(9): 1039–50.

[43] Sierra-Filardi, E., Nieto, C., Domínguez-Soto, A., Barroso, R., Sánchez-Mateos, P., Puig-Kroger, A., et al., 2014. CCL2 shapes macrophage polarization by GM-CSF and M-CSF: identification of CCL2/CCR2-dependent gene expression profile. Journal of Immunology (Baltimore, Md. : 1950) 192(8): 3858–67.

[44] Balkwill, F.R., 2012. The chemokine system and cancer. Journal of Pathology 226(2): 148–57.

[45] Ford, L.B., Cerovic, V., Milling, S.W.F., Graham, G.J., Hansell, C. a H., Nibbs, R.J.B., 2014. Characterization of conventional and atypical receptors for the chemokine CCL2 on mouse leukocytes. Journal of Immunology (Baltimore, Md. : 1950) 193(1): 400–11.

[46] Nibbs, R.J.B., Graham, G.J., 2013. Immune regulation by atypical chemokine receptors. Nat Rev Immunol 13(11): 815–29.

[47] Hansell, C.A.H., Hurson, C.E., Nibbs, R.J.B., 2011. DARC and D6: silent partners in chemokine regulation? 89(2): 197–206,

[48] Haller, H., Bertram, A., Nadrowitz, F., Menne, J., 2016. Monocyte chemoattractant protein-1 and the kidney. Current Opinion in Nephrology and Hypertension 25(1): 42–9.

[49] Panee, J., 2012. Monocyte Chemoattractant Protein 1 (MCP-1) in obesity and diabetes. Cytokine 60(1): 1–12.

[50] Rull, A., Rodríguez, F., Aragonès, G., Marsillach, J., Beltrán, R., Alonso-Villaverde, C., et al., 2009. Hepatic monocyte chemoattractant protein-1 is upregulated by dietary cholesterol and contributes to liver steatosis. Cytokine 48(3): 273–9.

[51] Camps, J., Rodríguez-Gallego, E., García-Heredia, A., Triguero, I., Riera-Borrull, M., Hernández-Aguilera, A., et al., 2014. Paraoxonases and chemokine (C-C motif) ligand-2 in noncommunicable diseases. Advances in Clinical Chemistry 63: 247–308.

[52] Gerard, C., Rollins, B.J., 2001. Chemokines and disease. Nature Immunology 2(2): 108–15.

[53] Raman, D., Sobolik-Delmaire, T., Richmond, A., 2011. Chemokines in health and disease. Experimental Cell Research 317(5): 575–89.

[54] Friedman, S.L., Ratziu, V., Harrison, S.A., Abdelmalek, M.F., Aithal, G.P., Caballeria, J., et al.,

2018. A randomized, placebo-controlled trial of cenicriviroc for treatment of nonalcoholic steatohepatitis with fibrosis. Hepatology 67(5): 1754–67.

[55] Gómez-Hernández, A., Beneit, N., Díaz-Castroverde, S., Escribano, Ó., 2016. Differential Role of Adipose Tissues in Obesity and Related Metabolic and Vascular Complications. International Journal of Endocrinology 2016: 1216783.

[56] Hotamisligil, G.S., 2006. Inflammation and metabolic disorders 1. Nature 444(1476-4687 (Electronic)): 860–7.

[57] Rull, A., Camps, J., Alonso-Villaverde, C., Joven, J., 2010. Insulin Resistance, Inflammation, and Obesity: Role of Monocyte Chemoattractant Protein-1 (orCCL2) in the Regulation of Metabolism. Mediators of Inflammation 2010: 1–11.

[58] Bruun, J.M., Lihn, A.S., Pedersen, S.B., Richelsen, B., 2005. Monocyte Chemoattractant Protein-1 Release Is Higher in Visceral than Subcutaneous Human Adipose Tissue (AT): Implication of Macrophages Resident in the AT. The Journal of Clinical Endocrinology & Metabolism 90(4): 2282–9.

[59] Yogarajah, T., Bee, Y.-T.G., Noordin, R., Yin, K.B., 2015. Increased peroxisome proliferator-activated receptor γ expression levels in visceral adipose tissue, and serum CCL2 and interleukin-6 levels during visceral adipose tissue accumulation. Molecular Medicine Reports 11(1): 515–20.

[60] Dandona, P., Aljada, A., Bandyopadhyay, A., 2004. Inflammation: the link between insulin resistance, obesity and diabetes. Trends in Immunology 25(1): 4–7.

[61] Wellen, K.E., Hotamisligil, G.S., 2005. Inflammation , stress , and diabetes. The Journal of Clinical Investigation 115(5): 1111–9.

[62] Vincent, H.K., Taylor, A.G., 2006. Biomarkers and potential mechanisms of obesity-induced oxidant stress in humans. International Journal of Obesity 30(3): 400–18.

[63] Yu, B.P., 1994. Cellular defenses against damage from reactive oxygen species. Physiological Reviews 74(1): 139–62.

[64] Fernández-Real, J.-M., Broch, M., Vendrell, J., Ricart, W., 2003. Insulin resistance, inflammation, and serum fatty acid composition. Diabetes Care 26(5): 1362–8.

[65] Bełtowski, J., Wójcicka, G., Górny, D., Marciniak, A., 2000. The effect of dietary-induced obesity on lipid peroxidation, antioxidant enzymes and total plasma antioxidant capacity. Journal of Physiology and Pharmacology : An Official Journal of the Polish Physiological Society 51(4 Pt 2): 883–96.

[66] Davì, G., Guagnano, M.T., Ciabattoni, G., Basili, S., Falco, A., Marinopiccoli, M., et al., n.d. Platelet activation in obese women: role of inflammation and oxidant stress. JAMA 288(16): 2008–14.

[67] Miao, L., St. Clair, D.K., 2009. Regulation of superoxide dismutase genes: Implications in disease. Free Radical Biology and Medicine 47(4): 344–56.

[68] Margis, R., Dunand, C., Teixeira, F.K., Margis-Pinheiro, M., 2008. Glutathione peroxidase family - an evolutionary overview. FEBS Journal 275(15): 3959–70.

[69] Cardoso, B.R., Hare, D.J., Bush, A.I., Roberts, B.R., 2017. Glutathione peroxidase 4: a new player in neurodegeneration? Molecular Psychiatry 22(3): 328–35.

[70] García-Heredia, A., Kensicki, E., Mohney, R.P., Rull, A., Triguero, I., Marsillach, J., et al., 2013. Paraoxonase-1 Deficiency Is Associated with Severe Liver Steatosis in Mice Fed a High-fat High-cholesterol Diet: A Metabolomic Approach. Journal of Proteome Research 12(4): 1946–55.

[71] Camps, J., Iftimie, S., García-Heredia, A., Castro, A., Joven, J., 2017. Paraoxonases and infectious diseases. Clinical Biochemistry 50(13-14): 804–11.

[72] Reuter, S., Gupta, S.C., Chaturvedi, M.M., Aggarwal, B.B., 2010. Oxidative stress, inflammation, and cancer: How are they linked? Free Radical Biology and Medicine 49(11): 1603–16.

[73] Musso, G., Cassader, M., Gambino, R., 2016. Non-alcoholic steatohepatitis: emerging molecular targets and therapeutic strategies. Nature Reviews Drug Discovery 15(4): 249–74.

[74] García-Ruiz, I., Solís-Muñoz, P., Fernández-Moreira, D., Grau, M., Muñoz-Yagüe, T., Solís-Herruzo, J.A., 2016. NADPH oxidase is implicated in the pathogenesis of oxidative phosphorylation dysfunction in mice fed a high-fat diet. Scientific Reports 6(1): 23664.

[75] Xu, L., Kitade, H., Ni, Y., Ota, T., 2015. Roles of chemokines and chemokine receptors in obesity-associated insulin resistance and nonalcoholic fatty liver disease. Biomolecules 5(3): 1563–79.

[76] Garcia, M.C., Amankwa-Sakyi, M., Flynn, T.J., 2011. Cellular glutathione in fatty liver in vitro models. Toxicology in Vitro 25(7): 1501–6.

[77] Koliaki, C., Szendroedi, J., Schlensak, M., Roden Correspondence, M., Kaul, K., Jelenik, T., et al., 2015. Adaptation of Hepatic Mitochondrial Function in Humans with Non-Alcoholic Fatty Liver Is Lost in Steatohepatitis Cell Metabolism Adaptation of Hepatic Mitochondrial Function in Humans with Non-Alcoholic Fatty Liver Is Lost in Steatohepatitis. Cell

Metabolism 21: 739–46.

[78] Arrese, M., Cabrera, D., Kalergis, A.M., Feldstein, A.E., 2016. Innate Immunity and Inflammation in NAFLD/NASH. Digestive Diseases and Sciences 61(5): 1294–303.

[79] Duarte, N., Coelho, I.C., Patarrão, R.S., Almeida, J.I., Penha-Gonçalves, C., Macedo, M.P., 2015. How Inflammation Impinges on NAFLD: A Role for Kupffer Cells. BioMed Research International 2015: 984578.

[80] Fabbrini, E., Sullivan, S., Klein, S., 2010. Obesity and nonalcoholic fatty liver disease: Biochemical, metabolic, and clinical implications. Hepatology 51(2): 679–89.

[81] Roh, Y. S., & Seki, E. 2018. Chemokines and Chemokine Receptors in the Development of NAFLD. In Obesity, Fatty Liver and Liver Cancer. Springer, Singapore. 1061:45-53.

[82] Obstfeld, A.E., Sugaru, E., Thearle, M., Francisco, A.-M., Gayet, C., Ginsberg, H.N., et al., 2010. C-C Chemokine Receptor 2 (CCR2) Regulates the Hepatic Recruitment of Myeloid Cells That Promote Obesity-Induced Hepatic Steatosis. Diabetes 59(4): 916–25.

[83] Yang, S.J., Iglayreger, H.B., Kadouh, H.C., Bodary, P.F., 2009. Inhibition of the chemokine (C-C motif) ligand 2/chemokine (C-C motif) receptor 2 pathway attenuates hyperglycaemia and inflammation in a mouse model of hepatic steatosis and lipoatrophy. Diabetologia 52(5): 972–81.

[84] Tacke, F., 2017. Targeting hepatic macrophages to treat liver diseases. Journal of Hepatology 66(6): 1300–12.

[85] Ren, R., Ocampo, A., Liu, G.-H., Izpisua Belmonte, J.C., 2017. Regulation of Stem Cell Aging by Metabolism and Epigenetics. Cell Metabolism 26(3): 460–74.

[86] Minciullo, P.L., Catalano, A., Mandraffino, G., Casciaro, M., Crucitti, A., Maltese, G., et al., 2016. Inflammaging and Anti-Inflammaging: The Role of Cytokines in Extreme Longevity. Archivum Immunologiae et Therapiae Experimentalis 64(2): 111–26.

[87] López-Otín, C., Blasco, M.A., Partridge, L., Serrano, M., Kroemer, G., 2013. The Hallmarks of Aging. Cell 153(6): 1194–217.

[88] Baylis, D., Bartlett, D.B., Patel, H.P., Roberts, H.C., 2013. Understanding how we age: insights into inflammaging. Longevity & Healthspan 2(1): 8.

[89] Franceschi, C., Campisi, J., 2014. Chronic Inflammation (Inflammaging) and Its Potential Contribution to Age-Associated Diseases. The Journals of Gerontology Series A: Biological Sciences and Medical Sciences 69 (6): 4–9.

[90] Fulop, T., Witkowski, J.M., Olivieri, F., Larbi, A., 2018. The integration of inflammaging in

age-related diseases. Seminars in Immunology 40 (12): 17–35.

[91] Wu, X., Cao, N., Fenech, M., Wang, X., 2016. Role of Sirtuins in Maintenance of Genomic Stability: Relevance to Cancer and Healthy Aging. DNA and Cell Biology 35(10): 1–34.

[92] Nelson, G., Wordsworth, J., Wang, C., Jurk, D., Lawless, C., Martin-Ruiz, C., et al., 2012. A senescent cell bystander effect: senescence-induced senescence. Aging Cell 11(2): 345–9.

[93] Yousefzadeh, M.J., Schafer, M.J., Noren Hooten, N., Atkinson, E.J., Evans, M.K., Baker, D.J., et al., 2018. Circulating levels of monocyte chemoattractant protein-1 as a potential measure of biological age in mice and frailty in humans. Aging Cell 17(2): e12706.

[94] Brouwers, B., Dalmasso, B., Hatse, S., Laenen, A., Kenis, C., Swerts, E., et al., 2015. Biological ageing and frailty markers in breast cancer patients. Aging 7(5): 319–33.

[95] Chiao, Y.A., Dai, Q., Zhang, J., Lin, J., Lopez, E.F., Ahuja, S.S., et al., 2011. Multi-Analyte Profiling Reveals Matrix Metalloproteinase-9 and Monocyte Chemotactic Protein-1 as Plasma Biomarkers of Cardiac Aging. Circulation: Cardiovascular Genetics 4(4): 455–62.

[96] Coppé, J.-P., Desprez, P.-Y., Krtolica, A., Campisi, J., 2010. The Senescence-Associated Secretory Phenotype: The Dark Side of Tumor Suppression. Annual Review of Pathology: Mechanisms of Disease 5(1): 99–118.

[97] Deo, R., Khera, A., McGuire, D.K., Murphy, S.A., de P. Meo Neto, J., Morrow, D.A., et al., 2004. Association among plasma levels of monocyte chemoattractant protein-1, traditional cardiovascular risk factors, and subclinical atherosclerosis. Journal of the American College of Cardiology 44(9): 1812–8.

[98] Franceschi, C., Garagnani, P., Vitale, G., Capri, M., Salvioli, S., 2017. Inflammaging and “Garb-aging”. Trends in Endocrinology and Metabolism: TEM 28(3): 199–212.

[99] Gordon, L.B., Rothman, F.G., López-Otín, C., Misteli, T., 2014. Progeria: A paradigm for translational medicine. Cell 156(3): 400–7.

[100] Ghosh, S., Zhou, Z., 2014. Genetics of aging, progeria and lamin disorders. Current Opinion in Genetics & Development 26: 41–6.

[101] Merideth, M.A., Gordon, L.B., Clauss, S., Sachdev, V., Smith, A.C.M., Perry, M.B., et al., 2008. Phenotype and Course of Hutchinson–Gilford Progeria Syndrome. New England Journal of Medicine 358(6): 592–604.

[102] Osorio, F.G., Ugalde, A.P., Mariño, G., Puente, X.S., Freije, J.M.P., López-Otín, C., 2011. Cell autonomous and systemic factors in progeria development. Biochemical Society Transactions 39(6): 1710–4.

[103] De Sandre-Giovannoli, A., 2003. Lamin A Truncation in Hutchinson-Gilford Progeria. Science 300(5628): 2055–2055.

[104] López-otín, C., 2005. From Immature Lamin to Premature Aging Molecular Pathways and Therapeutic Opportunities. Cell Cycle 4101(12): 1732–5.

[105] Osorio, F.G., Obaya, Á.J., López-Otín, C., Freije, J.M.P., 2009. Accelerated ageing: From mechanism to therapy through animal models. Transgenic Research 18(1): 7–15.

[106] Gonzalez, J.M., Pla, D., Perez-Sala, D., Andres, V., 2011. A-type lamins and Hutchinson-Gilford progeria syndrome: pathogenesis and therapy. Frontiers in Bioscience, 3: 1133–46.

[107] Cadiñanos, J., Varela, I., López-Otín, C., Freije, J.M.P., 2005. From Immature Lamin to Premature Aging: Molecular Pathways and Therapeutic Opportunities. Cell Cycle 4(12): 1732–5.

[108] Hamczyk, M.R., del Campo, L., Andrés, V., 2018. Aging in the Cardiovascular System: Lessons from Hutchinson-Gilford Progeria Syndrome. Annual Review of Physiology 80(1): 27–48.

[109] Villa-Bellosta R, Rivera-Torres J, Osorio FG, Acín-Pérez R, Enriquez JA, López-Otín C, Andrés V.., et al., 2013. Defective extracellular pyrophosphate metabolism promotes vascular calcification in a mouse model of Hutchinson-Gilford progeria syndrome that is ameliorated on pyrophosphate treatment. Circulation 127(24): 2442–51.

[110] Soria-Valles, C., Osorio, F.G., Gutierrez-Fernandez, A., De Los Angeles, A., Bueno, C., Menendez, P., et al., 2015. NF-[kappa]B activation impairs somatic cell reprogramming in ageing. Nat Cell Biol 17(8): 1004–13.

[111] Peinado, J.R., Quiros, P.M., Pulido, M.R., Marino, G., Martinez-Chantar, M.L., Vazquez-Martinez, R., et al., 2011. Proteomic Profiling of Adipose Tissue from Zmpste24-/- Mice, a Model of Lipodystrophy and Premature Aging, Reveals Major Changes in Mitochondrial Function and Vimentin Processing. Molecular & Cellular Proteomics 10(11): M111.008094–M111.008094.

[112] Carrero, D., Soria-Valles, C., López-Otín, C., 2016. Hallmarks of progeroid syndromes: lessons from mice and reprogrammed cells. Disease Models & Mechanisms 9(7): 719–35.

[113] Osorio, F.G., Navarro, C.L., Cadiñanos, J., López-Mejía, I.C., Quirós, P.M., Bartoli, C., et al., 2011. Splicing-directed therapy in a new mouse model of human accelerated aging. Science Translational Medicine 3(106): 106ra107.

[114] Sorriento, D., Pascale, A.V., Finelli, R., Carillo, A.L., Annunziata, R., Trimarco, B., et al., 2014. Targeting Mitochondria as Therapeutic Strategy for Metabolic Disorders. The Scientific

World Journal 2014: 1–9.

[115] Kozlov, A. V., Lancaster, J.R., Meszaros, A.T., Weidinger, A., 2017. Mitochondria-meditated pathways of organ failure upon inflammation. Redox Biology 13(April): 170–81.

[116] Sunny, N.E., Bril, F., Cusi, K., 2017. Mitochondrial Adaptation in Nonalcoholic Fatty Liver Disease: Novel Mechanisms and Treatment Strategies. Trends in Endocrinology and Metabolism: TEM 28(4): 250–60.

[117] Van Horssen, J., Van Schaik, P., Witte, M., 2017. Title: Inflammation and mitochondrial dysfunction: a vicious circle in neurodegenerative disorders? Inflammation and mitochondrial dysfunction: a vicious circle in neurodegenerative disorders? Neuroscience Letters.

[118] Willems, P.H.G.M., Rossignol, R., Dieteren, C.E.J., Murphy, M.P., Koopman, W.J.H., 2015. Redox Homeostasis and Mitochondrial Dynamics. Cell Metabolism 22(2): 207–18.

[119] Bournat, J.C., Brown, C.W., 2010. Mitochondrial dysfunction in obesity. Current Opinion in Endocrinology, Diabetes, and Obesity 17(5): 446–52.

[120] Westermann, B., 2010. Mitochondrial fusion and fission in cell life and death. Nature Reviews Molecular Cell Biology 11(12): 872–84.

[121] Eisner, V., Picard, M., Hajnóczky, G., 2018. Mitochondrial dynamics in adaptive and maladaptive cellular stress responses. Nature Cell Biology 20(7): 755–65.

[122] Mishra, P., Chan, D.C., 2016. Metabolic regulation of mitochondrial dynamics. 212(4): 379-387.

[123] Riera-Borrull, M., Rodríguez-Gallego, E., Hernández-Aguilera, A., Luciano, F., Ras, R., Cuyàs, E., et al., 2016. Exploring the Process of Energy Generation in Pathophysiology by Targeted Metabolomics: Performance of a Simple and Quantitative Method. Journal of the American Society for Mass Spectrometry 27(1): 168–77.

[124] Buck, M.D., O'Sullivan, D., Pearce, E.L., 2015. T cell metabolism drives immunity. The Journal of Experimental Medicine 212(9): 1345–60.

[125] Bonora, M., Patergnani, S., Rimessi, A., De Marchi, E., Suski, J.M., Bononi, A., et al., 2012. ATP synthesis and storage. Purinergic Signalling 8(3): 343–57.

[126] Pfanner, N., Warscheid, B., Wiedemann, N., 2019. Mitochondrial proteins: from biogenesis to functional networks. Nature Reviews Molecular Cell Biology: 20: 267–284 1.

[127] Milenkovic, D., Blaza, J.N., Larsson, N.-G., Hirst, J., 2017. The Enigma of the Respiratory Chain Supercomplex. Cell Metabolism 25(4): 765–76.

[128] Yuan, H.-X., Xiong, Y., Guan, K.-L., 2013. Nutrient sensing, metabolism, and cell growth control. Molecular Cell 49(3): 379–87.

[129] Fruman, D.A., Chiu, H., Hopkins, B.D., Bagrodia, S., Cantley, L.C., Abraham, R.T., 2017. The PI3K Pathway in Human Disease. Cell 170 (4): 605–35.

[130] Law, B.K., 2005. Rapamycin: An anti-cancer immunosuppressant? Critical Reviews in Oncology/Hematology 56(1): 47–60.

[131] Engelman, J.A., Luo, J., Cantley, L.C., 2006. The evolution of phosphatidylinositol 3-kinases as regulators of growth and metabolism. Nature Reviews Genetics 7(8): 606–19.

[132] Pezze, P.D., Ruf, S., Sonntag, A.G., Langelaar-Makkinje, M., Hall, P., Heberle, A.M., et al., 2016. A systems study reveals concurrent activation of AMPK and mTOR by amino acids. Nature Communications 7: 13254.

[133] Lopez-Guadamillas, E., Muñoz-Martin, M., Martinez, S., Pastor, J., Fernandez-Marcos, P.J., Serrano, M., 2016. PI3Kα inhibition reduces obesity in mice. Aging 8(11): 2747–53.

[134] Jiang, B.-H., Liu, L.-Z., 2008. Role of mTOR in anticancer drug resistance: Perspectives for improved drug treatment. Drug Resistance Updates 11(3): 63–76.

[135] Tee, A.R., Blenis, J., 2005. mTOR, translational control and human disease. Seminars in Cell & Developmental Biology 16(1): 29–37.

[136] Ching, C.B., Hansel, D.E., 2010. Expanding therapeutic targets in bladder cancer: the PI3K/Akt/mTOR pathway. Laboratory Investigation 90(10): 1406–14.

[137] Zoncu, R., Bar-Peled, L., Efeyan, A., Wang, S., Sancak, Y., Sabatini, D.M., 2011. mTORC1 Senses Lysosomal Amino Acids Through an Inside-Out Mechanism That Requires the Vacuolar H+-ATPase. Science 334(6056): 678–83.

[138] Saxton, R.A., Sabatini, D.M., 2017. mTOR Signaling in Growth, Metabolism, and Disease. Cell. 168(6):960-976.

[139] Guertin, D.A., Sabatini, D.M., 2005. An expanding role for mTOR in cancer. Trends in Molecular Medicine 11(8): 353–61.

[140] Fingar, D.C., Blenis, J., 2004. Target of rapamycin (TOR): an integrator of nutrient and growth factor signals and coordinator of cell growth and cell cycle progression. Oncogene 23(18): 3151–71.

[141] Zoncu, R., Efeyan, A., Sabatini, D.M., 2011. mTOR: from growth signal integration to cancer, diabetes and ageing. Nature Reviews Molecular Cell Biology 12(1): 21–35.

[142] Woods, A., Williams, J.R., Muckett, P.J., Mayer, F. V., Liljevald, M., Bohlooly-Y, M., et al.,

2017. Liver-Specific Activation of AMPK Prevents Steatosis on a High-Fructose Diet. Cell Reports 18(13): 3043–51.

[143] Garcia, D., Shaw, R.J., 2017. AMPK: Mechanisms of Cellular Energy Sensing and Restoration of Metabolic Balance. Molecular Cell 66(6): 789–800.

[144] Klionsky, D.J., Klionsky, D.J., Abdelmohsen, K., Abe, A., Abedin, M.J., Abeliovich, H., et al., 2016. Guidelines for the use and interpretation of assays for monitoring autophagy (3rd edition). Autophagy 12(1): 1–222.

[145] Zhang, Z., Yao, Z., Chen, Y., Qian, L., Jiang, S., Zhou, J., et al., 2017. Lipophagy and liver disease: New perspectives to better understanding and therapy. 97: 339-348.

[146] Filomeni, G., De Zio, D., Cecconi, F., 2015. Oxidative stress and autophagy: the clash between damage and metabolic needs. Cell Death and Differentiation 22(3): 377–88.

[147] Scherz-Shouval, R., Elazar, Z., 2007. ROS, mitochondria and the regulation of autophagy. Trends in Cell Biology 17(9): 422–7.

[148] Hansen, M., Rubinsztein, D.C., Walker, D.W., 2018. Autophagy as a promoter of longevity: insights from model organisms. Nature Reviews Molecular Cell Biology 19(9): 579–93.

[149] Cadwell, K., 2016. Crosstalk between autophagy and inflammatory signalling pathways: balancing defence and homeostasis. Nature Reviews. Immunology 16(11): 661–75.

[150] Schneider, J.L., Cuervo, A.M., 2014. Liver autophagy: much more than just taking out the trash. Nature Reviews. Gastroenterology & Hepatology 11(3): 187–200.

[151] Kaushik, S., Cuervo, A.M., 2012. Chaperone-mediated autophagy: a unique way to enter the lysosome world. Trends in Cell Biology 22(8): 407–17.

[152] Kaushik, S., Cuervo, A.M., 2018. The coming of age of chaperone-mediated autophagy. Nature Reviews Molecular Cell Biology 19(6): 365–81.

[153] Schneider, J.L., Cuervo, A.M., 2014. Autophagy and human disease: emerging themes. Current Opinion in Genetics & Development 26: 16–23.

[154] Ryter, S.W., Koo, J.K., Choi, A.M.K., 2014. Molecular regulation of autophagy and its implications for metabolic diseases. Current Opinion in Clinical Nutrition and Metabolic Care 17(4): 329–37.

[155] Kim, Y.C., Guan, K.-L., 2015. mTOR: a pharmacologic target for autophagy regulation. Journal of Clinical Investigation 125(1): 25–32.

[156] Cai, Z., Yan, L.-J., 2013. Rapamycin, Autophagy, and Alzheimer's Disease. Journal of Biochemical and Pharmacological Research 1(2): 84–90.

[157] Li, J., Kim, S.G., Blenis, J., 2014. Rapamycin: one drug, many effects. Cell Metabolism 19(3): 373–9.

[158] Ben Sahra, I., Laurent, K., Giuliano, S., Larbret, F., Ponzio, G., Gounon, P., et al., 2010. Targeting Cancer Cell Metabolism: The Combination of Metformin and 2-Deoxyglucose Induces p53-Dependent Apoptosis in Prostate Cancer Cells. Cancer Research 70(6): 2465–75.

[159] Shi, W.-Y., Xiao, D., Wang, L., Dong, L.-H., Yan, Z.-X., Shen, Z.-X., et al., 2012. Therapeutic metformin/AMPK activation blocked lymphoma cell growth via inhibition of mTOR pathway and induction of autophagy. Cell Death & Disease 3(3): e275–e275.

[160] Locasale, J.W., 2013. Serine, glycine and one-carbon units: cancer metabolism in full circle. Nature Reviews Cancer 13(8): 572–83.

[161] Mentch, S.J., Locasale, J.W., 2016. One-carbon metabolism and epigenetics: understanding the specificity. Annals of the New York Academy of Sciences 1363(1): 91–8.

[162] Ducker, G.S., Rabinowitz, J.D., 2017. Cell Metabolism Review One-Carbon Metabolism in Health and Disease. Cell Metabolism 25: 27–42.

[163] Moran-Salvador, E., Mann, J., 2017. Epigenetics and Liver Fibrosis. Cmgh 4(1): 125–34.

[164] Xu, W., Wang, F., Yu, Z., Xin, F., 2016. Epigenetics and Cellular Metabolism. Genetics & Epigenetics 8: 43–51.

[165] Friso, S., Udali, S., De Santis, D., Choi, S.-W., 2017. One-carbon metabolism and epigenetics. Molecular Aspects of Medicine 54: 28–36.

[166] Lee, J., Friso, S., Choi, S.-W., 2014. Epigenetic Mechanisms Underlying the Link between Non-Alcoholic Fatty Liver Diseases and Nutrition. Nutrients 6(8): 3303–25.

[167] Joven, J., Rull, A., Ferré, N., Escolà-Gil, J.C., Marsillach, J., Coll, B., et al., 2007. The results in rodent models of atherosclerosis are not interchangeable. Atherosclerosis 195(2): e85–92.

[168] Rodríguez-Sanabria, F., Rull, A., Beltrán-Debón, R., Aragonès, G., Camps, J., Mackness, B., et al., 2010. Tissue distribution and expression of paraoxonases and chemokines in mouse: the ubiquitous and joint localisation suggest a systemic and coordinated role. Journal of Molecular Histology 41(6): 379–86.

[169] Liang, W., Menke, A.L., Driessen, A., Koek, G.H., Lindeman, J.H., Stoop, R., et al., 2014. Establishment of a general NAFLD scoring system for rodent models and comparison to human liver pathology. PloS One 9(12): e115922.

[170] Heymann, F., Tacke, F., 2016. Immunology in the liver — from homeostasis to disease.

Nature Reviews Gastroenterology & Hepatology 13(2): 88–110.

[171] Scott, C.L., Zheng, F., De Baetselier, P., Martens, L., Saeys, Y., De Prijck, S., et al., 2016. Bone marrow-derived monocytes give rise to self-renewing and fully differentiated Kupffer cells. Nature Communications 7: 10321.

[172] Pérez-Carro, R., Sánchez-Alcudia, R., Pérez, B., Navarrete, R., Pérez-Cerdá, C., Ugarte, M., et al., 2014. Functional analysis and *in vitro* correction of splicing *FAH* mutations causing tyrosinemia type I. Clinical Genetics 86(2): 167–71.

[173] Florholmen-Kjær, Å., Lyså, R.A., Fuskevåg, O.-M., Goll, R., Revhaug, A., Mortensen, K.E., 2014. A sensitive method for the analysis of glutathione in porcine hepatocytes. Scandinavian Journal of Gastroenterology 49(11): 1–8.

[174] Rodríguez-Gallego, E., Riera-Borrull, M., Hernández-Aguilera, A., Mariné-Casadó, R., Rull, A., Beltrán-Debón, R., et al., 2013. Ubiquitous transgenic overexpression of C-C Chemokine Ligand 2: A model to assess the combined effect of high energy intake and continuous low-grade inflammation. Mediators of Inflammation 2013 (2013): 953841

[175] Velazquez-Villegas, L.A., Perino, A., Lemos, V., Zietak, M., Nomura, M., Pols, T.W.H., et al., 2018. TGR5 signalling promotes mitochondrial fission and beige remodelling of white adipose tissue. Nature Communications 9(1): 245.

[176] Takeda, T., Hosokawa, M., Takeshita, S., Irino, M., Higuchi, K., Matsushita, T., et al., 1981. A new murine model of accelerated senescence. Mechanisms of Ageing and Development 17(2): 183–94.

[177] Rossella, F., Polledri, E., Bollati, V., Baccarelli, A., Fustinoni, S., 2009. Development and validation of a gas chromatography/mass spectrometry method for the assessment of genomic DNA methylation. Rapid Communications in Mass Spectrometry 23(17): 2637–46.

[178] Satapati, S., Kucejova, B., Duarte, J.A.G., Fletcher, J.A., Reynolds, L., Sunny, N.E., et al., 2015. Mitochondrial metabolism mediates oxidative stress and inflammation in fatty liver. Journal of Clinical Investigation 125(12): 4447–62.

[179] Schriner, S.E., Linford, N.J., Martin, G.M., Treuting, P., Ogburn, C.E., Emond, M., et al., 2005. Extension of Murine Life Span by Overexpression of Catalase Targeted to Mitochondria. Science 308(5730): 1909–11.

[180] Nguyen, G., Park, S.Y., Le, C.T., Park, W.S., Choi, D.H., Cho, E.-H., 2018. Metformin ameliorates activation of hepatic stellate cells and hepatic fibrosis by succinate and GPR91 inhibition. Biochemical and Biophysical Research Communications 495(4): 2649–56.

[181] Mato, J.M., Lu, S.C., 2007. Role of S-adenosyl-L-methionine in liver health and injury. Hepatology 45(5): 1306–12.

[182] Li, N., Hua, J., 2017. Immune cells in liver regeneration. Oncotarget 8(2): 3628–39.

[183] Robinson, M.W., Harmon, C., O'Farrelly, C., 2016. Liver immunology and its role in inflammation and homeostasis. Cellular & Molecular Immunology 13(3): 267–76.

[184] Riera-Borrull, M., García-Heredia, A., Fernández-Arroyo, S., Hernández-Aguilera, A., Cabré, N., Cuyàs, E., et al., 2017. Metformin potentiates the benefits of dietary restraint: A metabolomic study. International Journal of Molecular Sciences 18(11): 2263-2279

[185] Frudd, K., Burgoyne, T., Burgoyne, J.R., 2018. Oxidation of Atg3 and Atg7 mediates inhibition of autophagy. Nature Communications 9(1): 95-108.

[186] Czaja, M.J., 2016. Function of Autophagy in Nonalcoholic Fatty Liver Disease. Digestive Diseases and Sciences 61(5): 1304–13.

[187] Yan, S., Huda, N., Khambu, B., Yin, X.-M., 2017. Relevance of autophagy to fatty liver diseases and potential therapeutic applications. Amino Acids 49(12): 1965–79.

[188] Rodriguez-Navarro, J.A., Kaushik, S., Koga, H., Dall'Armi, C., Shui, G., Wenk, M.R., et al., 2012. Inhibitory effect of dietary lipids on chaperone-mediated autophagy. Proceedings of the National Academy of Sciences of the United States of America 109(12): E705–14.

[189] Kjøbsted, R., Hingst, J.R., Fentz, J., Foretz, M., Sanz, M.-N., Pehmøller, C., et al., 2018. AMPK in skeletal muscle function and metabolism. The FASEB Journal 32(4): 1741–77.

[190] Ljubicic, V., Miura, P., Burt, M., Boudreault, L., Khogali, S., Lunde, J.A., et al., 2011. Chronic AMPK activation evokes the slow, oxidative myogenic program and triggers beneficial adaptations in mdx mouse skeletal muscle. Human Molecular Genetics 20(17): 3478–93.

[191] Smith, R.L., Soeters, M.R., Wüst, R.C.I., Houtkooper, R.H., 2018. Metabolic Flexibility as an Adaptation to Energy Resources and Requirements in Health and Disease. Endocrine Reviews 39(4): 489–517.

[192] Wai, T., Langer, T., 2016. Mitochondrial Dynamics and Metabolic Regulation. Trends in Endocrinology & Metabolism 27(2): 105–17.

[193] Lu, Y.-T., Li, L.-Z., Yang, Y.-L., Yin, X., Liu, Q., Zhang, L., et al., 2018. Succinate induces aberrant mitochondrial fission in cardiomyocytes through GPR91 signaling. Cell Death & Disease 9(6): 672-689

[194] He, W., Miao, F.J.-P., Lin, D.C.-H., Schwandner, R.T., Wang, Z., Gao, J., et al., 2004. Citric acid cycle intermediates as ligands for orphan G-protein-coupled receptors. Nature 429(6988):

188–93.

[195] Jin, H.J., Lee, H.J., Heo, J., Lim, J., Kim, M., Kim, M.K., et al., 2016. Senescence-Associated MCP-1 Secretion Is Dependent on a Decline in BMI1 in Human Mesenchymal Stromal Cells. Antioxidants & Redox Signaling 24(9): 471–85.

[196] Hasty, P., Sharp, Z.D., Curiel, T.J., Campisi, J., 2013. mTORC1 and p53. Cell Cycle 12(1): 20–5.

[197] Christy, B., Demaria, M., Campisi, J., Huang, J., Jones, D., Dodds, S.G., et al., 2015. p53 and rapamycin are additive. Oncotarget 6(18): 15802–13.

[198] Mariño, G., López-Otín, C., 2008. Autophagy and aging: new lessons from progeroid mice. Autophagy 4(6): 807–9.

[199] Mariño, G., Ugalde, A.P., Salvador-Montoliu, N., Varela, I., Quirós, P.M., Cadiñanos, J., et al., 2008. Premature aging in mice activates a systemic metabolic response involving autophagy induction. Human Molecular Genetics 17(14): 2196–211.

[200] Vilchez, D., Saez, I., Dillin, A., 2014. The role of protein clearance mechanisms in organismal ageing and age-related diseases. Nature Communications 5(1): 5659-72.

[201] Kaushik, S., Cuervo, A.M., 2015. Proteostasis and aging. Nature Medicine 21(12): 1406–15.

[202] Chew, A.L., Tan, W.Y., Khoo, B.Y., 2013. Potential combinatorial effects of recombinant atypical chemokine receptors in breast cancer cell invasion: A research perspective. Biomedical Reports 1(2): 185–92.

[203] Bartoli, C., Civatte, M., Pellissier, J.F., Figarella-Branger, D., 2001. CCR2A and CCR2B, the two isoforms of the monocyte chemoattractant protein-1 receptor are up-regulated and expressed by different cell subsets in idiopathic inflammatory myopathies. Acta Neuropathologica 102(4): 385–92.

[204] López-Otín, C., Galluzzi, L., Freije, J. M., Madeo, F., & Kroemer, G, 2016 .Metabolic control of longevity. Cell, 166(4), 802-821.

[205] Wang, K., & Klionsky, D. J, 2011. Mitochondria removal by autophagy. Autophagy, 7(3), 297-300.

Appendices

Appendice

UNIVERSITAT ROVIRA I VIRGILI
THE ROLE OF CHEMOKINE (C-C MOTIF) LIGAND 2 IN INFLAMMATION, OXIDATIVE STRESS, AGING AND METABOLISM
Fedra Nicaury Luciano Mateo

UNIVERSITAT ROVIRA I VIRGILI
THE ROLE OF CHEMOKINE (C-C MOTIF) LIGAND 2 IN INFLAMMATION, OXIDATIVE STRESS, AGING AND METABOLISM
Fedra Nicaury Luciano Mateo

BBA - Molecular Basis of Disease 1865 (2019) 1555–1566

Contents lists available at ScienceDirect

BBA - Molecular Basis of Disease

journal homepage: www.elsevier.com/locate/bbadis

Chemokine (C-C motif) ligand 2 gene ablation protects low-density lipoprotein and paraoxonase-1 double deficient mice from liver injury, oxidative stress and inflammation

Fedra Luciano-Mateo[a,b], Noemí Cabré[a,b], Salvador Fernández-Arroyo[a,b], Gerard Baiges-Gaya[b], Anna Hernández-Aguilera[a,b], Elisabet Rodríguez-Tomàs[b], Maria Mercado-Gómez[b], Javier A. Menendez[c,d], Jordi Camps[a,b,*], Jorge Joven[a,b,e,*]

[a] Universitat Rovira i Virgili, Department of Medicine and Surgery, Reus, Spain
[b] Unitat de Recerca Biomèdica, Hospital Universitari Sant Joan, Institut d'Investigació Sanitària Pere Virgili, Universitat Rovira i Virgili, Reus, Spain
[c] Program Against Cancer Therapeutic Resistance (ProCURE), Metabolism and Cancer Group, Catalan Institute of Oncology, Girona, Spain
[d] Girona Biomedical Research Institute (IDIBGI), Girona, Spain
[e] The Campus of International Excellence Southern Catalonia, Tarragona, Spain

ARTICLE INFO

Keywords:
Autophagy
Chemokine (C-C motif) ligand 2
Energy metabolism
Glutathione
Methionine cycle
Non-alcoholic fatty liver disease

ABSTRACT

The risk of non-alcoholic fatty liver disease increases with obesity. Vulnerability to oxidative stress and/or inflammation represents a crucial step in non-alcoholic fatty liver disease progression through abnormal metabolic responses. In this study, we investigated the role of CCL2 gene ablation in mice that were double deficient in low density lipoprotein receptor and in paraoxonase-1. Mass spectrometry methods were used to assess the liver metabolic response in mice fed either regular chow or a high-fat diet. Dietary fat caused liver steatosis, oxidative stress and the accumulation of pro-inflammatory macrophages in the livers of double deficient mice. We observed alterations in energy metabolism-related pathways and in metabolites associated with the methionine cycle and the glutathione reduction pathway. This metabolic response was associated with impaired autophagy. Conversely, when we established CCL2 deficiency, histologic features of fatty liver disease were abrogated, hepatic liver oxidative stress decreased, and anti-inflammatory macrophage marker expression levels increased. These changes were associated with the normalization of metabolic disturbances and increased lysosome-associated membrane protein 2, expression, which suggests enhanced chaperone-mediated autophagy. This study demonstrates that CCL2 is a key molecule for the development of metabolic and histological alterations in the liver of mice sensitive to the development of hyperlipidemia and hepatic steatosis, a finding with potential to identify new therapeutic targets in liver diseases.

Abbreviations: 4-HNE, 4-hydroxy-2-nonenal; AKT, protein kinase B; ALT, alanine aminotransferase; AMPK, AMP-activated protein kinase; AST, aspartate aminotransferase; Atg7, autophagy-related protein 7; CCL2, chemokine (C-C motif) ligand 2; CCR2, C-C chemokine receptor type 2; CD 11b, cluster of differentiation 11B; CD, standard diet; CD163, cluster of differentiation 163; CLEC4F, C-type lectin domain family 4 member F; CMA, chaperone mediated autophagy; CPLKO, triple deficient mice in CCL2, PON1 and LDLr; FAH, fumarylacetoacetate hydrolase; GC-MS-EI, gas chromatograph coupled to a quadrupole time-of-flight mass spectrometer with an electron impact source; GSH, glutathione; GSSG, glutathione disulfide; GTT, glucose tolerance test; HDL, high density lipoprotein; HFD, high fat diet; LAMP2A, lysosome associated membrane protein 2; LC3, microtubule-associated proteins 1A/1B light chain 3B; LDLr, low density lipoprotein receptor; mTOR, mammalian target of rapamycin; NADPH, nicotinamide adenine dinucleotide phosphate; NAFLD, non-alcoholic fatty liver disease; NASH, non-alcoholic steatohepatitis; P4EBP1, eukaryotic initiation factor 4E-binding protein 1; PI3K, phosphoinositide 3-kinase; PLKO, double deficient mice in PON1 and LDLr; PON1, paraoxonase-1; SAH, S –adenosylhomocysteine; SAM, S –adenosylmethionine; UHPLC, ultra-high-pressure liquid chromatography-quadrupole time of flight mass spectrometer

* Corresponding authors at: Unitat de Recerca Biomèdica, Hospital Universitari Sant Joan, Institut d'Investigació Sanitària Pere Virgili, Universitat Rovira i Virgili, Carrer Sant Joan s/n, 43201 Reus, Spain.
E-mail addresses: jcamps@grupsagessa.com (J. Camps), jjoven@grupsagessa.com (J. Joven).

https://doi.org/10.1016/j.bbadis.2019.03.006
Received 10 January 2019; Received in revised form 11 March 2019; Accepted 19 March 2019
Available online 21 March 2019
0925-4439/ © 2019 Elsevier B.V. All rights reserved.

UNIVERSITAT ROVIRA I VIRGILI
THE ROLE OF CHEMOKINE (C-C MOTIF) LIGAND 2 IN INFLAMMATION, OXIDATIVE STRESS, AGING AND METABOLISM
Fedra Nicaury Luciano Mateo

1. Introduction

The liver is vulnerable to inappropriate food ingestion, and ectopic fat accumulation induces non-alcoholic fatty liver disease (NAFLD). NAFLD has become the most common liver disease worldwide and encompasses a histological spectrum, ranging from simple steatosis to non-alcoholic steatohepatitis (NASH), which may progress to cirrhosis and hepatocellular carcinoma [1,2]. NASH is multifactorial and may be progressive, but the mechanisms affecting its development are too complex to be fully established in humans. Recent analytical tools are now available to explore the adaptive metabolic response to liver injury by examining the combined relationships among metabolic abnormalities, oxidative stress and inflammation, including paraoxonase 1 (PON1) and chemokine (C-C motif) ligand 2 (CCL2), as key molecules to understand the role of antioxidant defenses and monocyte recruitment in the liver [3–6]. PON1 may be found both in hepatocytes and in the circulation bound to lipoproteins and functions primarily as an effective molecule to modulate lipid peroxidation and the inflammatory response, likely influencing the production of CCL2 [7]. In this context, we have previously reported in experimental models that *pon1* deficiency or *ccl2* overexpression render mice prone to liver steatosis and metabolic alterations [8–10].

Excessive calorie intake is a major cause of liver injury and compromises the ability of hepatocytes to alter their metabolism (metabolic reprogramming) to trigger the adaptive response of intracellular sensors and signaling molecules necessary for liver homeostasis [11–13]. To be efficient, this adaptation requires substantial mitochondrial activity. However, oxidative stress and inflammation induce mitochondrial dysfunction and eventually cellular death, indicating that these processes and energy metabolism pathways may be interrelated and can interfere with reparative mechanisms [14]. Mechanistically, we hypothesize that the relationships among mitochondrial function and the roles of PON1 and CCL2 could be associated with at least two essential activities. The first involves the link between the citric acid cycle (CAC) and methionine and the consequent role in the maintenance of correct glutathione synthesis [15]. The second is associated with the regulation of autophagy-lysosomal function, an essential process for liver metabolic homeostasis that is highly dependent on AMP-activated protein kinase (AMPK)/mammalian target of rapamycin (mTOR) signaling in energy metabolism [16–18].

Herein, we explore the role of PON1 and CCL2 in liver disease and how oxidative stress and inflammation modulate hepatic intracellular signaling molecules and the adaptive metabolic response to fat-induced liver injury. Specifically, we investigated the alterations produced by the diet in mice triple deficient in the genes of low density lipoprotein receptor, PON1 and CCL2 (CPLKO mice), using as control groups wild type (WT) mice and mice double deficient in the low density lipoprotein receptor and PON1 (PLKO). These last animals have previously been used as a model of hyperlipidemia, hepatic steatosis and metabolic syndrome [8–10].

2. Results

2.1. Metabolic phenotypes, including liver histology and distribution of macrophages, were sensitive to CCL2 deficiency

PLKO and CPLKO mice had a significantly lower body weight than WT animals when given chow diet (CD). In contrast, weight increased similarly in all strains when fed high fat diet (HFD; Fig. 1A). Moreover, serum cholesterol, triglycerides and glucose concentrations were significantly higher in the HFD groups than in the CD groups, and PLKO and CPLKO mice had higher values than WT animals. All strains became glucose intolerant when fed HFD but without significant differences among strains, and serum glucose remained lower in mice with *ccl2* deficiency. Serum aspartate aminotransferase (AST) and alanine aminotransferase (ALT) activities were higher in PLKO mice than in WT animals, while CPLKO mice had levels of these enzymes similar to those of the WT group (Fig. 1B). These findings suggested a differential hepatic response that was confirmed histologically (Fig. 2). Minor fat accumulation was observed in PLKO mice fed CD, and prominent liver steatosis was observed when fed HFD. In contrast, CPLKO mice did not develop steatosis irrespective of the administered diet (Fig. 2A).

The immunohistochemical expression of 4-hydroxy-2-nonenal (4-HNE) was low in WT mice and very high in PLKO animals. The expression of 4-HNE in CPLKO mice was similar to that of WT animals, indicating a similar degree of oxidative stress (Fig. 2B). Again, the expected higher oxidative stress in *pon1*-deficient mice was averted by the added deficiency in *ccl2* (CPLKO), suggesting that CCL2 may potentially induce major metabolic changes, inhibit the inflammatory response, or both.

Differences between PLKO and CPLKO mice were observed through the differential abundance of liver macrophages with different phenotypes. PLKO mice fed a CD diet had a lower expression of C-type lectin domain family 4 member F (CLEC4F), indicating a lower amount of Kupffer cells. This alteration was corrected in CPLKO animals. However, we did not find any significant difference in this marker in mice given HFD (Fig. 3A). A significant subset of macrophages was positive for F4/80 antigen with expected potent phagocytic activity and reactive oxygen species (ROS) production capacity. PLKO mice did not change their relative abundance of these macrophages, but in mice deprived of *ccl2*, the relative proportion of F4/80+ cells remained significantly lower when fed either CD or HFD (Fig. 3B). A relatively low percentage of macrophages were positive for cluster of differentiation 11b (CD11b) staining, which increased in fat-challenged mice in all strains. CD11b is a marker of pro-inflammatory macrophages, and the increase was lower in CPLKO animals (Fig. 3C). Finally, to assess the putative reparative function of some macrophages and the functional adaptation to environmental challenges, we also measured CD163+ cells. This antigen is a marker of anti-inflammatory macrophages, and we found that PLKO mice had a significant decrease in the proportion of CD163-stained cells with respect to WT mice. The additional CCL2 deficiency counteracted such reduced expression (Fig. 3D). We also measured the hepatic mRNA expression of *CD11b* and *CD163*, which confirmed the immunohistochemical analyses in mice fed with CD, although we did not observe any significant differences in animals fed with HFD (Supplementary Fig. S1).

We used mice deficient in the C-C chemokine receptor type 2 (CCR2) gene to investigate whether CCR2-CCL2 signaling pathway is the responsible of the hepatic improvements observed in CPLKO mice. *Ccr2* deficient mice did not develop steatosis at 6 weeks of HFD treatment and showed a low amount of 4-HNE and F4/80 stained cells. These mice did not present any significant differences in the immunological stainings of CLEC4F, CD163 and CD11b with respect to WT animals (Supplementary Figs. S2 and S3).

Taken together, our findings indicate that CCL2 alters the metabolic phenotype of mice challenged with fat accumulation and may reshape the functional capacity of liver macrophages.

2.2. Oxidative stress and inflammation mediate energy metabolism-associated pathways

Targeted metabolomic analysis indicated that PLKO and CPLKO mice differ in their liver metabolism. Partial least square discriminant analysis visually indicates the role of the measured metabolites in discriminating among the different experimental groups. Separation among groups was more clearly shown in animals fed HFD, and the effects on the distribution among dietary groups were consistent. The standardized metabolite concentrations were represented as a heatmap, and most metabolites discriminated both genetic variations, including the effect of diet. Glycolysis and amino acid metabolism appear to be important to explain the differences superposed by *ccl2* deficiency, as shown by the ranked importance of metabolites without supervision via

UNIVERSITAT ROVIRA I VIRGILI
THE ROLE OF CHEMOKINE (C-C MOTIF) LIGAND 2 IN INFLAMMATION, OXIDATIVE STRESS, AGING AND METABOLISM
Fedra Nicaury Luciano Mateo

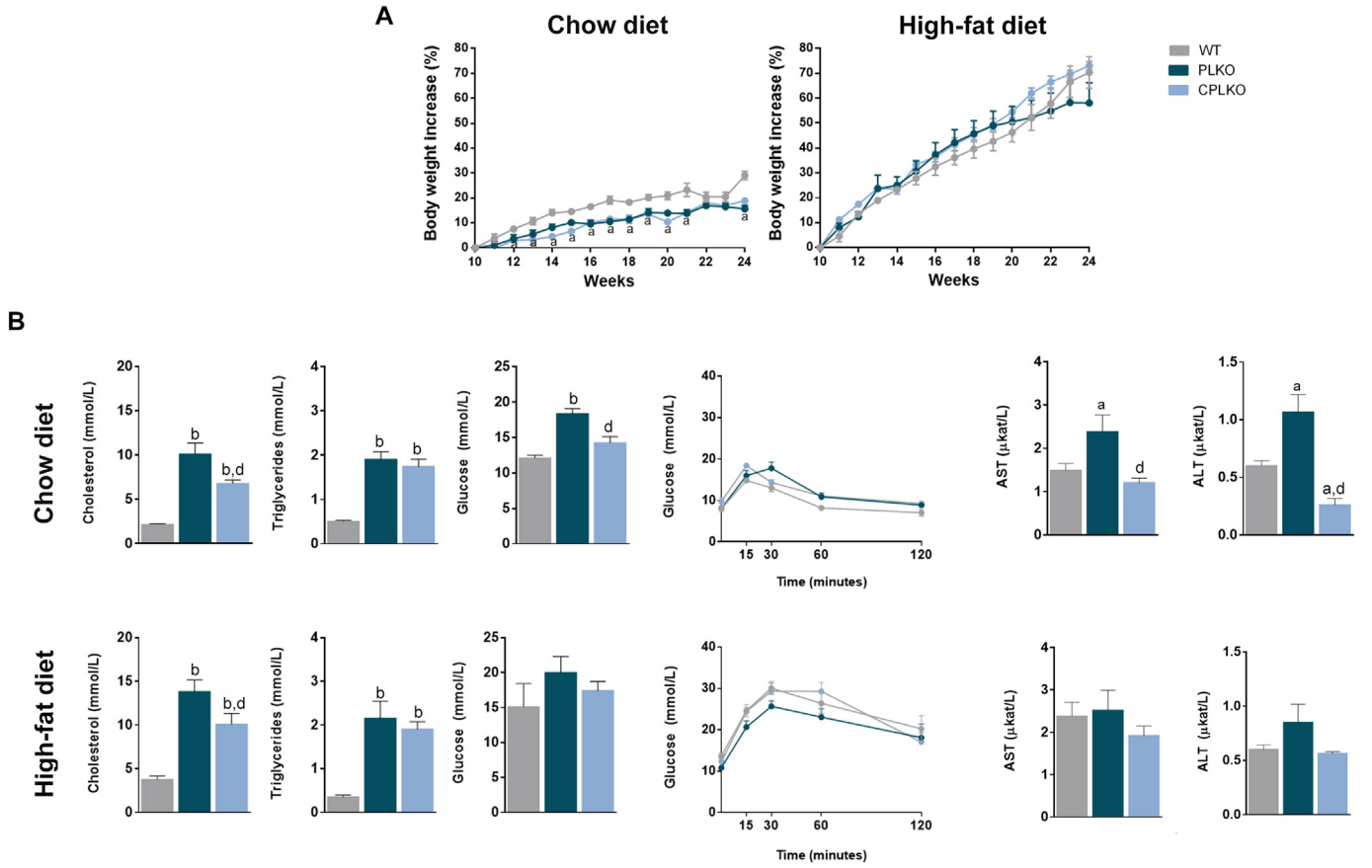

Fig. 1. Selected metabolic features in genetically modified mice. The results for (A) Body weight increase and (B) biochemical variables. PLKO denotes *ccl2*$^{+/+}$, *pon1*$^{-/-}$, *ldlr*$^{-/-}$ and CPLKO denotes *ccl2*$^{-/-}$, *pon1*$^{-/-}$, *ldlr*$^{-/-}$. Values are mean ± SEM (n = 8 per genotype and dietary condition) $^{a}P < 0.05$, $^{b}P < 0.001$, with respect to control littermates (WT); $^{c}P < 0.05$, $^{d}P < 0.001$, with respect to PLKO.

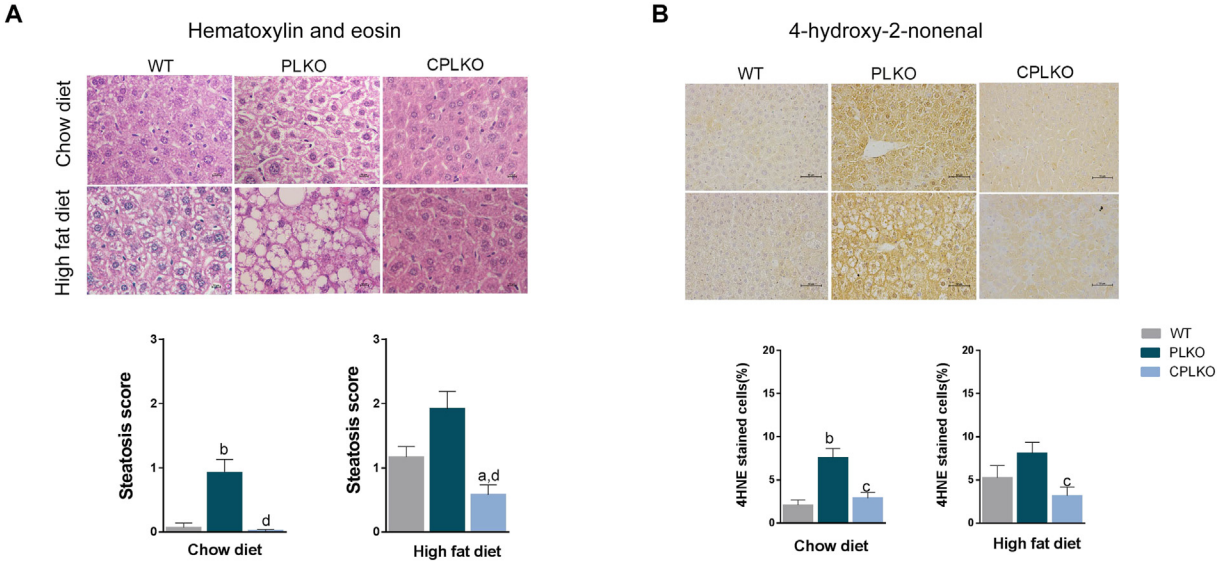

Fig. 2. Hepatic histological features. Representative microphotographs (bars indicate magnification) of liver sections stained with (A) hematoxylin and eosin and against (B) 4-hydroxy-2-nonenal (4-HNE). PLKO denotes *ccl2*$^{+/+}$, *pon1*$^{-/-}$, *ldlr*$^{-/-}$ and CPLKO denotes *ccl2*$^{-/-}$, *pon1*$^{-/-}$, *ldlr*$^{-/-}$. Values reported for the calculated steatosis score and 4HNE stained cells are mean ± SEM (n = 8 per genotype and dietary condition) $^{a}P < 0.05$, $^{b}P < 0.001$, with respect to control littermates (WT); $^{c}P < 0.05$, $^{d}P < 0.001$, with respect to PLKO.

random forest analysis (Fig. 4, Supplementary Table S1).

When comparing the metabolic response of PLKO and CPLKO mice with respect to normal (WT), we found an accumulation of glucose-6-phosphate together with increased proximal and distal metabolites, including fructose 6-phosphate, fructose 1,6-bisphosphate and ribose-5 phosphate, indicating a reduced entry of glucose carbon into mitochondrial biosynthetic metabolism and likely alterations in the pentose monophosphate shunt. In both strains, with minor dietary-induced

UNIVERSITAT ROVIRA I VIRGILI
THE ROLE OF CHEMOKINE (C-C MOTIF) LIGAND 2 IN INFLAMMATION, OXIDATIVE STRESS, AGING AND METABOLISM
Fedra Nicaury Luciano Mateo

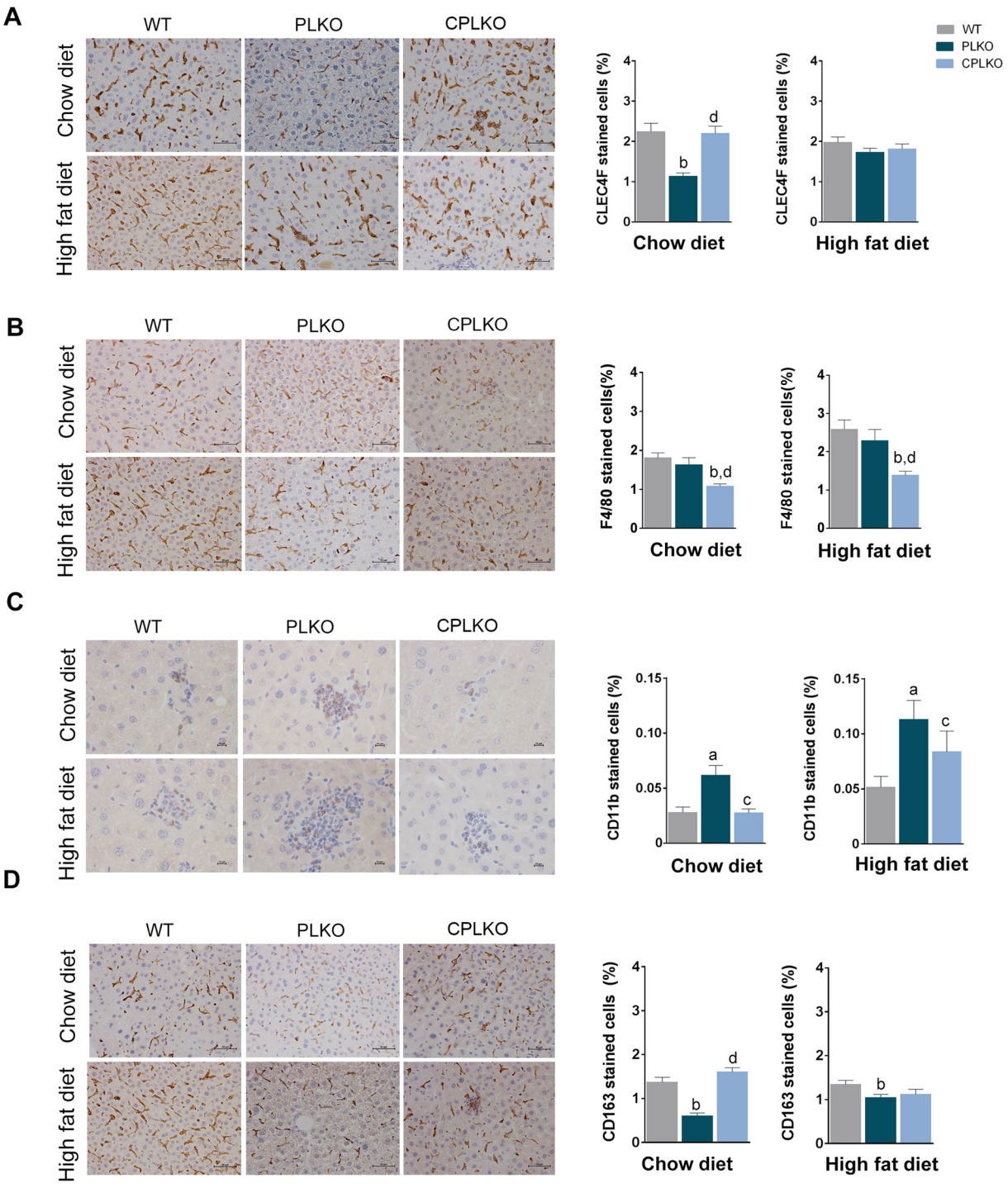

Fig. 3. Hepatic macrophage relative density. Representative microphotographs (bars indicate magnification) illustrating immunohistochemical staining of (A) C-type lectin domain family 4 member F (CLEC4F), (B) F4/80, (C) cluster of differentiation 11b (CD11b) and (D) cluster of differentiation 163 (CD163). PLKO denotes $ccl2^{+/+}$, $pon1^{-/-}$, $ldlr^{-/-}$ and CPLKO denotes $ccl2^{-/-}$, $pon1^{-/-}$, $ldlr^{-/-}$. Values for the calculated stained cells (%) are mean ± SEM (n = 8 per genotype and dietary condition) $^{a}P < 0.05$, $^{b}P < 0.001$, with respect to control littermates (WT); $^{c}P < 0.05$, $^{d}P < 0.001$, with respect to PLKO.

differences, there was an apparent decoupling between glycolysis and CAC (Fig. 5A, B). Therefore, the induced mutations result in a state of relatively reduced hepatic oxidative metabolism. However, the accumulation of lactate and β-hydroxybutyrate quantitatively differed according to the ingestion of calories and were more evident in comparisons between PLKO and CPLKO mice, suggesting potential alternatives to provide CAC feeding. Notably, mice deprived from CCL2 significantly improved the function of the glycolytic pathway and connections with CAC. Hepatic mitochondria also support relevant pathways related to the ability of 4-carbon intermediates to move into (anaplerosis) and out of (cataplerosis) the CAC without undergoing oxidation. These metabolic activities are required for shuttling reducing equivalents and biosynthetic substrates to other pathways, and the relative accumulation of CAC intermediates, lactate, ketone bodies and amino acids suggests that CCL2 may influence the flux of anaplerosis and cataplerosis-associated pathways (Fig. 5C). Taken together, our results suggest that PON1 and CCL2 are closely related and may affect metabolic activities with the potential for ROS formation in liver

UNIVERSITAT ROVIRA I VIRGILI
THE ROLE OF CHEMOKINE (C-C MOTIF) LIGAND 2 IN INFLAMMATION, OXIDATIVE STRESS, AGING AND METABOLISM
Fedra Nicaury Luciano Mateo

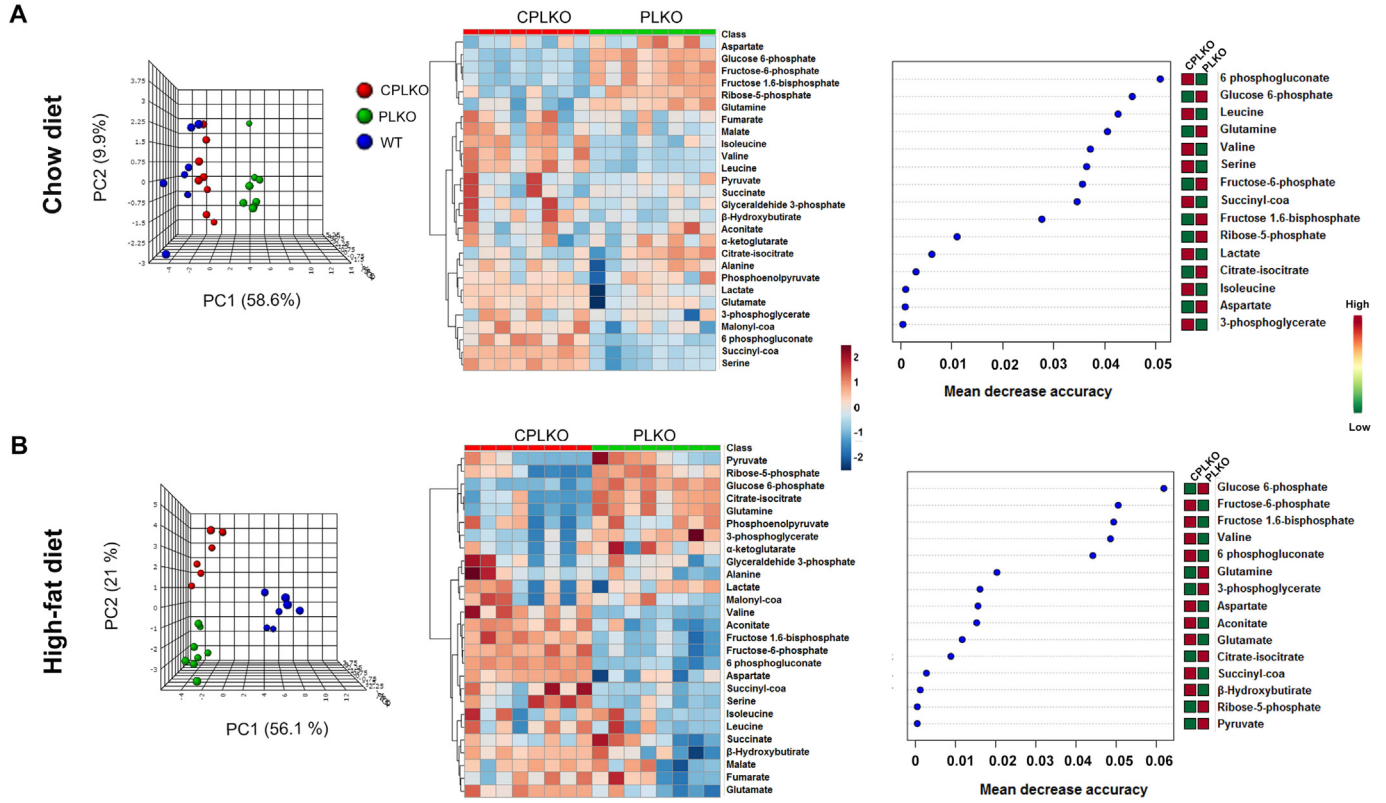

Fig. 4. Dietary-induced changes and the effect of *pon1* and/or *ccl2* ablation in hepatic energy-balance metabolites. From left to right in mice segregated by dietary conditions (A and B), partial least square discriminant analysis to visualize how measured metabolites discriminate among strains, heatmap built using standardized metabolite concentrations, and random forests to rank the importance of metabolites without supervision. PLKO denotes $ccl2^{+/+}$, $pon1^{-/-}$, $ldlr^{-/-}$ and CPLKO denotes $ccl2^{-/-}$, $pon1^{-/-}$, $ldlr^{-/-}$.

mitochondria, contributing to oxidative stress and inflammation under these conditions.

2.3. Oxidative stress-induced dysfunction in the liver methionine transmethylation and transsulfuration pathways may be restored by ccl2 deficiency

The liver regulates the flux of methionine through essential mechanisms affecting DNA, and protein methylation and the synthesis of the antioxidant glutathione. We observed significant differences in the levels of metabolites between PLKO and WT mice that were completely or partially averted in CPLKO animals (Supplementary Table S4, Fig. 6). For instance, there was a significant 4-fold decrease in methionine concentrations in PLKO mice when compared with the other strains, and the difference was maintained when fed CD or HFD. Homocysteine levels were also lower in PLKO mice, suggesting a significantly reduced flux in transmethylation. There were major changes in S-adenosylmethionine (SAM) and S-adenosylhomocysteine (SAH), substrate and product of essential methyltransferase reactions in PLKO mice. SAM levels were decreased in these animals, but differences only reached statistical significance when fed an HFD. In contrast, SAH levels increased dramatically, with a major impact on the SAM/SAH ratio. This decrease in the SAM/SAH ratio due to increased SAH correlated with homocysteine levels and probably suggests considerable alteration in the methylation status of hepatocytes. The SAM/SAH ratio in CPLKO mice was not different from that observed in WT mice, indicating reversal in causal mechanisms (Fig. 6). The reduced flux in methionine transmethylation of PLKO mice affects the efficient utilization of methionine for the synthesis of reduced glutathione (GSH) via the transsulfuration pathway. GSH is the most abundant antioxidant in hepatocytes and is critical for protecting cells from oxidative stress, acting as a free radical scavenger and inhibitor of lipid peroxidation. In PLKO mice, the GSH to GSSG ratio was extremely low, and we observed a greater mRNA expression of glutathione peroxidase and glutathione reductase than in WT and CPLKO animals (Supplementary Fig. S4). The GSH/GSSG ratio is an indicator of cellular health, and the reduced ratio indicates major cellular injuries because under normal conditions, reduced GSH represents up to 90% of cellular GSH. Interestingly, deficiency in CCL2 may be effective in maintaining hepatocytes' redox potential, but the levels were not completely reversed (Fig. 6). Our findings suggest that measurement of the GSH/GSSG ratio in the liver may bear usefulness in research focused on specific NAFLD therapeutics and the potential relationship between oxidative stress and epigenetic mechanisms.

2.4. Assessment of the role of ccl2 in hepatic autophagy-lysosomal function

In the liver, autophagy not only contributes to the maintenance of normal hepatocyte functions but also may respond to pathogenic changes. Autophagy was essentially suppressed or clearly reduced in genetically modified mice with respect to WT mice as assessed by low levels of microtubule-associated proteins 1A/1B light chain 3B (LC3) II/I ratio (Fig. 7), probably indicating a direct relationship with PON1 deficiency and high oxidative stress. We examined the autophagy-related protein 7 (Atg7), which was highly dependent on dietary conditions but did not significantly differ among strains. In contrast, mTOR was highly activated in genetically modified strains, as shown by the significant increase in the ratio between the phosphorylated and the nonphosphorylated forms. These changes probably refer to mTORC1 as indicated by a significantly higher expression of eukaryotic translation initiation factor 4E-binding protein 1 (P4EBP1) and were associated with low levels of AMPK activation. In addition, Akt was also highly

UNIVERSITAT ROVIRA I VIRGILI
THE ROLE OF CHEMOKINE (C-C MOTIF) LIGAND 2 IN INFLAMMATION, OXIDATIVE STRESS, AGING AND METABOLISM
Fedra Nicaury Luciano Mateo

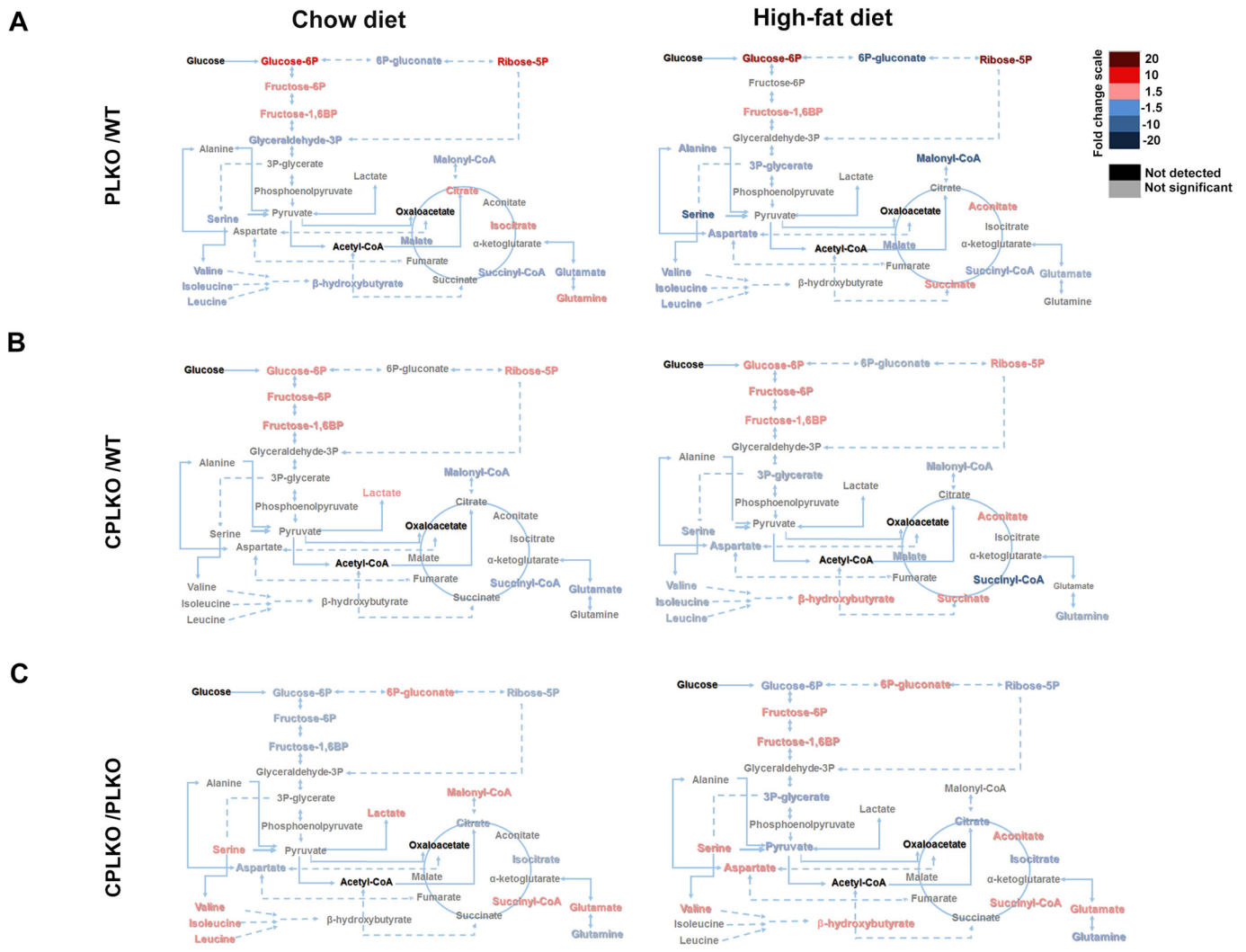

Fig. 5. The relative impact of dietary fat on the levels of metabolites associated with energy metabolism in the liver. Comparisons were made assessing fold-changes according to the legend in mice with *pon1* deficiency (A) and *pon1* and *ccl2* deficiency (B) with respect to control littermates and between both strains (C). PLKO denotes $ccl2^{+/+}$, $pon1^{-/-}$, $ldlr^{-/-}$ and CPLKO denotes $ccl2^{-/-}$, $pon1^{-/-}$, $ldlr^{-/-}$.

activated in PLKO and CPLKO mice. Considering the induced changes in liver histologic features and metabolic perturbations by the ablation of *ccl2* in PLKO mice, the lack of differential effects in the Akt/AMPK/mTOR pathway or the repression of autophagy appears noteworthy (Fig. 7). Then, we explored the expression of lysosome associated membrane protein 2 (LAMP2A), which was significantly increased in CPLKO mice with respect to PLKO mice levels, with even more dramatic effects when mice were fed HFD, suggesting a potential role of chaperone-mediated autophagy in the remission of oxidative stress (CMA). Taken together, our data indicate that PON1 deficiency is associated with decreased autophagosome formation, which is independent of CCL2. In contrast, CCL2 might affect CMA.

3. Discussion

In PLKO mice we found important liver alterations and energy stress. However, the additional ablation of CCL2, a key chemokine involved in the inflammatory response, partially or completely reverted most alterations in biochemical and histologic features. Essentially, we demonstrate the entwined roles of PON1 and CCL2 on the adaptive metabolic response to liver injury. Unbalanced nutritional status may lead to the accumulation of fat in hepatocytes, which sequentially induces mitochondrial dysfunction, oxidative stress, inflammation, and cell death. Remission through dietary interventions is uncommon, and our findings might have therapeutic and pathogenic implications in searching effective treatment procedures to reverse NAFLD and/or avoiding progression from simple steatosis to NASH.

The mechanisms establishing metabolic reprogramming in hepatocytes remains poorly understood. Overnutrition is causal in the altered expression of genes relevant for metabolism, oxidative stress and inflammation inducing epigenetic mechanisms responsible for the remarkable capacity of hepatocytes to switch their phenotypic status [9,19–21]. Hence, prevention of obesity and dietary restraint is a crucial first step in protecting the liver [22]. Reversibility of epigenetic mechanisms provides an interface between the host and environment. Here, we provide evidence indicating that oxidative stress probably interferes in the course of DNA and protein methylation through methionine metabolism and glutathione oxidation. The course of action may be substantially reversed, avoiding inflammation, which may provide a converging point between PON1 and CCL2 and are key mechanisms to explain the usefulness of epigenetic intervention through nutrition and drugs such as metformin and aspirin [23].

Our analysis of the coupled oxidation-inflammation system reveals in vivo a pivotal role in liver disease and potential alternative strategies capable of delaying NAFLD development. Deprivation of PON1, an important component of antioxidant defenses, results in increased

UNIVERSITAT ROVIRA I VIRGILI
THE ROLE OF CHEMOKINE (C-C MOTIF) LIGAND 2 IN INFLAMMATION, OXIDATIVE STRESS, AGING AND METABOLISM
Fedra Nicaury Luciano Mateo

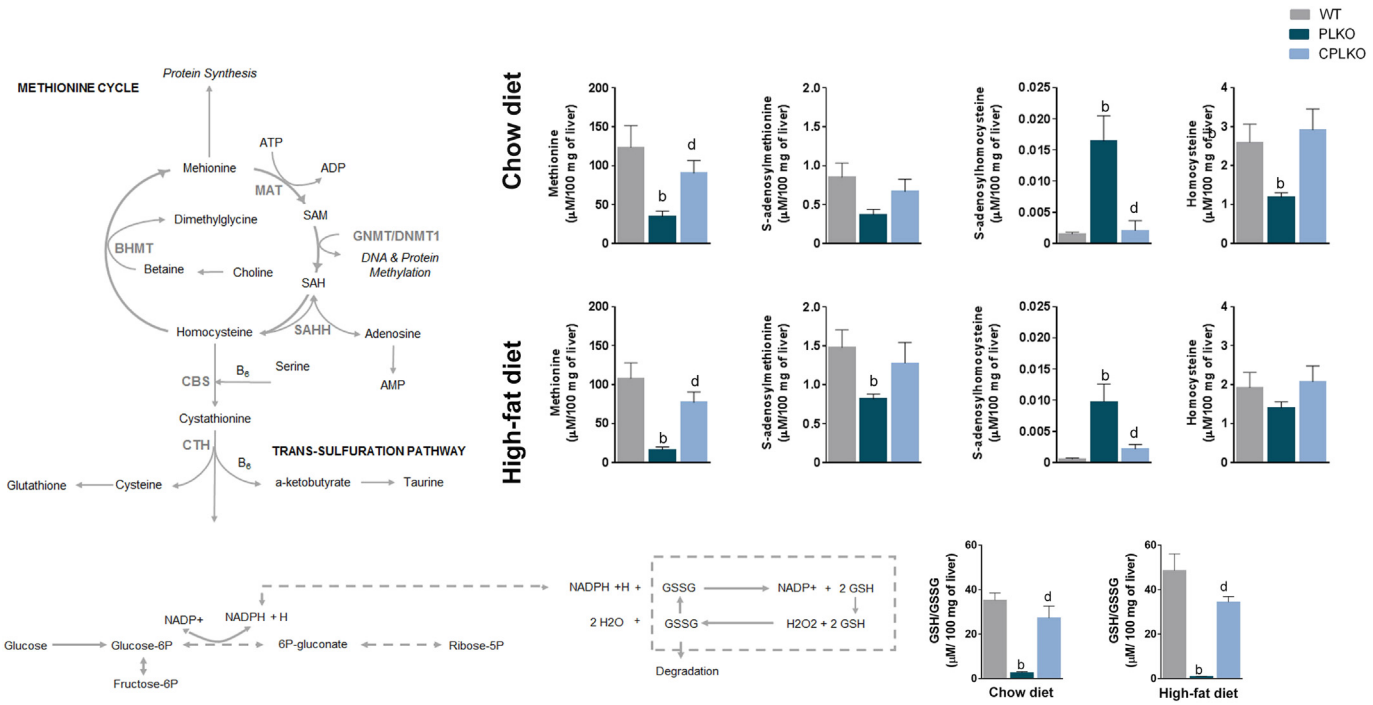

Fig. 6. The relative impact of dietary fat on the levels of metabolites associated with the methionine cycle and transsulfuration pathways in the liver. PLKO denotes *ccl2*$^{+/+}$, *pon1*$^{-/-}$, *ldlr*$^{-/-}$ and CPLKO denotes *ccl2*$^{-/-}$, *pon1*$^{-/-}$, *ldlr*$^{-/-}$. Values are mean ± SEM (n = 8 per genotype and dietary condition) $^{b}P < 0.001$, with respect to WT; $^{d}P < 0.001$, with respect to PLKO.

production of lipid peroxides, which correlated with fat accumulation and variations in the distribution of liver macrophages. Examination of energy metabolism in the livers of *pon1*-deficient mice suggested mitochondrial damage and decoupling from glycolysis, confirming that mitochondrial metabolism mediates oxidative stress and inflammation in fatty liver [24]. Mitochondrial damage can cause an imbalance between ROS production and removal, resulting in net ROS production. Potentially, overexpression of antioxidant defenses might improve lifespan and healthspan in mice [25]. The increase in glutathione peroxidase and glutathione reductase expression in PLKO mice can be interpreted as a mechanism of hepatocytes to defend against oxidative stress. Consequently, the GSH/GSSG ratio in these mice was extremely low in PLKO mice. This effect was also accompanied by a relative deficiency in methyl donors resembling the pro-oxidant, pro-inflammatory disturbances observed in mice fed methionine-choline deficient mice. Interestingly, most defects were completely reversed by the concomitant *ccl2* deficiency, most likely mediated by amelioration in macrophage functionality [26,27]. Although the liver has several types of immune cells such as natural killer cells, natural killer T cells, neutrophils, γδT cells, dendritic cells and lymphocytes T and B, macrophages represent one third of hepatic non-parenchymal cells and are considered the first response to liver injury, playing a major role in repair and regeneration processes [28].

Energy metabolism in the livers of CPLKO mice was also partially restored when compared with PLKO mice and suggested an important role of lactate and β-hydroxybutyrate as primary CAC substrates and in controlling the release of pro-inflammatory cytokines [29,30]. In addition, the restoration of branched chain amino acid metabolism observed in CPLKO mice might also contribute to the alleviation of liver steatosis and liver injury [31].

The AMPK signaling pathway coordinates autophagy and metabolism [32]. The heterotrimeric (αβγ) complex AMPK is a key player in maintaining cellular energy balance, and in these genetically modified mice, activation through phosphorylation at T172 of its catalytic subunit is significantly inhibited. Oxidative stress and energy stress may also differentially regulate AMPK activity through oxidation at several cysteine residues, a mechanism apparently dependent on the source of ROS, abundance of nutrients and the antioxidant capacity of cells [33]. AMPK activity and mTORC1 activation were inversely related, and autophagy was inhibited in both PLKO and CPLKO mice precluding the conjugation of LC3-I to phosphatidylethanolamine (LC3-II), which induced a low LC3-II/LC3-I ratio [34]. Therefore, the livers of these mice were deprived of a crucial mechanism to cope with a variety of cellular stresses. However, when we examined LAMP2A as a proxy for chaperone-mediated autophagy (CMA), we found that *pon1* deficiency altered this mechanism, which was completely reversed by the addition of *ccl2* deficiency. Accumulating evidence highlights the importance of autophagy in the maintenance of liver homeostasis and the involvement in the pathogenesis of NAFLD affecting hepatocytes and other hepatic cell types [18,35,36]. Our results suggest a possible link between CMA and NAFLD progression. CMA participates in protein quality control by degrading oxidized and damaged proteins under stress conditions and contributes amino acids through the degradation of proteins. The role of CMA in cellular fate has already been established by modulating carbohydrate and lipid metabolism, transcriptional programs, immune responses and the cell cycle through selective degradation of key enzymes in these pathways [37–39]. Indeed, it has been reported that high lipid concentrations can stimulate LAMP2A degradation through the modification of the lysosome membranes [40].

Previous studies suggest that the heterogeneous histological grades found in human biopsies were proportional to oxidative flux [24]. Our findings suggest that PON1 and CCL2 are key molecules modulating hepatic oxidative stress and inflammation that appear to be associated with increased oxidative metabolism, likely altering anabolic pathways. Both molecules are circulating in the blood at easily measurable concentrations and may represent possible predictive and diagnostic biomarkers of liver disease, but future research requires standardization of reagents and methods to overcome difficulties in interpretation [7]. Data may also suggest and/or potentiate novel therapeutic targets, which is important because there is no specific pharmacotherapy approved for NAFLD. For instance, it is plausible that increased PON1 activity may have beneficial effects in humans. Molecular mechanisms

UNIVERSITAT ROVIRA I VIRGILI
THE ROLE OF CHEMOKINE (C-C MOTIF) LIGAND 2 IN INFLAMMATION, OXIDATIVE STRESS, AGING AND METABOLISM
Fedra Nicaury Luciano Mateo

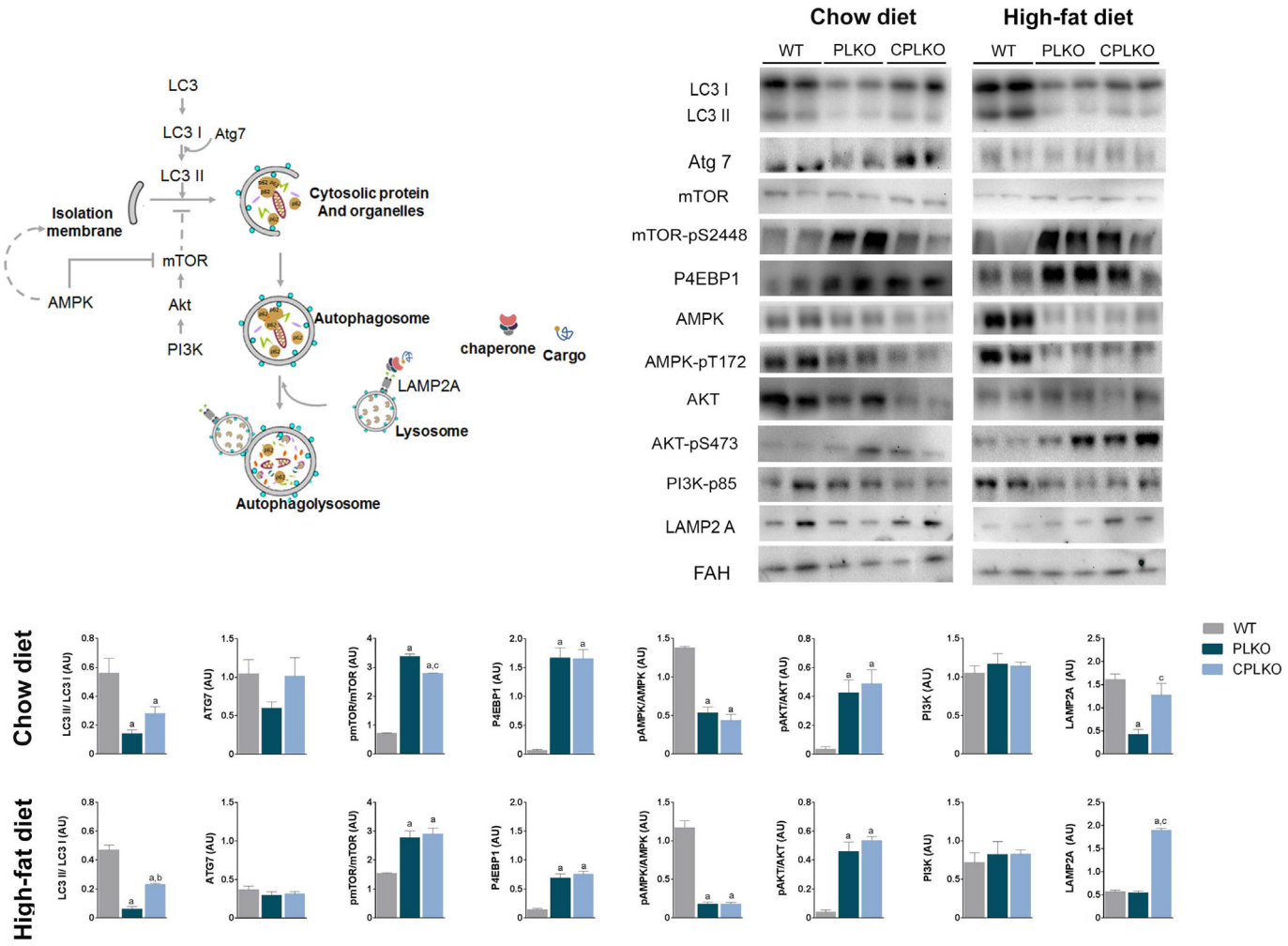

Fig. 7. Overall assessment of autophagy-lysosomal function through Western blot analysis of selected molecules, including microtubule-associated protein 1A/1B light chain 3B (LC3), autophagy-related protein 7 (Atg7), mammalian target of rapamycin (mTOR), mTOR-p S448, eukaryotic translation initiation factor 4E-binding protein 1 (P4EBP1), AMP-activated protein kinase (AMPK) AMPK-p T172, protein kinase B (AKT), AKT-pS473, phosphoinositide 3-kinase p85 subunit (PI3K-p85), lysosome associated membrane protein 2 (LAMP2A), and fumarylacetoacetate hydrolase (FAH). PLKO denotes *ccl2*$^{+/+}$, *pon1*$^{-/-}$, *ldlr*$^{-/-}$ and CPLKO denotes *ccl2*$^{-/-}$, *pon1*$^{-/-}$, *ldlr*$^{-/-}$. Representative bands are from pooled liver homogenates from randomly selected samples. Values for calculations are mean ± SEM (n = 8 per genotype and dietary condition); $^{a}P < 0.05$, $^{b}P < 0.01$, with respect to WT; $^{c}P < 0.05$, with respect to PLKO.

involved in the regulation of hepatic PON1 gene expression have not been explored, but several compounds may increase gene transcription, including probucol, several statins, vitamins and polyphenols (e.g., quercetin, naringenin, catechins, punicalagins, silymarin, and resveratrol) [41]. Similarly, polyphenol-rich foods may modulate plasma CCL2 in humans [42], and several anti-CCL2 antibodies and antagonists of its functional receptor (CCR2) are currently under investigation. Preclinical and clinical data on the dual CCR2/CCR5 inhibitor cenicriviroc are advanced in the path to approval (phase 3 trial) to specifically manage NASH and liver fibrosis [43,44]. Finally, our data also suggest that combination therapies are more likely to benefit patients with NAFLD than a single therapy and that drugs that may target AMPK activity and/or autophagy might be useful.

In summary, this study demonstrates that CCL2 is a key molecule for the development of metabolic and histological alterations in the liver of mice sensitive to the development of hyperlipidemia and hepatic steatosis, a finding with potential to identify new therapeutic targets in liver diseases.

4. Materials and methods

4.1. Mice generation, genotyping and experimental design

Low density lipoprotein receptor single deficient mice (*Ldlr*$^{-/-}$) and CCL2 single deficient mice (*ccl2*$^{-/-}$) were purchased from Jackson Laboratories (Bar Harbor, Maine, USA) and the University of California in Los Angeles kindly donated *pon1*$^{-/-}$ mice. All strains were backcrossed > 10 generations to ensure C57BL/6J genetic background. From their progeny, we first generated by breeding double-deficient mice in *pon1* and *ldlr* (*pon1*$^{-/-}$, *ldlr*$^{-/-}$; PLKO). Then, we generated another strain adding *ccl2* deficiency (*ccl2*$^{-/-}$, *pon1*$^{-/-}$, *ldlr*$^{-/-}$; CPLKO). PLKO mice and littermates without mutations (wild type, WT) were used as controls to investigate the effects of CCL2 deficiency. For some additional experiments, we used CCR2 single deficient mice (*Ccr*$^{-/-}$) purchased from Jackson Laboratories (Bar Harbor, Maine, USA), and fed a HFD.

Mice genotyping was performed using DNA isolated from the tail. *ccl2* and/or *pon1* mRNA expressions were analyzed from homogenized tails (Fig. 8) and livers (Supplementary Fig. S5) [45,46]. Handling of animals was performed by dedicated staff in accordance with current regulations and supervision by the Ethics Committee on Animal

UNIVERSITAT ROVIRA I VIRGILI
THE ROLE OF CHEMOKINE (C-C MOTIF) LIGAND 2 IN INFLAMMATION, OXIDATIVE STRESS, AGING AND METABOLISM
Fedra Nicaury Luciano Mateo

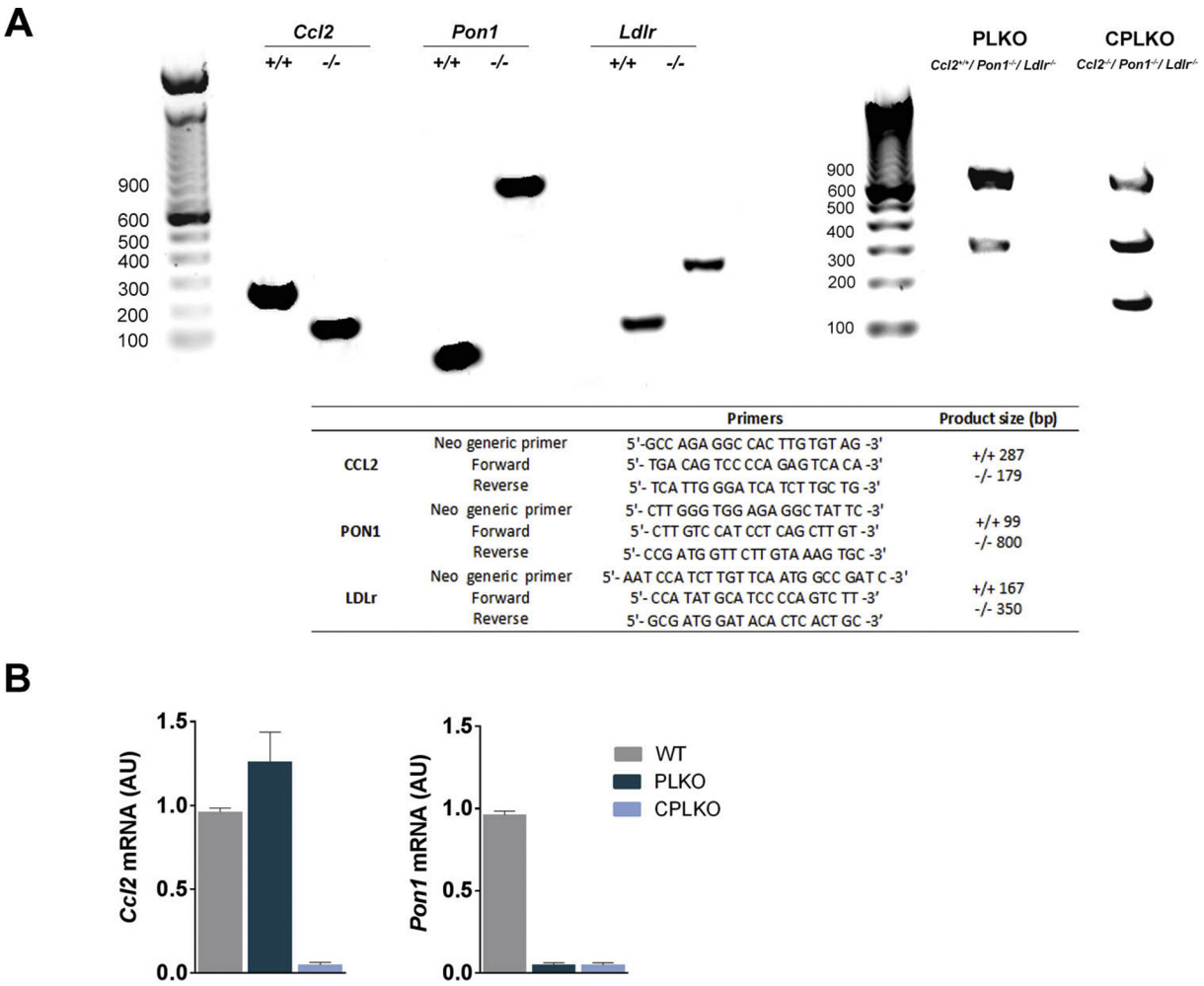

		Primers	Product size (bp)
CCL2	Neo generic primer	5'-GCC AGA GGC CAC TTG TGT AG -3'	+/+ 287 -/- 179
	Forward	5'- TGA CAG TCC CCA GAG TCA CA -3'	
	Reverse	5'- TCA TTG GGA TCA TCT TGC TG -3'	
PON1	Neo generic primer	5'- CTT GGG TGG AGA GGC TAT TC -3'	+/+ 99 -/- 800
	Forward	5'- CTT GTC CAT CCT CAG CTT GT -3'	
	Reverse	5'- CCG ATG GTT CTT GTA AAG TGC -3'	
LDLr	Neo generic primer	5'- AAT CCA TCT TGT TCA ATG GCC GAT C -3'	+/+ 167 -/- 350
	Forward	5'- CCA TAT GCA TCC CCA GTC TT -3'	
	Reverse	5'- GCG ATG GAT ACA CTC ACT GC -3'	

Fig. 8. Genotyping and liver mRNA expression in mice generation. (A) Electrophoretic assessment and primers used in genotyping. (B) Expression of *pon1* and *ccl2* mRNA in liver homogenates of 24-week-old male genetically modified mice and control littermates (WT). PLKO denotes $ccl2^{+/+}$, $pon1^{-/-}$, $ldl^{-/-}$ and CPLKO denotes $ccl2^{-/-}$, $pon1^{-/-}$, $ldlr^{-/-}$.

Experimentation of the Universitat Rovira i Virgili (protocols 4815 and GC-URV-0235-03.18.2014) following European guidelines (Directive 2010/63/EU).

Homozygous strains were viable and reproduced without difficulty under controlled temperature (22 °C), humidity (50%) and light/dark cycle 12/12 h in a stress-free environment and fed a CD prepared by Scientific Animal Food & Engineering, Augy, France and water ad libitum. The animals were randomly allocated to experimental groups, and the investigators responsible for the assessment of outcomes had no previous knowledge of the experimental group to which the animals belonged. No animals were excluded from the analysis. Selected male CPLKO, PLKO and WT mice (n = 16, each) at 10 weeks of age were allocated into two dietary groups (n = 8, each) to compare the *pon1*- and *ccl2*-related effects and to assess the differential response against caloric intake provided by CD or HFD (Ssniff Spezialdiäten GmbH, Soest, Germany), over 14 weeks. At the beginning of the study, other littermates (n = 3–4 for each strain) were used to confirm similar histologic features in their livers at this age. Information on supplied nutrients by both diets may be found in Supplementary Table S1.

4.2. Sample collection and biochemical analyses

One week before sacrifice, glucose tolerance tests (GTT) were performed on fasted (4 h) mice after intraperitoneal glucose (2 g/kg body weight) administration. Glucose concentrations were determined in blood from the tail immediately before and 15, 30, 60 and 120 min with test strips adapted to the Accuchek sensor system (Roche Diagnostics, Barcelona, Spain). At sacrifice, blood was obtained by intracardiac puncture to measure serum glucose, cholesterol, and triglyceride concentrations, and AST and ALT activities in an automated analyzer Roche Cobas Mira Plus (Roche Diagnostics).

4.3. Quantitative RT-PCR

Total RNA was extracted using the RNeasy kit (Qiagen, Barcelona, Spain) and was retrotranscribed using the Reverse Transcription System kit (Applied Biosystems; Invitrogen, Barcelona, Spain). Real-time PCR (qPCR) was conducted on a 7900HT Fast Real-Time PCR System using TaqMan Gene Expression Assays (Applied Biosystems). The results normalized according to the expression level of Beta-2-Microglobulin (B2M) mRNA.

4.4. Histological analyses and immunochemistry

Livers were frozen in liquid N_2 and stored at −80 °C and/or fixed in formalin (formaldehyde 3.7–4% buffered to pH = 7 and stabilized with methanol 1–1.5%) until analysis. Adequate sections were stained with hematoxylin and eosin to evaluate liver impairment according to a scoring system as described [47]. For immunohistochemistry, procedures were performed as described with few modifications [46]. Briefly,

UNIVERSITAT ROVIRA I VIRGILI
THE ROLE OF CHEMOKINE (C-C MOTIF) LIGAND 2 IN INFLAMMATION, OXIDATIVE STRESS, AGING AND METABOLISM
Fedra Nicaury Luciano Mateo

after deparaffinization and rehydration of 2 μm liver sections, antigens were retrieved in 0.15 mol/L sodium citrate or Tris 10 mM/EDTA 1 mM buffer at pH = 6 or pH = 9 in a microwave oven until reaching 90 °C. Bovine serum albumin (2%) and hydrogen peroxide (1%) were sequentially used to block nonspecific binding sites and endogenous peroxidase and rinsed with phosphate buffered saline. Then, sections were incubated with the corresponding primary antibody, the appropriate secondary antibody and detected with reagents described in Supplementary Table S2. All sections were counterstained with Mayer's hematoxylin and quantified via image analysis (at least 10 fields for each sample) using ImageJ software (National Institutes of Health, USA). To assess differences in oxidation and inflammation and to explore macrophage heterogeneity in healthy and diseased liver, we stained macrophages for CLEC4F, antigen F4/80, CD11b, CD163, and 4-HNE [11,48,49].

4.5. Western blot analyses

Frozen liver tissue (20 mg) from each animal was homogenized in 300 μL of lysis buffer composed of 0.25 M sucrose, 1 mM Pefabloc SC (Sigma-Aldrich, Saint Louis, MI, USA), and a phosphatase inhibitor cocktail (Hoffman-La Roche, Basel, Switzerland) using a sonicator (Branson Sonifer 150, Thistle Scientific, Glasgow, UK). Western blotting was performed by denaturing 50 μg of protein at 100 °C for 5 min in Laemmli sample buffer and β-mercaptoethanol. For protein separation, 8%–14% sodium dodecyl sulfate-polyacrylamide gel was used, and proteins were transferred onto a polyvinylidene difluoride or nitrocellulose membrane (Thermo Fisher, Barcelona, Spain). Before the primary antibody incubation, membranes were blocked with nonfat milk or bovine serum albumin at 5% in Tris, sodium chloride and 1% Tween-20 (pH = 7.4). Reagents and further details may be found in Supplementary Table S2. Bands were detected with a SuperSignal West Femto chemiluminescent substrate (Pierce, Rockford, IL, USA), and the analysis was performed with a ChemiDoc system (Bio-Rad Laboratories, Madrid, Spain). Bands were analyzed and quantified using Image Lab 2.0 software (Bio-Rad Laboratories). Specifically, we measured the expression of molecules involved in the regulation of energy metabolism and autophagy-lysosomal function, including the phosphoinositide 3-kinase p85 subunit (PI3K-p85), protein kinase B (AKT), phospho-AKT Ser 473 (AKT- pS473), mTOR, phospho-mTOR Ser 2448 (mTOR-pS2448), AMPK, AMPK- pT172, eukaryotic translation initiation factor 4E-binding protein 1 (P4EBP1), the microtubule-associated protein 1A/1B light chain 3B (LC3-I and LC3-II) and LAMP2A [16,50–52]. Fumarylacetoacetate hydrolase (FAH) was used as a reference protein.

4.6. Measurement of energy-balance metabolites in liver tissue (gas chromatography)

Metabolomic analysis was performed as previously reported [53]. Briefly, 100 mg of liver tissue was placed in 1 mL of methanol/water (8:2), mixed with D4-succinic acid (MeOH-D4s) as a standard at a final concentration of 0.01 μM, and homogenized with a Precellys 24 homogenizer (Izasa, Barcelona, Spain). Samples were stored at −20 °C for 2 h to precipitate the proteins and centrifuged at 15,000 rpm for 10 min at 4 °C. The supernatants were collected and stored at −80 °C. At the moment of analysis, samples were dried with N_2 and derivatized with methoxylamine hydrochloride dissolved in pyridine (40 mg/mL) and *N*-methyl-*N*-trimethylsilyl trifluoroacetamide. Analyses were performed with a 7890A gas chromatograph coupled with an electron impact source to a 7200 quadrupole time-of-flight mass spectrometer (GC-MS-EI) (Agilent Technologies, Santa Clara, USA).

4.7. Measurement of glutathione, glutathione disulfide and methionine cycle-related metabolites (liquid chromatography)

Metabolites were measured as described [54]. For the most common methionine cycle-related metabolites, 25 mg of liver tissue was added to 1 mL of an extraction solution containing methanol:water (8:2 v/v), 1% ascorbic acid (m/v) and 0.5% β-mercaptoethanol (v/v) and homogenized with Precellys 24 homogenizer (Izasa). After protein precipitation, samples were centrifuged at 14,000 rpm for 10 min at 4 °C, the supernatant was collected, dried under N_2, resuspended in 100 μL of ultrapure type 1 water containing 50 mM ammonium acetate + 0.2% formic acid and placed into vials for analysis. Five milliliters of sample was injected into an ultrahigh-pressure liquid chromatography-quadrupole time of flight mass spectrometer (Agilent Technologies, Santa Clara, USA) (UHPLC). To attain optimal results, GSH and GSSG were measured individually. Briefly, 50 mg of liver tissue was added to 500 μL of 100 mM N-ethylmaleimide, 152 mM NaCl in 1 mM acetic acid, and homogenized with a Precellys 24 homogenizer (Izasa). We used 200 μL of 8 M trichloroacetic acid for cell lysis and protein precipitation. Then, N-ethylmaleimide was removed by adding 10 mL of dichloromethane. Samples were centrifuged at 14,000 rpm, 4 °C for 10 min, and 10 μL were injected into the UHPLC. Data quantification was performed using the calibration curves of each standard.

4.8. Statistical analyses

We used the nonparametric Mann-Whitney *U* tests for comparisons between two groups according to the distribution of results in the measured variables. For comparing more than two groups, the Kruskal-Wallis was used. All statistical analyses and relevant graphics were performed with GraphPad Prism software 6.01 (GraphPad Software, San Diego, CA, USA), SPSS Software (IBM SPSS Statistics for Windows, Version 21.00 Armonk, NY: IBM Corp) and MetaboAnalyst 3.0 (www.metaboanalyst.ca). Differences were considered statistically significant when the *P* value was ≤ 0.05. Unless otherwise indicated, the results are expressed as the mean ± standard error of the mean.

Declarations of interest

The authors declare no commercial or financial conflicts of interest.

Author contributions

FLM, JAM, JC, and JJ contributed to conception and design of the experimental plan. FLM, NC, GBG, SFA, AHA, ERT, MMG and JAM made substantial contributions to acquisition, analysis and interpretation of data. FLM, JC, and JJ participate in drafting the manuscript. All authors participate in revising the manuscript critically for important intellectual content. The guarantors for the overall content are Jordi Camps and Jorge Joven.

Transparency document

The Transparency document associated with this article can be found, in online version.

Acknowledgment

The authors thank Dr. Diana Shih, from the Division of Cardiology of the University of California in Los Angeles, for the generous gift of a breeding pair of PON1-deficient mice. This study was funded by grant PI15/00285 from the *Instituto de Salud Carlos III* (Madrid, Spain), co-funded by the *Fondo Europeo de Desarrollo Regional* (FEDER), and by grant 60/U/2016 from the *Fundació La Marató de TV3* (Barcelona, Spain). We also acknowledge the support provided by the *Agència de Gestió d'Ajuts Universitaris i de Recerca* (Grant 2016FI_B 00352) and the *Universitat Rovira i Virgili* (Grant URVPFRB21545). The funders had no role in study design, data collection and analysis, decision to publish, or preparation of the manuscript.

UNIVERSITAT ROVIRA I VIRGILI
THE ROLE OF CHEMOKINE (C-C MOTIF) LIGAND 2 IN INFLAMMATION, OXIDATIVE STRESS, AGING AND METABOLISM
Fedra Nicaury Luciano Mateo

Appendix A. Supplementary data

Supplementary data to this article can be found online at https://doi.org/10.1016/j.bbadis.2019.03.006.

References

[1] G. Musso, M. Cassader, R. Gambino, Non-alcoholic steatohepatitis: emerging molecular targets and therapeutic strategies, Nat. Rev. Drug Discov. 15 (2016) 249–274, https://doi.org/10.1038/nrd.2015.3.
[2] V.T. Samuel, G.I. Shulman, Nonalcoholic fatty liver disease as a nexus of metabolic and hepatic diseases, Cell Metab. 27 (2018) 22–41, https://doi.org/10.1016/j.cmet.2017.08.002.
[3] M.C. Garcia, M. Amankwa-Sakyi, T.J. Flynn, Cellular glutathione in fatty liver in vitro models, Toxicol. in Vitro 25 (2011) 1501–1506, https://doi.org/10.1016/j.tiv.2011.05.011.
[4] C. Koliaki, J. Szendroedi, K. Kaul, T. Jelenik, P. Nowotny, F. Jankowiak, et al., Adaptation of hepatic mitochondrial function in humans with non-alcoholic fatty liver is lost in steatohepatitis, Cell Metab. 21 (2015) 739–746, https://doi.org/10.1016/j.cmet.2015.04.004.
[5] H.K. Vincent, A.G. Taylor, Biomarkers and potential mechanisms of obesity-induced oxidant stress in humans, Int. J. Obes. 30 (2006) 400–418, https://doi.org/10.1038/sj.ijo.0803177.
[6] R. Veteläinen, A. van Vliet, T.M. van Gulik, Essential pathogenic and metabolic differences in steatosis induced by choline or methione-choline deficient diets in a rat model, J. Gastroenterol. Hepatol. 22 (2007) 1526–1533, https://doi.org/10.1111/j.1440-1746.2006.04701.x.
[7] J. Camps, E. Rodríguez-Gallego, A. García-Heredia, I. Triguero, M. Riera-Borrull, A. Hernández-Aguilera, et al., Paraoxonases and chemokine (C-C motif) ligand-2 in noncommunicable diseases, Adv. Clin. Chem. 63 (2014), https://doi.org/10.1016/B978-0-12-800094-6.00007-8.
[8] A. García-Heredia, E. Kensicki, R.P. Mohney, A. Rull, I. Triguero, J. Marsillach, et al., Paraoxonase-1 deficiency is associated with severe liver steatosis in mice fed a high-fat high-cholesterol diet: a metabolomic approach, J. Proteome Res. 12 (2013) 1946–1955, https://doi.org/10.1021/pr400050u.
[9] A. Rull, F. Rodríguez, G. Aragonès, J. Marsillach, R. Beltrán, C. Alonso-Villaverde, et al., Hepatic monocyte chemoattractant protein-1 is upregulated by dietary cholesterol and contributes to liver steatosis, Cytokine 48 (2009) 273–279, https://doi.org/10.1016/j.cyto.2009.08.006.
[10] E. Rodríguez-Gallego, M. Riera-Borrull, A. Hernández-Aguilera, R. Mariné-Casadó, A. Rull, R. Beltrán-Debón, et al., Ubiquitous transgenic overexpression of C-C chemokine ligand 2: a model to assess the combined effect of high energy intake and continuous low-grade inflammation, Mediat. Inflamm. (2013) 1–19, https://doi.org/10.1155/2013/953841.
[11] F. Heymann, F. Tacke, Immunology in the liver — from homeostasis to disease, Nat. Rev. Gastroenterol. Hepatol. 13 (2016) 88–110, https://doi.org/10.1038/nrgastro.2015.200.
[12] L.A.J. O'Neill, E.J. Pearce, Immunometabolism governs dendritic cell and macrophage function, J. Exp. Med. 213 (2016) 15–23, https://doi.org/10.1084/jem.20151570.
[13] L. Xu, H. Kitade, Y. Ni, T. Ota, Roles of chemokines and chemokine receptors in obesity-associated insulin resistance and nonalcoholic fatty liver disease, Biomolecules 5 (2015) 1563–1579, https://doi.org/10.3390/biom5031563.
[14] A. Hernández-Aguilera, A. Rull, E. Rodríguez-Gallego, M. Riera-Borrull, F. Luciano-Mateo, J. Camps, et al., Mitochondrial dysfunction: a basic mechanism in inflammation-related non-communicable diseases and therapeutic opportunities, Mediat. Inflamm. 2013 (2013) 135698, , https://doi.org/10.1155/2013/135698.
[15] O.A. Lozoya, I. Martinez-Reyes, T. Wang, D. Grenet, P. Bushel, J. Li, et al., Mitochondrial nicotinamide adenine dinucleotide reduced (NADH) oxidation links the tricarboxylic acid (TCA) cycle with methionine metabolism and nuclear DNA methylation, PLoS Biol. 16 (4) (2018) e2005707, , https://doi.org/10.1371/journal.pbio.2005707.
[16] G. Filomeni, D. De Zio, F. Cecconi, Oxidative stress and autophagy: the clash between damage and metabolic needs, Cell Death Differ. 22 (2015) 377–388, https://doi.org/10.1038/cdd.2014.150.
[17] D.J. Klionsky, D.J. Klionsky, K. Abdelmohsen, A. Abe, M.J. Abedin, H. Abeliovich, et al., Guidelines for the use and interpretation of assays for monitoring autophagy (3rd edition), Autophagy 12 (2016) 1–222, https://doi.org/10.1080/15548627.2015.1100356.
[18] J.L. Schneider, A.M. Cuervo, Liver autophagy: much more than just taking out the trash, Nat. Rev. Gastroenterol. Hepatol. 11 (2014) 187–200, https://doi.org/10.1038/nrgastro.2013.211.
[19] M. Tous, N. Ferré, A. Rull, J. Marsillach, B. Coll, C. Alonso-Villaverde, et al., Dietary cholesterol and differential monocyte chemoattractant protein-1 gene expression in aorta and liver of apo E-deficient mice, Biochem. Biophys. Res. Commun. 340 (4) (2006) 1078–1084, https://doi.org/10.1016/j.bbrc.2005.12.109.
[20] A. Hernández-Aguilera, S. Fernández-Arroyo, E. Cuyàs, F. Luciano-Mateo, N. Cabre, J. Camps, et al., Epigenetics and nutrition-related epidemics of metabolic diseases: current perspectives and challenges, Food Chem. Toxicol. 96 (2016) 191–204, https://doi.org/10.1016/j.fct.2016.08.006.
[21] J. Lee, Y. Kim, S. Friso, S.W. Choi, Epigenetics in non-alcoholic fatty liver disease, Mol. Asp. Med. 54 (2017) 78–88, https://doi.org/10.1016/j.mam.2016.11.008.
[22] M. Riera-Borrull, A. García-Heredia, S. Fernández-Arroyo, A. Hernández-Aguilera, N. Cabré, E. Cuyàs, et al., Metformin potentiates the benefits of dietary restraint: a metabolomic study, Int. J. Mol. Sci. 18 (11) (2017), https://doi.org/10.3390/ijms18112263.
[23] E. Cuyàs, S. Fernández-Arroyo, S. Verdura, R.Á. García, J. Stursa, L. Werner, et al., Metformin regulates global DNA methylation via mitochondrial one-carbon metabolism, Oncogene. 37 (7) (2018) 963–970, https://doi.org/10.1038/onc.2017.367.
[24] S. Satapati, B. Kucejova, J.A. Duarte, J.A. Fletcher, L. Reynolds, N.E. Sunny, et al., Mitochondrial metabolism mediates oxidative stress and inflammation in fatty liver, J. Clin. Invest. 126 (4) (2016) 1605, https://doi.org/10.1172/JCI86695.
[25] S.E. Schriner, N.J. Linford, G.M. Martin, P. Treuting, C.E. Ogburn, M. Emond, et al., Extension of murine life span by overexpression of catalase targeted to mitochondria, Science. 308 (5730) (2005) 1909–1911, https://doi.org/10.1126/science.1106653.
[26] G. Nguyen, S.Y. Park, C.T. Le, W.S. Park, D.H. Choi, E.H. Cho, Metformin ameliorates activation of hepatic stellate cells and hepatic fibrosis by succinate and GPR91 inhibition, Biochem. Biophys. Res. Commun. 495 (4) (2018) 2649–2656, https://doi.org/10.1016/j.bbrc.2017.12.143.
[27] J.M. Mato, S.C. Lu, Role of S-adenosyl-L-methionine in liver health and injury, Hepatology 45 (2007) 1306–1312, https://doi.org/10.1002/hep.21650.
[28] N. Li, J. Hua, Immune cells in liver regeneration, Oncotarget. 8 (2) (2017) 3628–3639, https://doi.org/10.18632/oncotarget.12275.
[29] S. Hui, J.M. Ghergurovich, R.J. Morscher, C. Jang, X. Teng, W. Lu, et al., Glucose feeds the TCA cycle via circulating lactate, Nature. 551 (7678) (2017) 115–118, https://doi.org/10.1038/nature24057.
[30] Y.H. Youm, K.Y. Nguyen, R.W. Grant, E.L. Goldberg, M. Bodogai, D. Kim, et al., The ketone metabolite β-hydroxybutyrate blocks NLRP3 inflammasome-mediated inflammatory disease, Nat. Med. 21 (3) (2015) 263–269, https://doi.org/10.1038/nm.3804.
[31] T. Honda, M. Ishigami, F. Luo, M. Lingyun, Y. Ishizu, T. Kuzuya, et al., Branched-chain amino acids alleviate hepatic steatosis and liver injury in choline-deficient high-fat diet induced NASH mice, Metabolism. 69 (2017) 177–187, https://doi.org/10.1016/j.metabol.2016.12.013.
[32] M.M. Mihaylova, R.J. Shaw, The AMPK signalling pathway coordinates cell growth, autophagy and metabolism, Nat. Cell Biol. 13 (9) (2011) 1016–1023, https://doi.org/10.1038/ncb2329.
[33] D. Shao, S. Oka, T. Liu, P. Zhai, T. Ago, S. Sciarretta, et al., A redox-dependent mechanism for regulation of AMPK activation by Thioredoxin1 during energy starvation, Cell Metab. 19 (2) (2014) 232–245, https://doi.org/10.1016/j.cmet.2013.12.013.
[34] K. Frudd, T. Burgoyne, J.R. Burgoyne, Oxidation of Atg3 and Atg7 mediates inhibition of autophagy, Nat. Commun. 9 (2018) 95, , https://doi.org/10.1038/s41467-017-02352-z.
[35] M.J. Czaja, Function of autophagy in nonalcoholic fatty liver disease, Dig. Dis. Sci. 61 (5) (2016) 1304–1313, https://doi.org/10.1007/s10620-015-4025-x.
[36] S. Yan, N. Huda, B. Khambu, X.M. Yin, Relevance of autophagy to fatty liver diseases and potential therapeutic applications, Amino Acids 49 (12) (2017) 1965–1979, https://doi.org/10.1007/s00726-017-2429-y.
[37] J.L. Schneider, Y. Suh, A.M. Cuervo, Deficient chaperone-mediated autophagy in liver leads to metabolic dysregulation, Cell Metab. 20 (3) (2014) 417–432, https://doi.org/10.1016/j.cmet.2014.06.009.
[38] S. Kaushik, A.M. Cuervo, Degradation of lipid droplet-associated proteins by chaperone-mediated autophagy facilitates lipolysis, Nat. Cell Biol. 17 (6) (2015) 759–70, https://doi.org/10.1038/ncb3166.
[39] S. Kaushik, A.M. Cuervo, The coming of age of chaperone-mediated autophagy, Nat. Rev. Mol. Cell Biol. 19 (6) (2018) 365–381, https://doi.org/10.1038/s41580-018-0001-6.
[40] J.A. Rodriguez-Navarro, S. Kaushik, H. Koga, C. Dall'Armi, G. Shui, M.R. Wenk, et al., Inhibitory effect of dietary lipids on chaperone-mediated autophagy, Proc. Natl. Acad. Sci. U. S. A. 109 (12) (2012) E705–E714, https://doi.org/10.1073/pnas.1113036109.
[41] D. Martini, C. Del Bo', M. Porrini, S. Ciappellano, P. Riso, Role of polyphenols and polyphenol-rich foods in the modulation of PON1 activity and expression, J. Nutr. Biochem. 48 (2017) 1–8, https://doi.org/10.1016/j.jnutbio.2017.06.002.
[42] R. Beltrán-Debón, C. Alonso-Villaverde, G. Aragonès, I. Rodríguez-Medina, A. Rull, V. Micol, et al., The aqueous extract of Hibiscus sabdariffa calices modulates the production of monocyte chemoattractant protein-1 in humans, Phytomedicine. 17 (3–4) (2010) 186–191, https://doi.org/10.1016/j.phymed.2009.08.006.
[43] O. Krenkel, T. Puengel, O. Govaere, A.T. Abdallah, J.C. Mossanen, M. Kohlhepp, et al., Therapeutic inhibition of inflammatory monocyte recruitment reduces steatohepatitis and liver fibrosis, Hepatology. 67 (4) (2018) 1270–1283, https://doi.org/10.1002/hep.29544.
[44] S.L. Friedman, B.A. Neuschwander-Tetri, M. Rinella, A.J. Sanyal, Mechanisms of NAFLD development and therapeutic strategies, Nat. Med. 24 (2018) 908–922, https://doi.org/10.1038/s41591-018-0104-9.
[45] J. Joven, A. Rull, N. Ferré, J.C. Escolà-Gil, J. Marsillach, B. Coll, et al., The results in rodent models of atherosclerosis are not interchangeable, Atherosclerosis 195 (2007) e85–e92, https://doi.org/10.1016/j.atherosclerosis.2007.06.012.
[46] F. Rodríguez-Sanabria, A. Rull, R. Beltrán-Debón, G. Aragonès, J. Camps, B. Mackness, et al., Tissue distribution and expression of paraoxonases and chemokines in mouse: the ubiquitous and joint localisation suggest a systemic and coordinated role, J. Mol. Histol. 41 (2010) 379–386, https://doi.org/10.1007/s10735-010-9299-x.
[47] W. Liang, A.L. Menke, A. Driessen, G.H. Koek, J.H. Lindeman, R. Stoop, et al., Establishment of a general NAFLD scoring system for rodent models and comparison to human liver pathology, PLoS One 9 (2014) e115922, , https://doi.org/10.1371/journal.pone.0115922.
[48] C.L. Scott, F. Zheng, P. De Baetselier, L. Martens, Y. Saeys, S. De Prijck, et al., Bone

UNIVERSITAT ROVIRA I VIRGILI
THE ROLE OF CHEMOKINE (C-C MOTIF) LIGAND 2 IN INFLAMMATION, OXIDATIVE STRESS, AGING AND METABOLISM
Fedra Nicaury Luciano Mateo

marrow-derived monocytes give rise to self-renewing and fully differentiated Kupffer cells, Nat. Commun. 7 (2016) 10321, , https://doi.org/10.1038/ncomms10321.
[49] O. Krenkel, F. Tacke, Liver macrophages in tissue homeostasis and disease, Nat. Rev. Immunol. 17 (2017) 306–321, https://doi.org/10.1038/nri.2017.11.
[50] D.A. Fruman, H. Chiu, B.D. Hopkins, S. Bagrodia, L.C. Cantley, R.T. Abraham, The PI3K pathway in human disease, Cell 170 (2017) 605–635, https://doi.org/10.1016/j.cell.2017.07.029.
[51] P.D. Pezze, S. Ruf, A.G. Sonntag, M. Langelaar-Makkinje, P. Hall, A.M. Heberle, et al., A systems study reveals concurrent activation of AMPK and mTOR by amino acids, Nat. Commun. 7 (2016) 13254, , https://doi.org/10.1038/ncomms13254.
[52] R. Pérez-Carro, R. Sánchez-Alcudia, B. Pérez, R. Navarrete, C. Pérez-Cerdá, M. Ugarte, et al., Functional analysis and *in vitro* correction of splicing *FAH* mutations causing tyrosinemia type I, Clin. Genet. 86 (2014) 167–171, https://doi.org/10.1111/cge.12243.
[53] M. Riera-Borrull, E. Rodríguez-Gallego, A. Hernández-Aguilera, F. Luciano, R. Ras, E. Cuyàs, et al., Exploring the process of energy generation in pathophysiology by targeted metabolomics: performance of a simple and quantitative method, J. Am. Soc. Mass Spectrom. 27 (2016) 168–177, https://doi.org/10.1007/s13361-015-1262-3.
[54] Å. Florholmen-Kjær, R.A. Lysså, O.-M. Fuskevåg, R. Goll, A. Revhaug, K.E. Mortensen, A sensitive method for the analysis of glutathione in porcine hepatocytes, Scand. J. Gastroenterol. 49 (2014) 1–8, https://doi.org/10.3109/00365521.2014.964757.

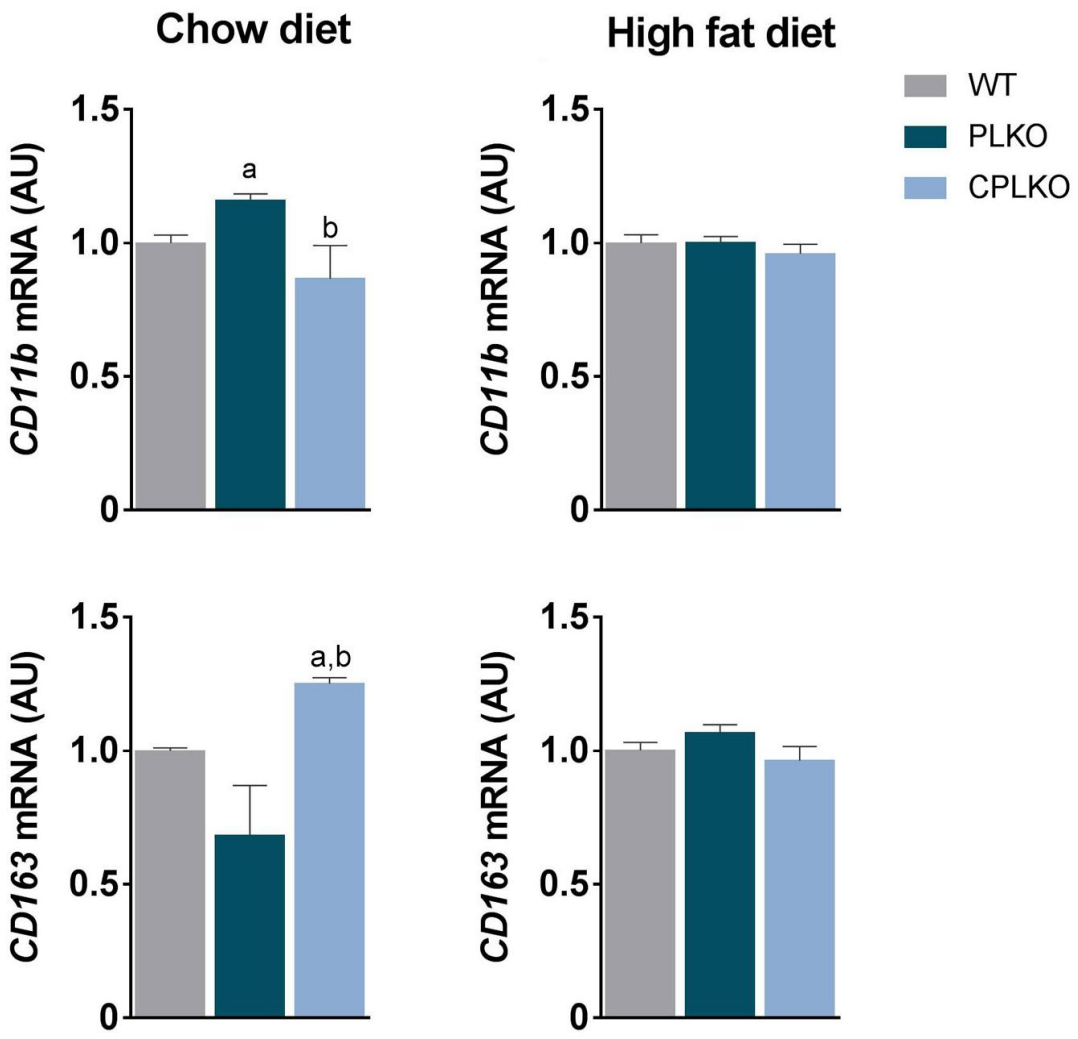

Supplementary Figure S1. Relative hepatic mRNA expression of CD11b and CD163 antigens in wild type (WT), PLKO and CPLKO mice. PLKO stands for *ccl2*$^{+/+}$, *pon1*$^{-/-}$, *ldl*$^{-/-}$ mice and CPLKO stands for *ccl2*$^{-/-}$, *pon1*$^{-/-}$, *ldlr*$^{-/-}$ animals. Values are mean ± SEM [a] $P < 0.05$, with respect to wild type mice; [b] $P < 0.05$, with respect to PLKO mice.

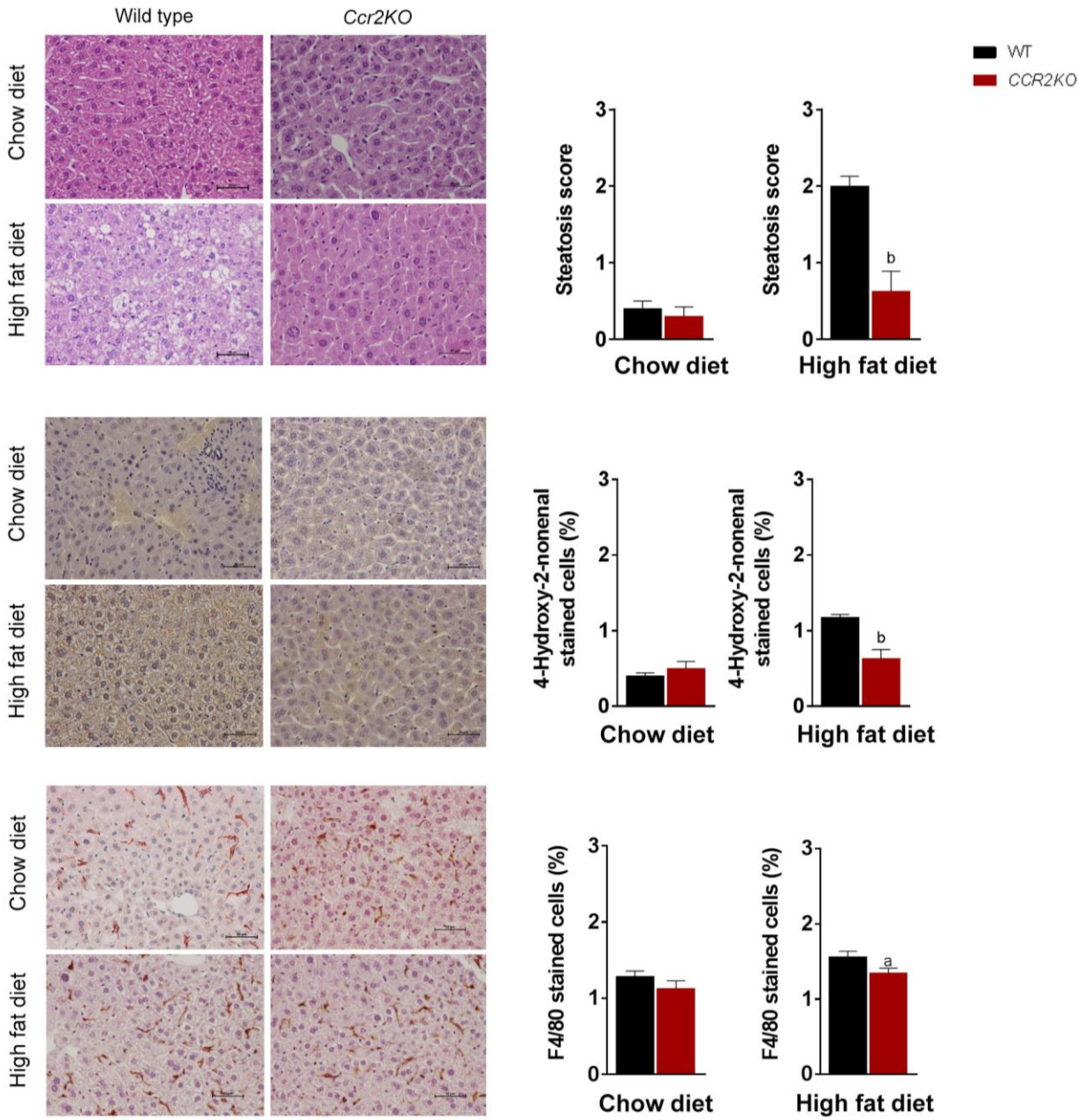

Supplementary Figure S2. Representative microphotographs (bars indicate magnification) of liver sections stained with hematoxylin and eosin and immunohistochemical staining against 4-hydroxy-2-nonenal (4-HNE) and F4/80 in wild type (WT) and *Ccr2* deficient mice (*ccr2KO*). Values reported for the calculated steatosis score, 4-HNE and F4/80 stained cells are mean ± SEM (n=8 per genotype and dietary condition) [a] $P < 0.05$, [b] $P < 0.001$, with respect to WT.

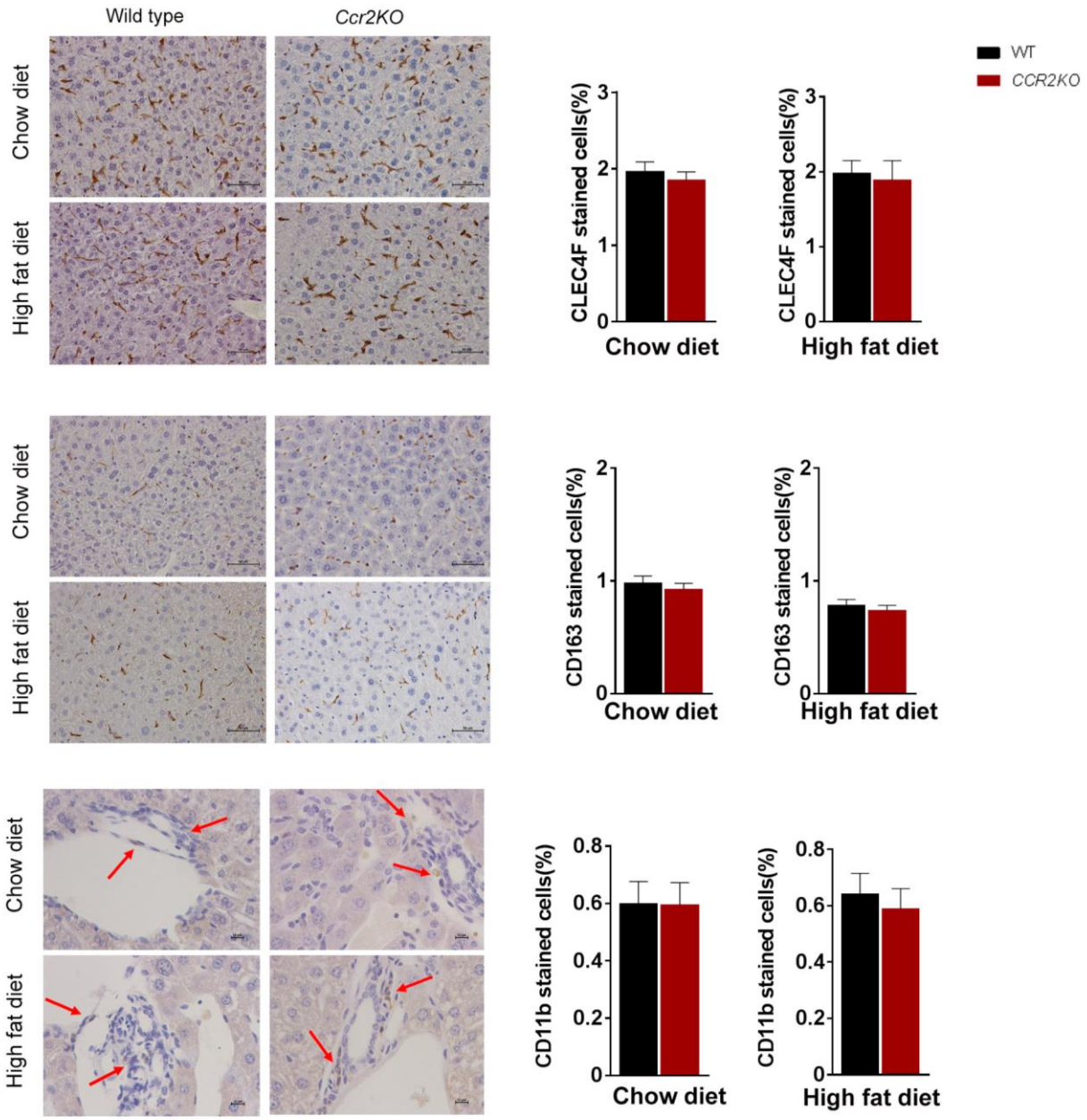

Supplementary Figure S3. Hepatic macrophage relative density. Representative microphotographs (bars indicate magnification) illustrating immunohistochemical staining against C-type lectin domain family 4-member F (CLEC4F), cluster of differentiation 163 (CD163), and cluster of differentiation 11b (CD11b), in wild type (WT) and *Ccr2* deficient mice (*ccr2KO).* Values reported for the calculated stained cells are mean ± SEM.

	WT		*PL KO*		*CPL KO*	
Metabolites	**CD**	**HFD**	**CD**	**HFD**	**CD**	**HFD**
Glucose 6-phosphate	18.9 (14.6 - 18.9)	39.4 (37.4 - 39.4)	228.6 (201.1 - 266.4) [b]	410.8 (299.1 - 445.3) [b]	39.5 (30.6 - 54.6) [b,d]	50.9 (49.3 - 64.9) [b,d]
Fructose-6-phosphate	2.6 (1.9 - 3.2)	4.5 (2.6 - 5.4)	13.9 (10.4 - 17.2) [b]	5.3 (4.6 - 7.5)	5.4 (4.1 - 6.06) [b,d]	13.4 (13.1 - 18.7) [b,d]
Fructose 1.6-bisphosphate	8.3 (7.6 - 8.6)	12.6 (10.9 - 12.9)	42.1 (30.7 - 45.7) [b]	17.3 (14.6 - 22.9) [b]	14.1 (12.1 - 18.8) [b,d]	42.4 (35.5 - 49.5) [b,d]
Glyceraldehide 3-phosphate	7.1 (5.3 - 7.1)	3.6 (1.2 - 5.4)	4.7 (4.4 - 5.8) [a]	3.3 (2.8 - 3.4)	6.1 (4.6 - 11.1)	3.2 (2.5 - 5)
3-phosphoglycerate	36.6 (18.3 - 72.9)	26.2 (25.7 - 45.6)	22.4 (19.6 - 24.4)	9.5 (9.2 - 1) [b]	27.1 (18.7- 33.6)	5.9 (4.7 - 7.4) [b,d]
Phosphoenolpyruvate	73.3 (58.0 - 148.6)	58.1 (57.8 - 82.4)	86.4 (67.6 - 95.6)	64.2 (53.1 - 75.6)	86.6 (72.7 - 89.9)	47.2 (39.3 - 68.6)
Pyruvate	18.7 (15.7 - 20.8)	13.5 (12 - 15.5)	16.7 (16.1 - 18.2)	14.9 (12.6 - 16.8)	16.6 (14.9 - 23.2)	11.7 (11.7 - 14.7) [d]
Lactate	4942.2 (4941.4 -1509.5)	6248 (4984.5 - 8331)	11273.9 (9990.7 - 13532.1)	8608.5 (5800.8 - 10465.9)	15947.9 (15799.6 - 16145.6) [b,d]	9058.5 (3654.5 - 11769.1)
6 phosphogluconate	40 (37.5 - 62.5)	30.3 (18.3 - 43.7)	8.5 (7.7 - 11.1) [b]	5.9 (4.5 - 7.4) [b]	34.4 (18.2 - 51.4) [d]	14.6 (6.1 - 23.5) [b, c]
Ribose-5-phosphate	7.3 (7.1 - 21.7)	3.4 (2.5 - 7.9)	77.5 (67.2 - 97.6) [b]	71.1 (51.1 - 97.6) [b]	14.9 (9.8 - 44.7) [b,d]	24.5 (13.5 - 56.0) [b,d]
Citrate-isocitrate	1.1 (0.8 - 1.5)	0.8 (0.3 - 2.)	3.4 (1.3 - 4.7) [a]	2.3 (1.7 - 3.4)	1.5 (0.9 - 2.3) [c]	0.3 (0.3 - 0.8) [d]
Aconitate	393.9 (232.5 - 461.5)	36.6 (23.6 - 45.8)	275.1 (238.6 - 328.9)	88.1 (72.1 - 130.7) [b]	268.7 (210.5 - 385.6)	279.4 (205.4 - 324.2) [b,d]
α-ketoglutarate	0.7 (0.5 - 0.8)	0.5 (0.7 - 0.8)	0.6 (0.5 - 0.6)	0.5 (0.4 - 0.6)	0.5 (0.4 - 0.6)	0.4(0.3 - 0.5)
Succinyl-coa	152.8 (152.8 - 173.7)	304.9 (281.2 - 304.9)	37.8 (29.2 - 44.2) [b]	13.3 (13.2- 14.5) [b]	121.8 (120.5 - 128.3) [b,d]	22.2 (19.4 - 62.2) [b,d]
Succinate	75.1 (55.5 - 82.9)	41.4 (38.1 - 57.7)	75.3 (70.7 - 81.2)	60.7 (47.1 - 83.6) [a]	73.9 (48.5 - 170.3)	64.9 (57.1 - 73.3) [b]
Fumarate	7.5 (5 - 9.3)	3.7 (3.2 - 7.1)	5.8 (4.2 - 6.01)	3.6 (2.3 - 5.3)	6.2 (3.9 - 9.7)	4.2 (3.8 – 7.1)
Malate	328.7 (163.7 - 469.9)	299.6 (170.1 - 299.6)	149.08 (107.7 -173.1) [a]	71.5 (58.3 - 121.8) [b]	247.4 (129.7 - 335.3)	103.9 (102.9 - 113.6) [b]
Malonyl-coa	9.7 (8.1 - 12.6)	6.1 (3.3 - 7.1)	4.7 (3.8 - 5.5) [b]	1.1 (0.9 - 1.4) [b]	5.7 (5.549 - 7.373) [b,d]	1.5 (0.5 - 2.1) [b]
β-Hydroxybutirate	14.8 (12.6 - 14.8)	9.8 (7.4 - 11.9)	9.01 (6.9 - 10.6) [b]	10.2 (7.7 - 13.4)	13.239 (9.505 - 25.309)	14.5 (13.6 - 15.2) [b,d]
Glutamate	229.1(211.8 - 417.8)	98.6 (97.3 - 103.4)	121.3 (84.2 - 145.4) [b]	47.6 (29.6 - 69.9) [b]	158.5 (136.5 - 202.5) [b,d]	132.2 (101.4 - 160.8) [d]
Glutamine	1.2 (0.9 - 2.2)	1.8 (0.6 - 3.1)	3.4 (3.1 – 4.4) [b]	2.4 (1.6 - 3.1)	1.6 (0.9 - 2.2) [d]	0.4 (0.4 - 0.7) [b,d]
Alanine	931.1 (847.1 - 1135.4)	879.6 (874.2 – 885.1)	896.8 (674.9 - 1094.1)	564.1 (470.9 - 707.7) [b]	908.1 (742.9 - 1112.7)	655.9 (568.2 - 1144.4)
Serine	1447.4 (804.6 - 2419.3)	1653.3 (1591.3 - 1715.3)	392.4 (305.4 - 446.3) [b]	150.5 (136.9 - 211.1) [b]	935.4 (876.1 - 1225.9) [d]	495.5 (205.9 - 725.3) [b, c]
Valine	292 (239.1 - 405.1)	345.8 (243.5 - 397.8)	141.9 (130.2 - 47.5) [b]	87.2 (85.3 - 91.4) [b]	283.9 (189.1 - 359.3) [d]	132.7 (108.8 - 148.1) [b, d]
Isoleucine	50.7 (43.6 - 53.9)	92.9 (81.8 - 92.9)	32.6 (30.9 - 38.1) [b]	21.4 (20.7 - 31.1) [b]	49.2 (36.3 - 50.9) [d]	25.9 (20.8 - 33.7) [b]
Leucine	578.6 (467.4 - 578.6)	770.4 (758.6 - 782.2)	277.9 (243.8 - 295.8) [b]	142.3 (133.3 - 215.6) [b]	517.6 (403.3 - 686.3) [d]	200.5 (160.1 - 260.1) [b]
Aspartate	204.5 (199.4 - 697.5)	506.1 (296.3 – 715.8)	310.3 (203.3 - 446.6)	146.3 (76.1 - 211.6) [b]	198.8 (161.9 - 281.9) [d]	290.3 (270.5 - 301.1) [b,d]

Supplementary table S1. Hepatic energy-balance metabolites. Values are expressed in μM/ 100 mg of tissue (mean (interquartile range)) illustrating dietary-based differences between standard chow diet (CD) or high fat diet (HFD) in all strains. PLKO denotes *ccl2*$^{+/+}$, *pon1*$^{-/-}$, *ldlr*$^{-/-}$ and CPLKO *ccl2*$^{-/-}$, *pon1*$^{-/-}$, *ldlr*$^{-/-}$; [a] P < 0.05, [b] P < 0.001, with respect to WT; [c] P < 0.05, [d] P< 0.001 with respect to PLKO.

Metabolite	*WT*		*PLKO*		*CPLKO*	
	CD	**HFD**	**CD**	**HFD**	**CD**	**HFD**
Homocysteine	2.4 (2.1 - 2.9)	2.3 (2.1 - 2.7)	1.2 (1 - 1.4)	1.441 (1 - 1.6)[d]	2.1 (1.4 - 4.1)	2 (1.4 - 2.7)
Choline-Dimethlyglycine	15 (10.8 - 22.6)	10 (7.4 - 10.4)	11.7 (6.7 - 15.1)	12.9 (9 - 18.8)[a]	27.9 (21.4 - 48.4)[a,d]	15.6 (9.6 - 20.9) [d]
Betaine	0.02 (0.01 - 0.06)	0.1 (0.01 - 0.2)	0.1 (0.04 - 0.09)	0.1 (0.04 - 0.1)	0.003 (0.003 - 0.01) [b,d]	0.04 (0.03 - 0.1) [d]
Methionine	99 (70.2 - 231.3)	99.4 (72 - 185.6)	28.9 (19.2 - 48.4)[b]	11.5 (8.7 - 27.9)[a]	89.3 (47.3 - 118.2)[d]	64.1 (51 -120)
SAM	0.6 (0.4 - 1.2)	1.4 (1.1 - 1.9)	0.4 (0.3 - 0.7)	0.9 (0.7 - 0.9) [a]	0.6 (0.4 - 1)	1.3 (0.5 - 1.7)
SAH	0.001 (0.001 - 0.002)	0.0003 (0.0001 - 0.001)	0.01 (0.01 - 0.03) [b]	0.01 (0.01 - 0.02)[b]	0.001 (0.0003 - 0.001)	0.001 (0.001-0.004)[a]
AMP	10 (8.4 - 11.4)	7.3 (5.3 - 8.5)	15.8 (9.1 - 26.1)	16.5 (13.6 - 20.1)[b]	8.5 (5.8 - 24)	12.2 (8.6 - 22.3)[a]
Cystathionine	0.004 (0.003 - 0.011)	0.007 (0.002 - 0.01)	0.004 (0.002 - 0.01)	0.002 (0.001 - 0.005)	0.004 (0.002 - 0.01)	0.003 (0.001 - 0.01)
Taurine	93.3 (85.9 - 210.2)	1827.3 (1291.8 - 2577.1)	363.3 (311.8 - 501.)[b]	1171.1 (1118.7 - 1695.8)	1192.9 (361.1 - 1769.5)[b]	1313.9 (356.5 - 2485.2)
Glutathione disulfide (GSSG)	13.4 (11.4 - 13.9)	8.4 (7.1 - 13.6)	240.605 (238.4 - 266.2) [b]	772.9 (543.1 - 7313.6)[b]	14.1 (10.1-21.4)[d]	15.3 (12.9 - 18.9)[a]
Glutathione (GSH)	439.7 (351.1 - 581.7)	453.2 (361.5 - 476.3)	653.328 (596.1 - 725.2)[b]	1171.1 (1118.7 - 1695.8)[a]	414.4 (320.1 - 475.6)[d]	513.8 (425.5 - 688.3)

Supplementary table S2. Metabolites in methionine cycle and transsulfuration pathway. Values are expressed in µM/ 100 mg of tissue (mean (interquartile range)) illustrating dietary-based differences between standard chow diet (CD) or high fat diet (HFD) in all strains. PLKO denotes *ccl2*$^{+/+}$, *pon1*$^{-/-}$, *ldlr*$^{-/-}$ and CPLKO *ccl2*$^{-/-}$, *pon1*$^{-/-}$, *ldlr*$^{-/-}$; [a] $P < 0.05$, [b] $P < 0.001$, with respect to WT; [c] $P < 0.05$, [d] $P < 0.001$ with respect to PLKO.

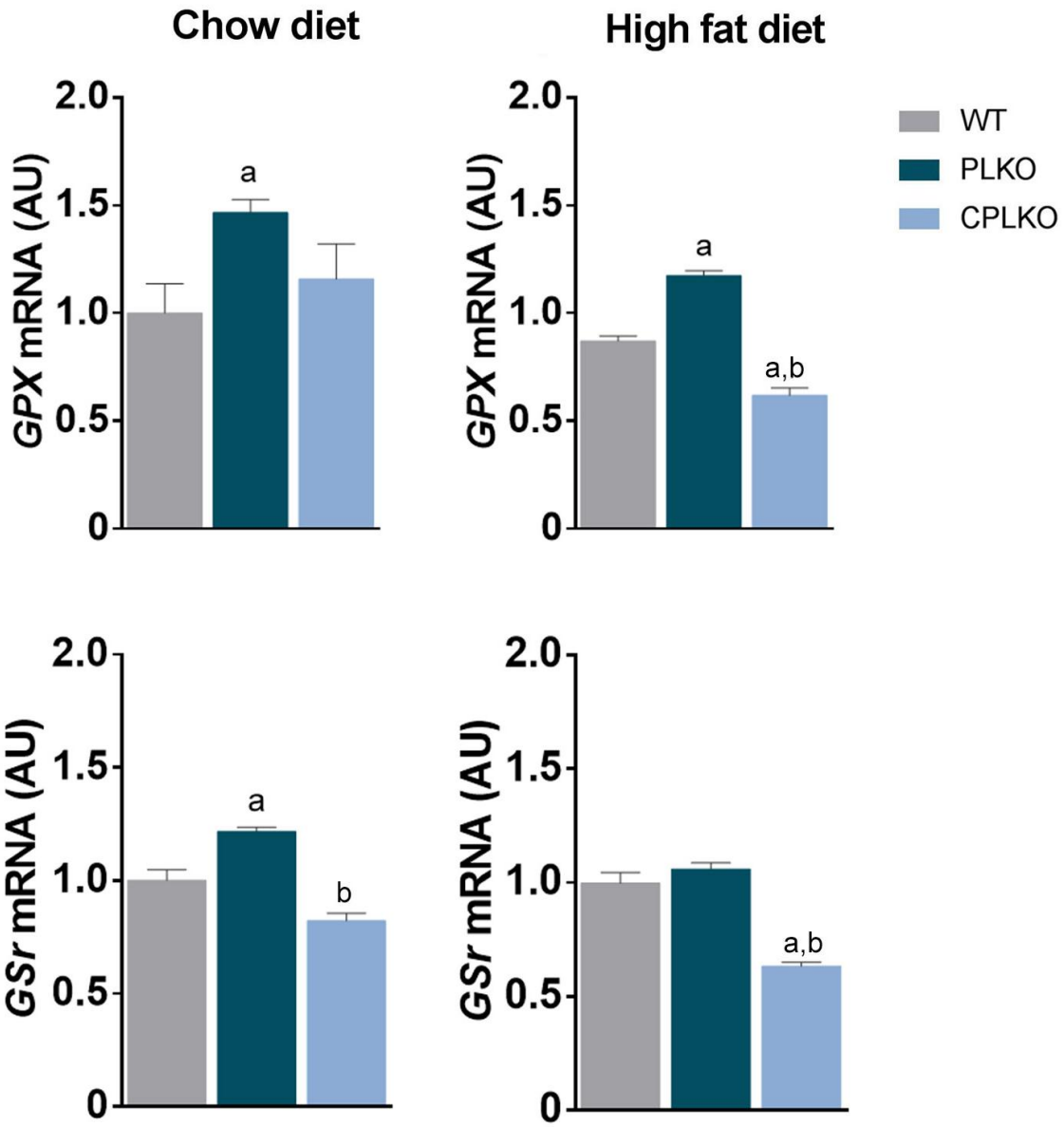

Supplementary Figure S4. Relative hepatic mRNA expression of glutathione peroxidase (*Gpx*) and glutathione reductase (*Gsr*) in wild type (WT), PLKO and CPLKO mice. PLKO stands for *ccl2*$^{+/+}$, *pon1*$^{-/-}$, *ldl*$^{-/-}$ mice, and CPLKO stands for *ccl2*$^{-/-}$, *pon1*$^{-/-}$, *ldlr*$^{-/-}$ animals. Values are mean ± SEM [a] $P < 0.05$, with respect to wild type mice; [b] $P < 0.05$, with respect to PLKO mice.

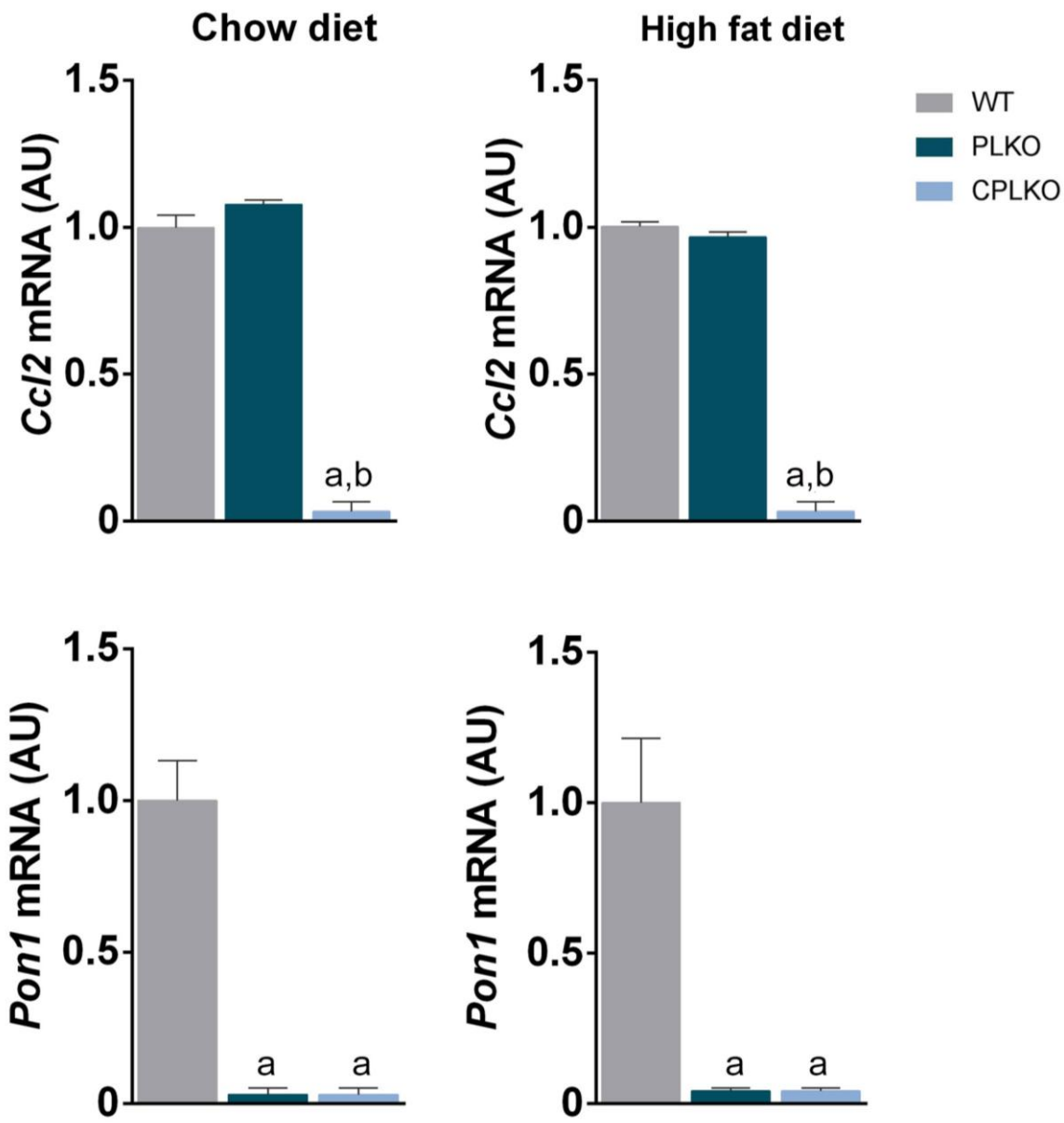

Supplementary Figure S5. Relative hepatic mRNA expression of the chemokine (C-C motif) ligand 2 (*Ccl2*) and paraoxonase-1 (*Pon1*) in wild type (WT), PLKO and CPLKO mice. PLKO stands for *ccl2*$^{+/+}$, *pon1*$^{-/-}$, *ldl*$^{-/-}$ and CPLKO stands for *ccl2*$^{-/-}$, *pon1*$^{-/-}$, *ldlr*$^{-/-}$. Values are mean ± SEM. [a] $P < 0.001$, with respect to wild type mice; [b] $P < 0.001$, with respect to PLKO animals.

	CD	HFD
Crude protein (%)	16.1	24.1
Crude fat (%)	3.1	34.6
Crude fibre (%)	3.9	7.2
Carbohydrate (available) (%)	71.8	24.8
Crude ash (%)	4.2	8.5
Nitrogen free extracts (%)	43.5	23.3
Energy density (Kcal/g (Kj/g))	3.3 (14.0)	5.7 (24)
Calories from protein (%)	19.3	19
Calories from fat (%)	8.4	60
Calories from carbohydrate (%)	72.4	21
Calcium (%)	1.4	1.0
Phosphorus (%)	1.0	0.7
Sodium (%)	0.5	0.2
Magnesium (%)	0.3	0.2
Potassium (%)	1.5	1.0
Chloride (%)	0.7	-
Caprid acid (C10:0) (%)	ND	0.04
Lauric acid (C12:0) (%)	ND	0.1
Myristic acid (C14:0) (%)	ND	0.4
Palmitic acid (C16:0) (%)	0.9	7.7
Palmitoleic acid (C16:1) (%)	0.03	0.9
Margaric acid (C17:0) (%)	ND	-
Stearic acid (C18:0) (%)	0.1	4.3
Oleic acid (C18:1) (%)	0.5	13.6
Linoleic acid (C18:2) (%)	1.3	4.8
Linolenic acid (C18:3) (%)	0.2	0.5
Arachidic acid (C20:0) (%)	ND	0.02
Paullinic acid (C20:1) (%)	ND	0.01
Arachidonic acid (C20:4) (%)	ND	0.5
Cholesterol (mg/kg)	ND	265
Lysine (%)	3.9	2
Methionine (%)	1.5	0.8
Cystine (%)	1.1	0.5
Met+Cys (%)	ND	1.3
Threonine (%)	ND	1.1
Tryptophan (%)	0.9	0.3
Arginine (%)	4.8	0.9
Histidine (%)	ND	0.8
Valine (%)	ND	1.6
Isoleucine (%)	ND	1.3
Leucine (%)	ND	2.4
Phenylalanine (%)	ND	1.3
Phe+Tyr (%)	ND	2.6
Glycine (%)	0.4	0.5
Glutamic acid (%)	ND	5.4
Aspartic acid (%)	ND	1.8
Proline (%)	ND	2.8
Alanine (%)	ND	0.8
Serine (%)	ND	1.4
Vitamin A (IU/kg)	7500	15000
Vitamin D_3 (IU/kg)	1000	1500
Vitamin E (IU/kg)	120	225
Vitamin K (as menadione) (mg/Kg)	2.5	20
Vitamin C (mg/Kg)	ND	30
Thiamin (B_1) (mg/Kg)	7	16
Riboflavin (B_2) (mg/Kg)	6.5	16
Pyridoxime (B_6) (mg/Kg)	2.6	18
Cyanocobalamin (B_{12}) (µg/Kg)	20	30
Nicotinic acid (mg/Kg)	75	45
Pantothenic acid (mg/Kg)	17	55
Folic acid (mg/Kg)	0.5	19
Biotin (µg/Kg)	40	310
Choline-Chloride (mg/Kg)	1600	2300
Inositol (mg/Kg)	ND	80
Iron (mg/Kg)	280	139
Manganese (mg/Kg)	90	82
Zinc (mg/Kg)	64	56
Copper (mg/Kg)	18	12
Iodine (mg/Kg)	ND	1.0
Selenium (mg/Kg)	ND	0.1
Cobalt (mg/Kg)	ND	0.1

Supplementary table S3. Nutritional composition of chow diet (CD) and high fat diet (HFD).

	Antigen	Antibody	1ry Dilution	2ry Antibody	2ry Dilution
Macrophage marker	F4.80	F4.80 antibody, ab100790 (Abcam, Cambridge, UK)	1:100	Goat α-rabbit HRP, P0448 (Dako, Agilent, California, USA)	1:200
Kupffer cells	CLEC4F	CLEC4F/CLECSF13 Antibody, AF2784 (AF2784, Minneapolis, USA)	1:100	Goat α-rabbit HRP, P0448 (Dako, Agilent, California, USA)	1:200
Pro-inflammatory macrophages marker	CD11b	CD11b antibody, ab133357 (Abcam, Cambridge, UK)	1:4000	Goat α-rabbit HRP, P0448 (Dako, Agilent, California, USA)	1:200
Anti-inflammatory macrophages markers	CD163	CD163, antibody, ab182422 (Abcam, Cambridge, UK)	1:500	Goat α-rabbit HRP, P0448 (Dako, Agilent, California, USA)	1:200
Oxidative stress marker	4HNE	Anti-HNE, MHN-100P (Genox, Baltimore, MD, USA)	1:1000	Goat anti-rabbit IgG, BA-1000 (Vector)	1:200
Insulin receptor	PI3K-p85	PI3K antibody, #4257 (Cell signalling, Massachusetts, USA)	1:1000	Goat α-rabbit HRP, P0448 (Dako, Agilent, California, USA)	1:5000
	Akt-p S473	p-Akt antibody, #4060 (Cell signalling, Massachusetts, USA)	1:1000	Goat α-rabbit HRP, P0448 (Dako, Agilent, California, USA)	1:5000
	Akt	AKT antibody, #4685 (Cell signalling, Massachusetts, USA)	1:1000	Goat α-rabbit HRP, P0448 (Dako, Agilent, California, USA)	1:5000
Energy sensors	mTOR-p S2448	pmTOR antibody,#2971 (Cell signalling, Massachusetts, USA)	1:1000	Goat α-rabbit HRP, P0448 (Dako, Agilent, California, USA)	1:2000
	mTOR	mTOR Antibody, #2972 (Cell signalling, Massachusetts, USA)	1:1000	Goat α-rabbit HRP, P0448 (Dako, Agilent, California, USA)	1:2000
	P4E-BP1	P4E-BP1 antibody #2855 (Cell signalling, Massachusetts, USA)	1:100	Goat α-rabbit HRP, P0448 (Dako, Agilent, California, USA)	1:5000
	AMPK-P T172	pAMPK antibody, #2531 (Cell signalling, Massachusetts, USA)	1:1000	Goat α-rabbit HRP, P0448 (Dako, Agilent, California, USA)	1:5000
	AMPK	AMPK antibody #2532S (Cell signalling, Massachusetts, USA)	1:1000	Goat α-rabbit HRP, P0448 (Dako, Agilent, California, USA)	1:5000
Autophagy markers	Atg7	Atg7 Antibody, #8558 (Cell signalling, Massachusetts, USA)	1:1000	Goat α-rabbit HRP, P0448 (Dako, Agilent, California, USA)	1:5000
	LC3	LC3B Antibody, #2775S (Cell signalling, Massachusetts, USA)	1:1000	Goat α-rabbit HRP, P0448 (Dako, Agilent, California, USA)	1:5000
	LAMP2A	LAMP2A antibody, ab125068 (Abcam, Cambridge, UK)	1:1000	Goat α-rabbit HRP, P0448 (Dako, Agilent, California, USA)	1:2000

Supplementary table S4. Antibodies and dilutions used in immunohistochemical and western blot analyses.

UNIVERSITAT ROVIRA I VIRGILI
THE ROLE OF CHEMOKINE (C-C MOTIF) LIGAND 2 IN INFLAMMATION, OXIDATIVE STRESS, AGING AND METABOLISM
Fedra Nicaury Luciano Mateo

List of publications and communications

Luciano-Mateo F, Cabré N, Fernández-Arroyo S, Baiges-Gaya G, Hernández-Aguilera A, Rodríguez-Tomàs E, Mercado-Gómez M Menéndez J.A; Camps J, Joven J. Chemokine (C-C motif) ligand 2 gene ablation protects low-density lipoprotein and paraoxonase-1 double deficient mice from liver injury, oxidative stress and inflammation. Biochim Biophys Acta Mol Basis Dis. 2019 Mar 21: S0925-4439(19)30080-8. doi: 10.1016/j.bbadis.2019.03.006**. Quartile: Q1**. **Impact factor: 5.1**

N. Cabré; **F. Luciano-Mateo**; S. Fernández-Arroyo; G. Baiges-Gaya; A. Hernández-Aguilera; M. Fibla; R. Fernández-Julia; M. Paris; F. Sabench; D. Castillo; J. A Menéndez; J. Camps; J. Joven. Laparoscopic sleeve gastrectomy in obesity promotes NAFLD remission by attenuating liver injury, oxidative stress and inflammation. Hepatology and Gastroenterology. 2019. **Item Status: submitted. Quartile: Q1**. **Impact factor: 7.7**

Arenas M, Rodríguez E, García-Heredia A, Fernández-Arroyo S, Sabater S, Robaina R, Gascón M, Rodríguez-Pla M, Cabré N, **Luciano-Mateo F**, Hernández-Aguilera A, Fort-Gallifa I, Camps J, Joven J. Metabolite normalization with local radiotherapy following breast tumor resection. PLoS One. 2018. 2018 Nov 16; 13(11):e0207474. doi: 10.1371/journal.pone.0207474. **Quartile: Q1**. **Impact factor: 2.8**

Hernández-Aguilera A, Fernández-Arroyo S, Cabre N, **Luciano-Mateo F**, Baiges-Gaya G, Fibla M, Martín-Paredero V, Menendez JA, Camps J, Joven J. Plasma Energy-Balance Metabolites Discriminate Asymptomatic Patients with Peripheral Artery Disease. Mediators Inflamm. 2018. Sep 20; 2018:2760272. doi: 10.1155/2018/2760272. **Quartile: Q2. Impact factor: 3.5**

Cabré N, **Luciano-Mateo F**, Arenas M, Nadal M, Baiges-Gaya G, Hernández-Aguilera A, Fort-Gallifa I, Rodríguez E, Riu F, Camps J, Joven J, Domingo JL. Trace element concentrations in breast cancer patients. Breast. 2018. Dec;42:142-149. doi: 10.1016/j.breast.2018.09.005. **Quartile: Q1**. **Impact factor: 2.9**

Garrido P, Rovira C, Cueto P, Fort-Gallifa I, Hernández-Aguilera A, Cabré N, **Luciano-Mateo F**, García-Heredia A, Camps J, Joven J, Garcia E, Vallverdú I. Effect of continuous renal-replacement therapy on paraoxonase-1-related variables in patients with acute renal failure caused by septic shock. Clin Biochem. 2018. Nov;61:1-6. doi: 10.1016/j.clinbiochem.2018.08.010. **Quartile: Q2 Impact factor: 2.3**

Luciano-Mateo F, Cabré N, Nadal M, García-Heredia A, Baiges-Gaya G, Hernández-Aguilera A, Camps J, Joven J, Domingo JL. Serum concentrations of trace elements and their relationships with paraoxonase-1 in morbidly obese women. J Trace Elem Med Biol. 2018. Jul;48:8-15. doi: 10.1016/j.jtemb.2018.02.023. **Quartile: Q2**. **Impact factor: 3.8**

Cuyàs E, Verdura S, Llorach-Pares L, Fernández-Arroyo S, **Luciano-Mateo F**, Cabré N, Stursa J, Werner L, Martin-Castillo B, Viollet B, Neuzil J, Joven J, Nonell-Canals A, Sanchez-Martinez M, Menendez JA. Metformin directly targets the H3K27me3 demethylase KDM6A/UTX. Aging Cell. 2018. May 8:e12772. doi: 10.1111/acel.12772. **Quartile: Q1**. **Impact factor: 7.6**

Iftimie S, García-Heredia A, Pujol-Bosch F, Pont-Salvadó A, López-Azcona AF, Hernández-Aguilera A, Cabré N, **Luciano-Mateo F**, Fort-Gallifa I, Castro A, Camps J, Joven J. Serum Paraoxonase-1 Concentration as a Potential Predictor of Urinary Bladder Cancer Recurrence. A Five Year Follow-Up Study. Arch Med Res. 2018. Feb;49(2):119-122. doi: 10.1016/j.arcmed.2018.04.011. **Quartile: Q3**. **Impact factor: 2.02**

Rovira J, Hernández-Aguilera A, **Luciano-Mateo F**, Cabré N, Baiges-Gaya G, Nadal M, Martín-Paredero V, Camps J, Joven J, Domingo JL .Trace Elements and Paraoxonase-1 Activity in Lower Extremity Artery Disease. Biol Trace Elem Res. 2018. ov;186(1):74-84. doi: 10.1007/s12011-018-1298-x. **Quartile: Q3**. **Impact factor: 2.4**

Arenas M, García-Heredia A, Cabré N, **Luciano-Mateo F**, Hernández-Aguilera A, Sabater S, Bonet M, Gascón M, Fernández-Arroyo S, Fort-Gallifa I, Camps J, Joven J. Effect of radiotherapy on activity and concentration of serum paraoxonase-1 in breast cancer patients. PLoS One. 2017. Nov 27;12(11):e0188633. doi: 10.1371/journal.pone.0188633. **Quartile: Q1**. **Impact factor: 2.8**

Riera-Borrull M, García-Heredia A, Fernández-Arroyo S, Hernández-Aguilera A, Cabré N, Cuyàs E, **Luciano-Mateo F**, Camps J, Menendez JA, Joven J. Metformin Potentiates the Benefits of Dietary Restraint: A Metabolomic Study. Int J Mol Sci. 2017. Oct 28;18(11). pii: E2263. doi: 10.3390/ijms18112263. **Quartile: Q2** . **Impact factor: 3.7**

Fort-Gallifa I, Hernández-Aguilera A, García-Heredia A, Cabré N, **Luciano-Mateo F**, Simó JM, Martín-Paredero V, Camps J, Joven J. Galectin-3 in Peripheral Artery Disease. Relationships with Markers of Oxidative Stress and Inflammation. Int J Mol Sci. 2017. May 4;18(5). pii: E973. doi: 10.3390/ijms18050973. **Quartile: Q2**. **Impact factor: 3.7**

Luciano-Mateo F, Hernández-Aguilera A, Cabre N, Camps J, Fernández-Arroyo S, Lopez-Miranda J, Menendez JA, Joven J. Nutrients in Energy and One-Carbon Metabolism: Learning from Metformin Users. Nutrients. 2017. Feb 10;9(2). pii: E121. doi: 10.3390/nu9020121. **Quartile: Q1** . **Impact factor: 4.2**

Riera-Borrull M, Rodríguez-Gallego E, Hernández-Aguilera A, Luciano F, Ras R, Cuyàs E, Camps J, Segura-Carretero A, Menendez JA, Joven J, Fernández-Arroyo S. Exploring the Process of Energy Generation in Pathophysiology by Targeted Metabolomics: Performance of a Simple and Quantitative Method. J Am Soc Mass Spectrom. 2016. Jan;27(1):168-77. doi: 10.1007/s13361-015-1262-3. **Quartile: Q2**. **Impact factor: 2.9**

Camps J, Hernandez-Aguilera A, Garcia-Heredia A, Cabre N, **Luciano-Mateo F,** Arenas M, Joven J. Relationships Between Metformin, Paraoxonase-1 and the Chemokine (C-C Motif) Ligand 2. Curr Clin Pharmacol. 2016. 11(4):250-258. doi: 10.2174/1574884711666160915152941.

Hernández-Aguilera A, Fernández-Arroyo S, Cuyàs E, **Luciano-Mateo F,** Cabre N, Camps J, Lopez-Miranda J, Menendez JA, Joven J. Epigenetics and nutrition-related epidemics of metabolic diseases: Current perspectives and challenges. Food Chem Toxicol. 2016. **Quartile: Q1**. **Impact factor: 3.9**

García-Heredia A, Riera-Borrull M, Fort-Gallifa I, **Luciano-Mateo F**, Cabré N, Hernández-Aguilera A, Joven J, Camps J. Metformin administration induces hepatotoxic effects in paraoxonase-1-deficient mice. Chem Biol Interact.2016. Oct;96:191-204. doi: 10.1016/j.fct.2016.08.006. **Quartile: Q2**. **Impact factor: 3.4**

Hernández-Aguilera A, Sepúlveda J, Rodríguez-Gallego E, Guirro M, García-Heredia A, Cabré N, **Luciano-Mateo F**, Fort-Gallifa I, Martín-Paredero V, Joven J, Camps J. Immunohistochemical analysis of paraoxonases and chemokines in arteries of patients with peripheral artery disease. Int J Mol Sci. 2015. 18;16(5):11323-38. doi: 10.3390/ijms160511323. **Quartile: Q2** . **Impact factor: 3.7**

Camps J, Rodríguez-Gallego E, García-Heredia A, Triguero I, Riera-Borrull M, Hernández-Aguilera A, **Luciano-Mateo F**, Fernández-Arroyo S, Joven J. Paraoxonases and chemokine (C-C motif) ligand-2 in noncommunicable diseases. Adv Clin Chem. 2014. 2014;63:247-308. **Quartile: Q1**. **Impact factor: 4.2**

Rodríguez-Gallego E, Riera-Borrull M, Hernández-Aguilera A, Mariné-Casadó R, Rull A, Beltrán-Debón R, **Luciano-Mateo F**, Menendez JA, Vazquez-Martin A, Sirvent JJ, Martín-Paredero V, Corbí AL, Sierra-Filardi E, Aragonès G, García-Heredia A, Camps J, Alonso-Villaverde C, Joven J. Ubiquitous transgenic overexpression of C-C chemokine ligand 2: a model to assess the combined effect of high energy intake and continuous low-grade inflammation. Mediators Inflamm. 2013. 2013;2013:953841. doi: 10.1155/2013/953841. **Quartile: Q2. Impact factor: 3.5**

Hernández-Aguilera A, Rull A, Rodríguez-Gallego E, Riera-Borrull M, **Luciano-Mateo F**, Camps J, Menéndez JA, Joven J. Mitochondrial dysfunction: a basic mechanism in inflammation-related non-communicable diseases and therapeutic opportunities. Mediators Inflamm. 2013. 2013;2013:135698. doi: 10.1155/2013/135698. **Quartile: Q2. Impact factor: 3.5**

Menendez JA, Joven J, Aragonès G, Barrajón-Catalán E, Beltrán-Debón R, Borrás-Linares I, Camps J, Corominas-Faja B, Cufí S, Fernández-Arroyo S, Garcia-Heredia A, Hernández-Aguilera A, Herranz-López M, Jiménez-Sánchez C, López-Bonet E, Lozano-Sánchez J, **Luciano-Mateo F**, Martin-Castillo B, Martin-Paredero V, Pérez-Sánchez A, Oliveras-Ferraros C, Riera-Borrull M, Rodríguez-Gallego E, Quirantes-Piné R, Rull A, Tomás-Menor L, Vazquez-Martin A, Alonso-Villaverde C, Micol V, Segura-Carretero A. Xenohormetic and anti-aging activity of secoiridoid polyphenols present in extra virgin olive oil: a new family of gerosuppressant agents. Cell Cycle. 2013. 15;12(4):555-78. doi: 10.4161/cc.23756. **Quartile: Q3**. **Impact factor: 3.3**

List of congress

EASL international congress 2019. Luciano-Mateo F.; Cabré N.; Baiges-Gaya G; Rodríguez-Tomás E; Hernández-Aguilera A; Fernández-Arroyo S; J Camps; J Joven. Metabolic inflammation: The role of chemokine C-C motif ligand 2 in the crosstalk between liver tissue and muscle. Vienna, Austria. 2019.

EASL international congress 2019. Cabré N; Luciano-Mateo F; Baiges-Gaya G; Fernández-Arroyo S; Hernández-Aguilera A; Camps J; Joven J. Integrated analysis of DNA methylation and mRNA expression profiles to identify target gens in non-alcoholic fatty liver disease. Vienna, Austria. 2019.

ESTRO 38 2019. Metabolic changes with the administration of radiotherapy in lung, head and neck cancer patients. Rodríguez E. Murcia M, Arguís M, Baiges-Gaya G, Cabré N, Luciano-Mateo F, Torres-Rayo M, Árquez M, Camps J; Joven J, Arenas M. Milán. Italy

87nd European Atherosclerosis Society Congress (EAS) 2019. Luciano-Mateo F; Cabré N; Baiges-Gaya G; Rodríguez-Tomás E; Hernández-Aguilera A; Fernández-Arroyo S; Camps J; Joven J. Systemic CCL2 overexpression promotes fibrosis and vascular alterations in a mouse model of accelerated aging. Maastricht, Netherlands. 2019.

Cell symposia: Aging and metabolism 2018. F Luciano-Mateo; N Cabré; G Baiges-Gaya; M Mercado-Gómez; I Rezola-Artero; E Rodríguez-Tomás; A Hernández-Aguilera; S Fernández-Arroyo; J Camps; J Joven. Overexpression of CCL2 promote systemic alterations in a mouse model of accelerated aging. Sitges, Spain 2018.

NAFLD international congress 2018. N. Cabré; F. Luciano Mateo; G. Baiges Gaya; S. Fernádez Arroyo; J. Camps; J.Joven. Energy metabolism in obesity reveals that nash requires targeting ampk/mtor – driven. Pathways. Geneva, Switzerland. 2018.

NAFLD international congress 2018. F Luciano-Mateo; N Cabré; G Baiges-Gaya; A Hérnadez-Aguilera; S Fernánd.ez-Arroyo; J Camps; J Joven. High fat high sucrose intake underlies the progression of simple steatosis to nonalcoholic steatohepatitis. Geneva, Switzerland. 2018.

86nd European Atherosclerosis Society Congress (EAS). Hernández-Aguilera, A.; Fernández-Arroyo, S.; Pantoja, C.; Mercado, M.; Luciano-Mateo, F.; Cabré, N.; Baiges, G.; Martin-Paredero, V.; Camps, J.; Joven, J. Energy metabolism as a potential source of biological markers in abdominal aortic aneurysm. Lisboa, Portugal, 2018

86nd European Atherosclerosis Society Congress (EAS). Cabré, N.; Luciano-Mateo, F.; Baiges, G.; Fernández-Arroyo, S.; Hernández-Aguilera, A.; Camps, J.; Joven, J. Bariatric surgery reverses DNA methylation modifying one carbon metabolism. Lisboa, Portugal, 2018

EASL international congress 2018. N. Cabré; F. Luciano Mateo; P. J. Àguila Hervás; M. Català; A. Hernández Aguilera; J. Camps; J. Joven. Effect of Bariatric surgery on non-alcoholic fatty liver disease:the role of macrophage mediated the sistemic inflammation. Paris, France. 2018

EASL international congress 2018. F. Luciano Mateo; N. Cabré; P. J. Àguila Hervás; M. Català; A. Hernández Aguilera; J. Camps; J. Joven. The multifactorial pathogenesis of nonalcoholic fatty liver disease: connecting inflammation and oxidation. Paris, France. 2018

XIII Congrés Català de Ciències de Laboratori Clínic. Hernández-Aguilera, A.; Fernández-Arroyo, S.; Pantoja, C.; Mercado, M.; Fort-Gallifa I.; Luciano-Mateo, F.; Cabré, N.; Baiges, G.; Martin-Paredero, V.; Camps, J.; Joven, J.. EL Metabolisme energètic com a potencial font de marcadors biològics en l'aneurisma d'aorta abdominal.Reus, Spain, 2018

XIII Congrés Català de Ciències de Laboratori Clínic. Baiges, G.; Hernández-Aguilera, A.; Pantoja, C.; Cabré N.; Luciano-Mateo, F.; Fort-Gallifa I.; Martin-Paredero, V.; Camps, J.; Joven, J. Fragments de degradació de la matriu extracel·lular com a possibles marcadors biològics en l'aneurisma d'aorta abdominal. Reus, Spain, 2018

XIII Congrés Català de Ciències de Laboratori Clínic. Cabré N.; Luciano Mateo F; Hernández Aguilera A.; Fernández Arroyo S.; Baiges Gaya G.; García Heredia A.; Camps Andreu J.; Joven J. El paper de l' α-cetoglutarat i el β-hidroxibutirat en la malaltia de l'esteatosi hepàtica no alcohòlica asociada a obesitat mòrbida: una aproximació metabolómica. Reus, Spain, 2018

EASL The International Liver Congress 2017.Cabré N.; Luciano-Mateo F; Hernández-Aguilera A.; Fernández-Arroyo S.; Baiges Gaya G.; García-Heredia A.; Camps Andreu J.; Joven J. Role of α-ketoglutarate and β-hydroxybutyrate in morbid obesity-associated non-alcoholic fatty liver disease: metabolomic approach. Amsterdam, Netherlands 2017.

EASL The International Liver Congress 2017. Luciano Mateo F; Cabré N. Casares; Hernández Aguilera A.; Baiges Gaya G.; García Heredia A.; Fernández Arroyo S.; Camps Andreu J.; Joven J. The role of chemokine (C-C motif) ligand 2 and the diet influence in the energy metabolism. Amsterdam, Netherlands 2017.

83nd European Atherosclerosis Society Congress 2015. A. Hernández Aguilera; N. Cabré Casares; F. Luciano Mateo; E. Rodríguez Gallego; M. Guirro Castellnou; S. Fernández Arroyo; R. Marine Casador; J. Camps Andreu; J. Joven. Expression of functional and silent receptors of CCL2 in human coronary arterie. Glasgow, United Kingdom. 2015.

83nd European Atherosclerosis Society Congress 2015. E. Rodríguez Gallego; R. Mariné Casador; M. Guirro Castellnou; A. Hernández Aguilera; F. Luciano Mateo; N. Cabré Casares; S. Fernádez Arroyo; J. Camps ; J. Joven. Inflammation and metabolism: The role of chemokine (C-C motif) ligand 2. Glasgow, United Kingdom. 2015.

12th International Meeting on Cholinesterases-Sixth International Conference on Paraoxonases. Cabré N, Luciano-Mateo F, Guirro M, Esther Rodríguez-Gallego E, Hernández-Aguilera A, García-Heredia A, Fernández-Arroyo S, Camps J, Joven J. Inflammation and oxidation in class III obesity: the role of chemokine (C-C motif) ligand 2 and paraoxonase 1. Elche, Spain 2015.

EASL international congress 2014. A. García Heredia; I. Fort; M. Riera Borrull; E. Rodríguez Gallego; A. Hernández Aguilera; F. Luciano Mateo; S. Fernández Arroyo; A. Abengochea; R. Marine Casador; M. Guirro Castellnou; J. Camps. Effect of Metformin in Paraoxonase-1 deficient mice. London, United Kingdom 2014.

EASL The International Liver Congress 2014. A Hernádez Aguilera; M. Riera Borrull; E. Rodríquez Gallego; R. Marine Casador; M. Guirro Castellnou; S. Fernández Arroyo; A. Garcia Heredia; F. Luciano Mateo; A. Martín Líndez; R. Beltrán Debón; J. Joven Maried. Ubiquitous transgenic overexpression of C-C chemokine ligand 2: A model to assess the combined effect of high energy intake and continuous low-grade inflammation. London, United Kingdom 2014.

82nd European Atherosclerosis Society Congress 2014. A. Garcia Heredia; I.Fort; M. Riera Borrull; E. Rodríguez Gallego; A. Hernández Aguilera; F. Luciano Mateo; S. Fernández Arroyo; A. Abengochea; R. Marine Casador; M. Guirro Castellnou; J. Camps. Effect of Metformin in Paraoxonase-1 deficient mice. Madrid, Spain. 2014.

82nd European Atherosclerosis Society Congress 2014. E. Rodríguez Gallego; S. Fernández Arroyo; M. Riera Borrull; A. Hernández Aguilera; M. Guirro Castellnou; R. Marine Casador; F. Luciano Mateo; A. Garcia Heredia; A. Martí Lindez; R. Beltrán Debón; J. Joven Maried. Metabolomics reveals that alterations in circulating aketoglutarate may be relevant in the assessment of morbid obesity-associated nonalcoholic fatty liver disease. Madrid, Spain. 2014.

82nd European Atherosclerosis Society Congress 2014. M. Riera Borrull; A. Hernández Aguilera; E. Rodríguez Gallego; A. Abengochea; S. Fernández Arroyo; F. Luciano Mateo; R. Marine Casador; M. Guirro Castellnou; J. Joven Maried. The action of metformin in hyperlipemic mice is modulated by the metabolic context. Madrid, Spain. 2014.

UNIVERSITAT ROVIRA I VIRGILI
THE ROLE OF CHEMOKINE (C-C MOTIF) LIGAND 2 IN INFLAMMATION, OXIDATIVE STRESS, AGING AND METABOLISM
Fedra Nicaury Luciano Mateo

UNIVERSITAT ROVIRA I VIRGILI
THE ROLE OF CHEMOKINE (C-C MOTIF) LIGAND 2 IN INFLAMMATION, OXIDATIVE STRESS, AGING AND METABOLISM
Fedra Nicaury Luciano Mateo